Microglia network homeostasis in health and disease

Dissertation

zur Erlangung des Grades eines

Doktors der Naturwissenschaften

der Mathematisch-Naturwissenschaftlichen Fakultät

und

der Medizinischen Fakultät

der Eberhard-Karls-Universität Tübingen

vorgelegt

von

Marc Welzer

aus Villingen-Schwenningen, Deutschland

2024

Tag der mündlichen Prüfung:	02.05.2024
Dekan der Math.-Nat. Fakultät:	Prof. Dr. Thilo Stehle
Dekan der Medizinischen Fakultät:	Prof. Dr. Bernd Pichler
1. Berichterstatter:	Prof. Dr. Mathias Jucker
2. Berichterstatter:	Prof. Dr. Olga Garaschuk
Prüfungskommission:	Prof. Dr. Mathias Jucker
	Prof. Dr. Olga Garaschuk
	Prof. Dr. Cornelius Schwarz
	Prof. Dr. Katja Schenke-Layland

Erklärung / Declaration:

Ich erkläre, dass ich die zur Promotion eingereichte Arbeit mit dem Titel:

„Microglia network homeostasis in health and disease“

selbständig verfasst, nur die angegebenen Quellen und Hilfsmittel benutzt und wörtlich oder inhaltlich übernommene Stellen als solche gekennzeichnet habe. Ich versichere an Eides statt, dass diese Angaben wahr sind und dass ich nichts verschwiegen habe. Mir ist bekannt, dass die falsche Abgabe einer Versicherung an Eides statt mit Freiheitsstrafe bis zu drei Jahren oder mit Geldstrafe bestraft wird.

I hereby declare that I have produced the work entitled **„Microglia network homeostasis in health and disease“***, submitted for the award of a doctorate, on my own (without external help), have used only the sources and aids indicated and have marked passages included from other works, whether verbatim or in content, as such. I swear upon oath that these statements are true and that I have not concealed anything. I am aware that making a false declaration under oath is punishable by a term of imprisonment of up to three years or by a fine.*

Tübingen, den ....

Datum / Date Unterschrift /Signatur

Für Theresa und Katrin

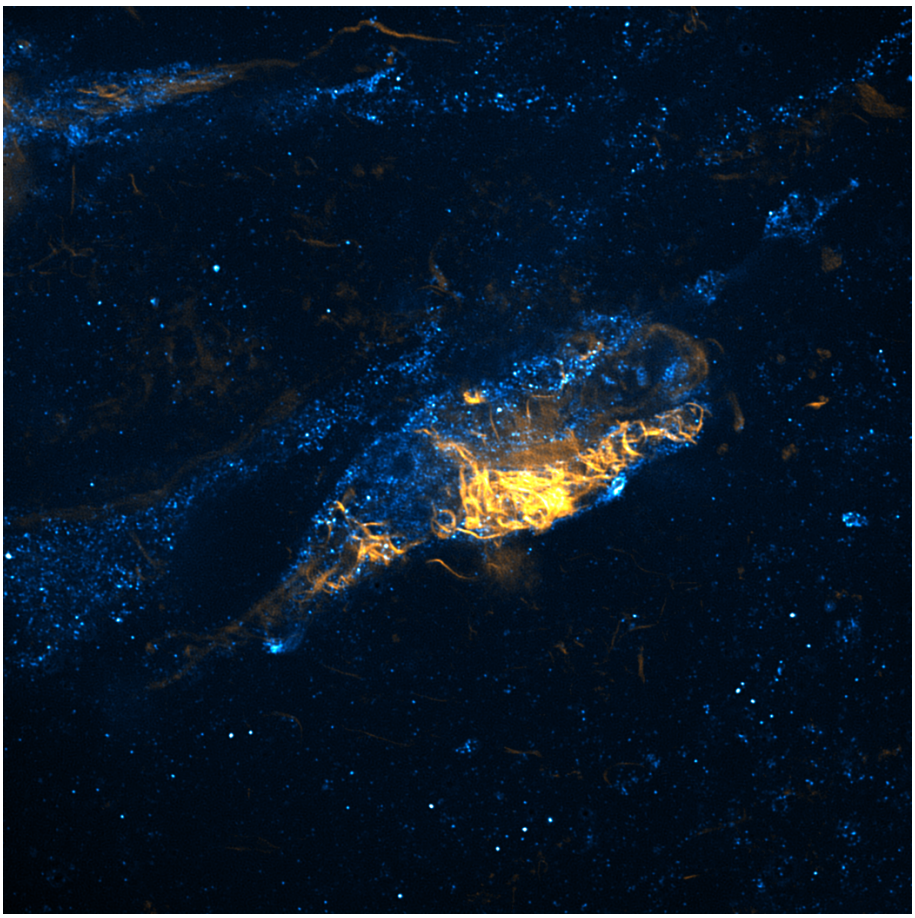

Contents

I Abstract

Microglia are the resident immune cells of the brain and play an important role in regulating brain function in health and disease. They are organized in a brain-wide network, with each cell having its own territory. It is generally recognized that microglia are long-lived cells, and individual cortical microglia can survive for a lifetime in a laboratory mouse. How the microglial network is maintained and how aging and disease affect the homeostasis of the network is not yet fully understood.

To investigate the homeostasis of the microglial network, I pursued two approaches. First, I describe my efforts to develop a new mouse model to study the response of the microglial network after ablation of individual microglia *in vivo*. The mouse model co-expresses the diphtheria toxin receptor (iDTR) and tdTomato dependent on Cre-recombination in a small percentage of microglial cells, rendering tdTomato-positive microglia susceptible to diphtheria toxin-induced cell death. Unfortunately, Cre-recombination of tdTomato and iDTR rarely, if ever, occurred in the same cell. Most likely, differences in length between the two loxP sites flanking the STOP cassette hampered success of this *in vivo* approach.

In the second part of the thesis, I describe the subsequent development of a novel hippocampal slice culture model as a simplified *in vitro* model to study microglia network homeostasis. In this model, the endogenous murine microglia were replaced by human induced pluripotent stem cells (iPSC)-derived microglia (iMics), facilitating the discovery of human microglial network changes. iMics in these chimeric hippocampal slice cultures differentiated and matured into microglia with a highly ramified morphology, transcriptional profile and network organization reminiscent of human microglia. In response to lipopolysaccharide stimulation or focal laser injury, iMics secrete pro-inflammatory cytokines or shield the injury site with their processes, respectively. Surprisingly, human colony-stimulating factor 1 (CSF1) was not required for iMic differentiation and survival in these chimeric hippocampal slice cultures, which contrasts with existing xenotransplantation models that express human CSF1. The observation that loss-of-function CSF1 receptor mutations diminish the integration of iMics into mouse brain slices suggests that cross-species ligand-receptor interactions of mouse CSF1 or interleukin 34 are sufficient for the differentiation and survival of iMics in the mouse brain slices.

To investigate how proteopathic lesions affect the homeostasis of this microglial network, chimeric slice cultures were combined with a recently developed α-synucleinopathy hippocampal slice culture seeding model. Similar to what has been observed in mouse models of α-synucleinopathy, also iMics in chimeric slice cultures develop α-synuclein inclusions that accumulate over time and show a transcriptional response associated with neurodegeneration such as upregulation of the inflammatory response and increased phagocytosis.

While the investigation of *in vivo* microglial network homeostasis will require further adjustments of the mouse model for targeted ablation of individual microglia, the here developed chimeric slice cultures provide an easily accessible and scalable platform for *in vitro* study of human microglia under both homeostatic as well as diseased conditions.

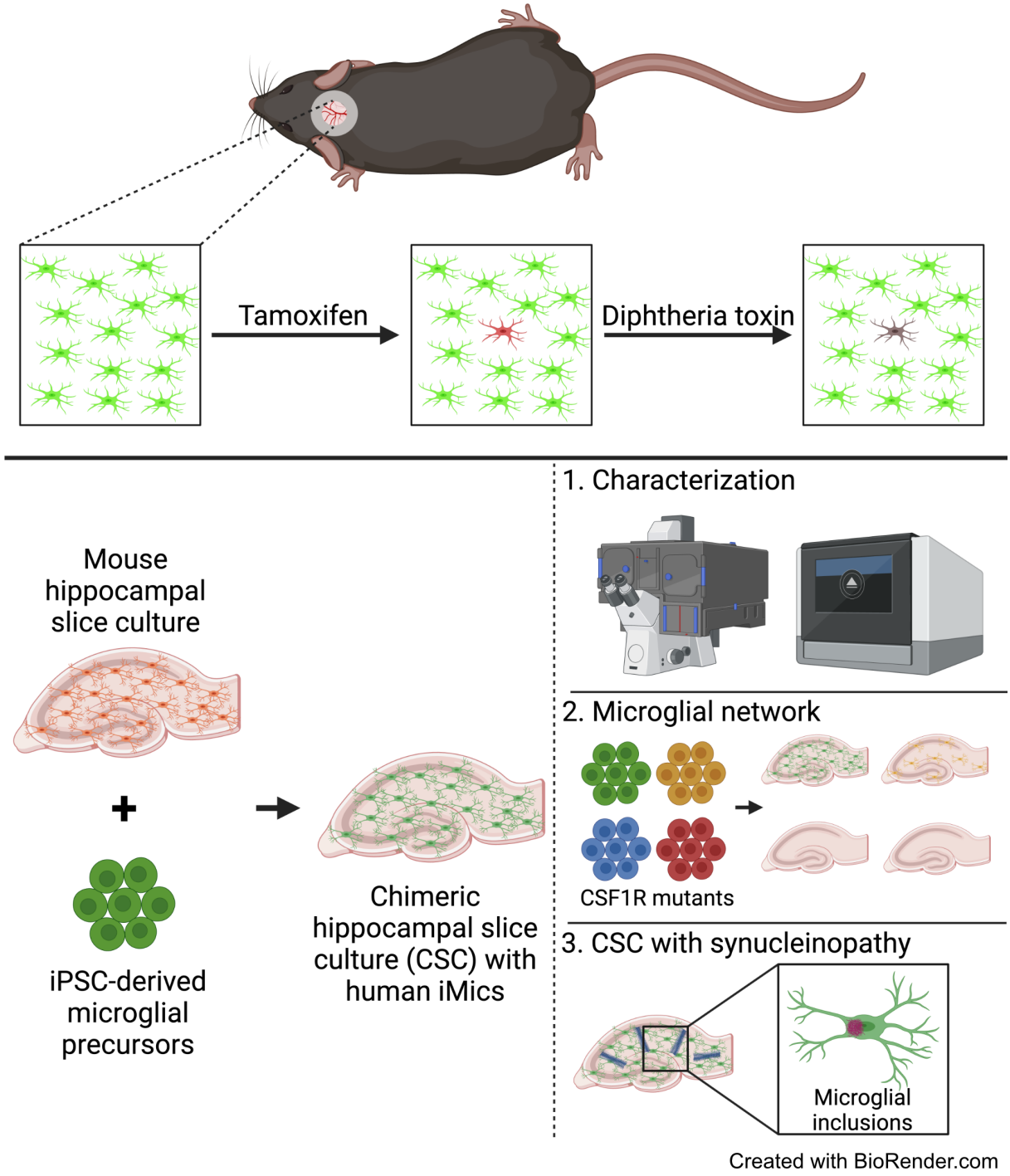

Figure 1.1 Graphical abstract
This work consisted of two main parts. First, *in vivo* experiments to study the homeostasis of the microglia network by targeted cell death of individual microglia (top). Second, the development of chimeric slice cultures using human iMics, including their characterization, studies of the microglia network in response to altered CSF1R signaling, and validation of CSC as a model for neurodegenerative diseases (bottom).

II Introduction

1 Microglia

Although microglia were described by Río-Hortega as early as 1919, they were overlooked in neuroscientific research for a long time (Sierra, Paolicelli, and Kettenmann 2019). It was not until the early 2000s that research on microglia gained popularity and has since grown exponentially (Paolicelli et al. 2022). Microglia are the primary immune cells of the brain. They are derived from primitive macrophages in the yolk sac and invade the human brain between 4.5 and 5.5 weeks of gestation, before the blood-brain barrier closes (Andjelkovic et al. 1998). In mice, this invasion occurs around embryonic day 8.5 (Ginhoux et al. 2010; Schulz et al. 2012; Stremmel et al. 2018). After this initial invasion of the brain, microglia are able to maintain their population through self-renewal (Ajami et al. 2007; Askew et al. 2017; Füger et al. 2017; Réu et al. 2017).

1.1 Microglia in health

1.1.1 Microglial functions in the brain

In the brain, microglia fulfill various functions both during development and in adulthood, including roles in maintaining homeostasis as well as responding to disease conditions (Figure 2.1). Most importantly, they surveil the brain with their motile processes in order to detect and phagocytose debris, dead or dying cells but also pathological insults such as microbes or protein aggregates (Davalos et al. 2005; Nimmerjahn, Kirchhoff, and Helmchen 2005). With their variety of surface receptors, microglia sense their environment to detect pathogen-associated molecular patterns of microbes and ‘eat-me’ signals of neurons, such as phosphatidylserine which is only present on the outside of the cell membrane under stress or apoptosis (Brown and Neher 2014). In response to immunological stimulation, microglia do not only clear unwanted material but also secrete pro- or anti-inflammatory cytokines to mediate the inflammatory reaction of the surrounding tissue (Borst, Dumas, and Prinz 2021; Colonna and Butovsky 2017; Liddelow et al. 2017). Additionally, microglia present antigens to peripheral immune cells invading the brain during inflammatory processes and react to inflammatory cytokines released in the periphery or by invading cells of the immune system, such as T-cells (Abdel-Haq et al. 2019; Franco and Fernández-Suárez 2015; Goddery et al. 2021; Moseman et al. 2020; Qin et al. 2008; Riazi et al. 2008). Microglia perform their immunological functions as part of the innate immune system. Moreover, recent publications described that microglia also show adaptive behavior in response to inflammatory stimuli and form an innate immune memory. Pro-inflammatory stimuli

early in life were shown to modulate the response of microglia in a mouse model of neurodegeneration through epigenetic modifications (Wendeln et al. 2018).

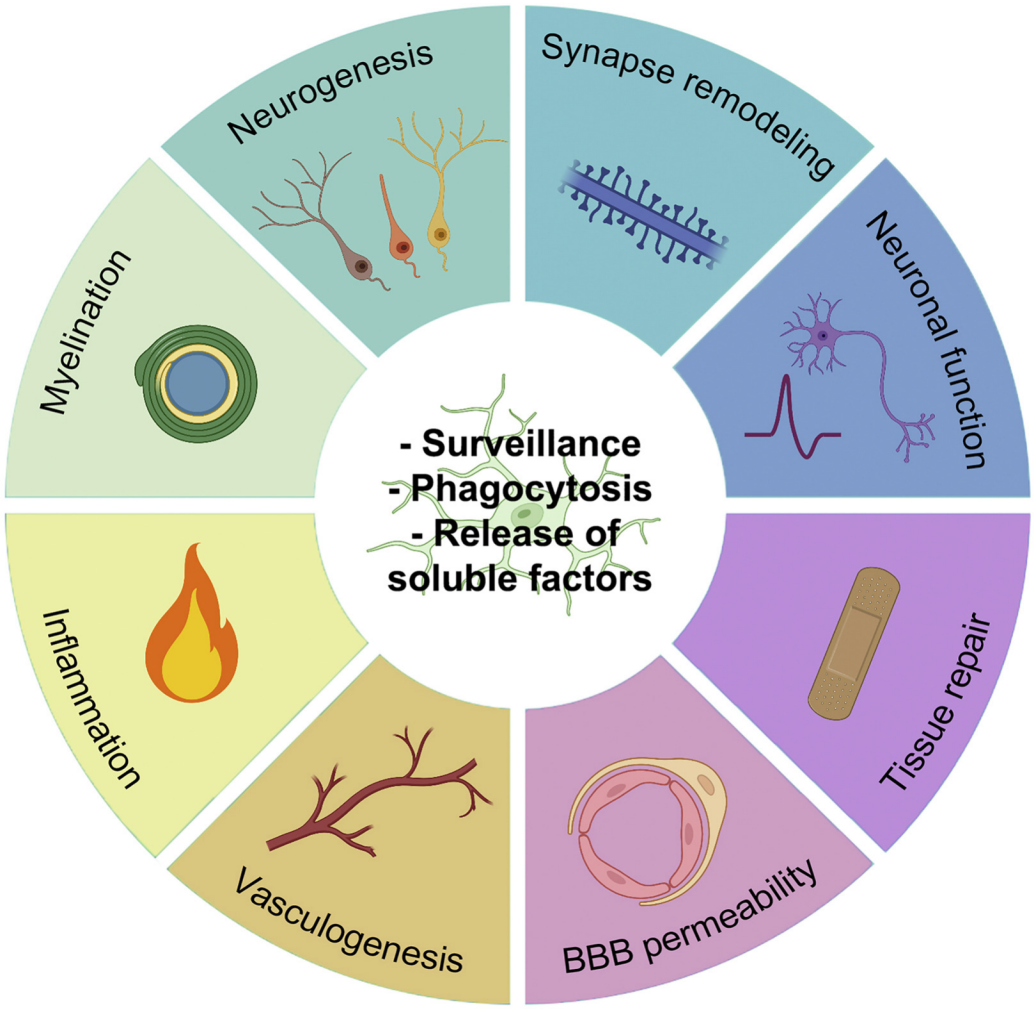

Figure 2.1 Microglia functions in health
Microglia have various functions in the healthy and diseased brain. From Paolicelli et al. 2022 with permission from Neuron - Cell Press

Besides their immunological function, microglia have several other tasks in the healthy brain, which they perform in coordination with other cell types in the central nervous system. For example, microglia are able to detect neuronal activity through expression of neurotransmitter receptors. Subsequently, they modulate neuronal activity by remodeling synapses through engulfing and phagocytosing synapses, but also by supporting the development of new synapses (Badimon et al. 2020; Eyo, Bispo, et al. 2018). The detection of neuronal activity prompts microglia to release neurotrophic factors such as brain derived neurotrophic factor (BDNF) or neurotoxic factors such as tumor necrosis factor α (TNFα) in order to modulate the neuronal network and synaptic plasticity (Parkhurst et al. 2013; Taylor et al. 2005). Vice versa, neuronal activity modulates microglial process dynamics (Cserép et al. 2020). While increased neuronal activity reduces microglial process movement and surveillance of their microenvironment, decreased neuronal activity such as during sleep or

anesthesia increases microglial process dynamics (Y. U. Liu et al. 2019). The modulation of neuronal activity as well as the phagocytosis of debris and apoptotic cells by microglia happens in a highly coordinated cooperation with astrocytes, another type of glia in the brain (Damisah et al. 2020; Vainchtein et al. 2018). Apart from this, astrocytes provide trophic support for microglia via Colony-stimulating factor 1 (CSF1) and Transforming Growth Factor β (TGFβ), while microglia modulate the inflammatory response of astrocytes to tissue injury (Baxter et al. 2021; Easley-Neal et al. 2019). Moreover, microglia regulate the permeability of the blood-brain barrier. Depending on the cytokines they are releasing, microglia can either increase or decrease the permeability of the blood-brain barrier. Upon secretion of pro-inflammatory cytokines such as interleukin 1β (IL1β) or interleukin 6 (IL6), the blood-brain barrier becomes leakier while the secretion of anti-inflammatory cytokines like interleukin 10 (IL10), Vascular Endothelial Growth Factor (VEGF), or TGFβ increases the tightness of the barrier (Ronaldson and Davis 2020). The secretion of VEGF also promotes angiogenesis in the brain which is especially important during the tissue repair process (Fantin et al. 2010).

This plethora of functions is also reflected in transcriptomics analyses of microglia. Interestingly, a couple of years ago, microglia were only considered to exist in three different states, as resting, homeostatic microglia, as pro-inflammatory M1-microglia or as anti-inflammatory M2-microglia, similar to what was known for peripheral and other tissue-resident macrophages (Paolicelli et al. 2022; Ransohoff 2016). However, the application of advanced single-cell RNA sequencing (scRNAseq) techniques in the field of microglia research showed that this view of only three substates was too simplified. In fact, a broad range of subclusters of microglia have been identified through scRNAseq of healthy, aging and diseased brains (Hammond et al. 2019; Sun et al. 2023). All of these subclusters of microglia are characterized by a specific subset of key genes that hint at their functional role in the brain. Microglia subclusters in the brain consist, amongst others, of proliferative, phagocytic, antigen-presenting, disease-associated and interferon response microglia (Galatro et al. 2017; Keren-Shaul et al. 2017; Olah et al. 2020; Sala Frigerio et al. 2019). The relative frequency of these microglia subsets is constantly changing in response to the developmental state of the brain or other environmental factors (Hammond et al. 2019). Additionally, microglia are not locked in one of these states but are rather dynamically changing. For example, when isolated from the brain, microglia rapidly lose their homeostatic profile and change into an ‘activated’, pro-inflammatory state. However, when put back into a brain environment, they quickly change back into their previous homeostatic state (Bennett et al. 2018; Gosselin et al. 2017).

The use of RNA sequencing technologies in microglia research has not only unraveled the dynamics of microglia states but also showed that there are drastic sex differences in microglia which changes the type of reaction to pathological insults or injury. Male microglia for example, have a higher immune activation in homeostatic conditions which in turn could be a modifier of disease risk for neurological

diseases. Female microglia in homeostatic conditions, however, have a neuroprotective phenotype which is even retained after being transferred into male brains (Guneykaya et al. 2018; Lynch 2022; Villa et al. 2018; Xu et al. 2023).

1.1.2 The role of microglia during development

Apart from their functions in adult brains, microglia are very important players in brain development. They are the first glia cell type present in the developing brain and play a major role in the maturation of the neuronal network (Colonna and Butovsky 2017). On the one hand, microglia secrete neurotrophic factors in order to promote neurogenesis and synaptogenesis while on the other hand they are also responsible for the limitation of axon outgrowth and pruning of excessive synapses (Schafer et al. 2012; Ueno et al. 2013). In addition to that, microglia induce programmed cell death of excessive neurons (Frade and Barde 1998; Sierra et al. 2010). The importance of microglial-induced neuronal cell death and synaptic pruning are exemplified by diseases caused by mutations in important microglial genes. Autosomal recessive mutations in Triggering receptor expressed on myeloid cells 2 (TREM2) or TYRO protein tyrosine kinase-binding protein (TYROBP), an adaptor protein of the TREM2 receptor, cause Nasu-Hakola disease, a disease characterized by psychotic symptoms, neurodegeneration and encephalopathy (Paloneva et al. 2002). Deficiencies in the fractalkine receptor CX3C motif chemokine receptor 1 (CX3CR1), a receptor important during synaptic pruning, lead to a transient increase in the number of dendritic spines and immature synapses in mouse models. In adulthood, these mice show autism-like behavior due to the lack of synaptic pruning (Paolicelli et al. 2011; Rogers et al. 2011; Zhan et al. 2014). Synaptic pruning is also affected by mutations in one of the three complement genes C1q, C3 or CR3 which then leads to a reduction of the segregation of eye-specific synaptic fields (Schafer et al. 2012). Additionally, it is hypothesized that microglia could play a role in neurodevelopmental disorders such as autism and schizophrenia in humans that show altered synaptic densities and might be caused by altered synapse elimination by microglia (Prinz, Jung, and Priller 2019).

Apart from their support and regulation of neuronal network maturation, microglia also directly interact with other types of glia and blood vessels during development. Microglia deliver trophic support for the generation and survival of oligodendrocytes during development, as well as for the formation of myelin by the secretion of Insulin-like growth factor 1 (IGF1) (Hagemeyer et al. 2017; Nemes-Baran, White, and DeSilva 2020; Wlodarczyk et al. 2017). However, this proposed microglial function has recently been questioned by a report of mice lacking microglia with normal oligodendrocyte maturation and myelination during development (McNamara et al. 2023). Lastly, microglia also regulate the vascularization of the developing brain by bridging endothelial tip cells (Fantin et al. 2010).

1.1.3 Microglia in healthy ageing

Since microglia function is largely influenced by the environment, the ageing brain is expected to have a major impact on microglia. In the ageing brain, microglia are exposed to various challenges such as dying and senescent neurons or other cell types and the accumulation of proteins and lipids (Borst et al. 2021; Marschallinger et al. 2020). Phenotypically, microglia undergo morphological changes and become dystrophic (Damani et al. 2011; Hefendehl et al. 2014; Streit et al. 2004). The soma size increases and microglia in the ageing brain become less ramified with fewer processes which in turn impairs their ability to surveil their microenvironment (Damani et al. 2011; Hefendehl et al. 2014). On a functional level, the ageing process leads to transcriptional changes of microglia. Expression of homeostatic genes, such as P2RY12, is downregulated and microglia adapt more activated, responsive substates (Galatro et al. 2017; Olah et al. 2018, 2020; Xu et al. 2023). Moreover, the reduction of homeostatic functions of microglia is also shown by a downregulation of TGFβ-expression, an important gene involved in the homeostatic functionality of microglia (Olah et al. 2018). The reduced expression of genes involved in cell adhesion, axonal guidance and receptors sensing the microglial environment shows reduced ability of microglia to perform their homeostatic functions (Galatro et al. 2017). Additionally, these changes also lead to reduced process motility of microglia and an impaired response to injuries of the brain, as shown by a slowed-down reaction of microglia to a laser lesion in aged mouse brains (Damani et al. 2011; Hefendehl et al. 2014). The reduced homeostatic functionality of microglia furthermore leads to a loss of their homogenous network distribution. As a consequence, aged microglia more often occur in clusters in which several microglia cluster together, while leaving other areas of the brain rather unoccupied (Hefendehl et al. 2014).

Conversely, microglia upregulate processes in ageing that are associated with their response to pathogens. Ageing microglia increase the expression of genes involved in antigen presentation, innate immune functions like interferon response, phagocytosis and reactive oxygen species (ROS) production (Olah et al. 2018, 2020; Xu et al. 2023). Moreover, transcriptomics analyses show altered lipid and iron metabolism as well as protein-degradation. Notably, two major subclasses of microglia emerge in the ageing mouse brain. Firstly, a subcluster called interferon-response microglia (IRM) is characterized by the upregulation of genes involved in the innate immune response and interferon response type I pathways (Ifit2, Ifit3, Ifitm3, Irf7, and Oasl2) and usually associated with a reaction to viral infections. Importantly, IRMs are also detectable in aged human brains (Olah et al. 2018; Sala Frigerio et al. 2019). Secondly, another subcluster called activated response microglia (ARM) emerges in ageing. This subcluster is characterized by upregulation of genes involved in inflammatory processes (Cst7, Clec7A, Itgax), antigen presentation via MHC II (CD74, Ctsb, Ctsd) and tissue regeneration (SPP1). Interestingly, many of these upregulated genes are known genetic risk factors of neurodegenerative

diseases such as Alzheimer's disease and multiple sclerosis (APOE, CD33, MS4A4A, TREM2). These genes are also highly upregulated in those diseases, indicating a connection between the regulation of this subcluster and the development of neurodegenerative diseases (also see section II.1.2.2) (Olah et al. 2018; Sala Frigerio et al. 2019). Furthermore, it has been described that another subpopulation of ageing microglia accumulates lipids and becomes dysfunctional with a decreased ability to phagocytose and an increased production of ROS and pro-inflammatory cytokines (Figure 2.2) (Marschallinger et al. 2020). The enrichment of these preactivated subclusters in ageing, however, is not only relevant for neurodegenerative diseases but also changes the reaction of microglia in response to other pathological insults such as LPS. Although there are conflicting reports on the exact changes in the microglial reaction to LPS with ageing, they agree on the fact, that aged microglia are not able to cope with peripheral inflammation as well as young microglia, leading to increased vulnerability of the brain (Norden, Muccigrosso, and Godbout 2015; Xu et al. 2023).

To summarize, aged microglia present an inflammatory, neurodegeneration-like phenotype with a complex change of their profile that is largely influenced by the aged environment of the brain (Keren-Shaul et al. 2017; Xu et al. 2023). However, ageing microglia are not only influenced by the ageing brain but also in return accelerate neurological decline. A recent study showed that aged microglia in a young brain environment are sufficient to trigger cognitive decline. In these mice, the reduced support with myelination by ageing microglia triggered deficits in learning and memory functions (Xu et al. 2023).

1.2 Microglia in disease

1.2.1 Neurodegenerative diseases

Neurodegenerative diseases are characterized by their progressive nature that leads to cognitive decline and ultimately a premature death of the patients (Brettschneider et al. 2015). They are mostly age-associated and are therefore a major challenge to health-care systems worldwide due to increased life expectancy and the ageing population, especially in industrialized countries (Fu, Hardy, and Duff 2018; Prusiner 2013). Alzheimer's disease (AD) is the most common neurodegenerative disease. Until 2050 it is expected that the annual number of new cases of AD will double. All cases of AD and other dementias are projected to accumulate costs of just under $1 trillion per year, in the United States alone (Alzheimer's Association Report 2023). Many of the most common neurodegenerative diseases are associated with a typical, disease-specific accumulation of proteins (Dawson, Golde, and Lagier-Tourenne 2018; Jucker and Walker 2018). AD is characterized by the extracellular accumulation of amyloid-β (Aβ) in amyloid plaques and intracellular accumulation of tau in neurofibrillary tangles (Glenner and Wong 1984; Grundke-Iqbal et al. 1986; Kosik, Joachim, and Selkoe 1986; Wood et al. 1986). In Parkinson's disease (PD), however, a protein called α-synuclein (αsyn) accumulates in Lewy

bodies (LB) and Lewy neurites (LN) which will be discussed in more detail later (Spillantini et al. 1997). Other common neurodegenerative diseases such as amyotrophic lateral sclerosis (ALS) (with accumulations of SOD1, TDP-43, FUS and C9ORF72 dipeptide repeat proteins), frontotemporal lobar dementia (FTLD) (TDP-43, FUS, C9ORF72 dipeptide repeat proteins and tau), Creutzfeldt-Jacob Disease (Prion protein) and Huntington's disease (huntingtin) are also characterized by a pathological accumulation of proteins (Prusiner 2013). In these neurodegenerative diseases, proteins not only accumulate but are also spreading across the brain in a prion-like fashion. In 1982, Stanley Prusiner first described prion protein as 'proteinaceous infectious particles' occurring in scrapie, a neurodegenerative condition in sheep, but nowadays prion-like processes are also accepted for proteinaceous aggregates in other human neurodegenerative diseases (Prusiner 1982, 2013). First, a native protein misfolds and then recruits more native proteins to misfold which leads to a subsequent aggregation of misfolded proteins into insoluble, degradation-resistant amyloid fibrils. This process exponentially accelerates and rapidly spreads the misfolded, aggregating proteins across the brain. The initial misfolded protein or protein aggregate is termed 'seed' and causes neurodegenerative pathological processes by either a gain of toxic functions or a loss of physiological function (Jucker and Walker 2018; Prusiner 2012).

Despite research on neurodegenerative diseases for over a century, many of the disease processes are still not entirely understood so that therapeutical options are currently limited and are mostly focused on symptomatic treatment while causative treatments remain scarce. In AD for example, current treatment options mostly entail the management of neurotransmitter deficits or the excess of neuronal stimulation that cannot stop the progressive degeneration of the brain (Alzheimer's Association Report 2023). Only recently, however, the first treatments tackling amyloid as a potential cause of AD have been approved by the United States Food and Drug Administration (Alzheimer's Association Report 2023). These treatments are all antibodies directed against Aβ in order to stop the progression of the disease which leads to a drastic reduction of amyloid plaques and a minor slow-down of cognitive decline (Alzheimer's Association Report 2023; Jucker and Walker 2023). Nevertheless, disease processes in neurodegenerative diseases need to be understood in more depth to develop more causative treatments that not only stop the progression of the diseases but are ideally also able to restore cognitive function or even prevent their development if biomarkers become available to 'screen' patients before disease-onset.

1.2.2 Microglia in neurodegenerative diseases and other diseases of the brain

When Alois Alzheimer first described AD, he mentioned glial cells with 'adipose saccules' (Alzheimer et al. 1995). Today, we know that Alzheimer most likely observed the accumulation of lipid droplets in glial cells. Nevertheless, AD research has primarily focused on neuronal deficits until the end of the

last century. Genome-wide association studies (GWAS) for AD revealed that many of the risk genes for AD are highly or exclusively expressed in microglia which turned the focus of AD research more towards the involvement of glial cells (Andrews, Fulton-Howard, and Goate 2020; Efthymiou and Goate 2017; Hollingworth et al. 2011; de Rojas et al. 2021; Sims et al. 2017). In line with this, scRNAseq studies of microglia in human AD and mouse models of AD revealed an upregulation of these GWAS hits in microglia, highlighting their important role in AD (Keren-Shaul et al. 2017; Olah et al. 2020; Sala Frigerio et al. 2019).

Already early in the disease, microglia are recruited to amyloid plaques where they phagocytose Aβ and clear plaques (Hickman, Allison, and Khoury 2008). Moreover, microglia provide a physical barrier against plaque expansion and by the secretion of APOE, microglia help with compaction of plaques (Parhizkar et al. 2019; Yuan et al. 2016). However, this initially beneficial role of microglia in AD leads to detrimental effects in later stages of the disease. The sustained activation of microglia by plaques leads to a dysfunctional microglial phenotype with decreased phagocytic activity and an increased release of pro-inflammatory cytokines such as IL1β and TNFα that have a neurotoxic effect on the surrounding environment (Hickman et al. 2008). Furthermore, microglia phagocytose neurons presenting 'eat-me' signals as a response to AD pathology. Conversely, this suppresses microglial homeostatic functions such as neuronal surveillance (Sun et al. 2023; Wang and Colonna 2019). The multifaceted role of microglia in AD is also highlighted by publications that involve microglia in the spreading of AD pathology to other brain regions and the amplification of amyloid plaques (Joshi et al. 2014; Venegas et al. 2017). In the white matter, microglia often appear filled with lipid droplets, the 'adipose saccules' Alois Alzheimer already described in 1907 (Alzheimer et al. 1995; Hou et al. 2022). These lipid droplets are derived from phagocytosed myelin debris of dying neurons. Similar to the lipid droplet accumulating microglia that occur with ageing, lipid droplet accumulating microglia in AD are dysfunctional microglia with a reduced phagocytic ability and increased production of reactive oxygen species and pro-inflammatory cytokines (Hou et al. 2022; Marschallinger et al. 2020).

In 2017 Keren-Shaul et al. identified disease associated microglia (DAM), a microglial cluster which is only present in a mouse model of AD. This microglial cluster is amongst others characterized by an upregulation of APOE and TREM2, two of the strongest risk factors for sporadic AD. Generally, DAM show an upregulation of genes involved in phagocytosis, lipid metabolism, inflammation and proliferation and a down-regulation of homeostatic markers (Figure 2.2) (Keren-Shaul et al. 2017). These gene expression changes are in line with the previously observed functional changes of microglia described above. APOE and TREM2 have been described to regulate microglial activation in the context of amyloid plaques but also in the context of ageing and other neurodegenerative diseases. For example, the ARM cluster of microglia, which is enriched in healthy ageing but especially in the context of AD, is dependent on APOE (Sala Frigerio et al. 2019). Vice versa, human transcriptomic analyses

suggest that protective mutations of APOE decrease expression of AD risk genes, potentially explaining a reduced disease risk, at least partially (Olah et al. 2018). In comparison to mice, human transcriptomic analyses showed that the DAM cluster does not occur as such in humans but that the gene expression changes are rather distributed over several different clusters, highlighting differences in the microglial reaction to AD between mouse and human and the urge to interpret results from mouse models with caution when translating them to humans (Sun et al. 2023). Apart from this, AD pathology also leads to an increased antigen-presentation by microglia via MHC class II and recruitment of immune cells from the periphery into the brain (Chen et al. 2023; Olah et al. 2020; Sala Frigerio et al. 2019). Interestingly, microglia have not only been described to be involved in Aβ pathology in AD, but also seem to drive tau pathology. The loss of the NLPR3 inflammasome in microglia led to decreased development of hyperphosphorylated tau and reduced accumulation of tau downstream of Aβ pathology in mouse models (Ising et al. 2019).

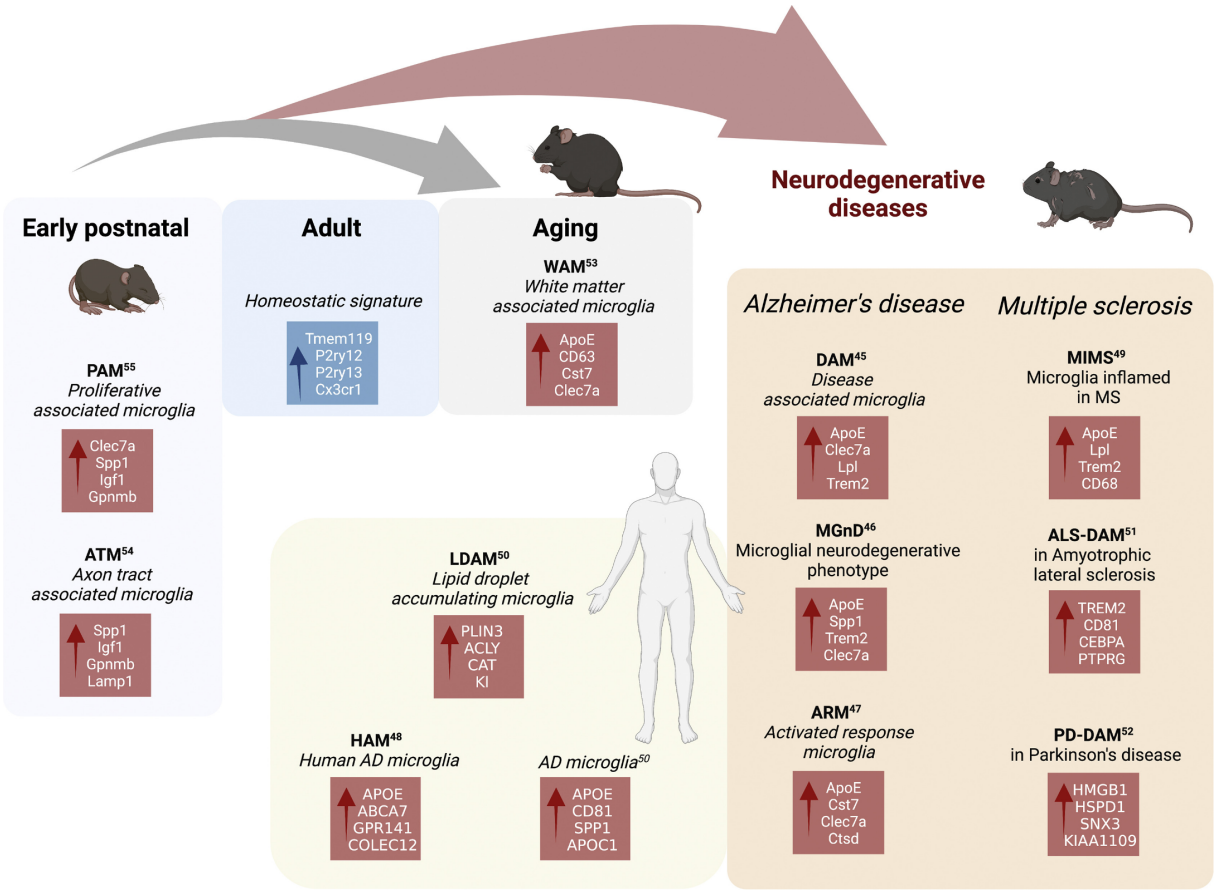

Figure 2.2 Microglial transcriptomic phenotypes in ageing and neurodegeneration
Depending on their environment (Age or disease), microglia adapt a plethora of transcriptomic phenotypes that influence cell function. These phenotypes are characterized by upregulation of context-dependent genes. From Paolicelli et al. 2022 with permission from Neuron - Cell Press

Similar to AD, microglia play an important role in the development and modulation of other neurodegenerative diseases. In 2017, Krasemann et al. compared microglial transcriptomics in mouse

models of different neurodegenerative diseases (ALS, AD and MS) and found that a microglial phenotype with decreased expression of homeostatic genes such as P2RY12 and CX3CR1 and an increased expression of genes such as APOE was common across diseases. They called this microglial phenotype microglial neurodegenerative phenotype MGnD (Figure 2.2) (Krasemann et al. 2017). In MS, microglia are involved in the formation of lesions where they strongly proliferate (Distéfano-Gagné et al. 2023; Kuhlmann et al. 2017). At the lesion sites, microglia appear foamy due to the lipids they are accumulating (Absinta et al. 2021). Additionally, microglia are at least partially involved in myelin damage, since microglia depletion is neuroprotective in mouse models of MS (Beckmann et al. 2018; Marzan et al. 2021; Nissen et al. 2018). Proposed mechanisms of microglial neurotoxicity in MS are the release of pro-inflammatory cytokines, activation of astrocytes into a neurotoxic phenotype by microglia and antigen-presentation to peripheral immune cells (Absinta et al. 2021; Healy et al. 2022; Liddelow et al. 2017). Conversely, microglia in MS are also involved in the process of remyelination (Patani et al. 2007).

Apart from neurodegeneration, microglia also seem to play an important role in neurodevelopmental disorders such as autism spectrum disorder. It has been suggested that a disbalance of synaptic pruning and modulation of neuronal circuits by microglia could be the cause for these diseases (Filipello et al. 2018; Petrelli, Pucci, and Bezzi 2016; Zhan et al. 2014).

Lastly, microglia also have a major influence on the outcome of stroke. Due to the lack of oxygen, neurons in areas with strong ischemia die and cause excitotoxicity. In these areas, microglia clear harmful debris. However, microglia can also have detrimental effects in stroke when neurons in the peri-infarct areas with milder ischemia and less oxygen deprival reversibly expose ‘eat-me’ signals to microglia which subsequently unnecessarily phagocytose these neurons (Brown and Neher 2014; Mari et al. 2004). Additionally, microglia shield damaged vessels in order to limit the bleeding into the brain parenchyma and later adapt a repair-associated microglial phenotype that promotes angiogenesis via VEGF (Mastorakos et al. 2021).

1.2.3 Synucleinopathies

Synucleinopathies are a group of neurodegenerative diseases characterized by the presence and prion-like spreading of αsyn inclusions in the brain. They mainly included PD, Dementia with Lewy Bodies (DLB) and Multiple System Atrophy (MSA) (Goedert, Jakes, and Spillantini 2017).

PD is a movement disorder with patients suffering from rest tremor, bradykinesia, muscular rigidity and a loss of postural reflexes but also non-motor symptoms such as constipation, anosmia and sleep disorders (Lang and Lozano 1998; Sveinbjornsdottir 2016). The cause of the motor symptoms is the degeneration of dopaminergic neurons in the substantia nigra pars compacta (Mhyre et al. 2012).

Histologically, PD is characterized by the accumulation of αsyn in so-called Lewy bodies in neuronal somas and Lewy neurites in neuronal processes (Spillantini et al. 1997). Within synuclein lesions it has been shown that αsyn is commonly phosphorylated at serine 129 (pS129), which might lead to increased accumulation of αsyn (Fujiwara et al. 2002). Due to its strong association with synuclein lesions, pS129 is frequently used as a marker for pathological synuclein lesions.

Similarly to PD, patients with DLB show Lewy pathology and suffer from parkinsonism, but additionally show cognitive symptoms and behavioral changes such as hallucinations (Outeiro et al. 2019).

Conversely, MSA is the most severe synucleinopathy with autonomic, cerebellar and cognitive symptoms in addition to parkinsonism (Ubhi, Low, and Masliah 2011). Histological hallmarks of MSA are the occurrence of αsyn inclusions in oligodendrocytes, so-called glial cytoplasmic inclusions as well as αsyn inclusions occurring in neurons (Spillantini et al. 1998; Spillantini and Goedert 2018).

As described earlier, a hallmark of PD and other synucleinopathies is the prion-like spreading of misfolded, aggregating protein, in this case αsyn (Goedert 2015). In PD, Braak and et al. staged this progression into several stages that showed the occurrence and spreading of Lewy pathology along axonally connected regions beginning in the peripheral nervous system of the gut and the olfactory bulb, to the brain stem and via the midbrain including the substantia nigra to the cortex (Braak et al. 2003). The prion-like spreading of αsyn pathology was also shown by two independent groups that implanted healthy embryonic tissue into the brain of PD patients in order to increase the availability of dopamine in the midbrain and found Lewy pathology in the engrafted tissue more than ten years after transplantation (Kordower et al. 2008; Li et al. 2008).

An important finding in PD research was the discovery of a missense mutation in αsyn that causes a familial form of PD. This mutation, Ala53Thr (A53T), facilitates aggregation of αsyn, initiating the cascade described above (Choi et al. 2004; Polymeropoulos et al. 1997; Serpell et al. 2000). Apart from mutations of αsyn, mutations in mitochondrial, lysosomal and autophagosomal pathways have been discovered in sporadic cases of PD that increase the risk of the disease (Billingsley et al. 2018; Hardy 2010; Zimprich et al. 2004).

1.2.4 Microglia in synucleinopathies

Similar to the already described role of microglia in AD and other neurological diseases, microglia also play an important role in PD and other synucleinopathies. This is highlighted by PD risk genes that are highly expressed in microglia such as LRRK2 and GBA (Feng et al. 2023; Zhang et al. 2016). Interestingly, mutations in the AD risk gene TREM2 have also been described to increase the risk for PD (Liu et al. 2016). However, the role of microglia in synucleinopathies has not yet been studied as extensively as for AD and it is therefore less clear if microglia can be causative for PD. Nevertheless, it is clear that

microglia have beneficial and detrimental roles in PD and other synucleinopathies. In synucleinopathies, microglia phagocytose both neuronal debris and extracellular αsyn in various forms: monomeric, oligomeric and fibrillar αsyn. The recognition and phagocytosis of αsyn is thought to be mediated mainly by Toll-like receptors and subsequently leads to pro- or anti-inflammatory cytokine secretion. While the phagocytosis of monomeric αsyn has been reported to also stimulate the beneficial secretion of anti-inflammatory cytokines, oligomeric and fibrillar αsyn species elicit the release of pro-inflammatory cytokines such as Il1β and TNFα and reactive oxygen species (Fellner et al. 2013; Feng et al. 2019; Hughes et al. 2019; Joers et al. 2017; Li et al. 2020). It has also been described that a pro-inflammatory environment can enhance αsyn aggregation leading to a vicious cycle of αsyn aggregation and the release of pro-inflammatory cytokines (Gordon et al. 2018).

The permanent stimulation of microglia with neuronal debris and extracellular αsyn additionally leads to sustained microgliosis which is characterized by microglial proliferation and activation. Morphologically, activated microglia in the proximity of synuclein lesions lose their highly ramified appearance and become more amoeboid cells with decreased branching of microglial processes (Joers et al. 2017).

Upon phagocytosis, αsyn is subjected to degradation via the autophagic-lysosomal pathway. This process of αsyn degradation is a crucial function of microglia in synucleinopathies. A microglia-specific knockout of autophagy in a mouse model of PD led to an increased death of dopaminergic neurons (Choi et al. 2020). Additionally, some PD risk genes play an important role in this pathway. LRRK2 has among others been linked to microglial phagocytosis and the assembly of autophagolysosomes (Feng et al. 2023; Li, Tan, and Yu 2014). On the other hand, GBA is a lysosomal enzyme responsible for the degradation of glucosylceramide. Moreover, a recent publication from my laboratory showed that microglial αsyn inclusions in mouse models of PD can be stained with amyloid binding dyes such as Luminescent Conjugated Oligothiophenes (LCOs). Although we were not able to determine the source of these inclusions, it is likely that they are derived from phagocytosed material and could potentially be amplified within microglia. However, it is not clear if these inclusions are an artifact of overexpression of αsyn in these models or also occur in human synucleinopathies (Tanriöver et al. 2020).

An additional important function of microglia in PD is the presentation of antigens to T-cells via MHCII which leads to the recruitment of peripheral T-cells and to both pro- and anti-inflammatory effects in the environment (Gate et al. 2021; Olesen et al. 2018; Thomsen et al. 2021).

Furthermore, microglia are implicated in the spreading of αsyn, although evidence is currently scarce. So far, only a few labs have reported that microglia are able to spread and seed αsyn lesions via the release of αsyn-containing exosomes using cell culture models of immortalized or primary mouse

microglia (Guo et al. 2020; Xia et al. 2019). Exosomal release and uptake of αsyn has also been suggested as one possible mechanism of neuron-to-neuron spreading of αsyn and has been shown to be enhanced when autophagic activity is decreased, possibly a mechanism of cells to cope with the increased burden of misfolded protein (Danzer et al. 2012; Grozdanov and Danzer 2018). Only recently, however, direct transfer of αsyn between microglia via nanotubes has been described as another mechanism of cell-to-cell transfer between microglia. In this study, the authors showed that microglia carrying a high burden of αsyn, transfer αsyn to other microglia with a lower αsyn burden via tunneling nanotubes in order to jointly degrade the aggregated protein (Scheiblich et al. 2021). However, the translational relevance of these processes for disease progression is so far not clear.

1.3 Microglial morphology and network

1.3.1 Microglial morphology

The morphology of microglia with a small soma and highly branched processes is unique in the brain. Unsurprisingly, microglial morphology and its dynamic changes have been an important part of microglial research. Before the arrival of RNA sequencing techniques, morphological analyses of microglia have been widely used to correlate the morphology with the activation status of microglia. When microglial activation was still viewed as resting microglia vs activated M1 or M2 microglia, a highly branched, ramified morphology of microglia was viewed as microglia in a resting state (Paolicelli et al. 2022; Vidal-Itriago et al. 2022). Today, we know that 'resting' microglia are in fact highly motile microglia in a homeostatic, surveillant state and that microglial activation occurs in a wide spectrum of activation states, depending on the stimulus. Conversely, microglia that adapted an ameboid morphology with decreased branching and ramification were formerly viewed as activated microglia (Paolicelli et al. 2022; Vidal-Itriago et al. 2022). Accordingly, ameboid microglia are for example associated with an increased release of pro-inflammatory IL-1β accompanied by reduced surveillance and decreased phagocytic capability (Abiega et al. 2016; Madry et al. 2018). Hence, it has been suggested that ameboid microglia should rather be viewed as dysfunctional microglia than activated (Krabbe et al. 2013).

Typical read-outs of microglial morphology are the volume of the soma, the number branch or terminal points and the total length of all processes. With this set of read-outs, morphological changes of microglia in ageing and neurodegeneration have been described. During ageing as well as in neurodegeneration, the size of the microglial soma increases, and the total process length and ramification of microglia decreases. This reflects their change from a homeostatic phenotype towards a phenotype reacting to the changing environment (Hefendehl et al. 2014; Hickman et al. 2018; Perry, Nicoll, and Holmes 2010; Streit et al. 2004). Furthermore, another study compared microglial

morphology between different species and found that microglial morphology is drastically different between the different species. Marmoset microglia were found to be the most ramified and complex microglia. Mammals in general were found to have more ramified and complex microglia compared to zebrafish and various reptiles (Geirsdottir et al. 2019).

Recently, more advanced methods to analyze microglial morphology are used that rely on highly automated, computational pipelines in order to reduce multiple sources of bias introduced in previous analyses. The selection of individual cells and individual parameters for the read-out could lead to a selection bias in previous studies. In contrast, the computational pipelines allow for an unbiased analysis of a huge number of cells and subsequent cluster analysis of microglia according to their morphology. These studies confirmed morphological changes of microglia in neurodegeneration and ageing but also found morphological differences between human and mouse microglia that previous studies failed to detect in that detail by clustering microglia using UMAP plots according to their morphology. These algorithms also detected morphological differences between male and female microglia and between microglia in different brain regions (Colombo et al. 2022; Salamanca et al. 2019). Importantly, however, it is not yet clear how these morphological differences correlate with functional states of different clusters of microglia.

1.3.2 Network organization of microglia

Depending on the brain region, microglia make up 5 to 12 % of cells in the brain and hereby form an evenly distributed network of cells with distinct territories for each cell (Lawson et al. 1990). Microglial density is generally higher in white matter areas of the brain as compared to gray matter (Mittelbronn et al. 2001). Moreover, microglial densities and the ratio of microglia to neurons varies between brain regions. The ratio of microglia to neurons is three times higher in the frontal cortex compared to the cerebellum or the hippocampus (Geirsdottir et al. 2019). The reason and the functional consequences of this are not known. However, it has been suggested that microglial density rather correlates with the density of synapses and not the number of neurons (Dos Santos et al. 2020). The cortex for example is the brain region with the highest synaptic density (Santuy et al. 2020). Thus, it is possible that the microglia to synapse ratio is stable throughout the brain and might reflect the homeostatic functions of microglia in maintaining and shaping neuronal network activity via effects on synapses.

The microglial network is built by clonal expansion of a rather small proportion of microglia progenitors that invade the brain early during development. Once established, the microglial network remains stable during life (Barry-Carroll et al. 2023; Tay et al. 2017). Microglia are able to self-renew without a known stem cell or precursor population present in the adult brain (Ajami et al. 2007; Askew et al. 2017; Füger et al. 2017; Réu et al. 2017). Only under extreme experimental conditions such as irradiation and blood-brain barrier damage, peripheral myeloid cells invade the brain in order to

differentiate into microglia-like cells and occupy microglial territory (Ajami et al. 2007; Ginhoux et al. 2010; Mildner et al. 2007). Precise mechanisms for how microglia occupy their assigned territory and how microglial numbers are regulated are not known. However, P2RY12 was shown to regulate translocation of microglia to regulate the microglial network (Eyo, Mo, et al. 2018). Additionally, it was suggested that contact inhibition between microglia via Syndecan-4 could be an important process in this regulation (Zhan et al. 2019). This process could also play an important role in the event of microglial cell death when the microglial network needs to replace the missing cell. In the olfactory bulb of mice, a brain area with one of the highest proliferation rates of microglia, a study found temporally coupled events of microglial cell death and proliferation. The authors also found that the dividing microglial cell usually was the second-closest cell to the apoptotic cell (Askew et al. 2017). Similarly, a study from my laboratory found that the rates of proliferation and apoptosis are almost equal, supporting the coupled process of apoptosis and proliferation (Füger et al. 2017).

Only in ageing and neuronal injury or neurodegeneration the microglial network undergoes major changes. In ageing, the number of microglia is stable but microglia tend to lose their even distribution over the parenchyma, possibly increasing the local susceptibility of the brain tissue to insults (Hefendehl et al. 2014). In neurodegeneration or neuronal injury, microglia locally expand in order to react to the injury (Füger et al. 2017; Olmedillas et al. 2023; Tay et al. 2017). After the injury is resolved, excess microglia undergo apoptosis and the microglial network returns to its pre-injury state (Tay et al. 2017).

1.3.3 Longevity of microglia

It is widely accepted that microglia, especially at a network level, are long-lived cells, yet current studies show conflicting results on the longevity of individual microglia in mice and humans. For human microglia, estimations range from a nearly full replacement of all microglia every four years (about 20 cycles per life) to hundreds of cycles of self-renewal of the entire microglial population (Askew et al. 2017; Réu et al. 2017). However, the methods used to obtain these estimations differed and might explain the variety of results. For example, the study estimating hundreds of cycles of self-renewal used staining for Ki67 in microglia (Askew et al. 2017). Ki67 is widely used as a marker for proliferating cells. However, Ki67-positive cells do not necessarily undergo division as Ki67-positive cells also might be blocked in the G_1-phase of the cell cycle. This phenomenon would lead to an overestimation of the proliferation rate of microglia (Busch et al. 2007). Hence, the authors acknowledged the need for a more precise method to estimate microglial proliferation rates and longevity in humans (Askew et al. 2017). Another study used radiocarbon dating of the DNA of microglia in order to avoid these challenges. The authors found that microglia had an average age of 4.2 years with some cells being more than 20 years old. Based on these data, they estimated that human microglia were replaced by

newly produced cells at a median rate of 28 % per year (Réu et al. 2017). Although radiocarbon dating is a very precise method, this method might underestimate the actual proliferation rate of microglia while precisely reflecting the longevity of microglia. The reason for this is, that it has been shown that newborn microglia in mice are much more likely to die shortly after division and not replace existing microglia in the network (Askew et al. 2017). These cells, however, would not be detected by radiocarbon-dating and only by Ki67 staining.

While estimations of microglia longevity and proliferation rates in humans are only possible in post-mortem samples, experimental procedures in mice allow for longitudinal analyses. A study from my laboratory followed individual microglia in the cortex throughout the life of mice via *in vivo* 2-Photon live cell imaging. The study calculated the average lifetime of microglia in mice to be 29 months, which is more than the entire lifetime of most mice (Füger et al. 2017). In contrast to this, another study used several methods to determine microglia turnover in the mouse brain. Labeling of dividing microglia with BrdU and γ-retroviral vectors that selectively transduce proliferating glial cells, revealed that proliferation rates of microglia were especially high in the dentate gyrus of the hippocampus and the olfactory bulb. In addition to this, the authors performed *in vivo* 2-Photon live cell imaging of microglia in the olfactory bulb. Consistently with the aforementioned methods, they found that microglia undergo a full turnover of their population every 96 days (Askew et al. 2017). A third study investigating microglial longevity used so-called microfetti mice, in which microglia are fluorescently labeled in four different colors which facilitates the detection of proliferation events post-mortem. Interestingly, the authors estimated a complete turnover of the microglial population in the olfactory bulb every 8 months, compared to 41 months in the cortex, explaining the differences between the two *in vivo* 2-Photon live cell imaging studies (Tay et al. 2017). In summary, the consensus of these studies is that microglia are mostly long-lived cells with a low turnover rate with a strong heterogeneity between different brain regions.

Besides homeostatic conditions, two studies also looked at the longevity of microglia in mouse models of AD. In the periphery of amyloid plaques, the microglial network is as stable as under non-diseased conditions with long-lived microglia. However, the proliferation rate of microglia in the periphery is higher with newborn microglia migrating towards the plaques (Füger et al. 2017). Additionally, the microglial turnover is increased in close vicinity to the plaques with coupled events of cell death and proliferation indicating that the pathology leads to a decreased survival of microglia (Olmedillas et al. 2023).

1.4 CSF1R and global microglia depletion

A crucial receptor for the differentiation, maintenance and survival of microglia is colony stimulating factor 1 receptor (CSF1R). While CSF1R in the brain is mainly expressed by microglia, its two ligands, IL34 and CSF1 are differentially expressed in the brain (Elmore et al. 2014; Paolicelli et al. 2022; Zhang et al. 2016). IL34 is mainly expressed in the gray matter by neurons, while CSF1 is mostly expressed by astrocytes, oligodendrocytes and microglia in the white matter (Badimon et al. 2020; Easley-Neal et al. 2019). CSF1R is a receptor tyrosine kinase that, upon binding of its ligands, dimerizes and is phosphorylated. This induces subsequent downstream signaling via the phosphorylation of ERK1/2 among others (Liu et al. 2012; Stanley and Chitu 2014). The importance of CSF1R signaling for microglia and the brain is highlighted by a disease called Hereditary diffuse leukoencephalopathy with spheroids, an autosomal dominant disease caused by loss-of-function mutations in CSF1R (Rademakers et al. 2012). The lack of functional CSF1R leads, among others, to a reduced number of microglia (Tada et al. 2016). Patients suffering from this disease experience dementia, parkinsonism, epileptic seizures and depression (Rademakers et al. 2012).

The importance of CSF1R signaling for microglia can be exploited in order to globally deplete and replace microglia for experimental purposes in mice but is also considered for potential therapeutic approaches for various neurological diseases (Han et al. 2022). The most popular compounds for this approach are PLX3397, PLX5622, GW2580 and BLZ945, all of which are small molecule inhibitors of CSF1R that are able to pass the blood-brain barrier (Coniglio et al. 2012; Conway et al. 2005; Han et al. 2022; Krauser et al. 2015). They stabilize CSF1R in its auto-inhibited state which leads to kinase inactivation and prevents substrate and ATP binding (Benner et al. 2020). All of these CSF1R inhibitors lead to a near complete loss of microglia in mice within days (Green, Crapser, and Hohsfield 2020; Han et al. 2022). As soon as the CSF1R inhibition is stopped, microglia begin to proliferate and repopulate the brain from the few remaining microglia. During this process, the microglia repopulation first exceeds microglial numbers from before the depletion but then regulates itself to decrease to the previous network density (Elmore et al. 2014; Huang et al. 2018). Currently, not much is known about the microglial subpopulation that survives CSF1R inhibition, but it is believed that a small, progenitor-like microglia subpopulation exists that is independent of CSF1R signaling and therefore resistant to its inhibition. This subpopulation highly expresses MAC2, a ligand of TREM2 (Zhan et al. 2020). In various mouse studies, it has been shown that microglial depletion and repopulation has beneficial effects in ageing mice and mouse models of neurodegeneration. In ageing, microglia depletion improves spatial memory and reverses synaptic and neuronal deficits in aged mice (Elmore et al. 2018). In a mouse model of AD, microglia depletion reduces neuroinflammation and neuronal loss although plaque-associated microglia are more resistant to CSF1R inhibition and microglial depletion did not affect

amyloid pathology (Spangenberg et al. 2016). Lastly, short-term microglia depletion improves remyelination in a mouse model of MS (Beckmann et al. 2018). In contrast to these beneficial effects, microglia depletion can also have detrimental effects that need to be taken into consideration. Microglia depletion in early development can lead to altered functional connectivity in the brain, leading to hyperactivity and anxiolytic-like behavior (Rosin, Vora, and Kurrasch 2018). Additionally, CSF1R inhibitors have unspecific effects on other receptors and cell types in the brain. PLX3397 for example not only inhibits CSF1R but also inhibits other tyrosine kinases such as C-KIT, PDGFRα and FLT3 (Green et al. 2020; Han et al. 2022). On a cellular level, BLZ945, PLX3397 and PLX5562 indirectly or directly lead to a reduction of oligodendrocyte progenitor cells which could have further adverse effects (Hagemeyer et al. 2017; Y. Liu et al. 2019). Moreover, cellular debris from the excessive microglia cell death during microglia depletion needs to be cleared by other cell types, e.g. astrocytes (Zhou et al. 2022). Besides effects on the brain, CSF1R inhibition also influences peripheral macrophages and other tissue-resident macrophages (Lei et al. 2020).

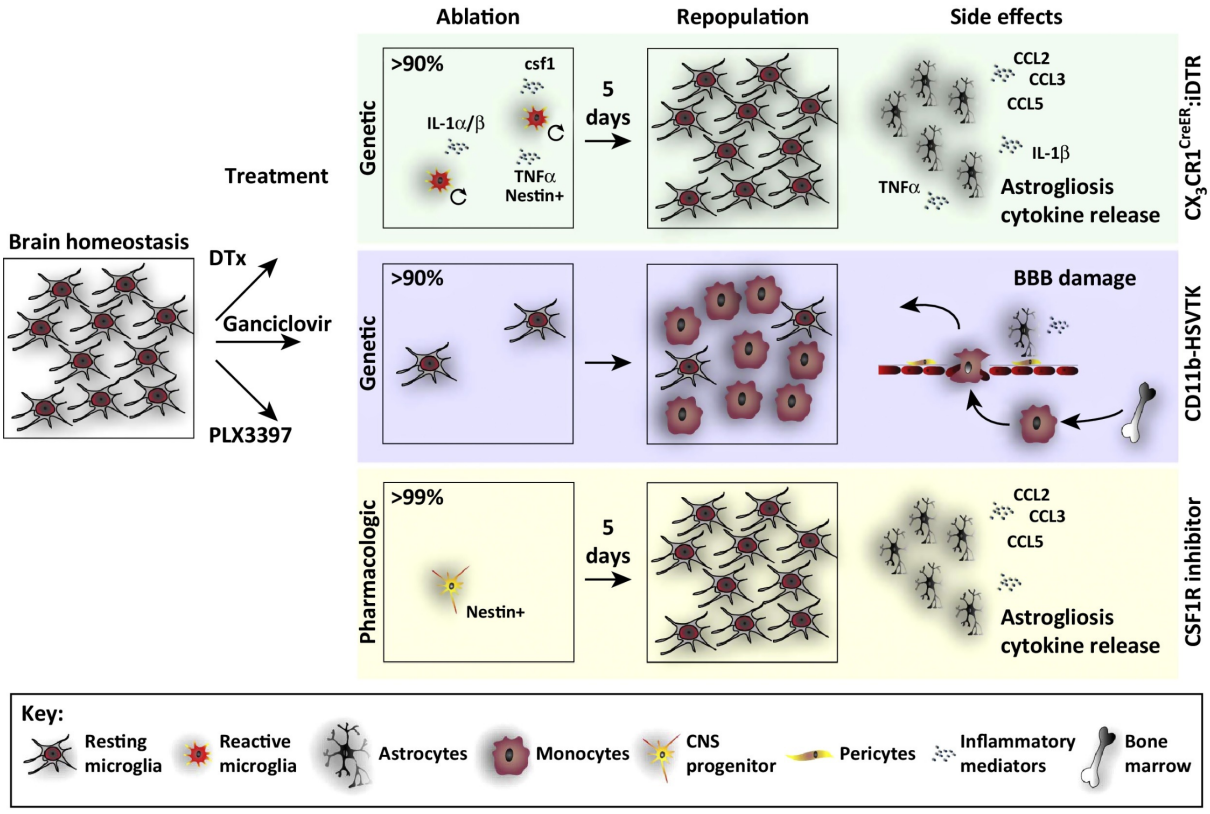

Figure 2.3 Strategies for global depletion of microglia
Strategies for the global depletion of microglia involve inhibition of CSF1R by PLX3397 and other similar compounds as well as genetic strategies that rely on the expression of iDTR or HSVTK. In the latter models, depletion is induced by the application of DT and ganciclovir, respectively. From Waisman et al. 2015 with permission from Trends in Immunology - Cell Press

Antibodies directed against CSF1R to block downstream signaling, that would be more specific than small molecule inhibitors, are, however, not commonly used to deplete microglia. They are able to deplete tissue-resident macrophages but do not affect microglia when applied peripherally (MacDonald et al. 2010).

In addition to inhibition of CSF1R, other approaches exist to selectively deplete microglia from the brain. One of these approaches is clodronate liposomes. These liposomes are selectively phagocytosed by phagocytic cells and processed within lysosomes. This releases clodronate which triggers apoptosis. However, this toxin-based approach causes cytokine release, astrogliosis and blood vessel damage. Furthermore, clodronate liposomes do not cross the blood-brain barrier and therefore need to be injected into the brain (Green et al. 2020; Han et al. 2019; Rooijen and Sanders 1994).

Apart from these drug-based approaches, there are genetic approaches in order to deplete microglia. Firstly, microglia specific expression of the receptor for diphtheria toxin (DTR) in combination with the injection of diphtheria toxin (DT), active DT or the thymidine kinase of herpes simplex virus (HSVTK) in combination with ganciclovir treatment can be used to induce apoptosis in microglia (Bruttger et al. 2015; Buch et al. 2005; Heppner et al. 2005; Varvel et al. 2012; Wang et al. 2016). The diphtheria toxin-based approaches cause cytokine release and astrogliosis while HSVTK-based approaches compromise the blood-brain barrier (Bruttger et al. 2015; Varvel et al. 2012; Waisman et al. 2015). The DT-based approaches will be explained in more detail later (see section II.2.1). Secondly, constitutive and conditional knock-out models of CSF1R exist. Constitutive CSF1R knock-out mice, however, suffer from developmental defects with skeletal and neurodevelopmental abnormalities (Cronk et al. 2018; Dai et al. 2002; Erblich et al. 2011; Li et al. 2006). This major drawback of constitutive CSF1R knock-out seems to be solved by so-called $Csf1r^{\Delta FIRE/\Delta FIRE}$ mice. The genomic deletion of a highly conserved super enhancer region, the fms-intronic regulatory element (FIRE), leads to a lack of tissue-resident macrophages in the brain, skin, heart, kidney and peritoneum in $Csf1r^{\Delta FIRE/\Delta FIRE}$ mice while other macrophages and monocytes are not affected. In contrast to constitutive CSF1R knock-out mice, $Csf1r^{\Delta FIRE/\Delta FIRE}$ mice are healthy and fertile without the aforementioned skeletal and neurodevelopmental abnormalities (Rojo et al. 2019).

Notably, a recent study used three cycles of microglia depletion and repopulation. Hereby the authors artificially induced an aged microglia phenotype in a young brain environment due to the high amount of proliferation. The authors estimated that each microglial cell in this model divides approximately 40 times. They then showed transcriptionally that microglia in this model developed an aged-like phenotype that affected the surrounding ‘young’ brain environment (Xu et al. 2023).

2 Approaches for targeted cell death

Since global depletion of microglia does not correspond to a physiologically occurring situation, approaches are needed that target individual microglia. Targeted cell death of individual microglia is of importance to study the microglial network. As discussed earlier, microglial cell death is a rare event (see section II.1.3.3) and thus can be modeled by approaches for targeted cell death of individual microglia. Besides brain-wide depletion of microglia via CSF1R inhibition, several methods exist that make the targeted death of individual cells possible (Figure 2.4).

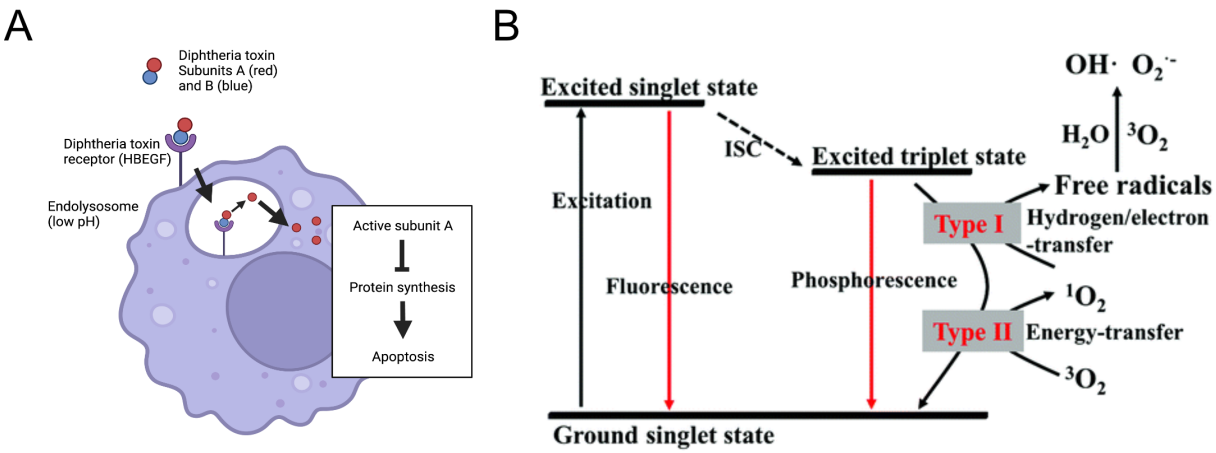

Figure 2.4 Approaches for targeted cell death
(A) Mode of action of Diphtheria toxin. DT consists of two subunits. Upon binding to iDTR (HBEGF) and processing in endolysosomes, the active A subunit of DT is released into the cytoplasm where it inhibits protein synthesis which leads to subsequent apoptosis. Created with Biorender.com according to Ruedl and Jung 2018 with permission from European Journal of Immunology – John Wiley and Sons **(B)** Generation of ROS by excitation of Hoechst 33342 (2Phatal) or a photosensitizing protein (for example KillerRed). Induction of ROS leads to apoptotic or necrotic cell death. Adapted from Zhao et al. 2021 with permission from Chemical Society Reviews

2.1 Diphtheria toxin

In contrast to humans, mice are not sensitive to Diphtheria toxin (DT) (Middlebrook and Dorland 1977; Pappenheimer Jr. et al. 1982). By expressing the human or simian heparin-binding epidermal growth factor-like growth factor (HBEGF), the receptor for DT (DTR), mouse cells can be sensitized to the toxin (Buch et al. 2005; Cha et al. 2003; Jung et al. 2002; Saito et al. 2001). Upon binding of DT, the toxin is endocytosed. Once in the cytoplasm, the toxic A subunit of DT inactivates elongation factor 2 which leads to a stop of protein synthesis and subsequent apoptosis (Figure 2.4 A) (Drazin, Kandel, and Collier 1971; Honjo et al. 1971; Pappenheimer Jr. et al. 1982). To prevent permanent and global expression of DTR, the most commonly used transgene is designed so that expression of DTR is blocked by a loxP-flanked STOP-cassette (Buch et al. 2005). In microglia, this approach has so far only been used for

global microglia depletion of about 80 % to 99 % of the microglial population (Bruttger et al. 2015; Parkhurst et al. 2013; Rubino et al. 2018). However, when dosing of Tamoxifen is adjusted to achieve low recombination efficiency by CreERT, a small subpopulation of microglia could be selectively targeted to express DTR. Intraperitoneal injection of DT would then lead to a selective ablation of these cells. Alternatively, a mouse model exists in which the expression of the A subunit of DT is blocked by a loxP-flanked STOP-cassette. Upon Cre-mediated recombination, the A subunit of DT is expressed in the target cell and induces apoptosis without the additional injection of DT (Lund et al. 2018).

2.2 2Phatal

2Phatal is a recently developed method for targeted apoptotic ablation of single cells (Hill et al. 2017). It is based on the photobleaching of the nucleus of the target cell which generates ROS and subsequently leads to apoptotic cell death of the target cell without inducing tissue damage to the surrounding area (Figure 2.4 B) (Hill et al. 2017). This is in contrast to frequently used laser ablation experiments that induce tissue burning and cell rupture (Hill et al. 2017). To use 2Phatal, the nuclear dye Hoechst 33342 is topically applied onto the brain during cranial window surgery (Damisah et al. 2020; Hill et al. 2017). Target cells can then be selectively ablated by focused scanning of the nucleus with a 2-Photon laser to induce apoptosis (Hill et al. 2017). After its application, Hoechst 33342 is cleared from the brain within a couple of days (Hill et al. 2017). So far, 2Phatal has been demonstrated in neurons, astrocytes, oligodendrocytes, pericytes and NG2 glia (Chapman et al. 2023; Damisah et al. 2020; Hill et al. 2017; Mills et al. 2022). However, microglia seem to not be labeled by Hoechst 33342 (Hill et al. 2017). Another disadvantage of the method is that Hoechst 33342 does not efficiently cross the blood-brain barrier which makes it necessary to apply the dye during surgery where minor leakage of the blood-brain barrier occurs (Choi et al. 2011; Hill et al. 2017). This limitation also restricts the time window during which 2Phatal can be performed since a reapplication of Hoechst 33342 to a later time point might be difficult.

2.3 Genetically encoded photosensitizers

Similarly to 2Phatal, photosensitizers are based on the induction of cell death by phototoxicity (Bulina et al. 2006; Liu et al. 2021). Photosensitizers are fluorescent proteins that are characterized by an especially high capability to generate ROS (Figure 2.4 B) (Liu et al. 2021). The phototoxicity of KillerRed for example, the most commonly used genetically encoded photosensitizer, is more than 1000-fold the phototoxicity of GFP (Pletnev et al. 2009). Upon prolonged excitation, either broadly by an epifluorescent light source or on a single cell level by confocal or 2-Photon lasers, photosensitizers lead to cell death (Auer, Vagionitis, and Czopka 2018; Buckley et al. 2017; Ertürk, Wang, and Sheng 2014; Liu et al. 2021; Williams et al. 2013). Depending on the localization of the protein within the cell,

targeted cells undergo either apoptotic or necrotic cell death (Liu et al. 2021). Other photosensitizing proteins are KillerOrange, SuperNova and miniSOG amongst others (Ruiz-González et al. 2013; Sarkisyan et al. 2015; Takemoto et al. 2013). Photosensitizers are either stably expressed in transgenic organisms or are delivered by viral or non-viral vectors to cells (Auer et al. 2018; Buckley et al. 2017; Ertürk et al. 2014; Liu et al. 2021; Williams et al. 2013). So far, the use of photosensitizers has been described for targeted cell death in neurons, oligodendrocytes and other cell types of mouse and rat OBSC, Caenorhabditis elegans and zebra fish (Auer et al. 2018; Buckley et al. 2017; Ertürk et al. 2014; Formella et al. 2018; Liu et al. 2021; Williams et al. 2013).

3 Model systems to investigate microglia

Their important role in plenty neurological conditions makes microglia a valuable target for different therapeutical approaches. However, microglial homeostasis and the tight balance between beneficial and detrimental effects need to be well understood so that it can be exploited in order to develop successful therapies. To this end, various model systems to investigate microglia, both *in vitro* and *in vivo,* exist which will be discussed in the following.

3.1 *In vitro* models

3.1.1 Immortalized cell lines

Of all model systems for microglia, immortalized cell lines are the model system with the easiest accessibility and handling. Many different immortalized microglia cell lines exist that were generated from mice, rats, macaques and humans. The most commonly used cell lines of these are the BV2 and N3/N9/N11/N13 mouse-derived lines and the HMO6 human-derived lines (Timmerman, Burm, and Bajramovic 2018). BV2 cells were generated by the transduction of neonatal primary mouse microglia with a retrovirus carrying the oncogenes v-raf and v-myc (Blasi et al. 1990). They express basic microglial markers and are responsive to LPS, Aβ or αsyn stimulation by phagocytosis of e.g. Aβ fibrils and an upregulation of ROS and pro-inflammatory genes (Blasi et al. 1990; Boza-Serrano et al. 2014; Kopec and Carroll 1998; Stansley, Post, and Hensley 2012; Timmerman et al. 2018). Similarly, N3/N9/N11/N13 cells, of which N9 are the most commonly used, were generated by transforming embryonic primary mouse microglia with v-myc or v-mil (Righi et al. 1989). These lines also express basic macrophage markers, have phagocytic capabilities and react to LPS or Aβ stimulation with the secretion of pro-inflammatory cytokines (Hickman et al. 2008; Righi et al. 1989).

The human HMO6 microglia line is derived from embryonic primary microglia from telencephalon tissue which were transduced with a retroviral vector carrying v-myc (Nagai et al. 2001). HMO6 microglia express the microglial marker CD11b and are able to secrete IL8 and TNFα in response to LPS

stimulation. However, when compared to primary microglia that were not immortalized, they fail to also release IL1β and IL6 (Ahn et al. 2008; Nagai et al. 2001; Timmerman et al. 2018).

Generally, immortalized microglia cell lines are only capable to reproduce the most basic functions of microglia and are therefore not suitable to recapitulate complex microglial interactions in the brain. Potentially, the process of immortalization might alter microglia but also the lack of a complex environment that supports microglia with trophic factors alters their phenotype (Bennett et al. 2018; Henn et al. 2009; Horvath et al. 2008; Stansley et al. 2012; Timmerman et al. 2018). Thus, immortalized microglia cell lines are mostly used to answer less complex research questions.

3.1.2 Primary cell culture: monocultures and organotypic brain slice cultures

Another approach to investigate microglia *in vitro* is primary cell culture. This includes both microglia monocultures and the cultivation of organotypic brain slice cultures.

Primary microglia can be isolated and cultivated from mice, rats, non-human primates and humans. To this end, microglia are usually isolated from brain tissue by tissue dissociation followed by density gradient centrifugation. Depending on the protocol this can lead to microglia single-cell cultures with up to 99 % purity (Stansley et al. 2012; Timmerman et al. 2018). Similarly to immortalized microglia, primary microglia reliably express markers of microglia, have phagocytic capabilities and react to various stimuli by the production of ROS and pro-inflammatory cytokines (Colton and Gilbert 1987; Maezawa et al. 2011; Takata et al. 2010). However, the loss of their complex 3D-environment in the brain and the loss of signaling with other brain cells lead to the loss of their homeostatic signature. In culture, primary microglia rapidly adapt an ‘activated’ phenotype with increased secretion of pro-inflammatory cytokines compared to *in vivo* (Cadiz et al. 2022; Dubbelaar et al. 2018; Gosselin et al. 2017; Maguire et al. 2022). Hence, the application of primary microglia cultures is limited, especially in the context of homeostasis.

In contrast to the preparation of monocultures of primary microglia, the preparation of organotypic brain slice cultures (OBSC) does not include the dissociation of brain tissue. OBSC are typically prepared from newborn rodents (Gähwiler et al. 1997; Humpel 2015), but can also be prepared from human tissue that is derived from resective brain surgery or tissue that is made available after abortions (Eugène et al. 2014; Schwarz et al. 2017, 2019; Wickham et al. 2020). To this end, the tissue is sliced into thin sections (250-350 µm thin) and cultivated on semipermeable membranes for several months (Barth et al. 2021; Novotny et al. 2016; Stoppini, Buchs, and Muller 1991). Since several slices can be obtained from one animal, multiple experimental conditions can be tested with slices from one animal and thus reduce animal numbers (Barth et al. 2021). While OBSC obtained from newborn rodents can be kept in culture for several months (Gähwiler et al. 1997), the preparation of OBSC from adult

rodents has proven to be much more difficult with OBSC only surviving a few weeks before the tissue degenerates (Humpel 2015). OBSC can be prepared from various brain regions. For rodents, OBSC from cortex, cerebellum, brain stem, hippocampus and retina have been described among others (Gähwiler et al. 1997). For humans, OBSC are mostly prepared from cortex or hippocampus due to tissue availability (Eugène et al. 2014; Schwarz et al. 2017, 2019; Wickham et al. 2020). A major advantage of OBSC compared to primary microglial culture is the conservation of the complex 3D tissue architecture and cell-cell interactions of all types (Gähwiler et al. 1997). However, since most OBSC are prepared from newborn rodents, they mostly reflect a developing stage of the brain (Humpel 2015). Interestingly though, a recent study showed signs of accelerated ageing and cellular senescence in OBSC. The extent of this accelerated ageing, however, is not yet further characterized (Liu et al. 2022). Additionally, the availability of human tissue is a limiting factor. Besides these drawbacks, the biggest disadvantage of OBSC is that the preparation causes axonal damage and subsequent tissue inflammation as shown by pronounced astro- and microgliosis which form a so-called 'glial scar' (Grabiec et al. 2017). Microglia in OBSC initially migrate towards the site of axonal damage on the surface of the culture but gradually readapt a more homeostatic phenotype within the first one to two weeks (Hailer, Jarhult, and Nitsch 1996; Heppner et al. 1998). After this initial inflammatory phase, microglia in OBSC readapt a more ramified morphology, reminiscent of the microglial morphology *in vivo* (Czapiga and Colton 1999; Hailer et al. 1996). On a transcriptomic level, microglia in OBSC are closer to microglia *in vivo* than to primary microglia *in vitro* despite still showing an 'activated' phenotype after three weeks in culture (Delbridge et al. 2020). Taken together, OBSC are a suitable model to study microglia in a state as close as possible to *in vivo* and in an environment which is as close as possible to the *in vivo* situation. Lastly, OBSC can also be used to model the pathology of various neurodegenerative diseases which is helpful to model the microglial reaction in this context (Barth et al. 2021; Croft et al. 2019; Novotny et al. 2016).

3.1.3 In vitro *graft models*

An extraordinary approach to study microglia in OBSC is the replenishment of OBSC endogenous microglia with isolated microglia from newborn and adult mice. The authors used regular OBSC and depleted microglia with clodronate. Subsequently, they grafted isolated microglia onto the tissue which then integrated at a similar density as the endogenous microglia. Moreover, the authors showed that grafted adult microglia adopted a morphology reminiscent of microglia *in vivo* (Masuch et al. 2016). However, this approach has neither been further characterized nor adapted widely by other labs.

3.1.4 Induced Pluripotent Stem Cells (iPSC)

The development of induced Pluripotent Stem Cells (iPSC) by Takahashi and Yamanaka in 2006 enabled a plethora of possibilities to study human cells in healthy and diseased conditions (Dolmetsch and Geschwind 2011; Shi et al. 2017; Takahashi and Yamanaka 2006). By overexpression of only four factors (Oct3/4, Sox2, c-Myc, and Klf4), they were able to generate pluripotent stem cells from somatic cells that are able to differentiate into cells from all three germ layers and have the capacity of infinite self-renewal (Takahashi and Yamanaka 2006). This discovery gave rise to the opportunity to study human cells and disease-associated mutations to an unprecedented extent and study patient-derived cell lines in order to recapitulate their individual genetic background (Dolmetsch and Geschwind 2011; Shi et al. 2017).

The differentiation of microglia from iPSC, however, has long proven difficult. Shortly after the discovery of their origin as primitive macrophages from the yolk sac (Ginhoux et al. 2010), several protocols to generate microglia from iPSC were published that mimicked the natural differentiation of microglia (Abud et al. 2017; Douvaras et al. 2017; Haenseler et al. 2017; Lee, Kozaki, and Ginhoux 2018; McQuade et al. 2018; Muffat et al. 2016; Pandya et al. 2017; Takata et al. 2017). Most of these protocols have in common, that they first drive iPSC into a mesoendodermal fate and then via hemogenic endothelium towards primitive hematopoiesis (via at least BMP4 and VEGF). These embryonic macrophage precursors are then expanded and supported by CSF1 and IL3. Lastly, differentiation into microglia-like cells and cultivation is achieved via CSF1 and IL34. This process usually takes between three and ten weeks (Lee et al. 2018; Speicher et al. 2019). Generally, one can distinguish between two major types of differentiation protocols: embryoid bodies (EB)-based and monolayer-based protocols. The use of EBs simulates cell signaling that is crucial for mesoendodermal specification that needs to be replaced by the addition of other factors and incubation under hypoxic conditions in monolayer-based protocols (Lee et al. 2018). Recently, a third major method to obtain microglia from iPSC was published. The authors induced expression of six transcription factors in order to generate microglia within only eight days and in large quantities (Dräger et al. 2022).

iPSC-derived microglia-like cells (iMicros) in monoculture express microglial markers such as P2RY12, Iba1 and TMEM119 (Douvaras et al. 2017; Muffat et al. 2016). Importantly, these microglia-specific markers (P2RY12, TMEM119) identify monoculture iMicros as microglia-like cells and differentiate them from other tissue-resident macrophages (Bennett et al. 2016; Chiu et al. 2013; Wes et al. 2016). Additionally, monoculture iMicros are phagocytically active, ramified, respond to stimulation and are able to secrete cytokines (Abud et al. 2017; Douvaras et al. 2017; Haenseler et al. 2017; Muffat et al. 2016; Pandya et al. 2017). In monoculture, iMicros exist in several different states and stimulation with brain-derived stimuli is also able to induce transcriptional states such as DAM, reminiscent of those

found *in vivo* as a response to pathological stimuli (Dolan et al. 2023; Sun et al. 2023). Nevertheless, cluster analysis of monoculture iMicros in comparison to *in vivo* microglia shows a lack of homeostatic signatures (Dubbelaar et al. 2018; Sun et al. 2023). Their transcriptional profile maps them closely to the differentiation steps and cultured primary human microglia while overlap with microglia *in vivo* is limited (Abud et al. 2017; Douvaras et al. 2017; Haenseler et al. 2017; Lee et al. 2018; Muffat et al. 2016). This is due to lacking cellular interactions with other cell types that naturally occur in the brain and influence the microglial transcriptome and functionality (Bennett et al. 2018; Bohlen et al. 2017; Dubbelaar et al. 2018; Gosselin et al. 2017).

In contrast, when cultured together with iPSC-derived neurons, astrocytes or both, iMicros are more ramified and less pro-inflammatory indicating a more 'homeostatic' phenotype (Abud et al. 2017; Haenseler et al. 2017; Vahsen et al. 2022). Additionally, transcriptomic analyses mapped co-cultured iMicros with microglia between embryonic development and postnatal microglia on day 3 (Takata et al. 2017). Overall, iMicros are a powerful tool to investigate disease-associated mutations and patient-derived cells and mimic *in vivo* microglia more closely than immortalized or primary microglia (Speicher et al. 2019; Stöberl et al. 2023). Findings from iMicros, however, should still be verified with more complex model systems as they mostly reflect early developmental stages and lack homeostatic signatures.

3.1.5 Cerebral organoids

Except for OBSC, all culture models described so far are comparably simple models in 2D. The advantage of 3D-models, however, is that they are able to more realistically reflect naturally occurring cell-cell interactions in the brain (Zhang et al. 2023). While tissue for the preparation of human OBSC is scarce, the development of cerebral organoids from iPSC increased the availability of human tissue for 3D-models. Cerebral organoids were first described by Lancaster et al. in 2013 (Lancaster et al. 2013; Lancaster and Knoblich 2014). They showed that cerebral organoids consist of various cell types including functional neurons and radial glia and can recapitulate characteristics of various brain regions (Lancaster et al. 2013). Moreover, the authors and others showed that cerebral organoids model human brain development until early postnatal stages (Gordon et al. 2021; Lancaster et al. 2013; Luo et al. 2016). Nowadays, several protocols are published to specifically differentiate organoids into defined brain regions such as cortex, hippocampus and midbrain (Jo et al. 2016; Paşca et al. 2015; Sakaguchi et al. 2015). Further studies showed that cerebral organoids contain not only neurons and radial glia, but also astrocytes, oligodendrocyte precursor cells and oligodendrocytes (Quadrato et al. 2017; Tanaka et al. 2020; Velasco et al. 2019). While all of these cell types are of neuroectodermal origin and hence induced during the differentiation process, microglia are derived from mesoderm (Hasselmann and Blurton-Jones 2020; Stöberl et al. 2023; Zhang et al. 2023). Since mesodermal and

endodermal lineage are not specifically inhibited in all protocols for the generation of cerebral organoids, it is still possible that iPSC differentiate spontaneously into this fate in these protocols (Qian, Song, and Ming 2019; Zhang et al. 2023). Although some protocols showed the presence of mesodermal precursors or even microglia, cerebral organoids are nevertheless widely considered to be devoid of microglia (Bodnar et al. 2021; Ormel et al. 2018; Pérez et al. 2021; Quadrato et al. 2017; Zhang et al. 2023). Unfortunately, the degree of this spontaneous differentiation seems to be stochastic and varies between different iPSC lines, experiments and protocols (Bodnar et al. 2021; Ormel et al. 2018; Zhang et al. 2023).

To overcome this limitation, several protocols exist in which cerebral organoids and microglia are differentiated separately. Subsequently, microglia precursors are engrafted into the organoids where they integrate and differentiate into microglia (Abud et al. 2017; Jin et al. 2022; Park et al. 2023; Song et al. 2019). However, the success of this engraftment is still varying between labs (Abud et al. 2017; Jin et al. 2022; Park et al. 2023; Zhang et al. 2023).

Microglia in cerebral organoids, no matter whether endogenously differentiated or engrafted, react to various stimuli such as blunt tissue damage, viral infection or LPS (Abud et al. 2017; Muffat et al. 2018; Ormel et al. 2018; Xu et al. 2021). Furthermore, they seem to interact with synapses and enhance neuronal maturation, recapitulating important functions of microglia (Park et al. 2023; Sabate-Soler et al. 2022; Schafer et al. 2012). Morphologically, they are more ramified than microglia in 2D model systems and transcriptionally resemble human microglia *in vivo* (Abud et al. 2017; Ormel et al. 2018; Popova et al. 2021). Still, microglia in cerebral organoids show artifacts of their *in vitro* environment, similar to primary microglia (Ormel et al. 2018; Popova et al. 2021). Namely, levels of the homeostatic markers TMEM119 and P2RY12 are lower than *in vivo* (Ormel et al. 2018).

3.2 *In vivo* models

Despite growing complexity and an increased quality of *in vitro* models, they still cannot fully recapitulate microglia phenotypes *in vivo*. The most frequently used organisms for the study of microglia *in vivo* are mammals and zebrafish (Sharma, Bisht, and Eyo 2021). To not exceed the scope of this thesis, I will only discuss the use of mice for the study of microglia *in vivo* since they are the best-defined model organism for microglia and most of the research presented here is derived from mice.

3.2.1 Mouse models

Due to the popularity of mice, a wide spectrum of tools and experimental methods are available to study microglia and their effects on the brain. This includes mouse lines for the targeted manipulation or visualization of microglia, as well as experimental tools such as viruses, drugs and small molecules.

One of the most commonly used genetic tools in biomedical research is the Cre/loxP system. Cre/loxP is a recombination system that allows for the excision or inversion of defined genetic sequences that are flanked by loxP-sequences (Sauer 1998; Sauer and Henderson 1989). In biomedical research, this recombination system is exploited to achieve expression or deletion of target genes but also to express reporter genes such as fluorescent proteins for the purpose of visualization or fate mapping (McLellan, Rosenthal, and Pinto 2017; Stifter and Greter 2020). By using specific promoters, the expression of Cre can be confined to a specific cell type in order to obtain cell-type specific expression or knock-out of any gene (McLellan et al. 2017). When the active enzyme, the Cre-recombinase, is fused to a mutated estrogen ligand-binding domain (CreER(T2)), the recombinase stays in the cytoplasm where it cannot induce recombination of the target sequence. Upon binding to 4-Hydroxytamoxifen, the active metabolite of tamoxifen, the fused enzyme is translocated to the nucleus where it recombines the target sequence. The necessity to inject Tamoxifen in this system, makes it controllable in time (Feil et al. 1996; McLellan et al. 2017).

For microglia, several different mouse lines exist, that use various promoters to achieve microglia-specific CreER-expression (Eme-Scolan and Dando 2020; Faust et al. 2023). However, these cell lines vary in cell-type specificity, recombination efficiency and rate of spontaneous recombination (rate of recombination without Tamoxifen), parameters that need to be taken into consideration in order to avoid undesired effects in other cell types or incomplete recombination in microglia (Faust et al. 2023). The most popular of these lines uses the promoter of CX3CR1 (Eme-Scolan and Dando 2020; Faust et al. 2023). Other promoters used for microglial CreER mouse lines include CD11b, , TMEM119, Hexb and P2RY12 (Chappell-Maor et al. 2020; Faust et al. 2023; Kaiser and Feng 2019; Masuda et al. 2020; McKinsey et al. 2020). On the one hand, CX3CR1-CreER mice have the highest recombination efficiency but on the other hand also show a comparably high rate of spontaneous recombination (2-10 %). Additionally, CX3CR1 and CD11b are promotors that are less specific to microglia and hence CreER expression under control of these promoters also affects other macrophages in the brain such as border-associated macrophages and peripheral immune cells such as circulating monocytes (Faust et al. 2023; Shi et al. 2018). In contrast to that, CreER-mice based on the promoters of TMEM119, Hexb and P2RY12 have been shown to be more microglia specific but are less efficient in inducing recombination (Faust et al. 2023). A recent approach that introduced a split Cre-enzyme under the CX3CR1-promoter and the other half of the enzyme under control of either Sall1 or Lyve1 achieved a distinction between microglia (Sall1-promoter) and border-associated macrophages (Lyve1) (Kim et al. 2021). Similar to CX3CR1-CreER, these binary Cre-transgenic mice showed fairly high rates of recombination (Faust et al. 2023; Kim et al. 2021).

Apart from CreER, microglia-specific promoters are also used to specifically label microglia in mice with reporter proteins. Some of the most commonly used lines are Iba1-EGFP and CX3CR1-EGFP (Hirasawa

et al. 2005; Jung et al. 2000). Similar to CreER mice, these promoters are not exclusive to microglia and also induce expression of the reporter in other myeloid cells. Hence, novel mouse models use promoters that are more specific to microglia such as TMEM119, Sall1 and Hexb (Eme-Scolan and Dando 2020; Kaiser and Feng 2019; Masuda et al. 2020; Takasato et al. 2004).

Besides genetic targeting of microglia in mice, several viral strategies exist in order to label or manipulate microglia. However, viral strategies generally face the problem of microglial immune activation (Klichinsky et al. 2020; Rosario et al. 2016). A first strategy of viral transduction of microglia is the use of a lentiviral microRNA9-regulated vector (Åkerblom et al. 2013; Barry-Carroll et al. 2023; Brawek et al. 2017). microRNA9 is expressed in all cells of the brain but microglia, so that the viral vector is degraded in all cells but microglia and is only expressed in microglia. This leads to a highly specific expression in microglia (Åkerblom et al. 2013). Another strategy is the use of adeno-associated viruses (AAV) in combination with vectors controlled by microglia-specific promoters. A recent publication optimized the capsid of AAV9 to maximize transduction of microglia while avoiding microglial immune activation (Lin et al. 2022).

This plethora of genetic and viral tools to visualize and manipulate microglia *in vivo* is used in various types of experiments. Visualizing microglia by fluorescent labeling is commonly used for 2-Photon *in vivo* imaging in order to observe microglial motility, network dynamics, reaction to tissue injury and Calcium signaling in microglia (Brawek et al. 2017; Cserép et al. 2020; Eme-Scolan and Dando 2020; Füger et al. 2017; Hefendehl et al. 2014; Hierro-Bujalance, Bacskai, and Garcia-Alloza 2018). Multicolor labeling of microglia, either genetically or virally transduced, has additionally been used for fate-mapping studies (Barry-Carroll et al. 2023; Tay et al. 2017). Another common read-outs of *in vivo* experiments is single-cell transcriptomics in order to dissect the various states of microglia (Keren-Shaul et al. 2017; Sala Frigerio et al. 2019; Sun et al. 2023; Xu et al. 2023).

Together with additional tools to investigate microglia such as microglia depletion and replacement (see section II.1.4), mouse models are frequently used to study the effect of microglia in neurodevelopment and neurological diseases (Beckmann et al. 2018; Elmore et al. 2014; Rosin et al. 2018; Spangenberg et al. 2019).

Despite this vast spectrum of models and experimental methods, mouse microglia are not the ideal model to recapitulate the phenotype of human microglia. Although humans share a similar genetic background with mice, many human genes enriched in microglia have only mouse orthologs with limited similarity or no orthologs at all (Hasselmann and Blurton-Jones 2020; Mancuso et al. 2019). This becomes especially clear when looking at AD risk genes. Of 44 AD risk genes that are enriched in microglia, only 29 have orthologs with a similarity larger than 60 % in mice. Among the genes that do not have convincing orthologs are important AD risk genes such as TREM2 (Hasselmann and Blurton-

Jones 2020; Mancuso et al. 2019). Apart from these genetic differences, human microglia were shown to age differently, have different gene expression patterns under homeostatic conditions and increased heterogeneity as compared to mouse microglia (Galatro et al. 2017; Geirsdottir et al. 2019; Masuda et al. 2019).

3.2.2 Chimeric mouse models

To overcome the aforementioned drawbacks of mouse microglia, several labs developed chimeric mice with xenotransplanted microglia. To this end, immunodeficient mice expressing human CSF1 were injected at a neonatal stage with iPSC-derived microglia or iPSC-derived microglial precursors (Abud et al. 2017; Fattorelli et al. 2021; Hasselmann et al. 2019; Mancuso et al. 2019; Svoboda et al. 2019). After transplantation, the microglia precursors stably integrate into the various regions of the brain and form a human microglial network (Hasselmann et al. 2019; Mancuso et al. 2019; Svoboda et al. 2019). Several studies showed that xenotransplanted human microglia are highly ramified, similar to human microglia *ex vivo* and functionally respond to stimuli such as LPS or focal laser injury, however differently to iPSC-derived microglia *in vitro* (Hasselmann et al. 2019; Svoboda et al. 2019). Transcriptomically, xenotransplanted human microglia closely resemble human microglia *ex vivo*, hence overcoming the prominent *in vitro* phenotype of all previously described model systems of human microglia (Hasselmann et al. 2019; Mancuso et al. 2019; Svoboda et al. 2019). When crossed with mouse models of AD, xenotransplanted microglia cluster around Aβ plaques where they downregulate homeostatic markers and adapt a disease-associated phenotype (Abud et al. 2017; Hasselmann et al. 2019). However, the microglial reaction to amyloid pathology was shown to differ between mouse and xenotransplanted human microglia. For example, Hasselmann et al. showed that only about one third of differentially-expressed genes (DEGs) found by Keren-Shaul et al in the classical DAM phenotype overlapped with the DEGs in xenotransplanted human microglia. Furthermore, Hasselmann et al. found hundreds of additional DEGs that were not part of the DAM signature, highlighting important differences between human and mouse microglia (Hasselmann et al. 2019; Keren-Shaul et al. 2017).

A novel approach that tries to improve xenotransplanted microglia was only published recently. Xenotransplanted microglia only interact with other brain cell types of mouse origin but lack interactions with human neurons and glia. In order to achieve the interaction of human microglia with other human brain cells *in vivo*, Schafer et al. xenotransplanted microglia-containing brain organoids into immunodeficient mice (Schafer et al. 2023). In contrast to the previously described xenotransplantation models, the mice for this transplantation approach did not require the expression of human cytokines due to interactions with other human brain cells (Hasselmann et al. 2019; Mancuso et al. 2019; Schafer et al. 2023). Xenotransplanted microglia within human brain organoids are actively

surveilling their environment, react to a focal laser injury and LPS and adapt a morphological appearance reminiscent of human microglia *ex vivo* (Schafer et al. 2023). Interestingly, the authors found that the human brain-like environment induced a human-specific microglial gene signature contrary to xenotransplanted microglia from Hasselmann et al. that still expressed some mouse-specific microglial genes indicating that the human brain environment shapes the phenotype of the transplanted microglia (Hasselmann et al. 2019; Schafer et al. 2023).

3.3 Comparison of model systems to investigate microglia

Model systems to investigate microglia can be divided into three main categories: 2D *in vitro* models, complex 3D *in vitro* models and *in vivo* models.

2D *in vitro* models of microglia, that include immortalized cell lines, primary microglia cultures and iPSC-models, are easily accessible for experiments and genetic manipulations (Hedegaard et al. 2020). Additionally, experiments with *in vitro* microglia can be performed at high throughput. However, *in vitro* models lack the complex 3D-architecture of the brain including cell-cell interactions that shape the microglial phenotype and transcriptome which differ significantly from *in vivo* microglia (Gosselin et al. 2017; Warden et al. 2023). Furthermore, *in vitro* models lack vascularization and interactions with the periphery of the brain (Hasselmann and Blurton-Jones 2020; Hedegaard et al. 2020). Hence, *in vitro* models of microglia are best suited to investigate basic cellular functions such as phagocytosis and secretion of cytokines (Hedegaard et al. 2020).

More complex *in vitro* systems to investigate microglia are cerebral organoids and OBSC. In contrast to 2D *in vitro* models they provide a more complex cellular architecture including multiple cell types and a brain-like organization (Hasselmann and Blurton-Jones 2020; Warden et al. 2023). Microglia in these models are transcriptomically less activated but still show artifacts of their *in vitro* culturing conditions (Ormel et al. 2018; Popova et al. 2021). Due to the more complex environment, they can be used to study cell-cell interactions between microglia and other cell types of the brain while combining this advantage with the previously mentioned easy accessibility for experiments and genetic manipulations (Hasselmann and Blurton-Jones 2020; Hedegaard et al. 2020; Warden et al. 2023).

The most complex model systems for microglia are *in vivo* models. ‘Pure’ mouse models and chimeric mice with xenotransplanted microglia are suited for complex modeling of diseases, allow for the investigation of brain region specific phenotypes of microglia and include a periphery of the brain that influences microglia (Hasselmann and Blurton-Jones 2020; Warden et al. 2023). On the one hand, xenotransplanted microglia resemble human microglia *ex vivo* as close as possible and can still be easily targeted for genetic manipulation (Hasselmann and Blurton-Jones 2020; Schafer et al. 2023; Warden

et al. 2023). On the other hand, chimeric mice need to be severely immunocompromised and experimental methods such as live cell imaging require complicated surgical procedures that limit the throughput of these experiments (Hasselmann et al. 2019; Mancuso et al. 2019; Schafer et al. 2023; Svoboda et al. 2019).

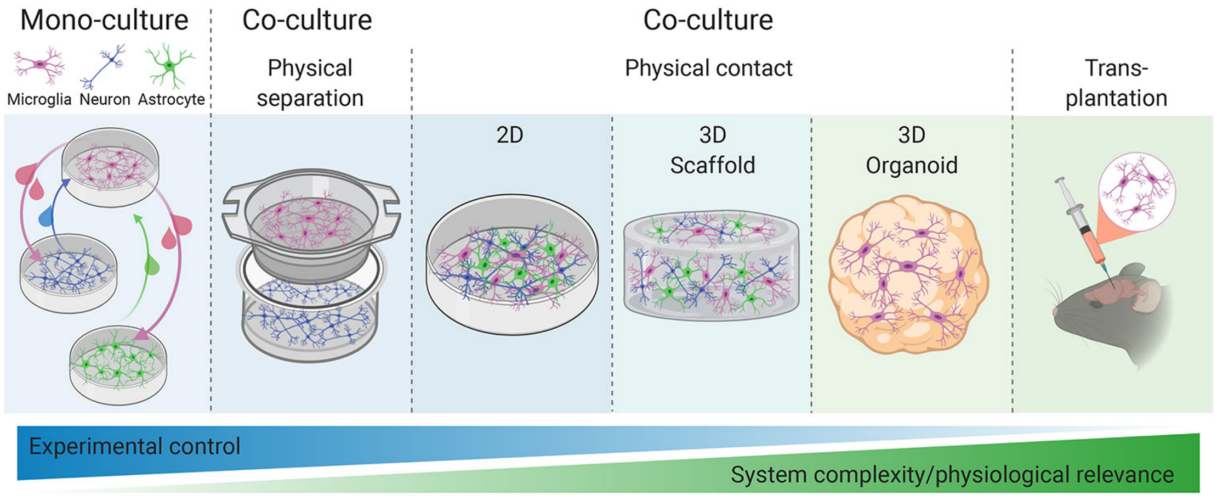

Figure 2.5 Model systems for microglia
Model systems for microglia range from comparably easy 2D cell culture models to complex xenotransplantation of iPSC-derived microglia into mice to study human microglia *in vivo*. With increasing complexity of the model system, the physiological relevance of the experiments increases but inversely, the experimental control over the model system decreases. From Hedegaard et al. 2020 published in Frontiers in Immunology under a Creative Commons CC-BY license (CC-BY 4.0)

In summary, *in vitro* models to investigate microglia guarantee as much control as possible over experimental parameters with high throughput but their reduced complexity leads to a reduced relevance. This is the opposite for *in vivo* models that are the most relevant model systems but are more difficult to control (Figure 2.5) (Hedegaard et al. 2020). Independent of the model system, species differences for microglia always need to be taken into consideration when planning experiments and interpreting results (Galatro et al. 2017; Geirsdottir et al. 2019; Hasselmann and Blurton-Jones 2020; Mancuso et al. 2019; Masuda et al. 2019).

4 Aims of the study

Microglia are organized in a brain-wide network with defined areas for each cell. It is generally recognized that microglia are very long-lived cells under homeostatic conditions, but that they proliferate in the event of injury or neurodegeneration. Depending on the brain region, most microglial cells survive the entire life of a mouse. Therefore, the death of microglial cells is a rare event during homeostasis but occurs more frequently in neurodegeneration. Whenever a microglial cell dies, a gap is created in the microglial network, so that the remaining cells must react to reoccupy the area of the dead cell. This process of homeostasis of the microglial network is not yet well understood.

The main goal of this work was to study how the microglial network is maintained. To this end, I pursued two approaches. The first step was to develop a novel mouse model that enables the selective ablation of individual microglia *in vivo*. The mouse model was designed so that a small percentage of microglia expressed diphtheria toxin receptor, making this subset of microglia susceptible to diphtheria toxin. Using 2-photon *in vivo* live imaging, I wanted to investigate the response of the microglial network after single cell death at different ages in the mouse brain.

Due to the complexity of *in vivo* models, a novel chimeric OBSC system (CSC) with human iPSC-derived microglia should be developed as a simplified model system for future investigation of the homeostasis of the microglia network under different conditions. For this purpose, human iPSC microglia should be transplanted onto microglia-depleted mouse OBSC. To establish this novel model system, I first sought to characterize CSC and compare the human microglia phenotype and network organization in CSC with human microglia *ex vivo* to demonstrate the suitability of the system for studying the microglia network. In addition, I aimed to induce neurodegenerative pathology in CSC by seeding with αsyn pff to confirm the suitability of CSC for modeling the microglial network response to neurodegeneration.

III Materials and Methods

1 General Materials

1.1 Antibodies and other compounds

1.1.1 Primary antibodies for immunofluorescence

Table 3.1 Primary antibodies for immunofluorescence

Antigen	Species	Dilution	Manufacturer	Antigen retrieval and Incubation Time
Iba1	goat polyclonal	1:250	Novus Biologicals NB100-1028	4°C ON
Iba1	rabbit polyclonal	1:250	Thermo Fisher Scientific PA521274	4°C ON
pS129	rabbit monoclonal	1:1000	AbCam ab51253	4°C ON
PU.1	rabbit monoclonal	1:250	Thermo Fisher Scientific MA5-15064	4°C ON
STEM101	mouse monoclonal	1:250	Takara Bio Y40400	4°C ON
tdTomato	goat polyclonal	1:250	SICGEN AB8181-200	4°C ON
TMEM119	rabbit polyclonal	1:100	AbCam ab185333	Antigen retrieval: Citrate Buffer + 0.05% Tween, 10 min 97 °C 4 °C, 3 days

1.1.2 Secondary antibodies for immunofluorescence

Table 3.2 Secondary antibodies for immunofluorescence

Antigen + Tag	Species	Dilution	Manufacturer	Incubation Time
Goat-Alexa 488	Donkey	1:250	Jackson ImmunoResearch 705-545-147	2 h at RT
Goat-Alexa 568	Donkey	1:250	Invitrogen A-11057	2 h at RT
Goat-Alexa 647	Donkey	1:250	Jackson ImmunoResearch 705-605-147	2 h at RT
Mouse-Alexa 488	Donkey	1:250	Jackson ImmunoResearch 715-545-150	2 h at RT
Mouse Alexa 647	Donkey	1:250	Jackson ImmunoResearch 715-605-151	2 h at RT
Rabbit-Alexa 488	Donkey	1:250	Jackson ImmunoResearch 711-545-152	2 h at RT
Rabbit-Alexa 568	Donkey	1:250	Invitrogen A10042	2 h at RT
Rabbit-Alexa 647	Donkey	1:250	Jackson ImmunoResearch 711-605-152	2 h at RT

1.1.3 Luminescent conjugated oligothiophenes

Table 3.3 Luminescent conjugated oligothiophenes

Name	Concentration used	Origin	Incubation Time
pFTAA	3 µM	Peter R. Nilsson Linköping, Sweden	30 min at RT
hFTAA	3 µM	Peter R. Nilsson Linköping, Sweden	30 min at RT

1.1.4 Antibodies for FACS

Table 3.4 Antibodies for FACS

Antigen + Tag	Species	Dilution	Manufacturer	Incubation Time
CD11b-Brilliant Violet785	Rat	1:100	BioLegend 101243	30 min 4°C
CD45-AF700	Rat	1:100	Bio-Rad Laboratories MCA1031A700T	30 min 4°C

1.1.5 Other antibodies

Table 3.5 Other antibodies

Antigen (+ Tag)	Species	Concentration	Manufacturer	Use
Mouse CSF1R	Rat	5 µg/ml	BioLegend 135539	Depletion of mouse microglia

1.2 Cell Culture Media and other chemicals

1.2.1 Cell culture media

Table 3.6 HSC preparation medium

Component	Manufacturer	Stock conc	Final conc
Minimum Essential Medium (-Phenolred)	Gibco 21935028	2x	1x
Glutamax	Gibco 35050-038	100x	1x
UltraPure Distilled Water	Invitrogen 10977035	-	-

Sterile filtered

Table 3.7 HSC culture medium

Component	Manufacturer	Stock concentration	Final concentration
Minimum Essential Medium	Gibco 32360034	1x	1x
Horse Serum (Heat-Inactivated)	Gibco 26050088	100 %	20 %
Glutamax	Gibco 35050-038	100x	0.5x
Ascorbic acid	Sigma-Aldrich A4403-100mg	25 %	0.00125 %
Insulin	Gibco 12585014	4 mg/ml	0.001 mg/ml
$CaCl_2$	Sigma-Aldrich 21115-100ml	1 M	1 mM
$MgSO_4$	Sigma-Aldrich 83266-100ml-F	2.5 M	2 mM
D-Glucose (water-free)	Roth X997.1		13 mM
Penicillin/Streptomycin	Gibco 15140122	100x	1x

pH = 7.28

Sterile filtered

Table 3.8 EB medium

Component	Manufacturer	Stock concentration	Final concentration
mTeSR+	Stem Cell Technologies 100-0276		
BMP4	Miltenyi Biotec 130-111-167	50 µg/ml	50 ng/ml
VEGF	Miltenyi Biotec 130-109-396	50 µg/ml	50 ng/ml
SCF	R & D Systems 255-SC-050	20 µg/ml	20 ng/ml
+Y-27632 on Day1	Stem Cell Technologies 72304	10 µM	10 nM

Table 3.9 EB differentiation medium

Component	Manufacturer	Stock concentration	Final concentration
X-Vivo15	Lonza		
h-M-CSF	Miltenyi Biotec 130-096-493	100 µg/ml	100 ng/ml
h-IL-3	Miltenyi Biotec 130-095-069	25 µg/ml	25 ng/ml
Penicillin/Streptomycin	Gibco 15140122	100x	1x
Glutamax	Gibco 35050-038	100x	1x
Beta-mercaptoethanol	Gibco 31350010	50 mM	55 µM

Table 3.10 iMic monoculture medium

Component	Manufacturer	Stock concentration	Final concentration
Dulbecco's Modified Essential Medium-F12	Gibco 12634010	1x	0.5x
Neurobasal A Medium	Gibco 10888-022	1x	0.5x
Beta-mercaptoethanol	Gibco 31350010	50 mM	50 µM
Glutamax	Gibco 35050-038	100x	1x
B27 Supplement with Vitamin A	Life Technologies 17504-044	50x	1x
h-M-CSF	Miltenyi Biotec 130-096-493	100 µg/ml	20 ng/ml
h-IL34	PeproTech 200-34	100 µg/ml	100 ng/ml

Table 3.11 Stempro Medium

Component	Manufacturer	Stock concentration	Final concentration
Stempro-34 SFM	Gibco 10639011		
Transferrin from human serum	Roche 10652202001		200 µg/ml
Glutamax	Gibco 35050-038	100x	1x
Penicillin/Streptomycin	Gibco 15140122	100x	1x
Ascorbic acid	Sigma-Aldrich A4403-100mg		0.5 mM

1-Thioglycerol	Sigma-Aldrich M6145		0.45 mM

Table 3.12 Serum-Free Differentiation Medium (SF-Diff)

Component	Manufacturer	Stock concentration	Final concentration
IMDM, GlutaMAX™ Supplement	Gibco 31980030		75 %
Ham's F-12 nutrient mix	Gibco 11765054		25 %
N-2 supplement	Gibco 17502001	100x	1x
B-27 supplement, serum-free	Gibco 17504001	50x	1x
BSA	Gibco 15260037	7.5 %	0.05 %
Penicillin/Streptomycin	Gibco 15140122	100x	1x

1.2.2 Buffers

Table 3.13 Dissection Buffer

Component	Manufacturer	Amount
1x HBSS	Self-made	10 ml
45 % D-Glucose	Self-made (0.9 g D-Glucose in 2 ml ddH_2O)	120 µl
DNAse I	SigmaAldrich	1 mg

Table 3.14 FACS buffer

Component	Manufacturer	Amount
1x HBSS	Self-made	48 ml
BSA 7.5 %	Gibco	666 µl (filtrated through 0.22 µm filter)
EDTA 0.5 M	Sigma-Aldrich	1 ml (filtrated through 0.22 µm filter)
Hepes 0.5 M	Roth	500 µl

Table 3.15 HBSS 10x

Component	Concentration
ddH_2O	Fill up to 1 l
NaCl	1.38 M
KCl	53.3 mM
KH_2PO_4	4.4 mM
Na_2HPO_4	3 mM
$NaHCO_3$	40 mM
Glucose	56 mM

1.2.3 Other chemicals

Table 3.16 Other chemicals

Compound	Manufacturer	Article number
Diphtheria toxin	Sigma-Aldrich	322326-1mg
Tamoxifen	Sigma-Aldrich	T5648-1g
NaCl 0.9% (for injections)	Pharmacy of the University Clinics Tuebingen	M25

LPS	Sigma-Aldrich	L6511-100mg
Calbryte 590	Biomol Feinchemikalien	ABD-20700
αSynuclein preformed fibrils	Ronald Melki Institut François Jacob, Fontenay-aux-Roses, France	-

1.3 Software

Table 3.17 Software and Plug-Ins

Software	**Source**
GraphPad Prism 9	GraphPad
R 4.3.1 & RStudio 2023.06.2+561	The R Foundation
FlowJo 10.6.2	FlowJo LLC
Imaris 9.7.2	Bitplane
FIJI 2.1.0/1.53c	Schindelin et al. 2012
Time Series Analyzer v3 for FIJI	https://imagej.nih.gov/ij/plugins/time-series.html
Huygens Essential 20.04	Scientific Volume Imaging B.V.
Serial Cloner 2.6.1	Serial Basics
SnapGene Viewer 7.0.2	SnapGene by Dotmatics

1.4 Statistics

All statistical analyses including the creation of figures were performed with either R or GraphPad Prism 9 (GraphPad Software, San Diego, California USA). Individual datapoints represent biological replicates with one to three technical replicates each, depending on the experiment. Error bars represent the standard error of the mean (SEM). P-values smaller than 0.05 were considered significant.

2 New mouse model does not allow to induce targeted microglia cell death to investigate microglial network homeostasis *in vivo*

2.1 Mice

2.1.1 Mice and breeding scheme

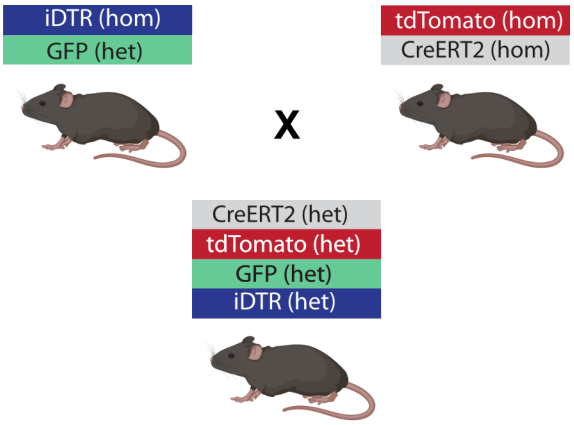

Figure 3.1 Breeding scheme of tdTom x iDTR mice
Breeding scheme of tdTom x iDTR mice. The Iba1-GFP transgene could only be bred heterozygously due to sterility of homozygotes. The two transgenes on the ROSA26 locus were introduced from two different homozygous lines to reduce excessive animals of an unwanted genotype.

For breeding of mice used for the targeted ablation of individual microglia, B6.Cg-Gt(ROSA)26Sor$^{tm14(CAG-tdTomato)Hze}$/J mice (R26-tdTomato; JAX number 007914) (Madisen et al. 2010) crossed to CD11b-CreERT2 mice (Füger et al. 2017), heterozygous B6.Cg-Tg(Aif1-EGFP)1Kohs/J- (short: Iba1-EGFP) (Hirasawa et al. 2005) mice and Iba1-EGFP mice crossed to B6-Gt(ROSA) 26Sor$^{tm1(HBEGF)Awai}$/J (R26-iDTR) (Buch et al. 2005) were used. The lines used in the experiment were crosses from these lines. First, the triple transgenic mice used in Füger et al. were bred by crossing R26-tdTomato (hom) x CD11b-Cre (hom) with Iba1-EGFP mice (het). Furthermore, a new 4x transgenic mouse line was bred for the second line used in the *in vivo* imaging experiments. R26-iDTR mice were crossed with Iba1-EGFP mice to obtain R26-iDTR (hom) x Iba1-EGFP mice (het) mice that were then crossed with R26-tdTomato (hom) x CD11b-Cre (hom) mice into a new 4x transgenic mouse line which was heterozygous for all four transgenes (Figure 3.1; called tdTom x iDTR mice). Both, male and female mice were included in all experiments. All animal experiments were performed in accordance with German Animal Protection Laws and were registered as N 08/19 G.

2.1.2 Mouse genotyping

Newborn animals were separated from their mother at 21 days of age into cages with all female or all male littermates. During this process, mice were marked with ear tags and the tissue from the marking

process was used for subsequent genotyping. DNA from tissue samples was extracted using the REDExtract-N-Amp™ Tissue PCR Kit (Sigma-Aldrich) according to the manufacturer's instructions. Presence of the transgene was tested via PCR and analyzed with a QIAxcel Advanced (Qiagen) with the QIAxcel DNA screening kit and the QIAxcel ScreenGel 1.5.0 software. For primers and protocols see the following sections:

R26-tdTomato	-	Section X.1.1
CD11b-CreERT2	-	Section X.1.2
R26-iDTR	-	Section X.1.3
Iba1-EGFP	-	Section X.1.4

2.1.3 Mouse injections

250 mg tamoxifen (Sigma-Aldrich) were dissolved in 25 ml corn oil (Sigma-Aldrich) while heating to 37 °C at 10 µg/µl and aliquots of 1 ml were stored at -20 °C. Aliquots were thawed and heated on a heating pad just before injection to reduce viscosity. Mice were injected intraperitoneally (i.p.) with 100 µg/g body weight tamoxifen twice 48 hours apart at the age of three months.

Diphtheria toxin (DT) (Sigma-Aldrich; 322326) was dissolved in 0.9 % NaCl injection solution at 1 mg/ml. Aliquots of 10 µl were stored at -80 °C. For injections, DT-stock was diluted 1:500 in 0.9 % NaCl injection solution and mice were injected i.p. with a total of 500 ng DT in a volume of 250 µl for five consecutive days. As vehicle control, mice were injected with 0.9 % NaCl injection solution as described above.

2.1.4 Cranial window surgery

For implantation of a cranial window, the surgical procedure was performed as described by Hefendehl et al. 2012. Mice were anesthetized with a mix of Fentanyl (0.05 mg/kg bodyweight), Midazolam (5 mg/kg bodyweight), Medetomidin (0.50 mg/kg bodyweight) in H_2O administered by i.p. injection. Additionally, preoperative analgesia was subcutaneously injected (Carprofen 5 mg/kg bodyweight). The depth of the anesthesia was assessed by testing for reflexes between the toes and once a deep anesthesia of the mice was assured, local anesthesia was applied subcutaneously with 0.05 ml of 2% Lidocain. Then, mice were placed on a heating pad to keep the body temperature stable and the head was fixed in a stereotactic frame. Eye ointment was applied to both eyes to prevent the eyes from drying out. After shaving the site of the surgery, a first midline incision of the skin was made from the neck to the front in between the eyes. Once the skin was moved towards the sides to expose the skull, the lateral muscles on each side of the skull were gently lifted from the skull. Next the entire surface of the skull was gently drilled and scratched with a forceps to roughen the surface for better long-term stability of the glue. Then, an adhesive (iBond, Heraeus) was applied onto the skull and to the sides

where the lateral muscles were lifted earlier and subsequently hardened with UV-light for 20 seconds. Next, venus flow dental cement (Dental Bauer) was applied to the sides and hardened with UV-light for 20 seconds. Afterwards, a custom-made coverslip (4 mm diameter, 0.13-0.16 mm thickness) was placed onto the skull in order to outline the region for the craniotomy with forceps for the subsequent drilling. Then the skull was drilled along the marked outline until only a very thin part of the skull remained. During the drilling process, the drill was permanently moved around and short breaks were done to avoid over-heating. The thickness of the remaining skull was tested by gently trying to push the center of the craniotomy with the back of forceps. Once the skull could be pushed down easily, tiny holes were carefully poked into the skull on both sides of the craniotomy while avoiding damage to the dura mater. PBS was dropped onto the craniotomy in order to flow through the tiny holes in the skull. This process separated the dura mater from the skull and allowed for the gentle removal of the skull with forceps without damaging the dura. Then, a new, heat-sterilized coverslip was placed onto the craniotomy and carefully pushed onto the brain. More dental cement was used to fix the coverslip and to connect the newly applied cement with the previously applied cement. The cement was hardened for one minute with UV light. Lastly, a custom-made titanium ring which allowed for stable repositioning during imaging was fixed with dental cement on the existing thin layer of cement on top of the skull and around the cranial window and hardened with UV light for one minute. If necessary, the skin of the mice was sutured and the antidot for the anesthesia was applied. The antidot consisted of Flumazenil (0.5 mg/kg bodyweight), Atipamezol (2.5 mg/kg bodyweight), Buprenorphin (0.1 mg/kg bodyweight) in H_2O administered by subcutaneous injection. Mice were monitored until they woke up and were fully mobile. Postoperative analgesia (Carprofen 5 mg/kg bodyweight) was administered subcutaneously twice per day for the first three days and subsequently according to the individual needs of the mice but at least every second day for a total of ten days after the surgery. During the first ten days after surgery wet food pellets were added into the cage to improve recovery of the mice from the surgical procedure. After the surgery, mice were kept alone in their cages to prevent injuries to the surgery site.

2.1.5 Mouse preparation and brain fixation

In order to prepare mice and isolate the brain, the animals were sacrificed with a lethal dose of ketamine (250 mg/kg bodyweight) and xylazine (20 mg/kg bodyweight) in 0.9 % NaCl. Once the mice died from the overdose, they were immediately transcardially perfused with ice-cold PBS. Then, the brain was removed and fixed in 4 % PFA for 48 hours. After fixation, brains were cryoprotected in 30 % sucrose for another 48 hours and snap-frozen in 2-Methylbutane until further processing.

2.2 Imaging

2.2.1 2-Photon in vivo imaging

2-Photon *in vivo* imaging was performed at a Leica DMLFS microscope equipped with a TCS SP2 scan head (Leica Microsystems, Bensheim, Germany) and a Spectra Physics (San Jose, California) MaiTai eHP laser. To achieve excitation of both EGFP and tdTomato, the MaiTai eHP laser was tuned to 1000 nm. A 25× HCX IRAPO water-immersion objective (0.95 NA; Leica Microsystems) was used for detection.

Earliest one week after cranial window surgery, mice were used for 2-Photon *in vivo* imaging. Anesthesia of mice was introduced with 3 % Isoflurane vapor mixed in pure oxygen. Once mice were deeply anesthetized, the window was cleaned with water and the titanium ring on the head was fixed to a custom-made head fixation system which was attached to the motorized stage of the microscope to enable precise relocalization of previously identified regions of interest (ROI) (Hefendehl et al. 2012). During imaging, mice were placed on a heating pad and deep anesthesia was maintained with 1 to 1.5 % Isoflurane vapor mixed in pure oxygen. Anesthesia was monitored closely during the entire imaging. Imaging was performed for a maximum of one hour per imaging session which was usually sufficient to image six ROIs.

2.2.2 Brain sectioning

Fixed brains were sectioned at 25 µm using a freezing-sliding microtome (SM2000 R; Leica Biosystems). The sections were collected in a 12-well plate with cryoprotection solution (35% ethylene glycol and 25% glycerol in PBS) to collect every 12^{th} section in one well.

2.2.3 Immunofluorescent staining and imaging

Sections were carefully mounted onto TOMO adhesive glass slides with a brush and dried for 1 hour at 37 °C or overnight at room temperature. Slides were blocked for two hours at room temperature in 5 % Normal Donkey Serum + 0.3 % Triton X-100 in PBS and subsequently incubation with the primary antibodies was performed in 2 % Normal Donkey Serum + 0.3 % Triton X-100 in PBS. Incubation conditions and antibody dilutions are indicated in Table 3.1. After incubation with the primary antibodies, slides were washed three times in PBS for 15 minutes each before secondary antibody incubation. Slides were incubated with secondary antibodies in 1 % Normal Donkey Serum + 0.3 % Triton X-100 in PBS for two hours at room temperate and finally washed again three times in PBS for 15 minutes. Finally, slides were dried for 15 minutes at 37 °C and coverslipped with Dako Fluorescence Mounting Medium. Slides were dried for 24h at RT before storage at 4°C.

Confocal images were acquired using an upright Zeiss LSM 880 NLO microscope with ZEN Black Software (Zeiss). All images were obtained using a water-immersion x20 Objective (W Plan-Apochromat x20/1.0, Carl Zeiss, Jena. To depict the morphology of microglia, z-stack images were acquired and maximum intensity projections were generated.

2.3 Image analysis

2.3.1 Analysis of immunofluorescent staining

In order to analyze the recombination rate of microglia, confocal images were imported into the Imaris software version 9.7.2 (Bitplane). Iba1 or tdTomato signal from the soma was semi-automatically reconstructed using the 'Spots' function of Imaris with a diameter of the 'Spots' which was as a large as the soma of a microglia. The number of somata per channel was then determined in order to calculate the percentage of tdTomato-positive microglia in relation to the total amount of microglia.

All images for figures were created with FIJI as maximum intensity projections.

2.3.2 Analysis of 2-Photon in vivo *imaging*

Huygens Essential (Scientific Volume Imaging B.V., Hilversum) was used to deconvolve all images acquired with 2-Photon live-cell imaging before further processing.

Then, all images of one ROI were imported into Imaris and fused into one movie of the position. Despite the stable head-fixation system, a small drift was visible between every two images that was corrected by reconstructing the soma of all tdTomato-positive microglia in all frames and using this reconstruction as a stable reference point for drift correction.

All images for figures were created with FIJI as maximum intensity projections.

2.4 FACS

2.4.1 Microglia isolation for FACS

In order to isolate microglia for FACS, mice were prepared as described above (see section III.2.1.5). Next, the skull was opened to remove the brain and the olfactory bulb and cerebellum were removed. Then, the brain was transferred into a petri dish with 1 ml of dissection buffer (Table 3.13) and minced with a scalpel before being transferred to Dounce homogenizers (Wheaton) in a total of 2 ml dissection buffer. After homogenization, the cell suspension was filtered through a 70 µm cell strainer into a 15 ml Falcon and centrifuged for 20 minutes at 300g without break. During centrifugation, isoprecoll solution was prepared (1 ml 10x HBSS + 9 ml Percoll (GE Healthcare)) and a gradient of 30 % Percoll, underlaid with 37 % Percoll with phenol red was prepared. Afterwards, the cell pellet was resuspended

in 5 ml 70 % Percoll and the gradient was underlaid by the 5 ml cell suspension before a gradient density centrifugation was performed at 800 g for 30 minutes without break. Microglia were enriched in the interphase between 37 % and 70 % Percoll and collected with a pipette. The microglia cell suspension was transferred into a new 15 ml Falcon and washed with FACS buffer (Table 3.14) by centrifugation at 300 g for 20 minutes without break. Subsequently, the supernatant was discarded and the residual volume was reduced to 200 µl. Microglia were resuspended in the residual volume and transferred into a 1.5 ml low-binding Eppendorf tube (Eppendorf). In order to stain microglia for FACS, the cell suspension was blocked with 1:100 mouse Fc block (BD Biosciences) on a spinning rotor at 4 °C. After 10 minutes, CD11b-Brilliant Violet 785-coupled (BioLegend) and CD45-A700-coupled (BioLegend) antibodies were added at a dilution of 1:100 and incubated for another 30 minutes at 4 °C. Subsequently, the cell suspension was washed once with FACS buffer by centrifugation at 300 g for 10 minutes and resuspended in 500 µl FACS buffer for FACS analysis.

2.4.2 FACS

FACS of microglia was performed at a Sony SH800. First, gating was performed to use only live cells for the subsequent gating with the forward scatter and the side scatter (Figure 3.2 A), then, cell doublets were removed using the forward scatter (Figure 3.2 B), before sorting microglia based on their expression of CD11b and CD45. All cells that showed high levels of CD11b, $CD11b^{high}$ and intermediate levels of CD45, $CD45^{intermediate}$ were considered microglia. Due to the tdTom-positive microglia that caused fluorescent bleedthrough into the CD45-channel, a second subpopulation with increased CD45 signal was visible on the right within the selected polygon (Figure 3.2 C). Lastly, microglia were sorted based on their endogenous EGFP and tdTomato fluorescence. A ‘GFP only’ and a ‘tdTom’ subpopulation were sorted into 1.5 ml low-bind Eppendorf tubes and stored at -80 °C for subsequent experiments. Unstained samples were used as gating controls.

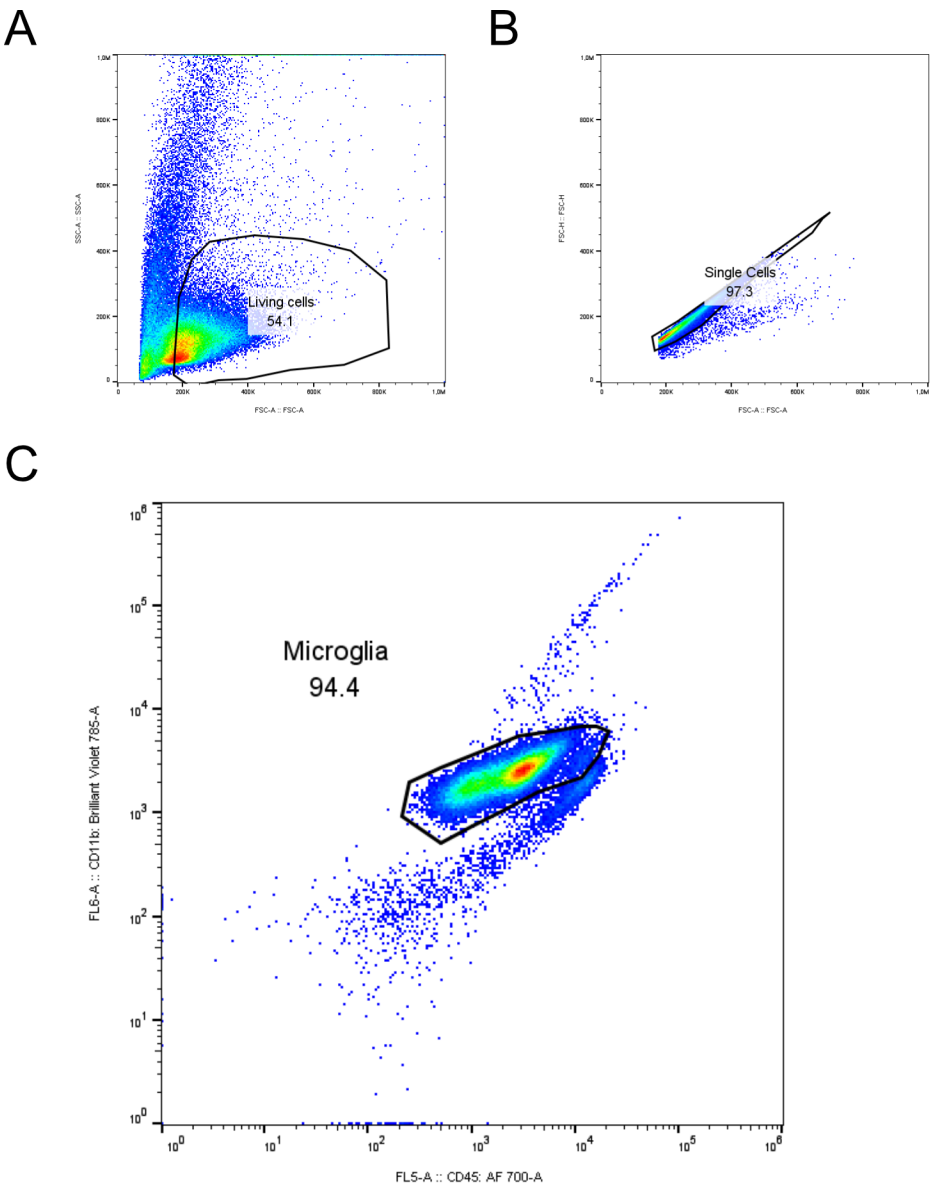

Figure 3.2 FACS gating
(A) Gating for living cells with forward scatter area plotted on the x-axis and side scatter area plotted on the y-axis. The gating is indicated as black polygon. **(B)** Gating for single cells to exclude doublets. Forward scatter area is plotted on the x-axis and forward scatter height is plotted on the y-axis. The gating is indicated as black polygon. **(C)** Gating for microglia as $CD11_b^{high}$ (y-axis)/ $CD45^{intermediate}$ (x-axis) cells. Gating is indicated as black polygon. Please note the second subpopulation on the right within the selected polygon which were tdTom-positive microglia that caused fluorescent bleedthrough into the CD45-channel.

2.5 PCR

2.5.1 DNA isolation

DNA from microglia sorted into 1.5 ml low-bind Eppendorf tube was isolated with a DNeasy Blood & Tissue Mini Kit (Qiagen) according to the manufacturer's instructions. DNA was stored at -20 °C until subsequent experiments were performed.

2.5.2 Primer and Protocols

Primers were designed using Serial Cloner 2.6.1 (Serial Basics).

Control PCR

```
ROSA26-F:     5’AAA GTC GCT CTG AGT TGT TAT 3’
ROSA26-tg_R: 5’CAT CAA GGA AAC CCT GGA CTA CTG 3’
```

Table 3.18 PCR mix Control PCR

ROSA26-F	0.2 µl
ROSA26-tg_R	0.2 µl
Mastermix (Sigma-Aldrich)	10 µl
	10.4 µl
Cell lysate	9.6 µl
	20 µl

1.	Incubate at	94 °C	for	2´
2.	Incubate at	94 °C	for	45 s
3.	Incubate at	60 °C	for	45 s
4.	Incubate at	72 °C	for	1´

Repeat steps 2 – 4 35 more times

5.	Incubate at	72 °C	for	2´
6.	Incubate at	4 °C	forever	

Product: 241 bp

The primers for the control PCR were designed to be specific for the ROSA26-iDTR transgene and would not generate a product for the ROSA26-tdTomato transgene.

No recombination PCR

STOP-F1: 5’AGG CTA CTG CTG ACT CTC AAC 3’

DTR-R1: 5’GCT GGT CCG TAG ATC CAG TG 3’

Table 3.19 PCR mix No recombination PCR

STOP-F1	0.2 µl
DTR-R1	0.2 µl
Mastermix (Sigma-Aldrich)	10 µl
	10.4 µl
Cell lysate	9.6 µl
	20 µl

1. Incubate at 94 °C for 2´
2. Incubate at 94 °C for 45 s
3. Incubate at 60 °C for 45 s
4. Incubate at 72 °C for 90 s

Repeat steps 2 – 4 35 more times

5. Incubate at 72 °C for 2´
6. Incubate at 4 °C forever

Products: No recombination: 840 bp

Recombination: No product due to the removed STOP-F1 binding sequence

Recombination PCR

DTR-Cre-F: 5’GTC CAG GGT TTC CTT GAT GAT G 3’

DTR-Cre-R: 5’CTG AGA TCC GGG TGG GAA TTA G 3’

Table 3.20 PCR mix Recombination PCR

DTR-Cre-F	0.2 µl
DTR-Cre-R	0.2 µl
Mastermix (Sigma-Aldrich)	10 µl
	10.4 µl
Cell lysate	9.6 µl
	20 µl

1.	Incubate at	94 °C	for	2´
2.	Incubate at	94 °C	for	45 s
3.	Incubate at	59 °C	for	45 s
4.	Incubate at	72 °C	for	90 s

Repeat steps 2 – 4 35 more times

5.	Incubate at	72 °C	for	2´
6.	Incubate at	4 °C	forever	

Products: No recombination: 4.6 kbp → not amplified due to short elongation period

Recombination: 801 bp

2.5.3 QIAxcel

Analysis of the PCR products was performed with a QIAxcel Advanced (Qiagen) with the QIAxcel DNA screening kit and the QIAxcel ScreenGel 1.5.0 software and compared to the projected PCR products from Serial Cloner 2.6.1.

2.6 Sanger sequencing

The PCR products of the 'Recombination PCR' were also used for Sanger sequencing of the products. To this end, the PCR DNA products were purified with a QIAquick PCR Purification Kit (Qiagen) according to the manufacturer's instructions. The sequencing primers were the same as used for the PCR amplification of the 'Recombination PCR' (DTR-Cre-F and DTR-Cre-R). Purified DNA samples together with the sequencing primers were sent to LGC genomics, Berlin for Sanger sequencing. Resulting chromatograms and sequences were analyzed using SnapGene Viewer 7.0.2 (SnapGene by Dotmatics) and Serial Cloner 2.6.1.

3 Development of a novel chimeric *in vitro* model to investigate human microglial network homeostasis and neurodegeneration

3.1 Induced pluripotent stem cells

3.1.1 iPSC culture

Different lines of human induced pluripotent stem cells (iPSC) were used for the described experiments (Table 3.21). iPSC were cultured on Geltrex -coated (Thermo Fisher Scientific) 6-well plates (Corning) in mTeSR$^+$ medium (Stemcell Technologies) at 37 °C and 5 % CO_2. Medium was changed after one day in culture (or after splitting) and subsequently every other day. Once about 80 % confluency was reached, iPSC were split using ReLeSR (Stemcell Technologies) for five minutes or used for differentiation. For the first day after splitting, 10 µM Y27632 (Rock inhibitor, Stemcell Technologies) was added to the medium to improve survival of iPSC.

Table 3.21 iPSC lines

Line	Origin
BIONi010-C	European Bank for Induced Pluripotent Stem Cell
BIONi010-C CAG-GFP	European Bank for Induced Pluripotent Stem Cell + CRISPR-edited in-house
KOLF2.1J (including CSf1R mutants)	The Jackson Laboratory
K5	Prof. Stefan Liebau, University of Tuebingen

3.1.2 iMic differentiation

iPSC-derived microglia (iMic) were differentiated as described by Haenseler et al. 2017 with minor changes. Once 80 % confluency of the iPSC was reached, the cells were washed once with PBS and then detached with ReLeSR for five minutes. Cells were then collected in DMEM/F12 (Gibco) + 0.1 % BSA (Gibco) (wash buffer) and centrifuged at 300 g for five minutes in a Heraeus Multifuge 3-SR. After aspiration of the supernatant, the iPSC-pellet was resuspended in 1 ml of EB medium (Table 3.8) and the cell number was counted with a Neubauer counting chamber (Neubauer Zählkammer Improved, Bard). In the meantime, an AggreWell800 plate in a 24-well plate format (Stemcell Technologies) was prepared. To this end 500 µl anti-adherence rinsing solution (Stemcell Technologies) was added to each well to be used and centrifuged at 1,300 g for five minutes. The anti-adherence solution was aspirated, each well was washed with 2 ml of wash buffer and 1 ml of EB medium was added.

Afterwards, in order to create embryoid bodies (EB), 3,000,000 iPSC were seeded into each of the prepared wells in another 1 ml of EB medium for a total of 2 ml EB medium per well supplemented with 10 µM of Y27632 for the first day. Subsequently, the cells were centrifuged at 800 g for three minutes without brake. EBs were kept at 37 °C and 5 % CO_2 and a partial medium exchange (75 %) was performed daily.

After five days, EBs were transferred from the AggreWell800 plate into 12 wells of 6-well plates in 2 ml EB Differentiation Medium (Table 3.9). To this end, EBs were flushed out of the microwells with a serological pipette and transferred into a 50 ml Falcon with EB Differentiation Medium where they were allowed to settle to the bottom of the falcon for a few minutes. Then, the medium was aspirated, the EBs were resuspended in EB Differentiation Medium and equally distributed (about 15 EBs per well). From here on, EBs were kept at 37 °C and 5 % CO_2 with weekly medium exchange.

Alternatively and only for one experiment, iMics were differentiated as described by Takata et al. 2017. In brief, once 80 % confluency of the iPSC was reached, the cells were washed once with PBS and then detached with ReLeSR for five minutes. Cells were then collected in DMEM/F12 (Gibco) + 0.1 % BSA (Gibco) (wash buffer) and centrifuged at 300 g for five minutes in a Heraeus Multifuge 3-SR. After aspiration of the supernatant, the iPSC-pellet was resuspended in 1 ml of mTeSR$^+$ medium and the cell number was counted with a Neubauer counting chamber (Neubauer Zählkammer Improved, Bard). Afterwards 10,000 cells per well were plated onto a Matrigel-coated (Corning) 6 well plate in Stempro Medium (Table 3.11) supplemented with the following cytokines during the differentiation process: Differentiation Day 0 (5 ng/mL BMP4, 50 ng/mL VEGF, and 2 µM CHIR99021 (Miltenyi Biotec)), Differentiation Day 2 (5 ng/mL BMP4, 50 ng/mL VEGF, and 20 ng/mL FGF2 (Miltenyi Biotec)), Differentiation Day 4 (15 ng/mL VEGF and 5 ng/mL FGF2), Differentiation Day 6 to 10 (10 ng/mL VEGF, 10 ng/mL FGF2, 50 ng/mL SCF, 30 ng/mL DKK-1 (), 10 ng/mL IL-6 (), and 20 ng/mL IL-3), Differentiation

Day 12 and 14 (10 ng/mL FGF2, 50 ng/mL SCF, 10 ng/mL IL-6, and 20 ng/mL IL-3). From Differentiation Day 16 on, the cells were fed with SF-Diff (Table 3.12) supplemented with 50 ng/mL h-M-CSF. A full medium exchange was performed every 3 days. Around Differentiation Day 20 to 25, when floating cells occurred, these cells were used for experiments. Until Differentiation Day 8, the cells were cultured in a hypoxia incubator at 37 °C with 5 % CO_2 and 5 % O_2 and were cultured at 37 °C with 5% CO_2 in normoxic conditions afterwards.

3.1.3 iMic precursor harvesting

After two to three weeks of differentiation in EB Differentiation Medium, EBs started to produce free-floating microglial precursor cells (pre-iMics). Pre-iMics were harvested weekly by collecting the supernatant cell culture medium during medium exchange. The cell culture medium was then filtered through a cell strainer (40µm, Greiner) to avoid a loss of EBs and the contamination of pre-iMics with EBs. The cell suspension containing the pre-iMics was centrifuged for five minutes at 300 g, the supernatant was aspirated and the pre-iMics were resuspended in 1 ml of iMic monoculture medium (Table 3.10) before determining the cell number with a Neubauer chamber. The desired amount of pre-iMics was then either plated for monoculture or transferred into an Eppendorf tube and centrifuged again at 300 g for five minutes for subsequent grafting onto HSC. The supernatant was aspirated and the cells were resuspended at a density of 10,000 cells/µl.

3.1.4 iMic monocultures

After harvesting of pre-iMics, the cells were plated in 6-wells plates at 100,000 pre-iMics per well in 2 ml iMic monoculture medium. iMic monocultures were kept at 37 °C and 5 % CO_2 and the medium was fully exchanged three times per week. After two weeks, iMics in monoculture were considered as differentiated cells.

3.2 Hippocampal slice cultures

3.2.1 Mice

For the preparation of hippocampal slice cultures (HSC), C57BL/6J (Jackson), heterozygous B6.Cg-Tg(Aif1-EGFP)1Kohs/J- (short: Iba1-EGFP) (Hirasawa et al. 2005) and heterozygous Thy1-hA53T-αSyn (short A53T) (van der Putten et al. 2000) were used. All animal experiments were performed in accordance with German Animal Protection Laws and were registered as N 04/19 M and N 03/20 G.

3.2.2 Mouse genotyping

To determine the genotype of Iba1-EGFP mice, prepared HSC were put under a standard fluorescence microscope and checked for fluorescence in the green channel. In order to genotype HSC from Thy1-hA53T-αSyn mice, a tail biopsy was obtained from the dead animal during the preparation process and used for subsequent genotyping. DNA from tissue samples was extracted using the REDExtract-N-Amp™ Tissue PCR Kit (Sigma-Aldrich) according to the manufacturer's instructions. Presence of the transgene was tested via PCR using the primers and PCR settings as indicated in section X.1.5 and analyzed with a QIAxcel Advanced (Qiagen) with the QIAxcel DNA screening kit and the QIAxcel ScreenGel 1.5.0 software.

3.2.3 Slice culture preparation and maintenance

HSC were prepared according to previously published protocols (Daniel et al. 2005; Novotny et al. 2016). Mouse pups, four to six days after birth, were decapitated using scissors. Next, the skull was exposed and carefully opened to remove the brain. Then, the brain was transferred into a Petri dish containing HSC preparation medium (Table 3.6) for further dissection. The hippocampi were removed and chopped into 350 µm thin slices using a tissue chopper (McIlwain). All slices were collected in a new dish with HSC preparation medium. Only intact slices were transferred onto sterile Millicell Cell Culture Inserts (Merck) (3-4 slices/insert) in 6-well plates (Corning) with 1.2 ml pre-warmed HSC culture medium (Table 3.7). The entire procedure was performed in a semi-sterile laminar flow hood. Usually, 18 to 24 intact slices were generated per pup. The cultures were kept at 37 °C and 5 % CO_2 with full medium exchange three times per week.

3.2.4 Microglia depletion and iMic grafting

In order to deplete endogenous mouse microglia from HSC, a mouse specific anti-CSF1R antibody (BioLegend, 5µg/ml) was added to the HSC culture medium. If not otherwise noted, the antibody treatment was performed throughout the entire experiment. Upon creation of a niche for microglial integration, pre-iMics were harvested as described above (see section III.3.1.3) and drop grafted onto HSC at 2-5 DIV of the HSC. To this end, pre-iMics were concentrated at 10,000 cells/µl and 1 µl of the cell suspension was added on top of each culture in order to create chimeric hippocampal slice cultures (CSC). Before the start of subsequent experiments, iMics were allowed to integrate and differentiate for at least 14 days.

3.2.5 Slice culture fixation

To fix HSC for subsequent immunofluorescent staining, HSC culture medium was aspirated, HSC were washed once with PBS and then fixed with 1.2 ml of 4 % PFA each underneath and on top of the insert for 2 hours at room temperature. After fixation, the PFA was removed and the HSC were washed three times for 15 min with PBS and subsequently stored at 4 °C in PBS for up to one month.

3.2.6 LPS treatment

After the generation of CSC at 14 DIV, a 'chronic' 7-day treatment with 25 ng/ml lipopolysaccharide (LPS) was started. 24 hours before the start of the treatment, HSC culture medium was refreshed and collected at the start of the treatment as 'baseline' sample. LPS was added for another three media changes on days 2, 4 and 6 six of the treatment. On day 5 of the 'chronic' LPS treatment, the HSC culture medium of different CSC derived from the same pup was refreshed and collected at treatment onset for an 'acute' LPS stimulus at 200 ng/ml on day 6 of the 'chronic' LPS treatment (corresponding to 20 DIV of the CSC). The experiment was terminated 24 hours after application of the 'acute' LPS stimulus for all conditions and the culture medium was collected for subsequent measurements.

3.2.7 Pff treatment

α-synuclein (αsyn) pathology was induced in HSCs 42 days after iMics were engrafted by α-synuclein pre-formed-fibrils (pff) (gifted by Ronald Melki) as described in Barth et al. 2021. In brief, 1 µl of 0.5 µg/µl αsyn-pff was added onto each CSC once and the cultivation was continued as usual. To analyze the progression of αsyn pathology and iMic responses, CSCs were either fixed at 3- and 5-weeks post-seeding with 4% PFA as described above (see section III.3.2.5) or used for scRNAseq as described below (see section III.3.3). Furthermore, HSC culture medium was collected 48 hours, 3 and 5 weeks after seeding for cytokine measurements.

3.2.8 Human brain slices

Healthy human access brain tissue was obtained from resective tumor surgeries in cooperation with the university hospital Aachen, sliced at 250 µm per slice and fixed in 4 % PFA, as described in Schwarz et al. 2017 and 2019. Informed written consent of the patients for tissue donation for scientific use was collected before surgery and approval of the institutional ethics board was obtained before the study (EK067/20). The donor patients, both male (50 and 66 years old) were both operated for removal of a tumor.

3.3 Sequencing

3.3.1 Microglia isolation

For single-cell RNA sequencing (scRNAseq) of iMics in CSC, iMics were isolated from CSC at 21, 42 and 77 DIV (with and without αsyn pff treatment) and compared to pre-iMics. For one biological replicate slices from 2.5 to 4 plates of CSC were pooled. Two biological replicates per group were used and pooled for the final scRNAseq analysis. CSC were carefully removed from the inserts using a cell lifter (VWR) and transferred to Dounce homogenizers (Wheaton) in 2 ml Dissection buffer as described above. After homogenization, the cell suspension was filtered through a 70 µm cell strainer into a 15 ml Falcon and centrifuged for 15 minutes at 400g without break. After centrifugation the supernatant was discarded and the cell pellet was resuspended in 80 µl of buffer from a mouse cell depletion kit according to the manufacturer's instructions (Miltenyi, 130-104-694). Afterwards, mouse cells were depleted according to the manufacturer's instructions. The remaining cells were centrifuged for 10 minutes at 400g and the pellet was resuspended in 100 µl of buffer. Then, the cell suspension was transferred into a low-bind 1.5 ml Eppendorf tube, the cell number was determined using a Neubauer counting chamber and the cell suspension was centrifuged for 10 minutes at 400g. The pellet was resuspended in PBS + 0.04 % BSA at 1000 cells per µl.

3.3.2 RNA library generation and single-cell RNA sequencing

A 10x scRNAseq library of the cell suspension was generated using the Chromium Next GEM Single Cell 3' Kit v3.1 kit on a Chromium Controller X with a Next GEM Chip G and a Dual Index Plate TT Set A according to the manufacturer's instructions. Quality control was performed as recommended with an Agilent TapeStation4200 D5000 High Sensitivity ScreenTape.

Further steps in the library generation were performed at the NGS Competence Center Tübingen using the NEBNext® Single Cell/Low Input RNA Library Prep Kit for Illumina® kit (New England BioLabs). scRNAseq was performed with the Illumina NovaSeq 6000 system and the NovaSeq 6000 SP Reagent Kit v1.5 (Illumina) at the NGS Competence Center Tübingen.

3.3.3 Single-cell RNA sequencing analysis

Analysis of scRNAseq data was performed at the Zentrum für Quantitative Biologie (QBiC) Tübingen by Dr. Jun-Hoe Lee. CellRanger analysis pipeline (v7.1.0) was used to process the 10x genomics single-cell RNA-sequencing data. Read alignment to the reference was performed and a matrix containing UMI counts per gene per cell (gene expression matrix) was generated. For dimensionality reduction analysis the Seurat R package (v4.3.0) was used. For cell clustering, the k-nearest neighbors of each cell were

determined based on Euclidean distance in PCA space, and the edge weights between any two cells were refined based on the shared overlap in their local neighborhoods (PCs:30, resolution: 0.8). The cell clusters were plotted using uniform manifold approximation and projection (UMAP) technique.

Finally, gene-expression levels were compared for pre-iMics and iMics 21 DIV, 42 DIV and 77 DIV for a selected set of genes as well as for a similar set of genes for iMics 42 DIV and 77 DIV from CSC with and without induced synucleinopathy.

Graphs were produced in RStudio with R version 4.1.3 (2022-03-10) mainly using the R package ggplot2 v3.4.2. Final reports were produced using the R package rmarkdown v2.21, with knitr v1.42.

3.4 Imaging

3.4.1 Immunofluorescent staining

Unsectioned HSC and CSC were used for immunofluorescent staining. To this end, HSC and CSC were carefully cut from the insert with a scalpel while they were still attached to the membrane in order to maintain top-down orientation for later imaging and stained in a 48-well plate (one separate well per condition). Only for TMEM119, antigen retrieval was performed as described in Table 3.1. Afterwards, slices were washed in PBS for ten minutes and transferred into blocking solution (5 % Normal Donkey Serum + 0.3 % Triton X-100 in PBS) in order to block unspecific binding. Slices were blocked for two hours at room temperature and subsequently incubation with the primary antibodies was performed in 2 % Normal Donkey Serum + 0.3 % Triton X-100 in PBS. Incubation conditions and antibody dilutions are indicated in Table 3.1. After incubation with the primary antibodies, slices were washed three times in PBS for 15 minutes each before secondary antibody incubation. Slices were incubated with secondary antibodies in 1 % Normal Donkey Serum + 0.3 % Triton X-100 in PBS for two hours at room temperate and finally washed again three times in PBS for 15 minutes. Finally, slices were mounted onto TOMO adhesive glass slides by carefully detaching them from the membrane with a brush, dried for 15 minutes at 37 °C and coverslipped with Dako Fluorescence Mounting Medium. Slides were dried for 24h at RT before storage at 4°C.

3.4.2 LCO staining

To stain microglial inclusions of αsyn, CSC were stained with Luminescent Conjugated Oligothiophenes (LCOs) that specifically bind amyloid fibrils such as αsyn fibrils. LCO staining was performed after incubation with fluorescently labelled secondary antibodies (see III .3.4.1). The LCO dyes pentamer-formyl thiophene acetic acid (pFTAA; 3 µM) or heptamer-formyl thiophene acetic acid (hFTAA; 3 µM) were applied for 30 minutes at room temperature in a dark humid chamber. Subsequently, slides were

washed three times for 15 minutes with PBS before they were mounted and coverslipped as described above.

3.4.3 Confocal imaging

Confocal images were acquired using an upright Zeiss LSM 880 NLO microscope with ZEN Black Software (Zeiss). All images were obtained using a water-immersion x20 Objective (W Plan-Apochromat x20/1.0, Carl Zeiss, Jena. To depict the morphology of microglial cells, z-stack images were acquired and maximum intensity projections were generated. Overview images were generated as tilescans of several z-stacks and subsequently maximum intensity projections were generated.

3.4.4 2-Photon live cell imaging

Movies of slice cultures with GFP-positive microglia (either CAG-GFP transgenic iMics or mouse HSC with Iba1-EGFP microglia) were acquired with an upright Zeiss LSM 880 NLO microscope, using an IR-optimized water-immersion x20 Objective (W Plan-Apochromat x20/1.0, Carl Zeiss, Jena). A MaiTai eHP (Spectra Physics) laser was used for two-photon excitation, tuned at 920 nm for exciting the GFP fluorescence. Emission was collected using Non-Descanned GaAsP detectors, with a 520/50 emission filter. Timelapse images were acquired at a resolution of 0.208 x 0.208 x 0.830 µm per voxel every 2 minutes. To induce a focal laser injury, the MaiTai eHP laser was tuned to 810 nm, set to point scan mode on lowest scanning speed with maximum power for 8 seconds. During acquisition the slice cultures were placed in a custom-made slice culture holder, that securely holds the inserts at the same position and orientation. Additionally, the slice cultures were submerged in pre-warmed CM and the entire imaging took place within a customized stage-top incubator to guarantee a stable imaging environment.

3.4.5 Calcium imaging

CSC 12 weeks after grafting and age-matched control HSC as well as HSC that were depleted for the entire experiment were used for Calcium imaging. To this end, Calbryte-590 AM (AAT Bioquest) was freshly dissolved at 4 mM in DMSO + 20 % Pluronic F-127 (Invitrogen) and subsequently diluted 1:200 in PBS before being applied on top of HSC/CSC for 30 minutes before imaging. Calcium imaging of entire slice cultures was performed at 10 Hz for three minutes using a Leica Thunder Imager with 5x magnification to capture the entire slice culture. During the imaging, slice cultures were kept at 37 °C and 5 % CO_2. After capturing baseline Calcium activity for all slices on an insert, 4-AP (100 µM) was added to the slice cultures and stimulated Calcium activity was measured as before.

3.5 Image analysis

3.5.1 Image processing

Huygens Essential (Scientific Volume Imaging B.V., Hilversum) was used to deconvolve all movies acquired with 2-Photon live-cell imaging before further processing.

All images for figures were created with FIJI as maximum intensity projections.

3.5.2 Morphological analysis of microglia

In order to analyze morphological parameters of microglia, confocal images were imported into the Imaris software version 9.7.2 (Bitplane).

First, nuclear signal such as derived from STEM101 (human nuclei) and PU.1 (microglia nuclei) was semi-automatically reconstructed using the 'Spots' function of Imaris. The number of nuclei per channel was then normalized to the total volume of the slice culture by reconstructing the entire slice culture with a very low absolute intensity threshold (Between 1 and 5 for 8-bit images) in the 'Surfaces' tool of Imaris. The reconstructed nuclear signal was also used to analyze the nearest-neighbor distance of microglia by using the implemented statistics for the 'Distance to Nearest Neighbour' in Imaris.

Next, the signal of Iba1-staining was used to reconstruct microglial morphology. To this end, microglia were semi-automatically reconstructed with the 'Surfaces' tool of Imaris based on the absolute intensity of the signal. Microglia that touched the borders of the image were excluded from the analysis. The resulting 3D-reconstruction of microglia was used to create a new channel in the image that removed all signal outside of the reconstructed microglia in order to improve the subsequent reconstruction with the 'Filaments' tool. The reconstruction of microglia with the 'Filaments' tool was then used to read out the morphological parameters 'Filament No. Dendrite Branch Pts' (Number of microglial branchpoints per cell as a measure of ramification) and 'Filament Length (sum)' (Length of all microglial processes per cell as a measure of ramification) in the 'Statistics' tab.

Lastly, the volume each microglia was governing (the volume of the convex hull), was calculated by using MATLAB 2021b and the MATLAB plug-in 'Convex hull' for Imaris which is available from the Imaris customer portal.

3.5.3 Analysis of microglia dynamics

To analyze microglial dynamics during 2-Photon live cell imaging, the microglial morphology was reconstructed as described above using the 'Surfaces' and 'Filaments' tool of Imaris (see section III.3.5.2). The reconstruction was performed for each timepoint of the movie and process movement was tracked by the 'Filaments' tool up to a distance of 10 µm between two timeframes.

In order to quantify the reaction of microglia to a focal laser injury, the injury site was reconstructed at the first frame after the lesion using the 'Spots' function of Imaris so that microglial processes were not yet present at the site. The resulting reconstruction of the injury was duplicated onto all timepoints and pixel values for the injury site were set to zero for all timepoints. Subsequently a vantage plot was calculated in Imaris (Spatial view) to calculate average pixel intensity in relation to the distance of the reconstructed injury site for all time points. In the next step, the intensity values for each movie were normalized to the highest value of the respective movie and averaged over all movies per group using MATLAB (see section XI.1.1.1).

3.5.4 Calcium imaging analysis

All calcium imaging movies were imported into FIJI and batch-processed. In FIJI, each movie was divided into 256 equally sized squares and the mean fluorescence intensity was measured for each of the ROIs at each of the 1,800 timepoints (Figure 3.3). The resulting measurements were then exported into an .csv-file for subsequent analysis in MATLAB. In MATLAB, a rolling average of ten subsequent timepoints was calculated for each of the ROIs and if the mean fluorescence intensity of the following timepoint was more than 0.5 % higher as the rolling average, this signal was counted as a spike. After detecting all spikes for one movie, a spike histogram of all ROIs was performed in which two timeframes were pooled into one bin (200 ms per bin). If a spike was detected for ten or more regions in one bin, this was counted as a spike to determine the synchronous spiking activity. Finally, the average spike amplitude, the general spike activity and the synchronous spike activity were calculated (see section XI.1.1.2 for scripts).

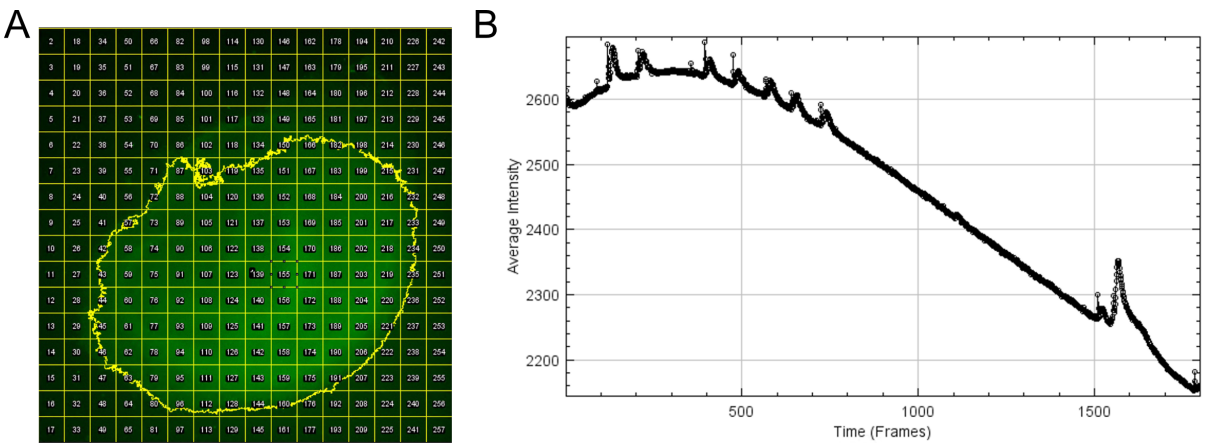

Figure 3.3 Analysis of Calcium imaging
(A) Calcium imaging movies were imported into FIJI and then the movies were divided into 256 squares of an equal size in which the mean fluorescence intensity was measured. **(B)** Resulting mean fluorescence intensity curve for one of the ROIs. For each of the 1,800 timepoints, the mean intensity was measured. Several spikes characterized by a rapid increase in the mean fluorescence intensity are visible. Overall, the mean fluorescence intensity was constantly decreasing due to bleaching.

3.5.5 Microglial inclusions

LCO-positive inclusions within iMics were analyzed with Imaris. iMics in tilescan images of entire CSC were 3D-reconstructed as described above with the 'Surfaces' tool of Imaris (see section III.3.5.2). Next, all voxels of the channel for the LCO signal (either from pFTAA or hFTAA) outside of the reconstructed microglial surfaces were set to 'Zero' in order to only see LCO-signal within iMics. LCO-positive signal within iMics in the newly created channel was then reconstructed with the 'Spots' tool of Imaris in order to quantify the number of microglia with LCO-positive inclusions and divided by the total number of iMics to obtain the relative amount of iMics with LCO-positive inclusions. Additionally, the LCO-positive signal was reconstructed with the 'Surfaces' function of Imaris in an intensity-based manner as described above for microglia and normalized to the total volume of the CSC to determine the relative volume of LCO-positive inclusions within iMics.

3.6 MSD

In order to measure secreted cytokine levels of CSC, slice culture medium was collected during the media change before the start of the treatment and during the treatment at the timepoints described in the respective sections and frozen until all samples were collected for further analysis. Cytokine levels were measured using a V-PLEX Human Proinflammatory Panel II (4-Plex, IL-1β, IL-6, IL-8, TNF-α) kit (Meso Scale Discovery). Samples were not diluted before measurement and measured according to the manufacturer's instructions with a Mesoscale Sector Imager 6000. For every measurement, internal reference samples were used. Data analysis was performed using the MSD discovery workbench software 3.0.

IV Results

1 New mouse model does not allow to induce targeted microglia cell death to investigate microglial network homeostasis *in vivo*

Our laboratory has previously shown that microglia in the mouse cerebral cortex are very long-lived cells, with an average lifespan of over 15 months. Thus, death of microglia in the mouse cerebral cortex occurs rarely (Füger et al. 2017). However, it is not well understood how microglia maintain their network, especially during aging and neurodegenerative disease, and how dying microglia are replaced in the mouse cortex. Three possibilities of how the microglial network could maintain itself are (Figure 4.1):

1. Network rearrangement without the addition of new cells to the network. Since only a small percentage of the entire network dies at a time, the remaining microglia only translocate into empty positions and reorganize their network in order to fill the empty spaces and still cover the entire brain (Eyo, Mo, et al. 2018; Olmedillas et al. 2023). Microglia division only happens remotely from time to time and leads to another minor reorganization of the network.
2. The empty space left by the dead cell is replenished by local division of close-by microglia which then migrate into the position of the dead cell. The dividing cell could either be the closest cell or a more remote cell as described for the olfactory bulb (2^{nd} closest microglia) (Askew et al. 2017).
3. The dead microglia cell is replaced by the invasion of peripheral immune cells that subsequently differentiate into microglia or microglia-like cells while the local microglial network does not react to the death event.

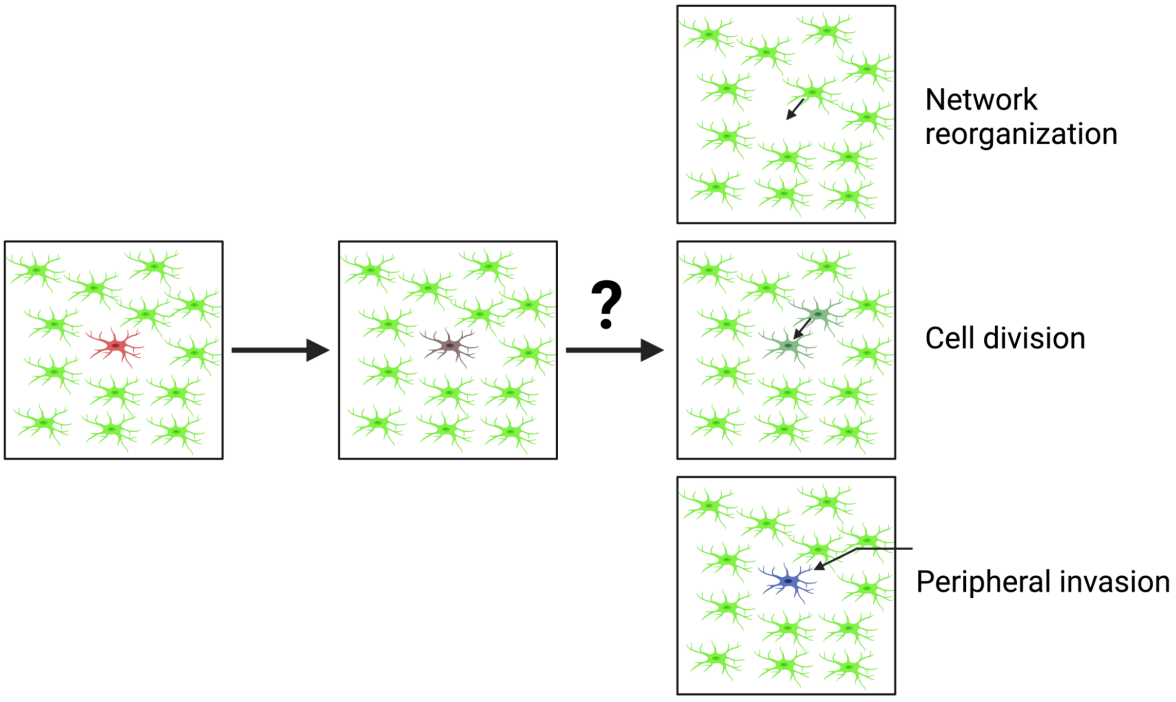

Figure 4.1 How does the microglial network react to the death of individual microglia
Scientific question of this study: In response to the targeted death of individual microglia (labelled by tdTomato (red); left and center) the microglial network could have three different responses: 1. Reorganization of the network without the addition of new cells to the network (top right) 2. Division of a neighboring cell from the first or second row and migration into the empty spot (center right) 3. Invasion of peripheral macrophages and integration into the empty position of the network (bottom right)

1.1 Development of a 4x transgenic mouse model to ablate individual microglia

In order to answer this question, a novel 4x transgenic mouse model (called tdTom x iDTR mice) was developed to observe the targeted ablation of individual microglia via 2-Photon *in vivo* imaging. To this end, a triple transgenic mouse line was used that was previously established in my laboratory (Füger et al. 2017). This mouse model expresses GFP in all microglia and additionally tdTomato (tdTom) in a small percentage of microglia in a Tamoxifen (Tam)-inducible manner. For this study, a fourth transgene was added so that these mice would also express an inducible human Diphtheria toxin receptor (iDTR) only in the tdTomato-positive microglia (Figure 4.2 A). In detail, to achieve microglia-specific expression, GFP expression was under control of the Iba1-promoter. Additionally, these mice expressed CreERT2, a Tamoxifen-inducible Cre-recombinase under the control of the CD11b-promoter which leads to its expression in microglia. Lastly, both the transgenes for tdTom and iDTR were targeted into the ROSA26 locus and under the control of a universal CAG-promoter. However, the

protein expression for both transgenes was blocked by a STOP-cassette that was flanked by two loxP-sites (Figure 4.2 B). Only upon Tam-induced Cre-recombination the STOP-cassette was removed and protein expression was started.

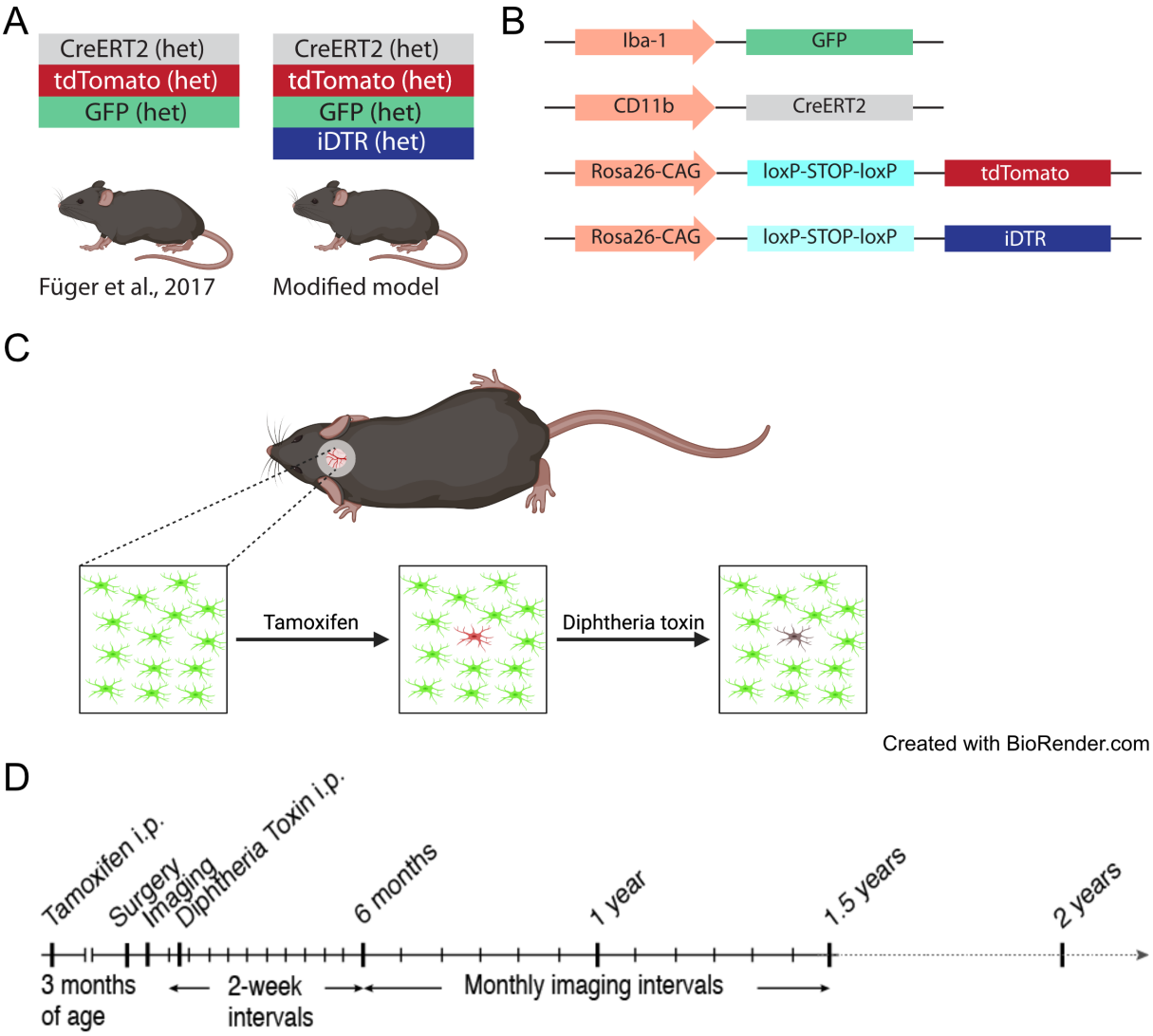

Figure 4.2 Development of a 4x transgenic mouse model to ablate individual microglia
(A) Schematic visualization of both mouse models used in this study. 3x transgenic CD11b-CreERT2;R26-tdTomato;Iba1-eGFP mice previously used in Füger et al., 2017, that expressed GFP in all microglia and Cre-recombination-dependent tdTomato. The newly developed tdTom x iDTR mouse model for this study additionally expressed the receptor for Diphtheria toxin (iDTR) in dependence of Cre-recombination. **(B)** Visualization of all four transgenes. Microglial expression of GFP was achieved under control of the Iba1-promoter (1st row). Expression of a Tamoxifen-inducible Cre-recombinase in microglia was achieved under the control of the CD11b-promoter (2nd row). Expression of tdTomato (3rd row) and iDTR (4th row) was inhibited by a floxed STOP-cassette. Upon Tamoxifen-induced Cre-recombination both transgenes were expressed under the control of the CAG promoter in the ROSA26 locus. **(C)** Experimental setup. Upon injection of a low dose of Tamoxifen, only a small percentage of microglia in tdTom x iDTR mice expressed tdTomato and iDTR. tdTomato allowed for the identification of iDTR-expressing cells in 2-photon *in vivo* imaging of mice that underwent cranial window surgery. After identification of ROIs, DT was applied in order to selectively ablate tdTomato-positive microglia. **(D)** Experimental timeline. Tamoxifen was injected at three months of age. Cranial window surgery was scheduled to be performed three weeks before DT-application at different ages for three different age groups. Two weeks after surgery, initial ROIs were identified and one week later, after successful relocalization of ROIs, DT was injected. Subsequently, mice were imaged biweekly for 2 months and afterwards in monthly intervals.

Similar to Füger et al., only a low dose of Tamoxifen was used at three months of age to induce Cre-recombination in a small subset of microglia in tdTom x iDTR mice. The sparse labeling of microglia with tdTom allowed for the visualization of iDTR-expressing microglia in which I aimed to induce apoptosis through injection with DT (Figure 4.2 C). For the study design, the mice were divided into three age groups. I planned to ablate individual microglia at 4 months of age for the young age group, at 10 months of age for the adult age group and at 22 months for the aged group. Mice underwent a surgical procedure to remove a part of the skull and implant a cranial window shortly before the start of observation. First, two weeks after surgery, initial ROIs with tdTom-positive microglia were identified via 2-Photon *in vivo* imaging. Then, another week later, all ROIs were reidentified to guarantee a stable cranial window and reliable repositioning of the ROIs. Subsequently, mice were treated with DT to induce targeted cell death of tdTom-positive microglia and reimaged one week after the treatment. Afterwards, mice were imaged biweekly until two months after treatment and scheduled for monthly imaging thereafter in order to see, in case of microglial division, if one of the two cells had a reduced lifetime compared to the other (Figure 4.2 D).

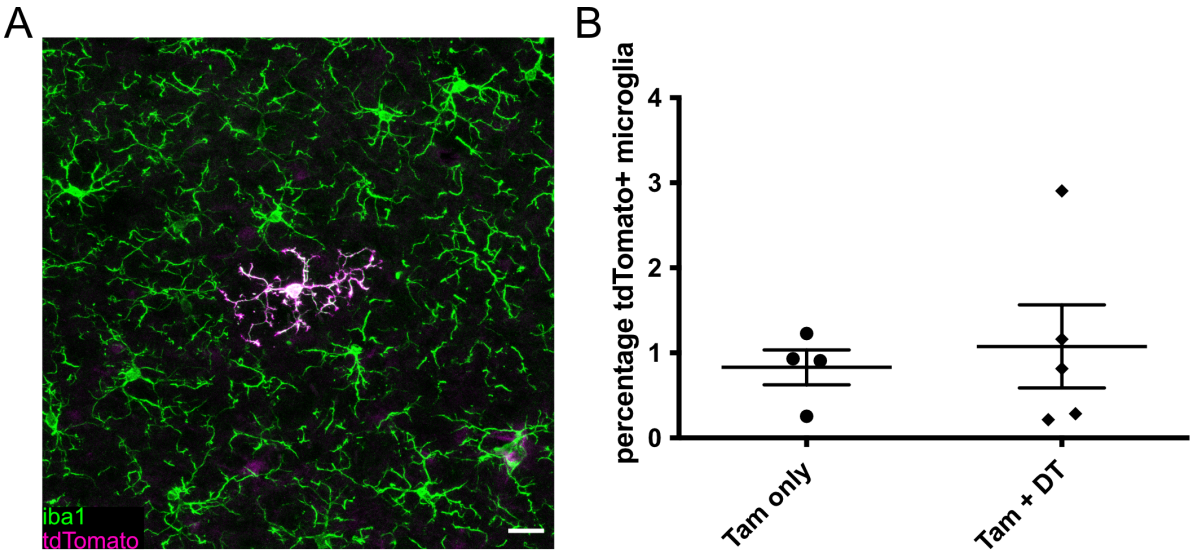

Figure 4.3 Dosing of Tamoxifen and DT
(A) Low dose of Tamoxifen as used in Füger et al. 2017 (2x 100 µg tamoxifen per gram bodyweight 48h apart) led to sparse tdTom (magenta) expression in only a small fraction of microglia (green). Scale bar: 20 µm. **(B)** Quantification of tdTomato positive microglia. Tamoxifen injection led to tdTomato expression in only 1 % of microglia four weeks after Tamoxifen injection. DT was injected at 500 ng per injection for five consecutive days but no significant differences in the percentage of tdTomato positive cells was found one week after the final DT injection. number of mice per group = 4-5; Mann-Whitney test p = 0.9048

Before starting *in vivo* imaging, dosing of Tamoxifen was tested in order to assess if the recombination efficiency in the novel tdTom x iDTR mouse model was similar to the triple transgenic mouse model used in Füger et al. To this end, tdTom x iDTR mice were injected twice 48 hours apart with 100 µg tamoxifen per gram bodyweight and sacrificed one month later. Low dose Tamoxifen injection led to sparse labeling of microglia with tdTom in addition to the global GFP labeling of microglia, similar to

the mouse model used in Füger et al. (Figure 4.3 A). Furthermore, to test the expression of iDTR in tdTom-positive microglia, tdTom x iDTR mice were injected with DT or NaCl as control one month after Tamoxifen treatment and sacrificed another one week later. Both control and DT-treated mice showed expression of tdTom in roughly 1 % of microglia, indicating that DT ablation of tdTom-positive microglia did not work as intended (Figure 4.3 B).

1.2 Targeted microglia cell death *in vivo*

1.2.1 2-Photon in vivo *imaging of tdTom x iDTR mice*

Next, I continued with 2-Photon *in vivo* imaging of tdTom x iDTR mice and started with the young age group that underwent Tamoxifen treatment at three months of age and DT treatment at four months of age. Additionally, one triple transgenic mouse of the Füger et al. mouse model was treated accordingly and used as a negative control. For the tdTom x iDTR mice, a total of ten ROIs in five mice were observed until six weeks after DT treatment. In none of the ten ROIs tdTom-positive microglia were ablated, however, in four positions tdTomato-positive microglia underwent cell division. The cell division events were observed between one and two weeks after the end of the DT treatment (Figure 4.4 A). Due to the remaining microglia in these ROIs being all GFP-positive only, it was not possible to determine with absolute certainty that some of these cells underwent DT-induced apoptosis, although for two ROIs in which the tdTom-positive microglia divided, potential cell death events were observed in close proximity to the tdTom-positive microglia. For the control mouse, neither cell death nor cell division events of tdTom-positive microglia were observed until six weeks after DT injection in four ROIs (Figure 4.4 B). All in all, these observations were in line with the previous experiment where no reduction in the ratio of tdTom-positive microglia could be observed after injection with DT (Figure 4.3 B), overall indicating that DT-induced ablation of tdTom-positive microglia did not work in this model.

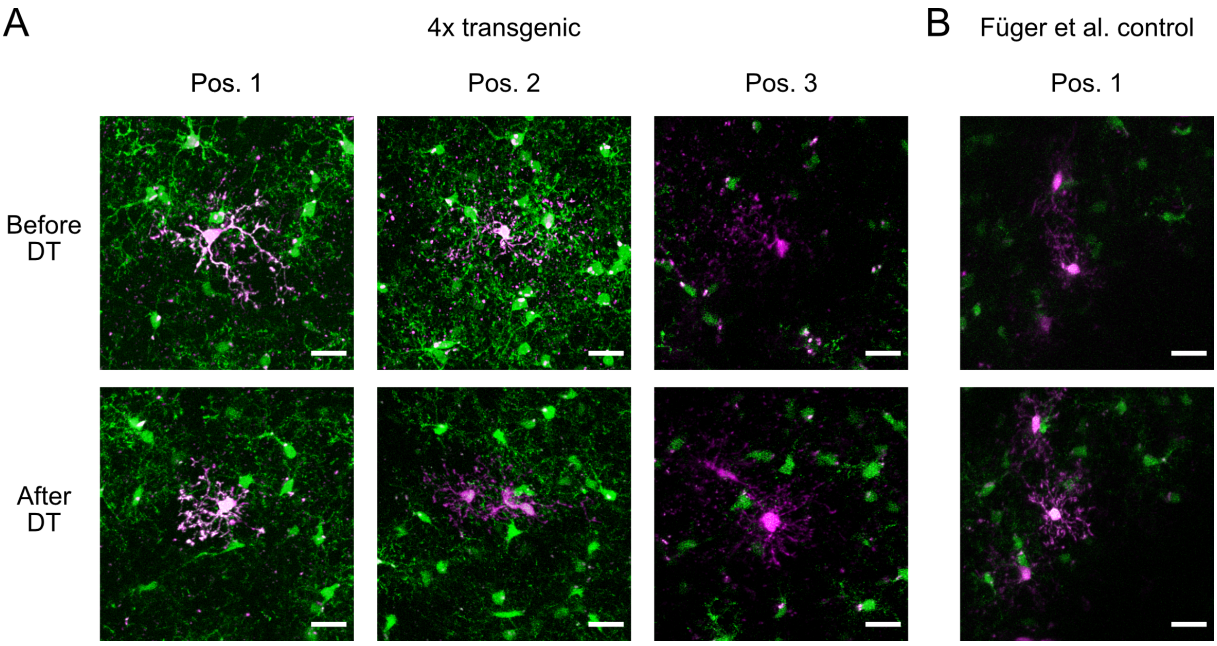

Figure 4.4 2-Photon *in vivo* imaging of tdTom x iDTR mice
(A) Representative 2-Photon *in vivo* images of three ROIs of tdTom x iDTR mice from the young age group before (upper row) and six weeks after DT application (bottom row). In none of the OIs DT was able to ablate tdTomato positive microglia. In four out of ten ROIs, division of tdTomato-positive cells was observed upon DT injection. Scale bars: 20 µm (B) Representative images from a 3x transgenic mouse as used in Füger et al. Neither ablation nor division of tdTomato-positive cells in any ROI was observed. Scale bars: 20 µm

1.2.2 Fluorescence activated cell sorting of tdTom x iDTR mice

To rule out that I did not miss DT-induced ablation due to the limited number of microglia observed in 2-Photon *in vivo* imaging, tdTom x iDTR mice were treated with Tamoxifen for four consecutive days at three months of age to induce a slightly higher rate of recombination and injected at four months of age with DT (three mice) or NaCl (two mice), respectively. One week later, mice were sacrificed, and microglia were isolated by fluorescence-activated cell sorting (FACS). Microglia were identified as $CD11b^{high}/CD45^{+}$ cells and afterwards sorted according to their GFP and tdTom signal. As expected, I identified two subpopulations in the NaCl-injected control mice. All microglia showed strong GFP expression while only 3.4 % of microglia were also positive for tdTom. Hence, the subpopulations were named ‘GFP only’ and ‘tdTom’. However, despite DT-treatment, the ratio of the ‘tdTom’ subpopulation remained at 3.4 %, which was again in line with the observations from previous experiments (Figure 4.5).

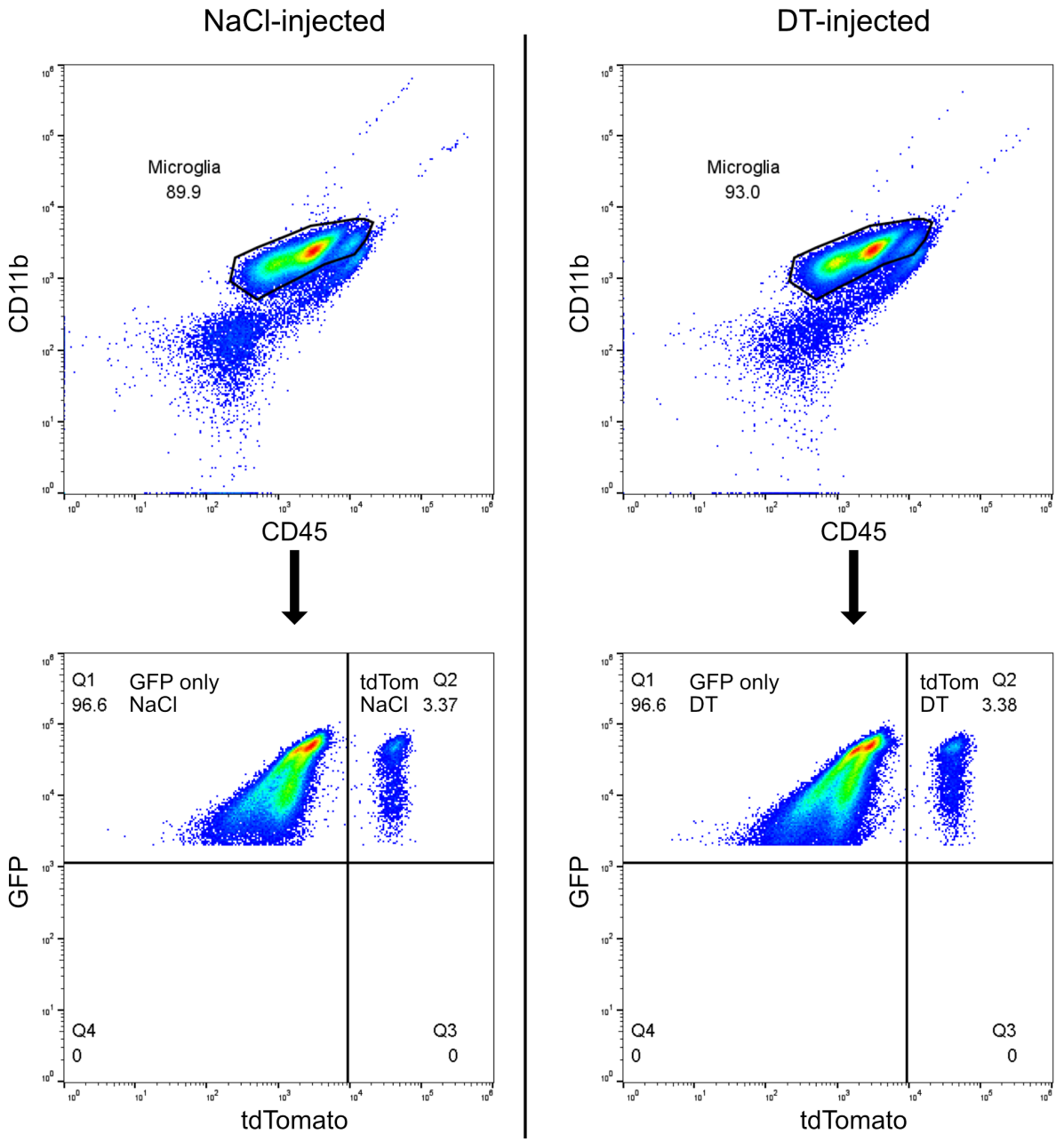

Figure 4.5 Fluorescence activated cell sorting of tdTom x iDTR mice
Gating of FACS experiments from tdTom x iDTR mice that were injected with Tamoxifen and subsequently treated with either NaCl or DT. Microglia were isolated via Percoll gradient and identified via their CD11b and CD45 flow cytometry signal. Then, microglia were sorted into two subpopulations according to their GFP and tdTom fluorescence intensity. DT-injected tdTom x iDTR mice had a similar percentage of tdTom-positive cells as NaCl-injected control animals.

In order to better understand why I was not able to selectively ablate tdTom-positive microglia in tdTom x iDTR mice, the respective subpopulations from each of the treatment groups were sorted for subsequent analysis. For both NaCl- and DT-injected mice, a ‘GFP only’ and a ‘tdTom’ subpopulation were obtained.

1.3 Analysis of recombination efficiency in tdTom x iDTR mice

My first approach to understand the problems I faced, was to analyze the recombination efficiency of the iDTR-transgene in the four samples obtained from the FACS experiment. To this end, I designed three PCR reactions that targeted the following parts of the transgene (Figure 4.6):

1. A PCR to show the expression of the iDTR transgene, independently of the recombination status. The primers were designed to specifically target the iDTR transgene so that the PCR would not be positive for the ROSA26-tdTom transgene. Hereafter, this PCR is called 'Control PCR'.
2. A PCR which was only positive if the iDTR transgene did not undergo Cre-recombination. The binding site of the forward primer was located in the STOP-cassette so that the binding sequence was excised upon Cre-recombination. Following, this PCR is called 'No recombination PCR'.
3. A PCR which was only positive if the iDTR transgene did undergo recombination. The forward primer bound in the promoter region and the reverse primer bound in the iDTR gene so that without recombination a PCR product of 4.6 kbp would be generated. However, the elongation phase of the PCR was designed to be too short to amplify the product. Only after recombination of the iDTR transgene, a product of 801 bp was amplified. Hereafter, this PCR is called 'Recombination PCR'.

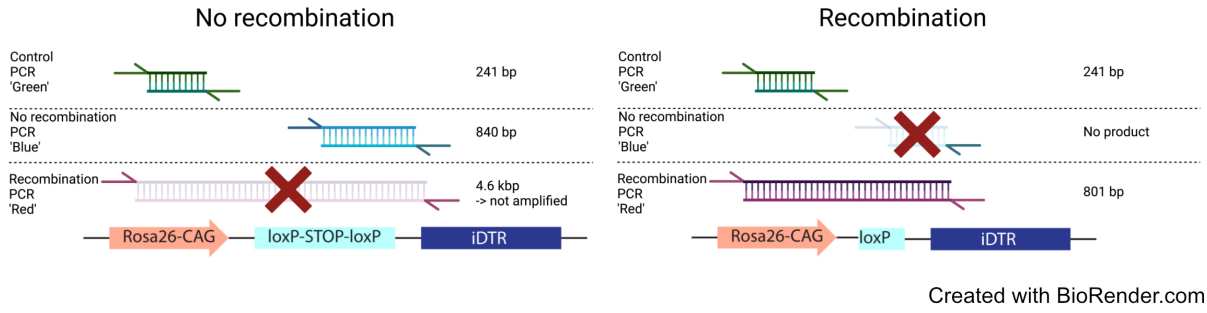

Figure 4.6 PCR analysis strategy of Cre-recombination efficiency in tdTom x iDTR mice
PCR analysis strategy to assess recombination efficiency of Cre in the iDTR transgene. 1. A control PCR in the ROSA26-locus specific for the iDTR-transgene showed the presence of the transgene independently of the recombination status ('Green'). 2. A PCR to specifically target the iDTR transgene if it has not undergone Cre-recombination. The forward primer was located in the STOP cassette and the reverse primer in the iDTR-gene. In case of recombination the forward primer would not bind to the transgene anymore ('Blue'). 3. A PCR specific for the iDTR transgene upon Cre-recombination. The forward primer was designed to bind in the ROSA26-CAG promoter and the reverse primer bound to the iDTR gene. Before recombination, this PCR would have a theoretical product of 4.6 kbp but the amplification time was set too short for the length of this product ('Red').

As expected, the 'Control PCR' was positive for all four subpopulations (GFP only and tdTom for both NaCl and DT treated mice), showing that the iDTR transgene was present in all subpopulations. However, since the tdTom population should not exist anymore after DT-treatment, the 'Control PCR'

showed that either the recombination of the iDTR transgene did not happen in tdTom-positive microglia or that the iDTR gene or the DT treatment itself did not work properly (Table 4.1).

Table 4.1 PCR Results Control PCR

FACS POPULATION	EXPECTED RESULT	ACTUAL RESULT	MATCH/MISMATCH?
GFP ONLY NACL	Positive	Positive	✓
TDTOM NACL	Positive	Positive	✓
GFP ONLY DT	Positive	Positive	✓
TDTOM DT	Negative (Population should not exist)	Positive	✗

Next, the 'No recombination PCR' was positive for all subpopulations from the previous FACS experiment, indicating that in all the subpopulations were microglia that did not undergo Cre-recombination for the iDTR transgene. For the GFP only subpopulations a positive result was expected, however, the positive result for both tdTom subpopulations showed that the recombination of the iDTR transgene did not take place in all the microglia of these subpopulations (Table 4.2).

Table 4.2 PCR Results No recombination PCR

FACS POPULATION	EXPECTED RESULT	ACTUAL RESULT	MATCH/MISMATCH?
GFP ONLY NACL	Positive	Positive	✓
TDTOM NACL	Negative	Positive	✗
GFP ONLY DT	Positive	Positive	✓
TDTOM DT	Negative (Population should not exist)	Positive	✗

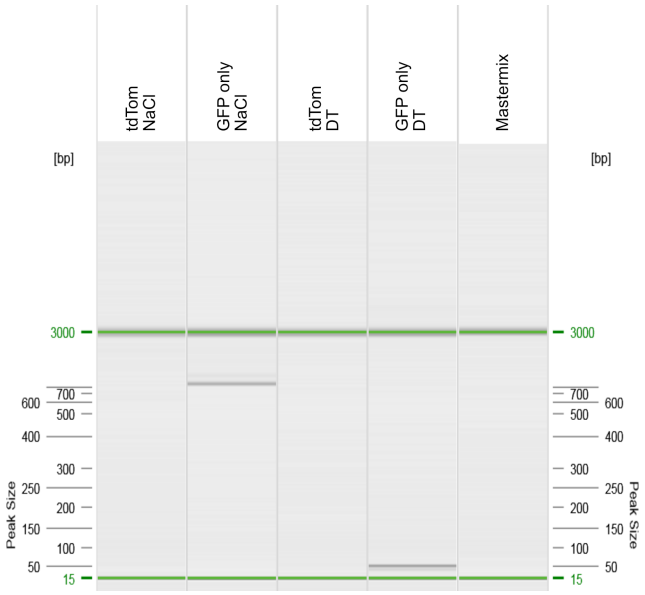

Figure 4.7 PCR Results Recombination PCR
PCR result of the PCR specific for the Cre-recombined iDTR-transgene. None of the tdTomato subpopulations nor the mastermix showed a band. Only the GFP only subpopulation from NaCl-injected tdTom x iDTR mice showed the expected band at 801 bp while the GFP only subpopulation from DT-injected mice showed an unspecific band at around 50 bp.

Lastly, I wanted to test if Cre-recombination did not work at all or if the recombination efficiency was too low compared to the tdTom transgene. The 'Recombination PCR' showed that the expected PCR product at 801 bp was only detectable in the GFP only subpopulation of control treated mice (Figure 4.7). Together with the result of the 'No recombination PCR' of this subpopulation, this showed that iDTR-recombination was functional and occurred in a fraction of GFP only microglia. However, these results showed that Cre-recombination did either not take place at all in the tdTom subpopulation or the fraction of recombination was too low in this subpopulation to detect the DNA by PCR amplification since only 3,000 cells in total were isolated for the tdTom subpopulation of NaCl-treated mice compared to 100,000 cells in the GFP only subpopulation.

Table 4.3 PCR Results Recombination PCR

FACS POPULATION	EXPECTED RESULT	ACTUAL RESULT	MATCH/MISMATCH?
GFP ONLY NACL	Negative	Positive → Sequencing	✘
TDTOM NACL	Positive	Negative	✘
GFP ONLY DT	Negative	Unspecific Band → Sequencing	✘
TDTOM DT	Negative (Population should not exist)	Negative	✓

Additionally, the 'Recombination PCR' of the DT-treated mice was negative for the tdTom subpopulation, again either due to no recombination or a too small fraction of recombination. Finally, the GFP only subpopulation of DT-treated mice showed an unspecific band at around 50 bp (Figure 4.7), indicating that DT-treatment might have led to apoptosis of iDTR-expressing microglia in the GFP only microglia (Table 4.3).

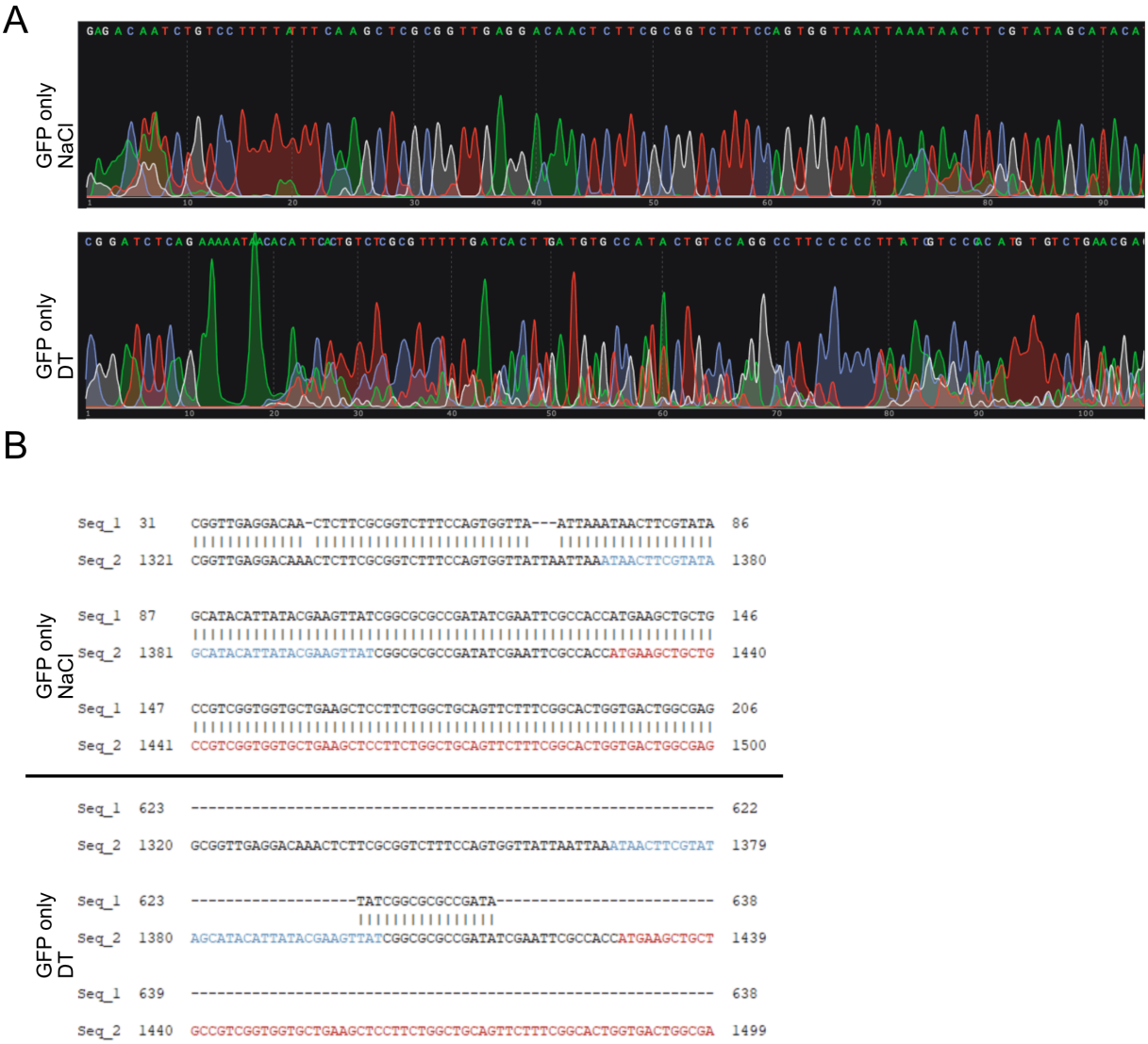

Figure 4.8 Sanger-sequencing of iDTR to confirm recombination
(A) Sanger chromatogram of the FACS subpopulations: 1. GFP-only NaCl-treated 2. GFP-only DT-treated. The chromatogram for NaCl treatment showed a clean chromatogram with easily identifiable peaks. The chromatogram for the DT-treatment, however, showed multiple peaks per position indicating several different sequenced fragments. **(B)** Alignment of the resulting sequences with the Cre-recombined transgene for iDTR. The sequence of the GFP-only NaCl-treated population perfectly aligned with the Cre-recombined transgene of iDTR, while the sequence for the GFP-only DT-treated population showed no matching sequence fragments.

Even though DT-treatment seemed to affect the fraction of GFP only microglia that underwent Cre-recombination, I wanted to know if the iDTR was intact and functional in tdTom x iDTR mice. To this end, I performed Sanger sequencing of iDTR in the GFP only FACS subpopulations of both NaCl-treated

and DT-treated mice (see Figure 4.5). In the previous PCR experiment, these subpopulations were the only ones for which the 'Recombination PCR' showed a result, although the band for the DT-treated mice seemed to be unspecific (see Figure 4.7 & Table 4.3). Sanger sequencing of the GFP only subpopulation from NaCl-treated mice showed clean Sanger chromatograms with easily identifiable base peaks. The respective chromatograms of DT-treated mice, however, showed multiple peaks per base which made it impossible to identify a clear sequence, a possible hint for fragmented DNA (Figure 4.8 A). Accordingly, the consensus sequence of DT-treated mice did not align with the sequence of iDTR. The identified sequence for NaCl-treated mice, however, aligned perfectly with the sequence of iDTR (Figure 4.8 B) (also see section X.2 for full alignments) (Buch et al. 2005).

Overall, Sanger sequencing showed that the iDTR sequence was intact and functional. The potential fragmentation of DNA upon DT-injection together with the failure to detect the expected band in the 'Recombination PCR' after DT-treatment in the GFP only subpopulation indicated that DT treatment successfully ablated iDTR expressing microglia. However, iDTR-recombination was not detectable in tdTom-positive microglia which explains why no targeted ablation of tdTom-positive microglia was possible during 2-Photon *in vivo* imaging of tdTom x iDTR mice.

2 Development of a novel chimeric *in vitro* model to investigate human microglial network homeostasis and neurodegeneration

These previous experiments demonstrate that in vivo models require a high investment of time, costs and animal numbers and are limited to low-throughput manipulations. Therefore, as a next step I tested whether *in vitro* culture models could offer a simplified, alternative system to study microglia homeostasis in various conditions. Because of the easy accessibility of *in vitro* models for treatments and experimental readouts and the complex 3D-architecture of hippocampal slice cultures (HSC) that more closely resembles *in vivo* conditions compared to other *in vitro* systems, I decided to turn to this model system. To facilitate the investigation of mutations in microglia and to study human microglia *in vitro*, a novel slice culture system was developed in which endogenous mouse microglia were replaced with human iPSC-derived microglia in order to improve current HSC models.

2.1 Generation of chimeric slice cultures

First, different conditions for the engraftment of iPSC-derived microglia (iMics) into HSC were tested. To test if iMics required a microglia-depleted niche or could coexist with endogenous mouse microglia, iMic precursors (pre-iMics), that were derived from iPSC according to the protocol by Haenseler et al. (Haenseler et al. 2017), were either grafted onto untreated HSC or HSC with a microglia-depleted niche.

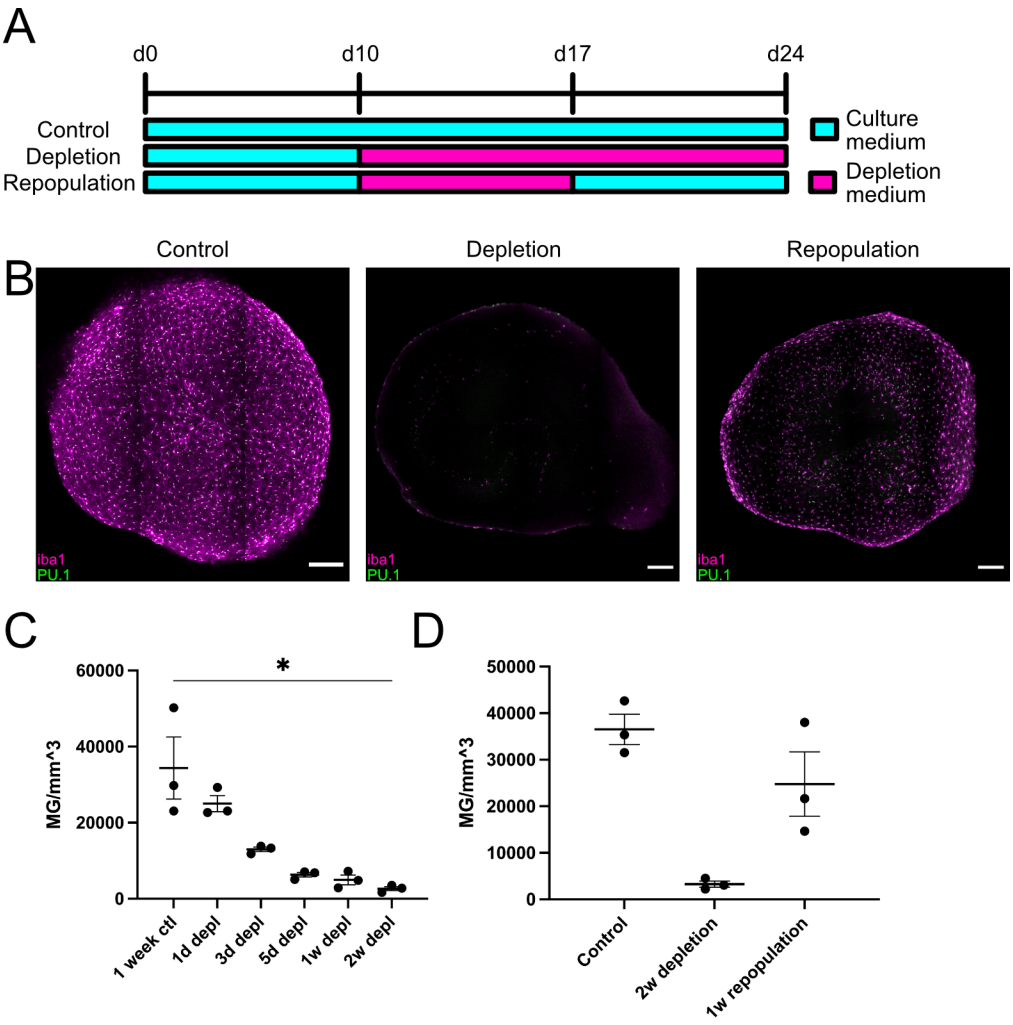

Figure 4.9 Depletion of mouse microglia in hippocampal slice cultures with a mouse-specific anti-CSF1R antibody
(A) Experimental timeline. All mouse HSC were allowed to adjust to culturing conditions for 10 days. The 'control' group was cultivated in regular culture medium for the entire experiment. The 'depletion' group was switched to culture medium supplemented with 5 µg/ml anti-CSF1R-antibody after 10 days for the rest of the experiment, while the 'repopulation' condition was switched back to not supplemented culture medium after 7 days of depletion. **(B)** Representative images of the three experimental groups. Microglia were stained against Iba1 (magenta) and PU.1 (green; microglia nuclei). After 2 weeks of depletion only 8 % of microglia were left in the hippocampal slice cultures. After one week back in regular culture medium, microglia were beginning to repopulate the culture. Scale bars: 200 µm **(C)** Microglia density of mouse HSC measured as microglia per volume. Depletion with a mouse-specific anti-CSF1R-antibody led to a sharp decrease in microglia cell numbers over time. n (groups)=6; number of independent experiments per group = 3; Kruskal-Wallis test with Dunn's multiple comparison test p = 0.0077**(D)** Microglia density of mouse HSC measured as microglia per volume. After removal of the anti-CSF1R-antibody, microglia repopulate the hippocampal slice cultures within a week. n (groups)=3; number of independent experiments per group = 3; Kruskal-Wallis test with Dunn's multiple comparison test p = 0.025

In order to create a niche for iPSC-derived microglia, endogenous mouse microglia in HSC, prepared from four to six days old C57BL6/J (B6) mice, were depleted with a mouse-specific α-CSF1R-antibody (5 µg/ml; BioLegend) after an accommodation period to the culturing conditions of ten days (Figure 4.9 A). Within one week, antibody treatment of HSC lead to an 85.6 % depletion of mouse microglia (Figure 4.9 B-C, p = 0.0077). However, upon removal of the antibody, the remaining mouse microglia

were able to quickly repopulate the HSC to 68 % of the original density within one week (Figure 4.9 D, p = 0.025).

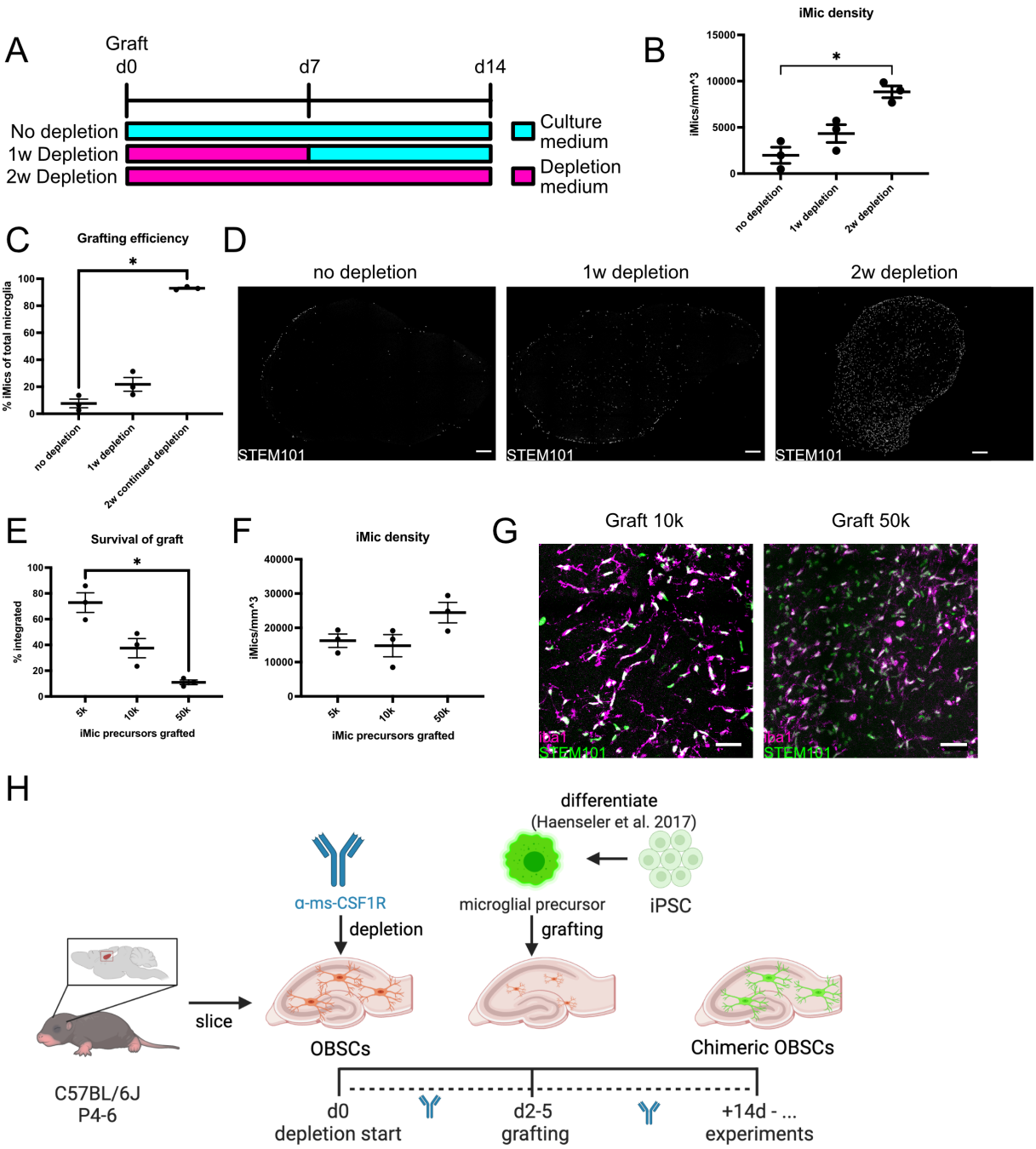

Figure 4.10 Optimization of iMic grafting conditions
(A) Experimental timeline. iMics were grafted at the day of preparation for all conditions. The 'control' group was cultivated in regular culture medium for the entire experiment. The '1w Depletion' and the '2w Depletion' groups were cultured in culture medium supplemented with 5 µg/ml anti-CSF1R-antibody from the start of the experiment but only the '1w Depletion' group was switched back to regular culture medium. **(B)** iMic density of CSC measured as iMics per volume. Continuous depletion of mouse microglia led to a higher number of iMics integrated into the slice cultures. n (groups)=3; number of independent experiments per group = 3; Kruskal-Wallis test with Dunn's multiple comparison test p = 0.0107 **(C)** Grafting efficiency of CSC calculated by dividing the number of iMics (STEM101-positive cells) by the total number of microglia (PU.1-positive cells). Continuous depletion of mouse microglia led to a higher grafting efficiency. n (groups)=3; number of independent experiments per group = 3; Kruskal-Wallis test with Dunn's multiple comparison test p = 0.0036 **(D)** Representative images of three grafting paradigms. iMics were stained against STEM101 (white; human nuclei). Only few STEM101-positive cells were visible

in the 'no depletion' and '1w Depletion' groups, while STEM101-positive cells are spread over the culture in the '2w Depletion' group. **(E)** Survival of the grafted amount of pre-iMics, calculated by dividing the number of iMics 7 days after grafting by the size of the graft (x-axis). n (groups)=3; number of independent experiments per group = 3; Kruskal-Wallis test with Dunn's multiple comparison test p = 0.0036 **(F)** Microglia density of CSC measured as microglia per volume. Different amounts of grafted pre-iMics did not lead to significantly different amounts of integrated cells 7 days after grafting. n (groups)=3; number of independent experiments per group = 3; Kruskal-Wallis test with Dunn's multiple comparison test p = 0.1964 **(G)** Representative images of two different amounts of grafted pre-iMics 7 days after grafting. A graft size of 10k cells led to a lower number of STEM101-positive cells (green) while iMics in cultures with a graft size of 50k cells showed lower Iba1-levels (magenta). Scale bar: 20 µm **(H)** Experimental set-up. Hippocampal slice cultures were prepared from 4-6 days old C57BL6/J mice. Endogenous mouse microglia were depleted throughout the entire experiment by CSF1R-inhibition and pre-iMics differentiated from human iPSC according to Haenseler et al. (2017) were grafted at 2-5 DIV. After 14 days of differentiation CSC were used for experiments.

After establishing the creation of a microglia-depleted niche, pre-iMics were grafted onto HSC to create chimeric hippocampal slice cultures (CSC), either on untreated HSC or HSC with microglia depletion for one or two weeks (Figure 4.10 A). Only a continuous depletion for 2 weeks with α-msCSF1R-antibody yielded high cell counts and grafting efficiencies. When depleting endogenous microglia throughout the entire experiment, 93 % of total microglia were of human origin, also showing that the α-CSF1R-antibody used, does not affect human microglia. Inversely, without endogenous microglia depletion, iMics did barely integrate and only made up 7.6 % of total microglia which was only slightly improved to 22 % when depleting for one week (Figure 4.10 B-D; Panel B: p = 0.0107; Panel C: p = 0.0036). This indicates that iMics required the sustained depletion of mouse microglia throughout the entire experiment and were dependent on the resulting niche.

Next, to determine the optimal number of precursors to graft, three different pre-iMics cell numbers were tested for grafting. While the survival of the graft was decreasing with increasing size of the graft from 73 % (5,000 cells grafted) to 11 % (50,000 cells grafted) (Figure 4.10 E; p = 0.0036), the resulting number of integrated cells did not differ significantly (Figure 4.10 F, p = 0.1964). However, immunofluorescent staining of the different conditions revealed a decreased expression of Iba1 when grafting 50,000 precursors, indicating a slower differentiation of the precursors (Figure 4.10 G). Therefore, for all subsequent experiments mouse microglia were permanently inhibited with a mouse specific α-CSF1R-antibody and a graft size of 10,000 cells per HSC was used (Figure 4.10 H).

After establishing the protocol, the protocol was retested with various iPSC-lines and a second differentiation protocol for microglia precursors in order to make the model system more accessible and reproducible for other laboratories. While different lines and protocols yielded varying amounts of integrated iMics after 14 days in vitro (DIV) (6400 iMics/mm^3 – 16200 iMics/mm^3), they all integrated in high numbers with a grafting efficiency between 93.6 % and 97.4 % (Figure 4.11 A, B; Panel A: p = 0.0014; Panel B: p = 0.2357) and differentiated into highly ramified iMics (Figure 4.11 C), demonstrating the accessibility of CSC for a broad research community. For all further experiments, unless otherwise noted, the EB-based protocol with the BIONi010C line was used.

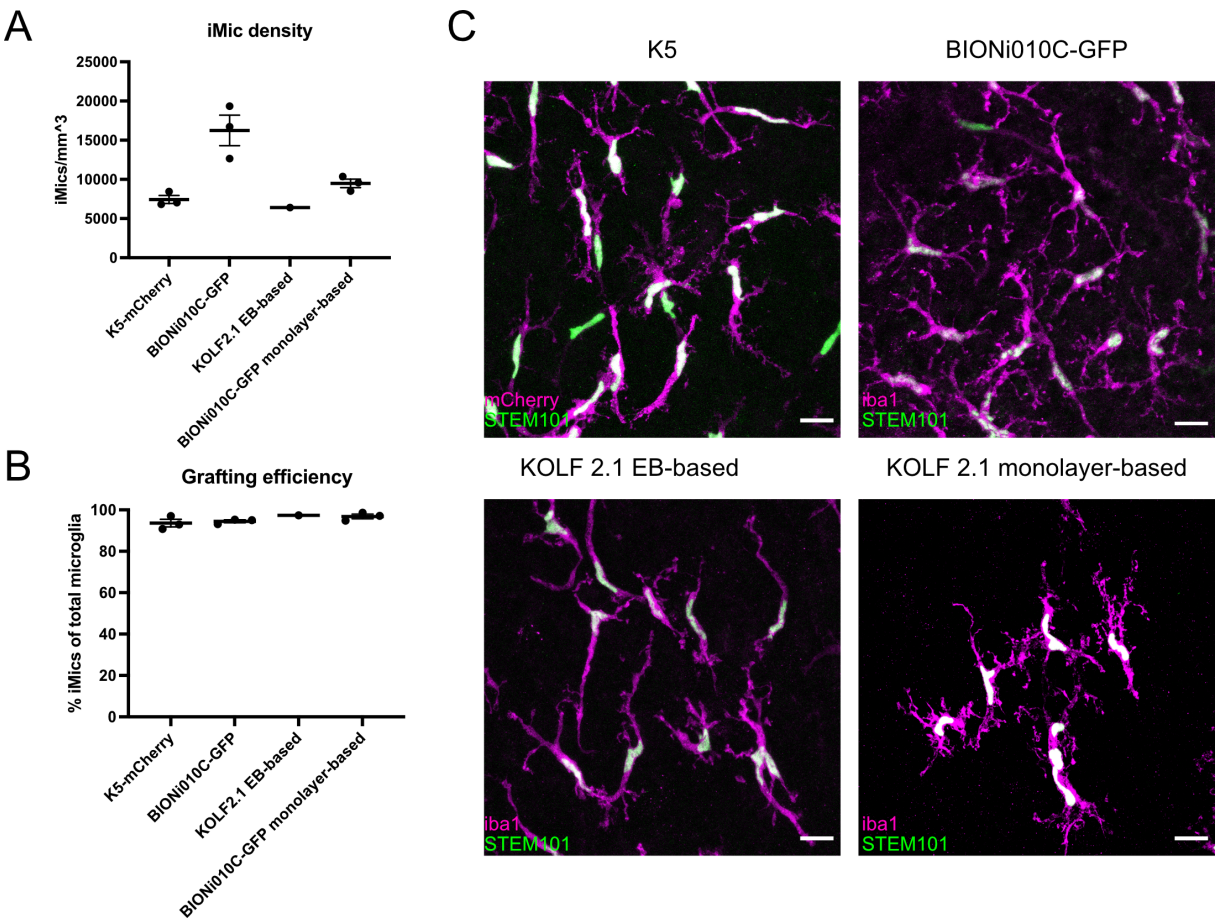

Figure 4.11 CSC with different iPSC lines and differentiation protocols
(A) Microglia density of CSC measured as microglia per volume. pre-iMics derived from different iPSC-lines (K5-mCherry, BIONi010C, KOLF2.1) and different microglia differentiation protocols (EB-based and monolayer-based) integrated in high numbers into mouse HSC. Kruskal-Wallis test with Dunn's multiple comparison test; p = 0.0014 **(B)** Grafting efficiency of CSC calculated by dividing the number of iMics (STEM101-positive cells) by the total number of microglia (PU.1-positive cells). iMics derived from different iPSC-lines (K5-mCherry, BIONi010C, KOLF2.1) and different microglia differentiation protocols (EB-based and monolayer-based) made up between 93.6 % and 97.4 % of total microglia in CSC 14 days after grafting. Kruskal-Wallis test with Dunn's multiple comparison test; p = 0.2357 **(C)** Representative images of iMics in Chimeric slice cultures 14 days after grafting derived from different iPSC-lines and differentiation protocols. iMics in all conditions were highly ramified as visualized by mCherry-expression (K5, magenta) or Iba1 staining (other conditions, magenta). STEM101 (green) was used to confirm human identity of the cells. Scale bars: 20 µm

2.2 Characterization of iMics in chimeric slice cultures

In order to validate CSC, a characterization of CSC and iMics in CSC was performed on a cellular and functional level. First, iMics morphology and network organization was investigated in comparison to mouse microglia in HSC and human microglia *ex vivo*. Furthermore, the functionality of iMics in CSC was assessed by 2-Photon live cell imaging and cytokine measurements and additionally profiled iMics on a transcriptional level. Lastly, I performed Calcium-imaging as a viability readout of CSC.

2.2.1 Morphological characterization of iMics in chimeric slice cultures

First, immunofluorescent staining of iMics in CSC at different timepoints was performed against Iba1 to visualize microglial morphology. From 7 DIV until 42 DIV a morphological maturation of iMics in CSC could be observed. Furthermore, overview images of the entire CSC revealed an even distribution of iMics over the entire slice culture (Figure 4.12 A). Quantification of the number of iMics in CSC and the percentage of iMics as compared to the total amount of microglia (grafting efficiency), revealed that iMics amount and grafting efficiency stabilized after 4 weeks at around 8000 iMics/mm^3 which is close to the reported microglia density in the mouse hippocampus (Keller, Erö, and Markram 2018) (5990 microglia/mm^3; Figure 4.12 B dotted line) and 97 % of all microglia were human-derived (Figure 4.12 B, C; Panel B: p = 0.1417; Panel C: n (groups)=6; p = 0.9547). In order to validate microglial identity of the cells, immunofluorescent staining against Iba1, PU.1 and TMEM119 was performed. All markers were expressed after 4 weeks, confirming a microglial identity of the cells (Figure 4.12 D). These findings were then further validated and several morphological and network parameters of iMics in CSC after 21 DIV (3 w) and 42 DIV (6 w) were compared with human ex vivo microglia derived from resective human brain surgery and mouse microglia in HSC. To this end, microglia from various sources were reconstructed with the 'Spots' and 'Filaments' tool of Imaris.

To assess the distribution of iMics throughout CSC, a Nearest-Neighbor-Distance (NND) approach based on the coordinates of the nucleus of each cell was used. The nearest neighbor distance of iMics in CSC was compared with the other aforementioned groups and a Kruskal-Wallis analysis with Dunn's multiple comparison test was performed. No significant differences between iMics in CSC and human microglia *ex vivo* were found. The mean NND for iMics at 42 DIV (31.95 µm) was almost identical to the mean NND of human microglia *ex vivo* (32.42 µm). While mouse microglia in HSC at 42 DIV had a comparably shorter NND (27.69 µm) indicating a higher density of mouse microglia in HSC (Figure 4.12 E; p = 0.0006).

The total number of branchpoints per cell was slightly, but not significantly increasing from 21 DIV (5.55 per cell) to 42 DIV (6.10 per cell) and overall very similar to human *ex vivo* microglia (4.77 per cell) (Figure 4.12 F; p = 0.3844). Similarly, the total process length per iMic in CSC slightly increased from 147 µm at 21 DIV to 160 µm at 42 DIV and was close to human *ex vivo* microglia at 133 µm (Figure 4.12 G; p = 0.8680). Furthermore, the volume each of the microglia surveilled was compared by reconstructing the cells with the 'Filaments' tool in Imaris and calculating the volume of the convex hull. For all groups, the volume each microglia surveilled was not significantly different. On average, iMics in CSC surveilled 4283 µm^3 per cell at 21 DIV and 5964 µm^3 per cell at 42 DIV, compared to 6959 µm^3 per cell for human *ex vivo* microglia (Figure 4.12 H; p = 0.4667). Overall, these analyses suggest that iMics in CSC mature morphologically to a similar ramification and distribute similarly compared to

human microglia *ex vivo*. Especially the high similarity of the network organization between iMics in CSC and human microglia *ex vivo* showed that CSC develop a human microglial network within mouse brain tissue *in vitro* which is reminiscent of the homeostatic human microglial network *ex vivo*.

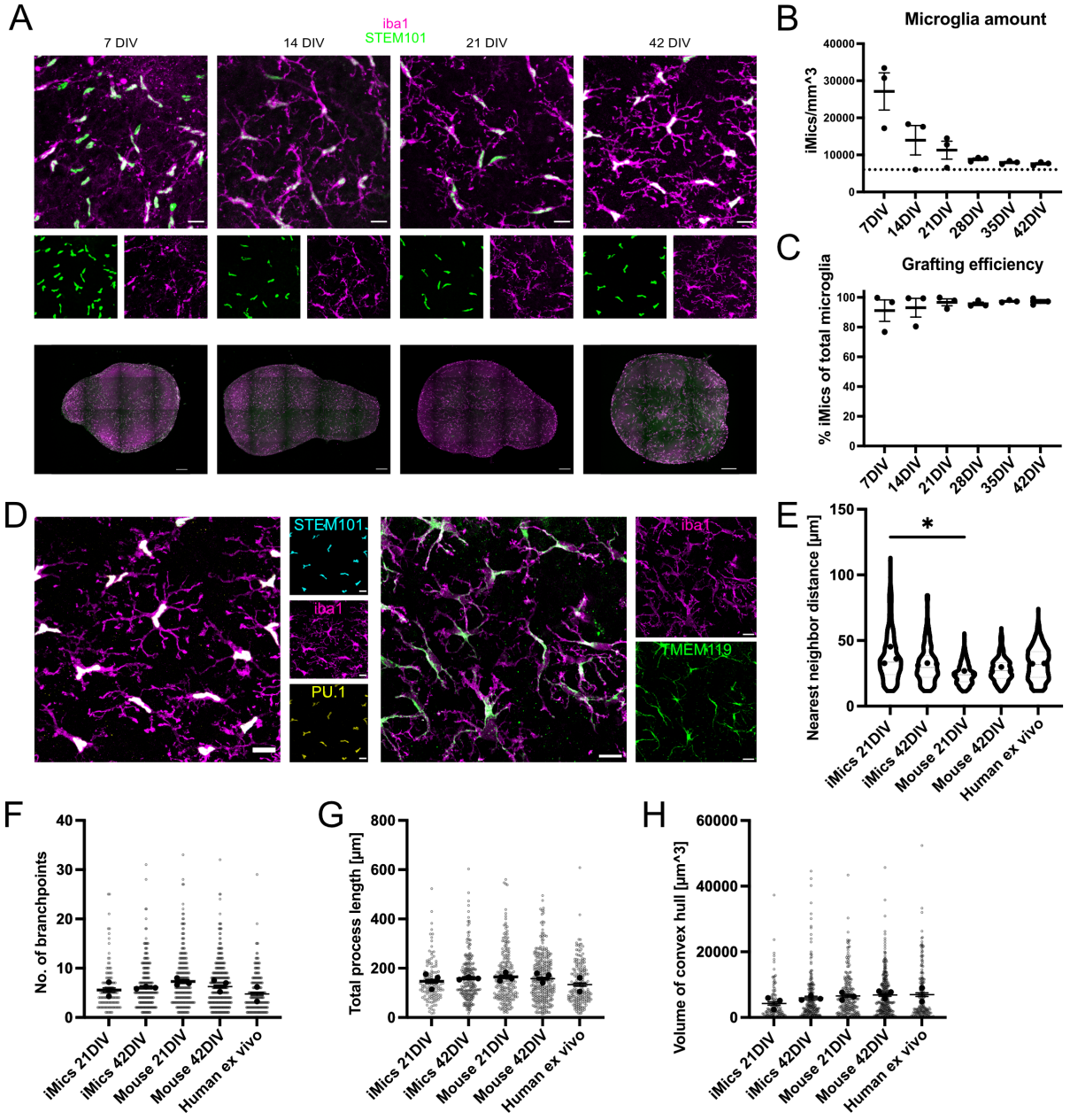

Figure 4.12 iMics are stably integrating into mouse hippocampal slice cultures and maturing towards a human *ex vivo* microglia-like phenotype

(A) Representative images of CSC at different timepoints of differentiation. iMics were stained against Iba1 (magenta) and STEM101 (green; human nuclei). Close-up images showed morphological maturation of iMics in CSC over time by increasing ramification of processes. Overview images (bottom row) showed an even distribution of iMics throughout the culture. Scale bars: 20 µm (Close-ups) and 200 µm (overview images). **(B)** iMic density of CSC measured as iMics per volume. After decreasing over the first three weeks, the density of iMics (counted as STEM101-positive cells) stabilized at around 8000 cells/mm³. The dotted line indicates microglial density in the mouse hippocampus at 5990 cells/mm³. n (groups)=6; number of independent experiments per group = 3; Kruskal-Wallis test p = 0.1417 **(C)** Grafting efficiency of CSC calculated by dividing the number of iMics (STEM101-positive cells) by the total number of microglia (PU.1-positive cells). After three weeks the grafting efficiency stabilized above 95 %. n (groups)=6; number of independent experiments per group = 3; Kruskal-Wallis test with Dunn's multiple comparison test p = 0.9547 **(D)** Representative immunofluorescent images of microglial markers. The left panel shows STEM101-positive cells also expressing Iba1 and PU.1. The right panel shows the

expression of hTMEM119 in Iba1-positive cells. Scale bars: 20 µm **(E)** Nearest neighbor distance [µm] of iMics in CSC compared to endogenous mouse microglia and *ex vivo* human microglia. Localization of cell somata was reconstructed with the Spots mode of Imaris 9.7.2. The mean of all microglia from one well is indicated as black dot, individual values are indicated via Violin-plots. n (groups)=5; number of independent experiments per group = 2-3; Kruskal-Wallis test with Dunn's multiple comparison test p = 0.0006 **(F - H)** Number of branch points (F), total process length [µm] (G) and volume of convex hull (=surveilled volume per cell) [µm^3] (H) of iMics in CSC compared to endogenous mouse microglia and *ex vivo* human microglia. Cells were reconstructed with the filaments mode of Imaris 9.7.2. The mean of all microglia from one well is indicated as black dot, individual values are indicated as gray dots. n (groups)=5; number of independent experiments per group = 2-3; Kruskal-Wallis test with Dunn's multiple comparison test F: p = 0.3844**; G:** p = 0.8680**; H:** p = 0.4667

2.2.2 Functional characterization of iMics in chimeric slice cultures

Moreover, in order to analyze iMics functionality, 2-Photon live cell imaging of BIONi010C-iMics 21 DIV endogenously expressing GFP was performed to compare their homeostatic process movement with mouse microglia in Iba1-EGFP HSC. Z-stacks of one position were acquired every 2 minutes for 20 minutes and cells were subsequently reconstructed with the 'Filaments' tool of Imaris to track process movement over time. Overlay of z-stacks from different time points indicated homeostatic process movement (Figure 4.13 A; colorful terminal points of processes) and quantification of process movement did not reveal a significant difference between grafted iMics in CSC and endogenous mouse microglia in HSC (means: iMics 21 DIV: 0.02902 µm/s; Mouse 21 DIV: 0.02925 µm/s) (Figure 4.13 B; p = 0.8203).

A common assay to test functionality of microglia, is to induce a focal laser injury to the tissue to test for a quick reaction of microglia to shield the injury site. For this purpose, a laser beam (810 nm, 8 sec) was applied to a random spot in the tissue and z-stacks were acquired every 2 minutes for 30 minutes to observe the subsequent reaction. Both iMics in CSC and endogenous mouse microglia in Iba1-EGFP HSC were found to quickly react to the laser injury (Figure 4.13 C; magenta circle) by moving their processes towards the injury site within minutes. Similar to above, colorful spots in the merge images indicate movement of the cells. The reaction to laser injury was then quantified by plotting the normalized fluorescent intensity of the iMics/microglia channel against the distance to the lesion site. Before the lesion, both iMics and endogenous mouse microglia showed a random distribution of the fluorescent intensity. After the injury, the normalized fluorescent intensity quickly increased close to the injury site and peaked after 30 minutes, while the fluorescent intensity remained randomly distributed in the more distant parts. The reaction for both iMics in CSC and endogenous mouse microglia was very similar, indicating functionality of iMics in CSC (Figure 4.13 D).

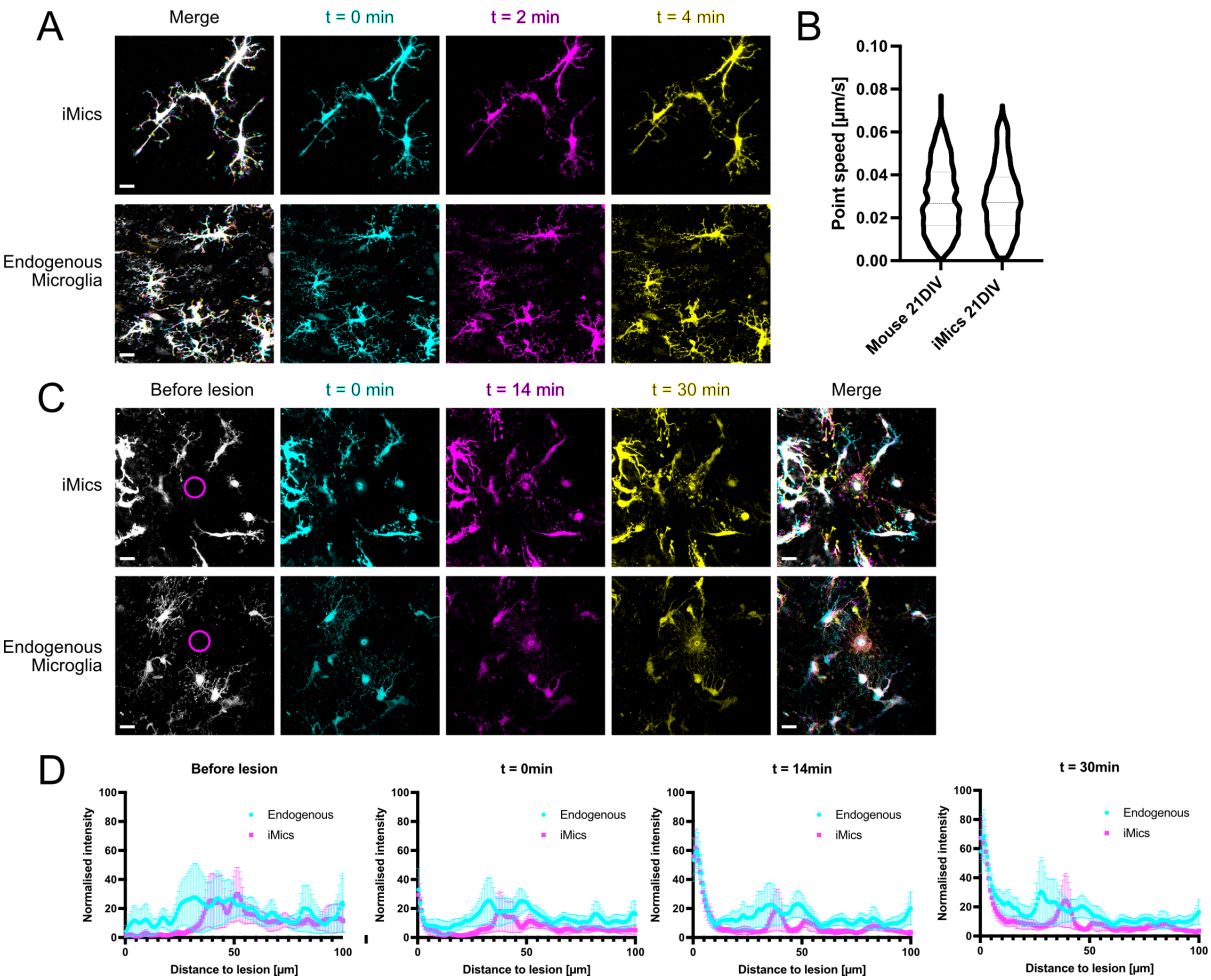

Figure 4.13 iMics in chimeric slice cultures are motile and respond to focal laser injury
(A) Representative images of homeostatic movement of iMics in CSC (upper row) and endogenous mouse microglia in HSC (bottom row) at 21 DIV. Shown are images for 0 min (cyan), 2 min (magenta) and 4 min (yellow). The cyan, magenta and yellow processes in the merge images show process movement of the cells. Scale bars: 20 µm **(B)** Violin plots of the speed of process movement. Processes in 30 min movies (2 min intervals) were tracked semi-automatically with Imaris. Mann-Whitney-Test: p = 0.8203; n (mouse 21 DIV) = 769 (tracked processes); n (iMics 21 DIV) = 390 **(C)** Representative images of the response to a focal laser injury of iMics in CSC (upper row) and endogenous mouse microglia in HSC (bottom row) at 21 DIV. Shown are images before the lesion (white; not included in the merge image) for 0 min (cyan), 14 min (magenta) and 30 min (yellow) after the lesion. The cyan, magenta and yellow processes in the merge images show process movement towards the injury site and the formation of a barrier. Scale bars: 20 µm **(D)** Normalized intensity of the fluorescence of iMics (magenta) and endogenous mouse microglia (cyan) plotted against the distance from the injury site for 4 different time points (before the lesion, 0 min, 14 min and 30 min after the laser lesion). Note the sharp increase over time of the intensity close to the lesion site (0-10 µm distance) for both groups. n (Endogenous) = 9 movies from independent cultures = n(iMics); Mean ± SEM

Furthermore, the ability of iMics in CSC to secrete pro-inflammatory cytokines was tested. For this purpose, CSC were treated with either a chronic low dose LPS stimulus (25 ng/ml) for 7 days or with an acute high-dose stimulus (200 ng/ml) for 24 hours in order to simulate a bacterial infection. The concentration of human pro-inflammatory cytokines in the culture medium was measured using a human-specific cytokine panel on the Mesoscale (MSD) platform. Treatment started at 14 DIV (Figure 4.14 A). While human cytokines were measurable neither in the untreated control condition nor in LPS treated HSC without human iMics (or only at a low level), both the chronic and the acute LPS stimulus

elicited a diverse pro-inflammatory cytokine release in CSC. An increase in IL1β, TNFα, IL8 and IL6 was measured. Interestingly, only for IL8 the release levels were at the same level between the two different LPS paradigms. For all other measured cytokines, the acute LPS stimulus elicited the highest cytokine release (Figure 4.14 B). All in all, these results indicated that iMics in CSC were capable of functionally reacting to diverse stimuli.

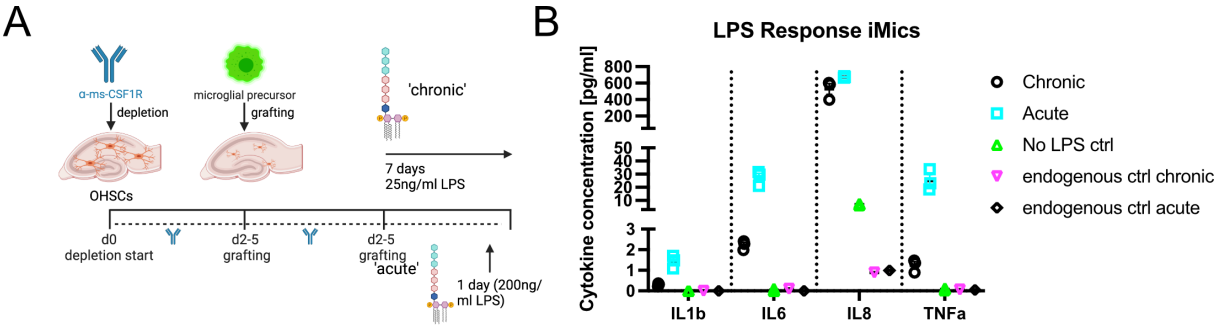

Figure 4.14 iMics in chimeric slice cultures respond to a pro-inflammatory LPS stimulus
(A) Experimental set-up. 14 days after grafting chronic low dose treatment (25 ng/ml LPS) with LPS was started and continued for 7 days, while acute high dose treatment (200 ng/ml LPS) was started 20 days after grafting and lasted for 24 hours **(B)** Human-specific mesoscale measurements of four pro-inflammatory cytokines showed an increase in cytokine secretion into the cell culture medium after stimulation of CSC after chronic and acute LPS stimulation compared to unstimulated CSC and stimulated HSC with endogenous mouse microglia only (endogenous ctrl). n (groups)= 5; number of independent experiments per group = 3

2.2.3 Transcriptional characterization of iMics in chimeric slice cultures

Next, iMics were characterized on a transcriptional level in order to investigate their maturation and differentiation in CSC for an extended period of time. Single cell RNA sequencing (scRNAseq) was performed in pre-iMics and iMics in CSC at 3, 6 and 11 weeks *in vitro*. scRNAseq showed a down-regulation of genes associated with proliferation (CENPF, SPC24 and MKI67) from the precursor stage towards differentiating microglia over time. Additionally, homeostatic markers of microglia, such as P2RY12, CX3CR1 and CSF1R, as well as genes involved in immunological functions of microglia such as the complement system and antigen presentation, were upregulated, indicating that iMics were more and more differentiating towards mature microglia over time. Furthermore, increased expression of P2RY12, CX3CR1 and OLFML3, markers specific for microglia (Chiu et al. 2013; Wes et al. 2016), identified iMics in CSC as microglia and distinguished them from peripheral macrophages and monocytes. At 11 weeks *in vitro*, however, iMics in CSC showed a strong downregulation of homeostatic markers, such as P2RY12, CX3CR1 and CSF1R, and a drastic upregulation of genes previously associated with aging and neurodegeneration. At 11 weeks, iMics showed upregulation of the complement system and antigen presentation but also strongly upregulated genes involved in antigen presentation, phagocytosis and other disease-associated microglia (DAM) genes, such as APOE and TREM2 (Keren-Shaul et al. 2017). Furthermore, iMics in CSC upregulated genes involved in the

interferon response which were previously identified as key genes of a microglial subpopulation called interferon-responsive microglia (IRM), a subpopulation of microglia associated with aging (Olah et al. 2020; Sala Frigerio et al. 2019). All in all, these results indicated that iMics in CSC differentiate into homeostatic microglia within six weeks but that CSC at 11 weeks *in vitro* showed signs of aging or degeneration and iMics reacted to this changed environment by adapting an IRM or DAM-like phenotype (Figure 4.15).

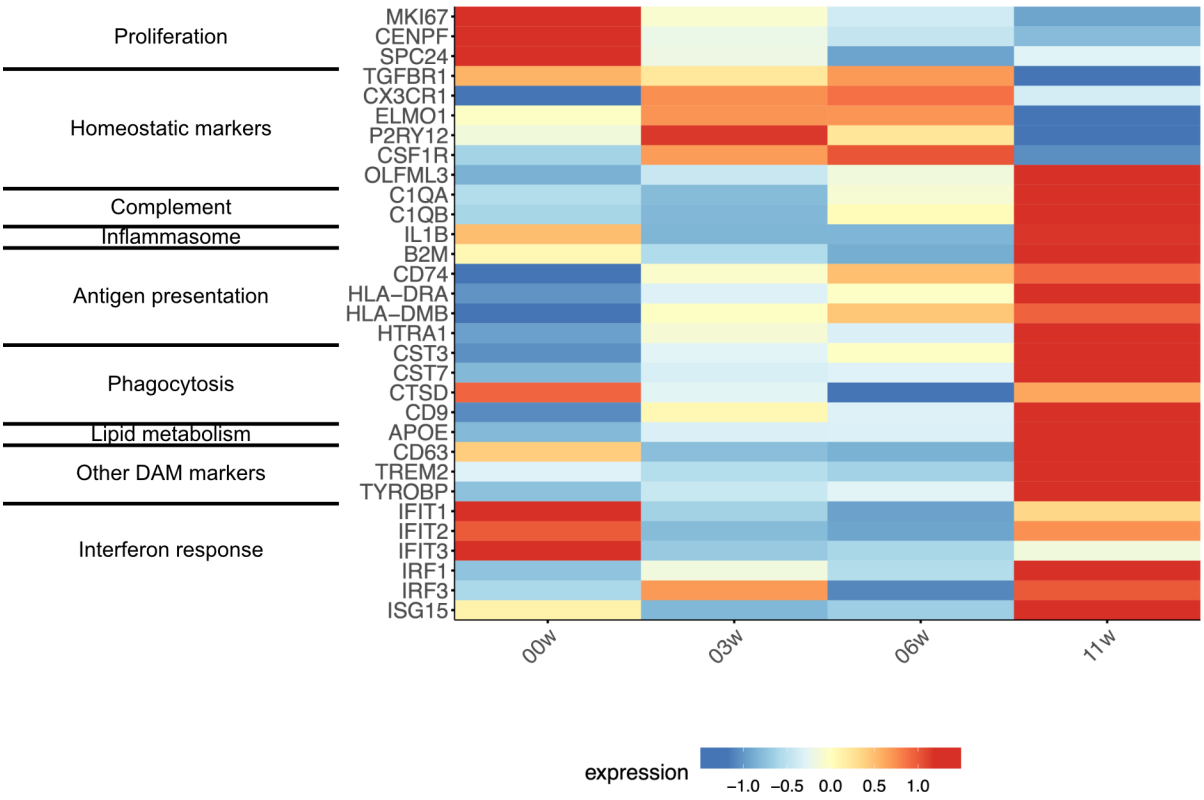

Figure 4.15 RNA sequencing of iMics in chimeric slice cultures
Heatmap depicting differentially expressed genes from scRNAseq of pre-iMics and iMics in CSC at 3, 6 and 11 weeks *in vitro*. Genes involved in proliferation were rapidly downregulated and key microglial homeostatic markers showed increased expression from precursors to 6w *in vitro*. At 11 weeks, homeostatic markers were downregulated and inflammation, neurodegeneration and aging-associated genes were strongly upregulated.

2.2.4 Electrophysiological characterization of chimeric slice cultures

Lastly, the viability of the new culture system was determined by measuring the electrical activity of CSC by calcium imaging of entire slice cultures. Control HSC, microglia depleted HSC and CSC were incubated with Calbryte590-AM, a small-molecule calcium sensor, after 12 weeks, and calcium activity was recorded for three minutes at ten Hertz. Subsequently, images were analyzed with FIJI and MATLAB. Each timepoint at which at least 10 ROIs were spiking simultaneously was defined as synchronous spiking. While stimulation with 4-AP led to a significant increase in spike rate, no

significant differences between the different culturing conditions were found, neither for unstimulated nor for 4-AP stimulated cultures (Figure 4.16; A: p = 0.6691; B: p = 0.6259; C: p = 0.3080).

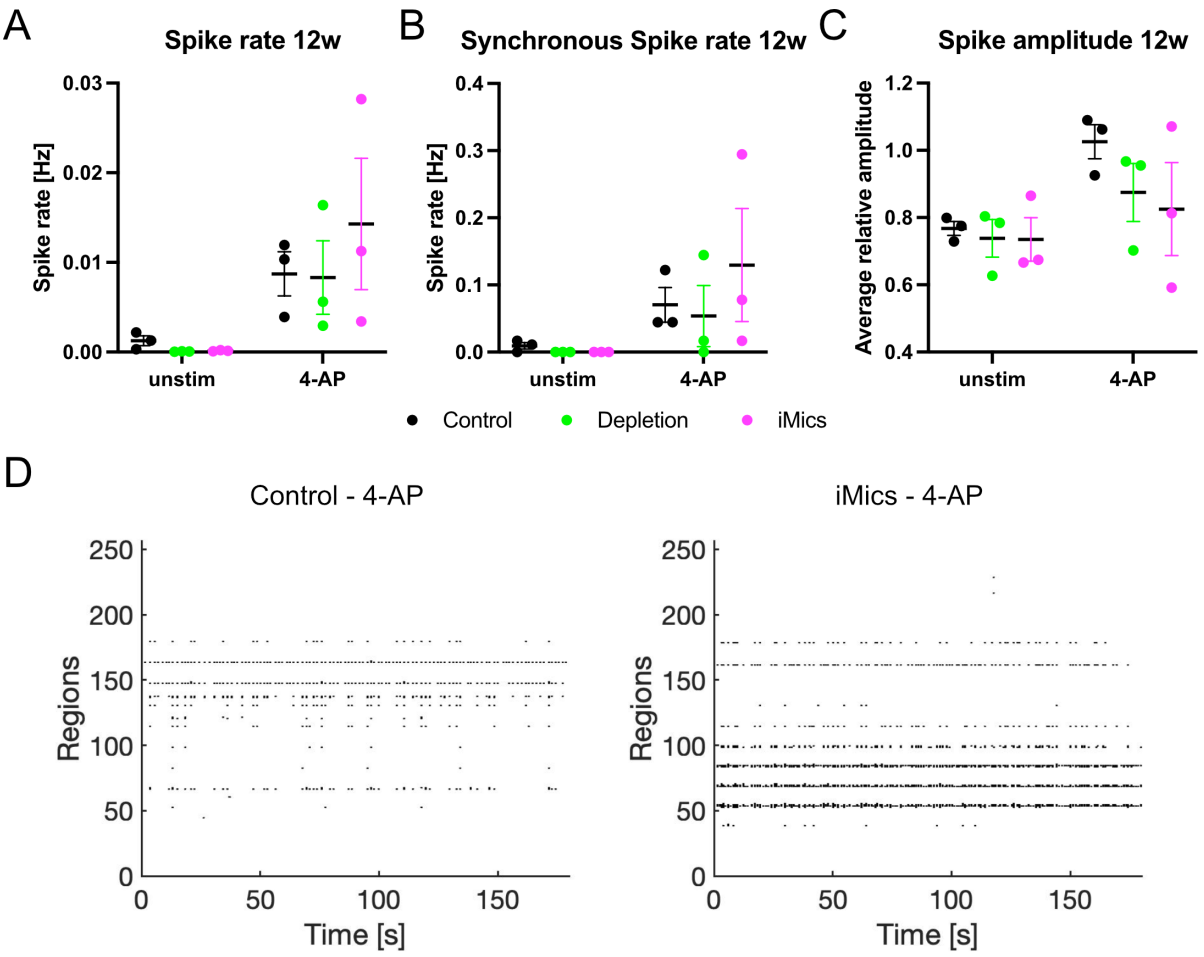

Figure 4.16 Chimeric slice cultures are electrophysiologically active
(A - C) Spike rate (A), synchronous spiking activity (B) and average spike amplitude (C) during calcium imaging of HSC with mouse microglia (control), without any microglia (depletion) and CSC (iMics) in baseline conditions and with 4-AP stimulation. No significant differences for the different culturing conditions were detected (A: p = 0.6691; B: p = 0.6259; C: p = 0.3080) **(B)** Spike activity pattern of control mouse HSC (left) and CSC (right) during Calcium imaging of the entire slices with 4-AP stimulation. For the purpose of analysis, each image was divided into 256 ROIs (Y-axis). Each measurement was performed for 3 min at 10 Hz.

Together with the detailed analysis of iMics, calcium imaging revealed that CSC are a viable culture system for 12 weeks with human iMics that closely resemble human microglia *ex vivo* in their morphological, functional and transcriptional phenotype, as well as in their network organization and thus could be used to study human microglial network homeostasis *in vitro*.

2.3 Modelling of synucleinopathies in chimeric slice cultures

As microglia play a major role in several neurodegenerative diseases, CSC were also validated in the context of neurodegenerative pathology. To this end, synucleinopathy was induced in CSC according to a previously established protocol in the laboratory (Barth et al. 2021) and the reaction of iMics to

the pathological insult was characterized by immunofluorescent staining, cytokine profiling and scRNAseq five weeks after seeding.

2.3.1 Induction of synucleinopathy in chimeric slice cultures

Before the induction of synucleinopathy, CSC were generated as described above. HSC were prepared from four to six days old B6 mice and endogenous mouse microglia were replaced by iMics. At 42 DIV αsyn pff were drop-seeded onto CSC and cultivated for another 35 days (Figure 4.17 A). 35 days after seeding, CSC were fixed in PFA and the resulting pathology was assessed via immunofluorescent staining against Iba1 and pS129-αsyn, a marker for pathology-associated forms of αsyn (Fujiwara et al. 2002). iMics were found to be evenly distributed and pS129-positive αsyn pathology was also widely detectable (Figure 4.17 B). Thus, the induced synucleinopathy in CSC was comparable to the described pathology in HSC with endogenous mouse microglia (Barth et al. 2021). However, since iMics in CSC were differentiated from human iPSCs, this enabled the possibility to study the properties and responses of human microglia in synucleinopathy in a novel model system.

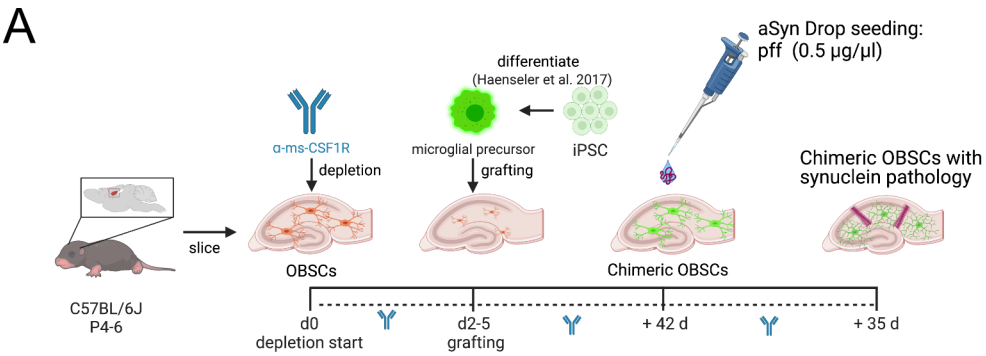

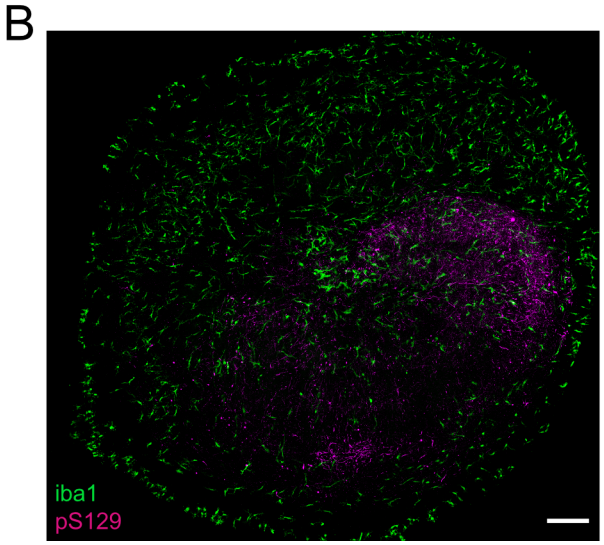

Figure 4.17 CSC can be induced with synucleinopathies and develop pS129+-inclusions after seeding with αsyn-pff
(A) Experimental set-up. Six weeks after grafting 1µl α-syn pre-formed fibrils (0.5 µg/µl) was drop-seeded onto CSC to induce synucleinopathy and cultivation was continued for another 5 weeks. **(B)** Overview image of a CSC that was treated according to the above experimental scheme. iMics were stained with Iba1 (green) and pathological synuclein was stained against pS129 (magenta). Scale bar: 200 µm

2.3.2 Microgliosis and microglial inclusions in chimeric slice cultures with synucleinopathy

One of the most prominent microglial phenotypes in synucleinopathies, such as PD, is microgliosis which is amongst others characterized by the proliferation of microglia. In order to test if microgliosis in CSC is detectable, the density of iMics was determined three and five weeks after treatment with αsyn-pff in CSC derived from A53T-transgenic mice. A53T-transgenic mice are a common model of synucleinopathy with neuronal αsyn inclusions and prominent motor symptoms (van der Putten et al. 2000). For both timepoints, iMic densities in synucleinopathy-induced CSC was doubled compared to untreated CSC, while iMic density remained stable over time within each condition showing microgliosis in CSC after induction of synucleinopathy (Figure 4.18 A; $p = 0.0398$).

Next, I aimed to find out if iMics in CSC treated with αsyn-pff would also develop microglial inclusions with αsyn, as recently described by my laboratory in different mouse models of synucleinopathy (Tanriöver et al. 2020) and in αsyn-pff treated HSC (Barth et al. 2021). Interestingly, microglial inclusions of αsyn cannot be detected with immunofluorescent staining against pS129. Therefore, pentameric formyl thiophene acetic acid (pFTAA), a luminescent conjugated oligothiophene (LCO) that binds to amyloid structures such as αsyn fibrils (Tanriöver et al. 2020), was used to detect these inclusions. For quantification of microglial inclusions, CSC were stained for human microglia (Iba1 and STEM101) together with pFTAA. Microglial inclusions were present in both CSC derived from B6 and A53-transgenic mice engrafted with BIONi010C and KOLF2.1 iMics, respectively (Figure 4.18 B).

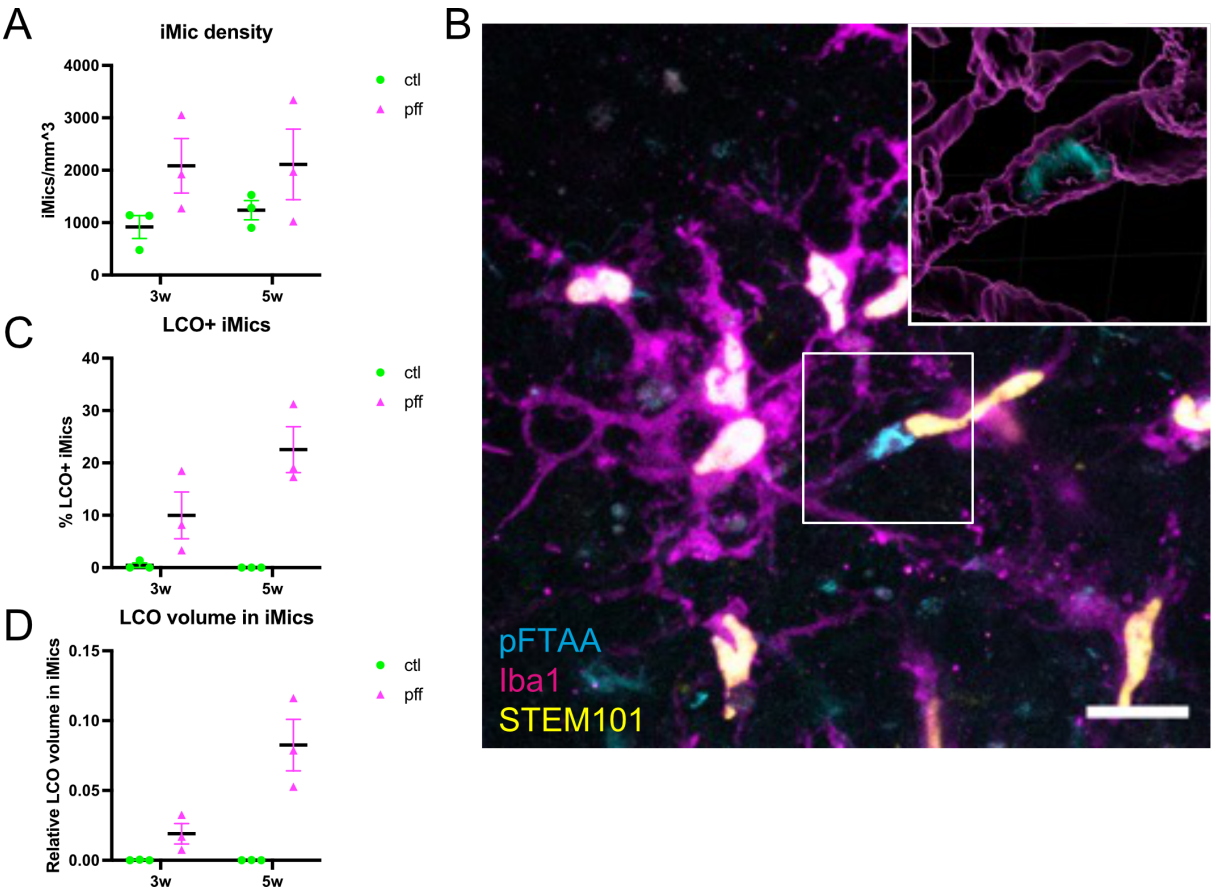

Figure 4.18 Microgliosis and inclusions in iMics in CSC
(A) iMic density of CSC measured as iMics per volume. Higher microglial densities were seen three and five weeks after pff-treatment, indicating microgliosis as response to induced synucleinopathy. number of independent experiments per group = 3; 2-Way ANOVA p (pff-treatment) = 0.0398 **(B)** Representative image of iMics (magenta) in α-syn pre-formed fibrils-treated CSC that showed intracellular pFTAA (cyan, amyloid-binding dye) inclusions. Human nuclei were stained with STEM101 (yellow). Scale bar: 20µm **(C)** Quantification of iMics with LCO+ inclusions in synucleinopathy-induced CSC. LCO+ inclusions could not be detected in untreated CSC, while LCO+ inclusions increased from three to five weeks. number of independent experiments per group = 3; 2-Way ANOVA p (pff-treatment) = 0.0018 **(D)** Relative LCO volume within iMics. Only LCO-signal within iMics was quantified and the relative volume of LCO signal within iMics was calculated by dividing the absolute volume of LCO within iMics by the total volume of the culture and multiplied by 100. No LCO signal was present in control CSC, while the relative volume of LCO increased from three to five weeks. number of independent experiments per group = 3; 2-Way ANOVA p (pff-treatment) = 0.0059

In order to exclude that the detected microglial inclusions are not derived from the initial seed material but from endogenously amplificated αsyn fibrils, microglial inclusions were quantified three and five weeks after pff treatment of CSC prepared from A53T-transgenic mice. Three weeks after pff-treatment roughly 10 % of iMics were positive for LCO-inclusions. Two weeks later, the percentage of LCO-positive iMics increased to more than 20 %. Moreover, the relative volume of LCO signal within iMics was quantified in order to exclude that iMics only shared the initial burden of the seed and redistributed the inclusions. No LCO signal was detected within iMics in untreated CSC. However, LCO signal was detected three weeks after seeding and was almost fourfold increased two weeks later in αsyn-pff-treated CSC indicating that endogenously amplificated αsyn fibrils were incorporated in

microglial inclusions of αsyn and not only the initial seed was phagocytosed (Figure 4.18 C, D; Panel C: p = 0.0018; Panel D: p = 0.0059). Overall, these results showed that microgliosis and microglial inclusions are reproducible in iMics in CSC.

2.3.3 Inflammatory and transcriptomic response of iMics in chimeric slice cultures with synucleinopathy

Next, the functional response of iMics in CSC with synucleinopathy from B6 mice was characterized. To this end, pro-inflammatory cytokines in the culture medium were measured at different time points via a human-specific cytokine panel using the MSD platform and compared to untreated CSCs.

48 hours after pff-treatment, all measured cytokines were significantly increased compared to control CSC indicating a strong response to the initial seed. After three and five weeks, however, the levels of the pro-inflammatory cytokines IL1β, IL6 and TNFα went back to baseline levels. Only levels for IL8 remained elevated over the concentrations of control CSC over time (Figure 4.19 IL1β: p = 0.0167**;** IL6: p = 0.1155; IL8: p = 0.0020; TNFα: p = 0.0466). All in all, iMics in CSC showed a diverse pro-inflammatory response to synucleinopathy with a strong initial response and a weak, sustained elevation of IL-8 levels.

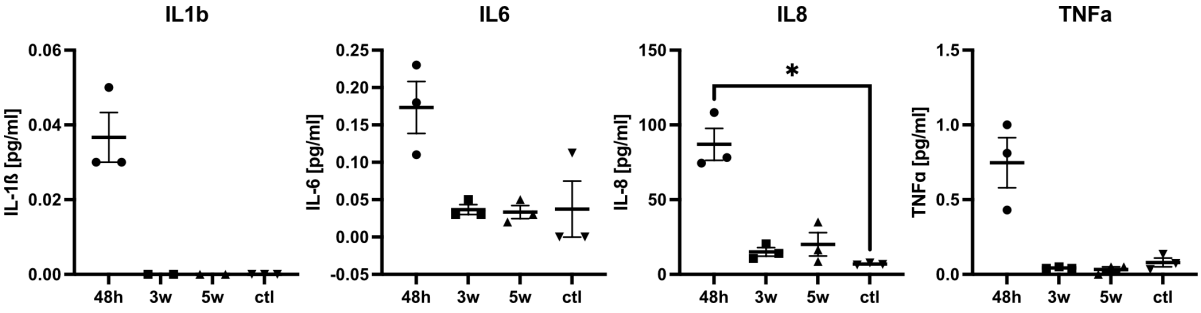

Figure 4.19 Inflammatory response of iMics in CSC to the induction of synucleinopathy
Human-specific mesoscale measurements of four pro-inflammatory cytokines showed an increase in cytokine secretion into the cell culture medium after α-syn pff treatment. Cytokine secretion peaked at 48 h after the treatment and decreased over time back to control levels for all 4 cytokines. Only for IL8, cytokine levels remained above baseline level for an extended period of time. n (groups)=4 per cytokine; number of independent experiments per group = 3; Kruskal-Wallis test with Dunn's multiple comparison test IL1β: p = 0.0167**;** IL6: p = 0.1155; IL8: p = 0.0020; TNFα: p = 0.0466

Lastly, in order to investigate the transcriptional response of iMics in CSC with synucleinopathy and to see if DAM-genes were upregulated in iMics upon induction of disease as described in the literature (Keren-Shaul et al. 2017; Krasemann et al. 2017), scRNAseq was performed on CSC from B6 mice which were treated with αsyn-pff at 6 weeks *in vitro* and cultivated for another five weeks and compared to age-matched control CSC and to the baseline transcriptome at 6 weeks *in vitro*. As expected from the previous scRNAseq timeline (Figure 4.15), iMics in CSC for both treatment and control conditions,

downregulated the key microglial homeostatic markers P2RY12, CX3CR1, CSF1R and HEXB at 11 weeks *in vitro*.

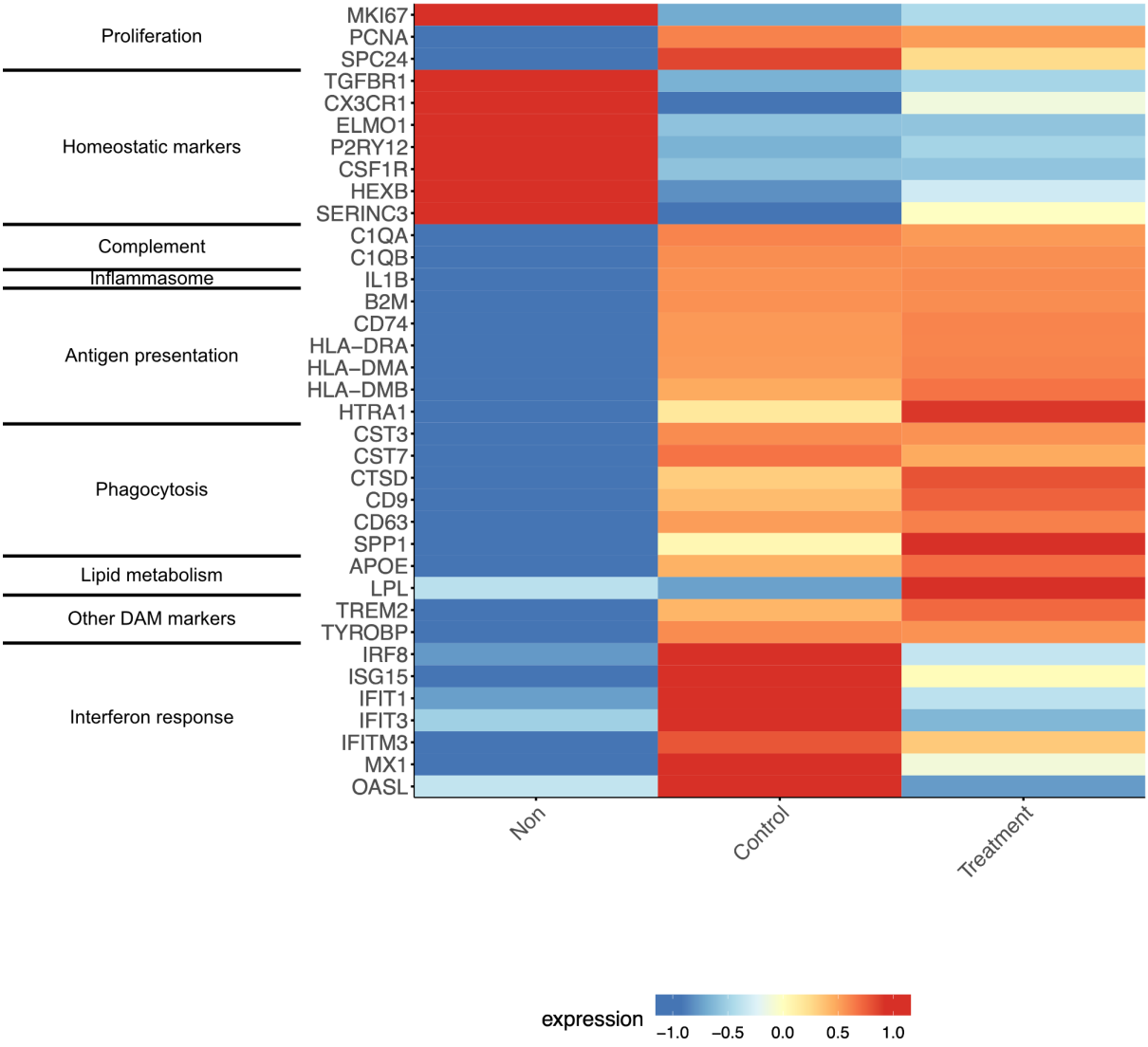

Figure 4.20 Single cell RNA sequencing of iMics in chimeric slice cultures with synucleinopathy
Heatmap depicting differentially expressed genes from scRNAseq analysis of iMics in CSC with αsyn pathology for 5 weeks (Treatment) compared to the baseline (Non; iMics 6 weeks *in vitro*) and age-matched control CSC (Control). At 11 weeks *in vitro* both groups showed an upregulation of proliferation-associated genes as compared to 6 weeks. Moreover, both groups downregulated homeostatic microglial genes and upregulated neurodegeneration and aging associated pathways. iMics in control CSC at 12 weeks showed mostly an aging-associated IRM phenotype while iMics in CSC with synucleinopathy showed a higher upregulation of phagocytosis-associated and other DAM genes.

Moreover, compared to 6 weeks *in vitro* both groups upregulated genes involved in proliferation, complement, inflammation, antigen presentation, phagocytosis, interferon response and other DAM genes with increasing time *in vitro*, indicating a general activation of microglia towards a degeneration and aging phenotype (Keren-Shaul et al. 2017; Krasemann et al. 2017; Sala Frigerio et al. 2019). When comparing αsyn pff-treated and untreated CSC at 11 weeks *in vitro*, iMics from control CSC showed a stronger upregulation of interferon response genes, further highlighting a pronounced aging-

associated transcriptional phenotype at 11 weeks *in vitro*. In contrast to that, iMics from seeded CSC showed a stronger upregulation of classical DAM genes, such as APOE, LPL, TREM2 and TYROBP showing amongst others, a changed reaction to lipids. Furthermore, iMics from treated CSC upregulated phagocytosis-associated genes, while expression levels of complement and antigen presentation associated genes were comparable between the groups. Overall, this shows that iMics in CSC with synucleinopathy do not only react to the aging culture by transitioning into IRM-like microglia but also react to the induced neurodegenerative pathology by upregulation of DAM markers that have initially been described for AD (Keren-Shaul et al. 2017) (Figure 4.20).

2.4 iMic network in chimeric slice cultures in the absence of human cytokines

2.4.1 Differentiation of CSF1R mutant iPSC into iMic precursors

The current dogma in immunology states that mouse CSF1 and IL34 cannot bind to human CSF1R (Elmore et al. 2014; Rathinam et al. 2011; Sieff 1987), which is further supported by recent microglia chimeric mouse models (Hasselmann et al. 2019; Mancuso et al. 2019). However, iMics in CSC do not require supplementation of human cytokines to the system for integrating and differentiating into mature microglia with an evenly distributed, similarly dense microglia network when compared to human microglia *ex vivo*. In order to understand these opposing findings, CSF1R E633K loss-of-function mutant iPSC on the background of the KOLF2.1J line (Pantazis et al. 2022) were used to prove that iMics in CSC are dependent on CSF1R signaling for their integration, differentiation and survival. Patients with the E633K mutation in CSF1R suffer from Hereditary diffuse leukoencephalopathy with spheroids (Rademakers et al. 2012), an autosomal dominant disease which is among others characterized by a reduced number of microglia in the brain (Tada et al. 2016), showing the importance of CSF1R for a proper microglia network homeostasis. Additionally, these patients experience dementia, parkinsonism, epileptic seizures and depression.

First, to obtain pre-iMacs for grafting onto microglia-depleted HSC, iPSC from the four different lines ($CSF1R^{+/+}$ WT, $CSF1R^{+/E633K}$ heterozygous, $CSF1R^{E633K/E663K}$ homozygous and $CSF1R^{-/-}$ KO) were differentiated as described above. Mesodermal fate induction and generation of EBs was not different for any of the lines showing the independence of CSF1R during this step (Figure 4.21 1st row). During the next step of the differentiation protocol, EBs serve as 'factories' for the production of iMic-precursors (pre-iMics). However, before producing actual pre-iMics, EBs first produce less differentiated and smaller precursor cells. This stage of differentiation was still observed for all genotypes. About a week after producing these smaller precursors, EBs start to generate vast amounts

of the desired pre-iMics, characterized by their larger size and a bright halo in phase-contrast microscopy.

This stage of pre-iMics can then be used for monocultures, co-cultures with neurons or for engraftment. Only CSF1R$^{+/+}$ WT and CSF1R$^{+/E633K}$ heterozygous EBs were able to generate this final stage of precursors while CSF1R$^{E633K/E663K}$ homozygous and CSF1R$^{-/-}$ KO EBs were unable to transition to this stage (Figure 4.21 2nd row). Accordingly, only CSF1R$^{+/+}$ WT and CSF1R$^{+/E633K}$ heterozygous pre-iMics were able to attach and differentiate in monoculture (Figure 4.21 3rd row). As expected, this experiment showed that CSF1R signaling is necessary for differentiation of iPSC into microglia in monoculture.

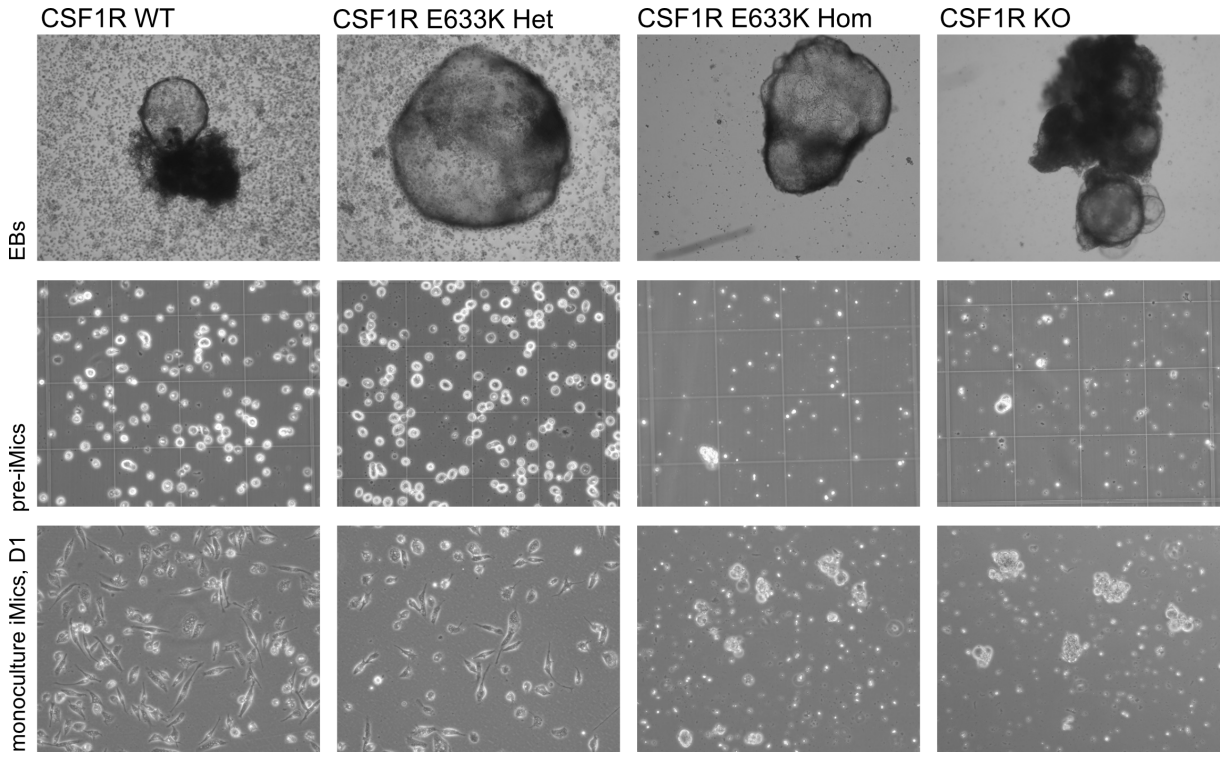

Figure 4.21 CSF1R signaling is required for *in vitro* differentiation of iMics
Initial steps of differentiation from iPSC to pre-iMics in KOLF2.1J iPSC harboring WT (1st column), heterozygous (2nd column) or homozygous E633K mutant (3rd column) or KO CSF1R (4th column). No differences were observed in EB formation efficiency and EB morphology (1st row). However, CSF1R$^{E633K/E663K}$ and CSF1R$^{-/-}$ lines failed to produce proper iMic-progenitor cells, which were much smaller and less abundant compared to CSF1R$^{+/+}$ and CSF1R$^{+/E633K}$ (2nd row). Additionally, pre-iMics plated in monoculture did not differentiate when harboring no functional CSF1R (3rd row, 3rd and 4th column). CSF1R$^{+/+}$ and CSF1R$^{+/E633K}$ pre-iMics both attached to the plate and showed first signs of morphological differentiation by extending processes. EBs imaged at 4x magnification, pre-iMics and iMics imaged at 10x magnification.

2.4.2 Integration of CSF1R mutant iMic precursors into chimeric slice cultures

After showing that CSF1R$^{+/E633K}$ heterozygous iPSC can be successfully differentiated into microglia in monoculture, the same four lines were used to generate CSC and the amount of integrated iMics was assessed at 7, 14 and 28 DIV.

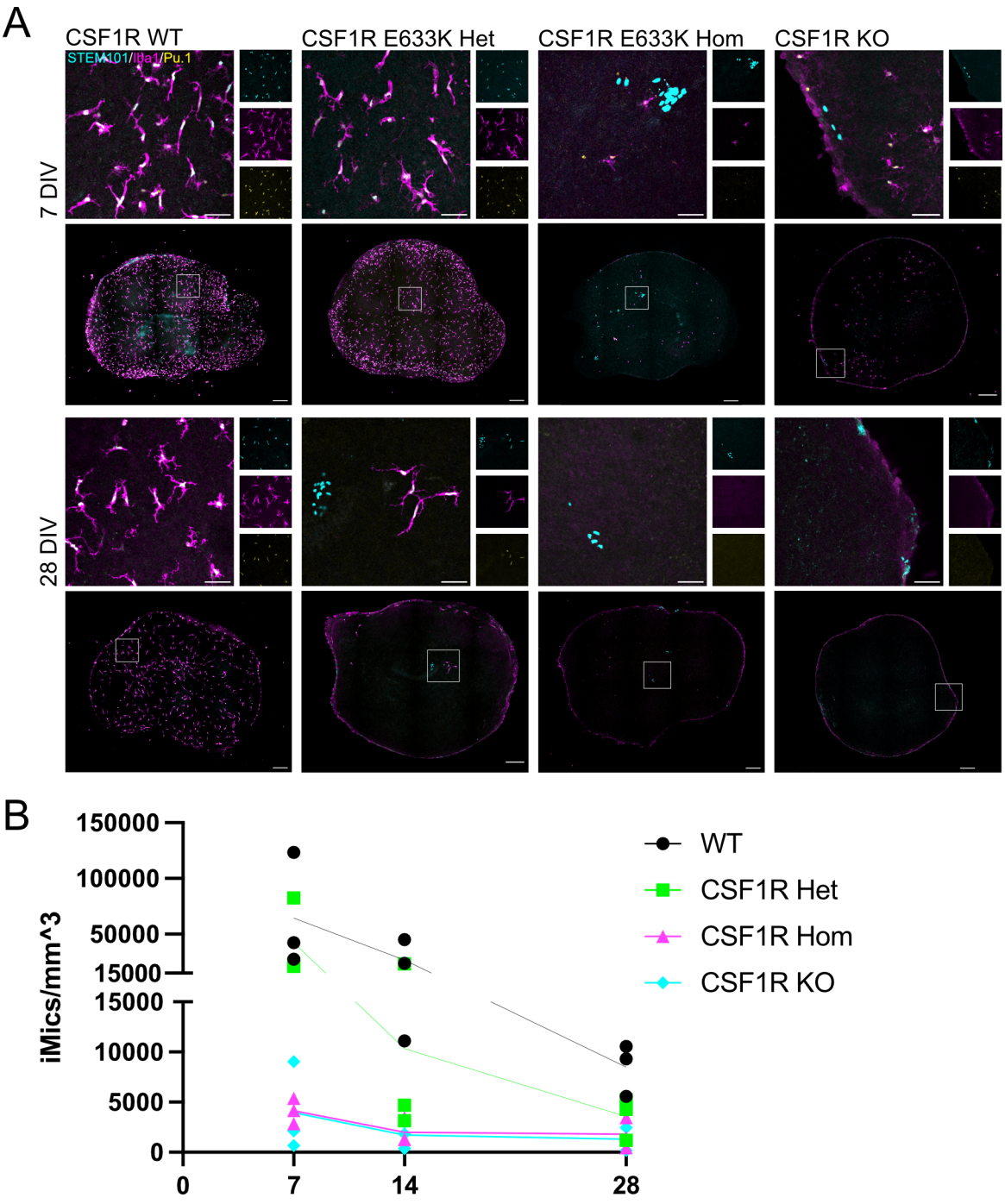

Figure 4.22 Intact CSF1R signaling is necessary for integration, differentiation and survival of iMics in CSC

(A) Representative images of the integration and survival of WT and CSF1R mutant microglial precursors in CSC at 7 and 28 DIV. iMics were stained against Iba1 (magenta), STEM101 (cyan; human nuclei) and PU.1 (yellow). WT iMics (1st column) showed a stable integration and morphological differentiation into ramified, evenly distributed iMics. $CSF1R^{+/E633K}$ heterozygous iMics (2nd column) integrated to a similar extent as WT iMics at 7 DIV but showed decreased survival at 28 DIV. Only few $CSF1R^{E633K/E663K}$ homozygous and $CSF1R^{-/-}$ KO pre-iMics (3rd and 4th column) integrated at 7 DIV but did not survive until 28 DIV. Scale bars: 200 µm **(B)** iMic density of CSC measured as iMics per volume for WT CSF1R mutant iMics. WT iMics showed an expected initial decrease of microglia numbers with a stabilization after 14 to 28 DIV. $CSF1R^{+/E633K}$ heterozygous iMics initially integrated to a similar extent but were not able to survive until 28 DIV, while $CSF1R^{E633K/E663K}$ homozygous and $CSF1R^{-/-}$ KO iMics only integrated in small numbers. number of independent experiments per group = 3; 2-Way ANOVA p (genotype) = 0.0053

As expected, due to the failed differentiation of $CSF1R^{E633K/E663K}$ homozygous and $CSF1R^{-/-}$ KO EBs into pre-iMics, the generation of CSC from both lines was not successful and only a few 'pre-iMics' integrated into CSC. Only small clusters of human cells (STEM101) that were negative for both microglial markers Iba1 and PU.1 were found.

More interestingly, $CSF1R^{+/E633K}$ heterozygous pre-iMics (42349 iMics/mm^3) integrated to a similar extent into CSC as compared to $CSF1R^{+/+}$ WT pre-iMics (64414 iMics/mm^3) and also showed a similar morphological phenotype at 7DIV, indicating that integration and the initial stages of differentiation are still possible in CSC despite the impaired CSF1R signaling in the heterozygous mutants. Similar to $CSF1R^{+/+}$ WT iMics, the number of $CSF1R^{+/E633K}$ heterozygous iMics declined sharply at 14 DIV, but, in contrast to the WT iMics did not stabilize after this initial decline. While the number of $CSF1R^{+/+}$ WT iMics remained constant at around 10,000 iMics/mm^3, only a few $CSF1R^{+/E633K}$ heterozygous iMics survived until 28 DIV (3574 iMics/mm^3) (Figure 4.22; Panel B: $p = 0.0053$). In addition to drastically reduced survival, $CSF1R^{+/E633K}$ heterozygous iMics did not seem to mature morphologically.

Their morphology still resembled iMic morphology at 7 DIV while $CSF1R^{+/+}$ WT iMics at 28 DIV were more ramified and less elongated compared to their appearance at 7 DIV. Overall, these results showed that intact CSF1R signaling is not only necessary for the initial steps of differentiation from iPSC to pre-iMics but is also necessary for iMic differentiation, survival and network homeostasis in CSC. Due to the absence of supplemented human ligands of CSF1R, these experiments show that mouse ligands of CSF1R can bind to human CSF1R and induce downstream signaling.

All in all, I present the development of a model that allows for the investigation of network homeostasis of human microglia *in vitro*. This model system is able to recapitulate features of microglia in homeostatic conditions at morphological, functional and transcriptional levels. Furthermore, in proof-of-principle experiments, the suitability of CSC to investigate microglia in both healthy and neurodegenerative conditions was demonstrated. Additionally, the homeostatic microglial network was shown to be dependent on CSF1R signaling in CSC. Lastly, iMics in a CSC model of seeded synucleinopathy were shown to react by profound microgliosis and upregulation of DAM-associated genes to the pathology and thus modeled the microglial network in disease-conditions.

V Discussion

1 New mouse model does not allow to induce targeted microglia cell death to investigate microglial network homeostasis *in vivo*

The microglial network is very stable over the entire life (Füger et al. 2017). Due to the important role of microglia in the brain, it is paramount to understand how the homeostatic microglial network is maintained and if ageing or neurological diseases can affect the network homeostasis. Various studies have shown that microglia are very long-lived cells, and that microglial cell death is a rare event (Füger et al. 2017; Réu et al. 2017). In contrast to the rare cell death of microglia, current depletion experiments of microglia make use of global depletion approaches that usually ablate 80 to 99 % of microglia (Waisman et al. 2015). Microglial network homeostasis in the context of the cell death of single microglia, however, is not yet understood.

Before this study, only one group showed that in the microglial network a dead cell is replaced by migration of a neighboring cell and proliferation of the second-closest cell (Askew et al. 2017). However, this finding is from the olfactory bulb, a brain region known for its several fold higher proliferation rate of microglia in comparison to other areas such as the cortex (Tay et al. 2017). Due to the very different proliferation rates between the two regions, it is possible that different mechanisms exist to cope with the death of individual microglia. Since more cells undergo apoptosis in the olfactory bulb at the same time (0.69 %), the disturbance to the entire network is higher as compared to the cortex where most microglia survive the entire lifetime of a mouse. Hence, it is imaginable that the disturbance in the cortex is so small that a rearrangement of the neighboring microglia is sufficient to reoccupy the 'lost' territory. Lastly, another possibility is the invasion of peripheral immune cells and the subsequent differentiation into microglia-like cells. So far, this phenomenon has only been described under extreme conditions, namely irradiation to destroy the blood-brain barrier (Bruttger et al. 2015; Xu et al. 2020).

1.1 Development of a 4x transgenic mouse model to ablate individual microglia

The goal for this project was to investigate microglial network homeostasis in the mouse cortex when ablating single cells. Additionally, I sought to compare network homeostasis between age groups and in neurodegeneration to detect functional deficits in this process that could explain the age-dependent susceptibility to neurodegenerative diseases. To this end, a previous mouse model of the laboratory to sparsely label microglia via Cre-recombinase for 2-Photon *in vivo* imaging was combined with a model for Cre-dependent expression of iDTR (Buch et al. 2005; Füger et al. 2017) (Figure 4.2). The

sparse tdTomato-positive microglia were hypothesized to also express iDTR and therefore these microglia would be susceptible to DT for targeted microglial cell death. In summary, this model would allow the visualization of all microglia via EGFP-expression and the selection of ROIs depending on the low percentage of tdTomato-positive microglia to know in advance which cells would be ablated upon DT injection.

When using the Iba1-EGFP and CD11b-CreERT transgenes for *in vivo* experiments, not only microglia are expressing EGFP or CreERT, respectively, but all myeloid cells express the transgenes (Eme-Scolan and Dando 2020). This includes other long-lived myeloid cells such as border-associated macrophages in the brain and short-lived, circulating myeloid cells in the periphery. Unspecific expression of both transgenes, however, only had minor effects for my experiments. EGFP expression under the Iba1-promoter was mostly used for visualization purposes in 2-Photon live cell imaging. Morphologically, microglia can be distinguished from circulating blood monocytes. However, distinguishing microglia from border-associated macrophages is not possible on a morphological level. Yet, microglia are far more common in the brain, so that most likely, only a few border-associated macrophages were included in the live-cell imaging. For FACS, and all subsequent analyses, peripheral myeloid cells were excluded by perfusion with PBS during the preparation of the mice. However, border-associated macrophages were likely included in the sorting. Yet, it is unlikely that the small number of border-associated macrophages compared to the number of microglia changes the interpretation of the results.

Unspecific expression of CreERT in the used mouse model also led to an unspecific expression of tdTomato and iDTR as a consequence of Tam-induced recombination. CD11b, however, is a marker for myeloid cell differentiation, so myeloid precursors in the periphery were not affected by the recombination (van Lochem et al. 2004). Consequently, the short lifetime of peripheral myeloid cells should lead to an exchange of cells with recombined transgenes after a few weeks, similar to what has been described for CX3CR1-CreER mice (Faust et al. 2023). In this project, injection of DT was scheduled earliest four weeks after Tam, so that a full exchange of peripheral myeloid cells should have been completed beforehand. Hence, tdTomato and iDTR expression only persisted in long-lived myeloid cells, e.g. microglia and border-associated macrophages. Like the aforementioned unspecific expression of EGFP under Iba1-control and for the same reasons, the influence of the unspecific recombination of tdTomato and CD11b should be limited.

We showed with Immunofluorescence that a low-dose injection of Tamoxifen induced a low rate of recombination of the tdTomato transgene, resulting in labeling of roughly 1 % of microglia with tdTomato (Figure 4.3). This result was in line with the observations my laboratory made in Füger et al.

(2017). However, due to a lack of appropriate antibodies for iDTR, I was not able to determine the recombination rate of the iDTR transgene.

1.2 Diphtheria toxin and proliferation of tdTomato-positive microglia

For this study, iDTR mice were selected and combined with an existing mouse model from the laboratory. The Cre-dependent expression of iDTR allowed for a cell-type specific and temporally controllable ablation of cells. Previous studies that used iDTR for the ablation of microglia used a global depletion approach which ablated more than 90 % of microglia. In these experiments, mice suffered from impaired learning, astrogliosis and increased cytokine production in the brain (Bruttger et al. 2015; Parkhurst et al. 2013). The authors of these studies attributed the side effects of DT-mediated depletion to the lack of microglia in general and to the massive accumulation of cell death over a short time window. In this study, by injecting a low dose of Tam, only a minority of microglia, the tdTomato-positive microglia, was hypothesized to express iDTR. Assuming that the recombination efficiencies for tdTomato and iDTR are similar, this approach would make 1 % of microglia susceptible to DT. These microglia were then ablated at a later timepoint by the injection of DT. Since my approach only led to the death of about 1 % of microglia and hence to only a fraction of the amount of cell death of the previous studies, the occurrence of these side effects of DT-mediated ablation was unlikely.

When injecting mice with DT four weeks after Tam application, I could not find a reduction in the ratio of tdTomato-positive cells via immunofluorescent staining (Figure 4.3). Due to the high variability of this result, I nevertheless continued with 2-Photon observations *in vivo*. In these experiments I was able to reliably follow predefined ROIs over several weeks. Similar to my immunofluorescent staining, I was not able to selectively ablate tdTomato-positive microglia as designed. Additionally, I even observed proliferation of some of the tdTomato-positive microglia (Figure 4.4). Further FACS analysis revealed that there was also no reduction of the tdTomato population at a brain-wide level (Figure 4.5). The potential reasons for these challenges are the following:

1. Mutations in the iDTR-transgene led to a dysfunctional iDTR, so that DT had no effect anymore.
2. The DT concentration was too low.
3. iDTR was not expressed in tdTomato-positive microglia.

I then sought to further investigate the mouse model to discover the reason for the challenges I faced.

Analysis of the GFP only and tdTom subpopulations from both DT-treated and NaCl-treated mice from the FACS experiment revealed that recombination of the iDTR transgene was only detectable in the GFP only subpopulations (Figure 4.7 & Table 4.3). However, I cannot exclude that PCR was not sensitive enough to detect possible recombination of iDTR in the tdTomato subpopulations. Since both subpopulations only consisted of 3000 to 4000 cells, a low recombination efficiency might have led to

only a few recombined cells and hence a false-negative result. The detected signal for the GFP only subpopulation from NaCl-treated mice corresponded to the expected length of the PCR, hence showing that recombination of the transgene generally worked. However, upon DT-treatment, an unspecific band was still detectable at a size of 50 bp, a potential sign for DNA fragmentation and cell death (Figure 4.7). This indicates that iDTR was intact and that the DT-concentration used was appropriate to induce cell death. I could further substantiate this finding by Sanger sequencing of iDTR and did not find any mutations in the iDTR transgene of NaCl-treated mice. Upon DT-treatment, the chromatogram obtained by Sanger sequencing showed overlapping peaks for all positions, indicating that no intact DNA was amplified (Figure 4.8). Hence, these results indicate that the problems I faced were likely caused by non-overlapping expression of the iDTR transgene with the tdTomato transgene.

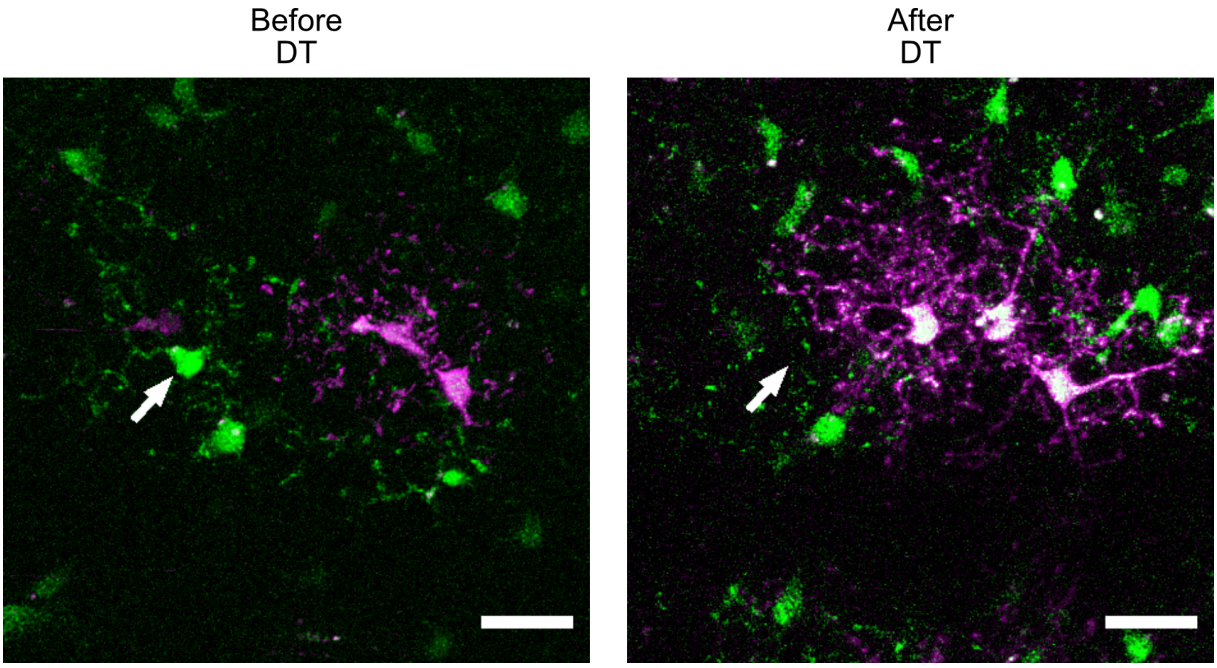

Figure 5.1 Death of GFP only microglia
Representative 2-Photon *in vivo* images of a ROI with a dying GFP only microglia from a tdTom x iDTR mice from the young age group before (left) and four weeks after DT application (right). Note that the tdTom-positive microglia are not the microglia closest to the dying cell but the proliferating microglia then migrated towards the territory of the dead cell. Scale bar: 20 µm

When further investigating the proliferation of tdTomato positive cells upon DT-injection, I was able to observe disappearing microglia that were only positive for GFP. Interestingly, the GFP only microglia that was ablated was always in close proximity to the subsequently proliferating tdTomato-positive microglia. However, it was never the microglia closest to the dying cell (Figure 5.1). Although I did not quantify the distance of the tdTomato-positive microglia to the dying cell further due to the small number of observed proliferation events, this result is reminiscent of the results by Askew et al. who found that the proliferation event mostly occurred in the second-closest microglia to the dying cell (Askew et al. 2017). Since proliferation of tdTomato-positive microglia did not occur in the control mice

without iDTR (from Füger et al. 2017) an effect of DT itself could be excluded. Thus, the most likely explanation for the proliferation is that recombination of iDTR occurred in some microglia without recombination of the tdTomato transgene. This hinted at a stochastic process for the recombination which would be independent for the two Cre-dependent transgenes. This would result in a random distribution of the recombination of the transgenes. Due to the low dose of Tam, however, which resulted in a recombination rate of only about 1 %, the probability for the recombination of both transgenes in one cell, would be very low, so that I would most likely miss these with the limitation of imaging only a few ROIs. This stochastic process would also explain why I did not see a change in the ratio of tdTom-positive cells in the FACS experiment, since GFP only and tdTomato-positive microglia would be ablated at the same ratio. The absence of detectable recombination by PCR in the tdTomato-positive subpopulation from the FACS experiment does also not contradict this explanation. Assuming a recombination rate of 1 % for the iDTR transgene in the tdTomato-positive subpopulation, this would lead to a total of 30 to 40 tdTomato-positive microglia that underwent recombination for iDTR, a cell number which is likely below the limit of detection for this experiment.

Alternative to the use of iDTR, other methods for targeted cell death are 2Phatal and the use of photosensitizers such as KillerRed. Compared to iDTR, both methods have significant disadvantages which is why a decision against using them was made. On the one hand, 2Phatal would be ideally suited to control which cell is targeted in any field of view and hence could be used to target tdTomato-positive microglia (when using in the Füger et al. mice), but also to target directly neighboring GFP only microglia and microglia further away from the tdTomato-positive microglia. This would facilitate the observation of the reaction of a single neighboring microglia towards a dying cell in the network. On the other hand, this theoretically high flexibility to observe microglial network homeostasis is contrasted by the inability of Hoechst 33342 to label microglial nuclei. Thus, it cannot be used to ablate individual microglial cells (Hill et al. 2017). Additionally, the dye needs to be applied during cranial window surgery. Due to the inability of Hoechst 33342 to cross the blood-brain barrier, minor damages to the barrier that occur during surgery are necessary for the dye to penetrate the brain parenchyma and to label nuclei (Choi et al. 2011; Hill et al. 2017). After administration, the dye only stays in the tissue for a few days (Hill et al. 2017). In order to guarantee homeostatic conditions after surgery and to reduce the stress for the mice, my experimental schedule included a two-week recovery window after surgery. Hence, 2Phatal was not compatible with my experiment. Similar to 2Phatal, photosensitizers allow for more control of which cells are targeted for ablation compared to iDTR. However, no mouse model expressing a photosensitizing protein is commercially available. Thus, the only available option for the *in vivo* use of photosensitizers is the use of viral vectors. The biggest disadvantage of using viral vectors for the delivery of genetic information to microglia is the subsequent activation of microglia (Klichinsky et al. 2020; Rosario et al. 2016). Thus, an observation of

the microglial network would not be possible under homeostatic conditions and was therefore not suitable for my aims.

1.3 The distance between loxP sites

The most likely explanation for the unsuccessful ablation of tdTomato-positive microglia is, that recombination of the two transgenes did not occur in the same cell. Hence, the majority of cells that underwent Cre-mediated recombination only had one recombined transgene, either tdTomato or iDTR. Contrary to our expectations, recombination did not take place at all or only rarely took place for both transgenes within one microglia and was thus not detected by my experiments. I hypothesize that Cre recombination for two transgenes is a stochastic process, meaning that even if Cre-mediated recombination takes place for one transgene, this does not influence the probability of recombination for the second transgene. In my experimental set-up, in which I aimed for a recombination rate of 1 %, this would be especially meaningful. In numbers, an entirely stochastic process for the recombination would mean that 0.01 % of all microglia were expressing both transgenes. For *in vivo* imaging, this would mean that only 1 % of tdTomato-positive microglia would also express iDTR. Hints that this hypothesis is true, although not proven, are the PCR band for iDTR recombination in the GFP only subpopulation of microglia and the proliferation of some tdTomato-positive microglia upon DT injection which did not occur in the control animals. Hence, DT-iDTR interaction led to a proliferation event which is only explainable by cell death of a GFP only microglia.

A further problem of the experimental design was the difference between the distances between the two loxP-sites flanking the respective STOP-cassettes. For tdTom the distance between the two loxP-sites was only 0.9 kbp, while for iDTR the distance was 3.8 kbp. Several groups reported that the distance between the loxP-sites influences the leakiness and recombination efficiency of the transgenes (Faust et al. 2023; Glaser, Anastassiadis, and Stewart 2005). The shorter the distance, the leakier the transgene, meaning the more recombination occurs without Tam-induction of Cre-recombination. Furthermore, the shorter the distance between the loxP-sites, the higher the recombination efficiency. For us, this means that the recombination rate for tdTom was higher than for the iDTR transgene. Since I adjusted the dose of Tam according to the recombination rate of tdTom, the recombination rate of iDTR was likely even lower than 1 %, making it even more unlikely to find cells with recombination of both transgenes. However, increasing the dose of Tam would not solve this problem because the recombination rates for tdTom and iDTR would always be different and thus would always lead to many tdTom-positive microglia that would not express iDTR. The best possibility to avoid this problem is the use of fusion proteins, in which iDTR is fused to the fluorescent reporter so that identification of the target cell is always possible. Several years ago, a group published a mouse model for Cre-dependent expression of iDTR fused to mCherry under the control of the CSF1R

promoter (Schreiber et al. 2013). In combination with Iba1-EGFP and CD11b-Cre, this triple transgenic mouse model could be an alternative option for future *in vivo* studies.

2 Development of a novel chimeric *in vitro* model to investigate human microglial network homeostasis and neurodegeneration

The first part of this study proved a general problem of *in vivo* experiments. They usually require a high investment of resources such as animal numbers and time. However, when they fail, *in vivo* experiments do not allow for quick, flexible adjustments to the same extent as *in vitro* experiments due to official regulations for animal experiments (in Germany). In contrast to that, *in vitro* experiments can be modified and adapted to fit different purposes more easily. For example, my laboratory published OBSC models that mimic AD-like or PD-like pathology and can both be performed on a WT mouse background (Barth et al. 2021; Novotny et al. 2016). However, in the microglia field, several publications showed drastic differences between microglia *in vivo* and *in vitro* (Bennett et al. 2018; Gosselin et al. 2017). Thus, the more *in vivo*-like a model system is, the more relevant its results are for microglia research. Additionally, there are well known differences between human and mouse microglia, especially in the context of neurodegenerative diseases (Geirsdottir et al. 2019; Hasselmann and Blurton-Jones 2020; Mancuso et al. 2019; Masuda et al. 2019). Several human microglial risk genes for neurodegeneration do not have a proper mouse ortholog (Hasselmann and Blurton-Jones 2020; Mancuso et al. 2019).

The current methodological spectrum in microglia research comprises various *in vitro* models ranging from immortalized cell lines to 2D and 3D models using human iPSC-derived microglia which however show a strong *in vitro* phenotype. Furthermore, more complex 3D models, namely OBSC, can closely mimic complex cell-cell interactions in the brain but are almost entirely generated from rodents. On the other hand, the recent development of chimeric mice with xenotransplanted iPSC-derived microglia allowed for the first time the study of human microglia in an *in vivo* environment (Hasselmann et al. 2019; Mancuso et al. 2019). For this reason, these mice are one of the most relevant model systems to study microglia. Yet, a major drawback of chimeric mice is that they need to be immunodeficient to allow for xenotransplantation and thus limit their lifetime and complicating their housing conditions.

Despite current model systems covering a broad range of complexity and relevance, a need for an *in vitro* model system of human microglia with a microglial phenotype as close to *in vivo* as possible was identified. A recent publication attempted the generation of chimeric hippocampal slice cultures by transplanting iPSC-derived microglia onto HSC but only showed data for 14 DIV (Ogaki, Ikegaya, and Koyama 2022). In order to be able to study microglia over a longer period of time than the previous

study, mouse OBSC as the *in vitro* system with the highest complexity of cell-cell interactions was used and combined with human iPSC-derived microglia by replacing endogenous mouse microglia with human microglial precursors to generate CSC. The generation, characterization and validation of this novel model system as well as two applications in the context of microglial homeostasis and neurodegeneration will be discussed in the following.

2.1 Chimeric slice cultures as a model to study microglia

First, in order to generate CSC, a niche was created by depleting endogenous mouse microglia for engraftment of iPSC-derived microglial precursors, similar to what is done in some xenotransplantation models (Fattorelli et al. 2021; Mancuso et al. 2019). Engraftment without previous depletion of mouse microglia led to a grafting efficiency of less than 10 %. When using continued depletion throughout the entire experiment, 93 % of microglia in CSC were of human origin (Figure 4.10). Interestingly, when only depleting for one week after engraftment of the precursors or stopping depletion of endogenous mouse microglia at a later time point of the experiment, endogenous mouse microglia reemerged and suppressed human microglia (data not shown). This phenomenon is in contrast to xenotransplanted mice that only need a one-time depletion of microglia and will be discussed later (see section V.2.2).

The most commonly used method to deplete microglia *in vitro* and *in vivo* is PLX3397, a small molecule inhibitor of CSF1R. PLX3397 and Clodronate were also the methods of choice to deplete endogenous microglia by Ogaki et al. However, PLX3397 seemed to totally prevent human microglia integration while Clodronate depletion resulted in 80 % replacement of mouse microglia by human microglia (Ogaki et al. 2022). However, to generate a suitable model system to investigate human microglia, the aim was to achieve a full exchange of microglia. The results by Ogaki et al. showed the necessity to specifically deplete mouse microglia without affecting human microglia, thus making the use of PLX3397 and other unspecific CSF1R-inhibitors impossible for the aims of this thesis. Hence, a mouse-specific anti-CSF1R antibody was used which made differentiating human microglia while simultaneously suppressing mouse microglia possible. Another major advantage of using an anti-CSF1R antibody as compared to PLX3397 is the high specificity of the antibody which avoids off-target effects that usually occur by the action of PLX3397 on other receptors than CSF1R. Additionally, one of the major drawbacks of the use of antibodies for microglia depletion, a lacking penetration of the blood-brain-barrier, is not relevant for an *in vitro* model system. This is because the antibody can be applied directly to the CSC via supplementation into the medium without the need to pass a blood-brain barrier. Depletion of mouse microglia with an anti-CSF1R antibody is similarly efficient as PLX3397 and depletes 85 % of microglia within a week and more than 90 % within two weeks (Figure 4.9) (Green et al. 2020). In line to published results for PLX3397 or PLX5622 (Elmore et al. 2014; Huang et al. 2018), a small microglial population remains that is resistant to CSF1R inhibition and is able to repopulate the

slice culture within a week. Due to limited collection of different time points, however, the previously described 'overshoot' phenomenon during repopulation events was not observed.

As described above, a need for a model that bridges the gap between current *in vitro* models and chimeric mice with xenotransplanted microglia was identified. One of the biggest challenges when working with iPSC, especially in more complex 3D models, is the lack of reproducibility and high variability between different cell lines (Stöberl et al. 2023). For CSC, three different iPSC lines and two different protocols for the generation of microglia precursors were tested and robust integration for all conditions was shown (Figure 4.11). This highlights the reproducibility of this approach.

2.1.1 Morphology and functionality of iMics in chimeric slice cultures

The most important characteristic of a model system is that it needs to mimic the 'real', i.e. the *in vivo* situation, as closely as possible. For microglia models, the most relevant properties of a model by which it is evaluated are morphological characteristics of microglia, their network organization, their functionality under homeostatic conditions and under pathology-like stimuli and lastly their transcriptional phenotype.

The comparison of morphological parameters between studies, especially for human tissue, is difficult. Hence, it is important to use appropriate controls in these experiments to obtain good reference values for the analysis. The morphology of microglia is not only influenced by the activation status of microglia, for which it has been used as a read-out, but is also influenced by other, less controllable parameters. Geirsdottir et al. showed that the morphology of microglia is different between species but also between different brain regions within a species. For example, the number of branch points in the human cortex and hippocampus is almost double compared to the cerebellum (Geirsdottir et al. 2019). Additional parameters influencing the morphology of microglia and its analysis are sample preparation, differing analysis pipelines and software and most importantly for human tissue the post-mortem delay. Post-mortem delay has been shown to induce transcriptional changes in microglia and hence could also influence microglial morphology (Heng et al. 2021). The results of this thesis were not affected by post-mortem delay since human *ex vivo* tissue was obtained from brain surgery and hence the tissue could be fixed immediately to obtain a 'gold standard' as a reference. However, the scarce availability of human tissue only allowed for the analysis comparison of microglia in the prefrontal cortex to microglia in the hippocampus in CSC. Nevertheless, very similar morphological properties of human iMics in CSC, mouse microglia in HSC and human microglia *ex vivo* were found, proving successful morphological differentiation and maturation of human iMics in CSC towards a highly ramified microglial appearance (Figure 4.12). Additionally, a morphological maturation of human iMics in CSC over time towards a more ramified phenotype for all analyzed morphological parameters was detected. Conversely, morphological differences between human microglia *ex vivo*, human iMics in

CSC and mouse microglia in HSC were not observed. Similarly, it was not possible to determine if human iMics in CSC are morphologically closer to human microglia *ex vivo* or mouse microglia in HSC. What eventually determines the morphological appearance of microglia is not known, is it the species and region they are derived from or is the local environment that differs between species and brain regions, although some evidence suggests that it could be a combination of both (Bennett et al. 2018). The study by Geirsdottir et al. was one of the studies with the most detailed information about microglial morphology across species and brain regions and includes data from microglia in the human and mouse hippocampus (Geirsdottir et al. 2019). iMics in CSC are less ramified compared to human and mouse microglia in the hippocampus (Geirsdottir et al. 2019), potentially indicating a more activated or primed and less homeostatic phenotype of iMics in CSC. Decreased homeostatic morphology in CSC, however, could be interpreted as an *in vitro* phenotype of microglia, although it is only minor compared to other 2D and 3D *in vitro* models to investigate microglia. However, the results of the previously mentioned study also differed from the results of this thesis for human microglia *ex vivo*, hence raising the question if the observed differences between the published results and iMics in CSC are more likely due to differences in the methodology and not due to an activation phenotype or a lack of microglial maturation.

In addition to microglial morphology, the network organization of iMics in CSC was also analyzed by analyzing the nearest neighbor distance (NND) and the microglial number per volume. Similar to the morphological analysis, no differences between iMics in CSC and the other experimental groups were detected (Figure 4.12). Thus, iMics in CSC not only morphologically resembled human microglia *ex vivo*, but also had a similar network organization. Yet, microglial NND values from the literature usually are in the range between 40 and 50 µm in the brain compared to 30 – 35 µm in CSC (Barry-Carroll et al. 2023; Hefendehl et al. 2014; Mancuso et al. 2019). Age differences between 1.5 months old CSC and three-week-old mice in Barry-Carroll et al. and three-month-old mice in Hefendehl et al., could explain the differences. Barry-Carroll et al. for example showed that the NND decreases during development between the embryonic stages and p21. Hefendehl et al. on the other hand showed a decrease of the NND with ageing, hence mapping iMics in CSC to an ageing or activated phenotype. However, since this difference was also detected for human microglia *ex vivo* as 'gold standard', methodological differences could again explain the minor differences. In contrast to the other studies, neither HSC nor CSC nor the human tissue slice were cut before staining and imaging so that tissue of 250 – 300 µm thickness was mounted compared to 25 to 80 µm thin sections in other studies. During this process, the compression of the tissue by the coverslip might be higher for thicker tissue and hence artificially reducing the NND for iMics in CSC. Since NND and the density of microglia are inversely correlated, similar results were obtained for the comparisons of the microglial density. Although quite similar to the published density of microglia in the mouse hippocampus (5990 microglia/mm^3), the density of

iMics in CSC (7600 microglia/mm^3) was slightly increased (Keller et al. 2018) (Figure 4.12). Like before, this could be a possible hint at a primed or aged phenotype of iMics in CSC.

In addition to read-outs obtained post-fixation, functional characteristics of iMics in CSC were also assessed by 2-Photon live cell imaging. iMics in CSC were shown to actively monitor their territory and respond to a functional laser injury to a similar extent as mouse microglia in HSC (Figure 4.13). Both methods and experimental readouts are commonly used to assess microglial functionality. Again, absolute comparisons to other studies are difficult due to differences in analysis pipelines and the used software for process tracking. Thus, comparisons of iMics in CSC with endogenous mouse microglia functionality are most important. Furthermore, qualitative assessment of the homeostatic process movement and the injury reaction revealed high similarities between iMics in CSC and published results (Hasselmann et al. 2019; Hefendehl et al. 2014). During homeostasis, iMics in CSC have a stationary soma and only move their processes, similar to what has been described *in vivo*. Similarly, microglia only move their processes but not their soma to the injury site upon focal laser injury within minutes.

Lastly, both chronic and acute LPS stimulation induced a broad cytokine response, including secretion of TNFα, IL1β, IL6 and IL8 (Figure 4.14). Despite LPS not being a physiological stimulus of microglia in the brain, it is commonly used as a proof-of-principle experiment due to the strength of the stimulation. The broad cytokine response of iMics in CSC to LPS is in line with results from primary microglial cell culture. In contrast to this, immortalized microglial cell lines are not able to elicit such a broad response and usually only secrete one or two cytokines upon stimulation (Ahn et al. 2008; Nagai et al. 2001; Timmerman et al. 2018). Furthermore, acute 24h stimulation with a high dose of LPS elicited a stronger response for all measured cytokines than a lower dose chronic stimulation for 7 days. Possible explanations for this are the higher dose of the acute stimulus or tolerance mechanisms induced by the chronic stimulation and could be further investigated by adjusting concentrations and extending the panel of tested cytokines, including anti-inflammatory cytokines (Wendeln et al. 2018).

Besides the performed functional experiments, microglia have several more, important functions under homeostatic conditions that were not further investigated in this thesis. This comprises phagocytic capability including the phagocytosis of synapses and neuronal debris, functionality of the complement system and antigen presentation. Testing for these functions, however, would have exceeded the scope of this thesis and usually is not performed in similar studies, such as in the first studies describing chimeric mice with xenotransplanted microglia (Hasselmann et al. 2019; Mancuso et al. 2019).

2.1.2 Transcriptional profile of iMics in chimeric slice cultures

Transcriptional profiling of microglia is a widely used method to determine microglial phenotypes. Here, scRNAseq was performed to characterize the transcriptional profile of iMics in CSC regarding their homeostatic profile and developmental age. However, due to time constraints, analysis on a single cell level including clustering and pseudo-time analysis was not yet finished when this thesis was written so that the different experimental groups were only analyzed as a bulk. Once completed, single cell analysis will reveal the heterogeneity of the iMics population in CSC in order to see how well different subclusters of microglia that exist *in vivo* are recapitulated by this novel model system.

We found that iPSC-derived microglial precursors highly expressed genes associated with proliferation, iMics in CSC at 3 and 6 weeks *in vitro*, showed a pronounced homeostatic signature and at 11 weeks of age, a signature similar to the described IRM phenotype was found (Olah et al. 2020; Sala Frigerio et al. 2019) (Figure 4.15). The homeostatic microglial signature at 3 and 6 weeks in culture included high expression of key homeostatic markers P2RY12, CX3CR1 and CSF1R. Additionally, expression of the microglia specific marker OLFML3 was shown, identifying iMics in CSC as microglial cells and distinguishing them from other tissue-resident and circulating macrophages. Besides their homeostatic markers, iMics expressed genes involved in important microglial functions at low levels. This included phagocytosis, complement, inflammasome and antigen presentation. However, the expression of other important microglial markers such as TMEM119 and Sall1 (data not shown) could not be detected. In contrast to that, I could show TMEM119 protein expression in iMics by immunofluorescent staining (Figure 4.12 D). Hence, the sequencing depth of scRNAseq was most likely too low to detect expression of these genes and possibly could be shown by more sensitive bulk RNA sequencing. Nevertheless, TMEM119 and Sall1 seemed to be only lowly expressed. This could be a hint that at this timepoint, iMics in CSC were not yet fully matured and rather corresponded to developmental stages of microglia. Although no direct comparison was performed so far, iMics in CSC seemed to differentiate into more *in* vivo-like microglia in comparison to other *in vitro* models due to the high expression of the key homeostatic markers.

Between 6 and 11 weeks *in vitro*, however, transcriptional profiling revealed a major shift in gene expression. At 11 weeks, homeostatic markers were strongly downregulated, and genes involved in antigen presentation, inflammasome, complement and phagocytosis were highly upregulated. Furthermore, genes involved in lipid metabolism, i.e. APOE and other genes previously associated with the DAM signature were found to be upregulated as well as genes associated with an increased interferon response. The detected gene expression changes were in line with the IRM phenotype which was described for human and mouse ageing (Olah et al. 2020; Sala Frigerio et al. 2019). This raises the question if CSC undergo accelerated ageing due to culturing conditions. In 2022, a group

published that brain ageing is modelled in OBSC based on the upregulation of genes related to cellular senescence (Liu et al. 2022). The reported changes already occurred after 8 weeks *in vitro* and thus could explain the observed ageing phenotype for iMics after 11 weeks. However, according to these data, a strong ageing phenotype was already detectable at 8 weeks, suggesting that age-related changes should be visible already at 6 weeks, which were not detectable in CSC. A possible explanation for this discrepancy is that the generation of CSC requires depletion of microglia directly from the beginning and is thus limiting the formation of a glial scar. Since the glial scar is characterized by strong microgliosis and astrogliosis, a reduction of inflammatory cytokines is probable in CSC (Grabiec et al. 2017). Since inflammation is one of the hallmarks of ageing, the reduction of the glial scar in CSC could have a beneficial effect and delay ageing of the slice culture by a few weeks (Ferrucci et al. 2020).

Overall, transcriptional profiling of iMics in CSC revealed that CSC are indeed filling the gap between current *in vitro* and *in vivo* systems to study microglia because iMics adapt a homeostatic, *in* vivo-like transcriptional profile. As a more complex *in vitro* model, they also offer the opportunity for low-throughput screens. The potential accelerated ageing of CSC is especially interesting for neurodegeneration research as age is the most important risk factor for the development of these diseases. This aspect, however, first needs to be further investigated.

2.2 iMics in chimeric slice cultures are independent of supplementation with human cytokines

The methodology of CSC and chimeric mice with xenotransplanted microglia is very similar. For the generation of iPSC-derived microglia, similar protocols are used (Fattorelli et al. 2021; Hasselmann et al. 2019; Mancuso et al. 2019). Depending on the protocol for chimeric mice, both methods rely on the depletion of endogenous microglia to create a niche for the integration of human iPSC-derived microglial precursors (Fattorelli et al. 2021; Mancuso et al. 2019). Other protocols for the generation of chimeric mice, however, do not deplete endogenous microglia (Hasselmann et al. 2019; Svoboda et al. 2019). Depending on which of the different immunodeficient mouse models is used, grafting efficiency in these mice ranges from 20 % to 80 % of total microglia in the mouse brain (Fattorelli et al. 2021; Hasselmann et al. 2019; Svoboda et al. 2019). By permanently depleting endogenous mouse microglia in CSC with a mouse specific anti-CSF1R antibody, a 97 % exchange of mouse microglia with human iMics was achieved which was stable for several weeks and thus higher compared to the grafting efficiency of current xenotransplantation mouse models (Figure 4.12 C). A recent publication used a similar approach for chimeric mice. The authors discovered a PLX3397-resistant CSF1R variant to continue depletion of endogenous microglia even after engraftment (Chadarevian et al. 2022). Besides the relevance of this mutation for xenotransplantation models, this study also opens up new possibilities for therapeutical approaches for neurodegenerative diseases and other diseases in which

microglia play a crucial role. Replacing microglia in the human brain with engineered microglia could help to correct disease-associated mutations such as TREM2 variants for AD or Nasu-Hakola disease. Since an existing microglial network does not allow for the efficient xenotransplantation of microglia, this approach was so far impossible (Abud et al. 2017). A PLX3397-resistant CSF1R variant, however, would make depletion of endogenous microglia possible without affecting the engineered microglia that are engrafted (Chadarevian et al. 2022).

The biggest difference between CSC and chimeric mice, however, is the supplementation of human cytokines to the system. CSC can be generated and sustained without further supplementation of human cytokines such as hCSF1 or hIL34. In contrast to this, all published protocols for the generation of chimeric mice use mice with humanized knock-in alleles for at least hCSF1 (Fattorelli et al. 2021; Hasselmann et al. 2019; Mancuso et al. 2019; Svoboda et al. 2019). This is based on the current dogma in immunology that the mouse cytokines mCSF1 and mIL34 cannot bind to the human receptor hCSF1R which is crucial for microglial differentiation, maturation and survival (Elmore et al. 2014; Rathinam et al. 2011; Sieff 1987).

2.2.1 The role of CSF1R for microglial differentiation and survival

Due to these differences, further investigations were necessary to determine how iMics are capable to differentiate into microglia and survive in CSC without any human cytokines. To this end, iPSC lines were used that are heterozygous or homozygous for a loss-of-function mutation in CSF1R, as well as a CSF1R KO line based on an isogenic background. CSF1R signaling was shown to be crucial for the first steps of differentiation from iPSC to microglial precursors. In these steps, the cells were still treated with hCSF1 and hIL3. While mesodermal induction and EB formation were successful independent of CSF1R background, only the WT and $CSF1R^{+/E633K}$ heterozygous line were able to produce proper iMic precursor cells. The homozygous $CSF1R^{E633K/E633K}$ and the CSF1R KO line seemed to be stuck in an earlier differentiation step and only produced smaller, less differentiated precursor cells that were neither able to integrate and further maturate in CSC nor to differentiate in monoculture (Figure 4.21). Hence, the most interesting line for further observations was the $CSF1R^{+/E633K}$ heterozygous line as it was able to produce morphologically normal iMic precursors that successfully integrated into CSC at 7 DIV. Accordingly, hCSF1 in the differentiation medium provided a strong enough cue for differentiation *in* vitro. Upon grafting, it was not possible to determine if remaining hCSF1 from the differentiation medium supported the successful integration of iMics into CSC or if the endogenous mouse cytokines induced CSF1R signaling. However, iMics on a $CSF1R^{+/E633K}$ heterozygous background were not able to survive until 28 DIV, in contrast to the isogenic WT control, demonstrating the need for intact CSF1R signaling in CSC (Figure 4.22). Thus, the importance of CSF1R signaling for microglial differentiation and survival was confirmed in line with the existing literature (Elmore et al. 2014).

2.2.2 Cross-species interaction of CSF1 and CSF1R

With this approach, however, it was impossible to determine how CSF1R signaling is induced in CSC. CSF1R has two known ligands, CSF1 and IL34. According to a blastp alignment (https://blast.ncbi.nlm.nih.gov/Blast.cgi?PAGE=Proteins), the sequence identity of hCSF1 and mCSF1 as well as of hIL34 and mIL34 is each only about 70 %, making it reasonable to assume that cross-species binding affinity of the cytokines with CSF1R might be impaired but not necessarily fully depleted. This might also explain the differences between chimeric mice and CSC. In their paper describing the development of chimeric mice with xenotransplanted microglia, Hasselmann et al. further investigated the necessity of hCSF1 knock-in for their mice. A lack of hCSF1 expression led to a total failure of integration of human microglia into the mouse brain. By heterozygous expression of hCSF1 they could show a dose-dependent effect as a partial survival of human microglia was observable (Hasselmann et al. 2019). For the homozygous hCSF1 knock-in, this suggests that the presence of hCSF1 provides human microglia with a competitive advantage over mouse microglia, but the presence of mouse microglia also shows that murine microglia can differentiate and survive in the presence of hCSF1, demonstrating cross-species binding of hCSF1 and mCSF1R or strong enough signaling via mIL34.

In CSC, similar conditions were tested but then an inverse approach was used. When endogenous murine microglia were not depleted, neither integration nor survival of human iMics in CSC was seen (Figure 4.10 C). This corresponds to the experiment by Hasselmann et al. in which the mice did not express hCSF1 (Hasselmann et al. 2019). The murine microglia in this scenario have a competitive advantage over human microglia due to their assumed higher binding affinity to mCSF1 so that human microglia cannot integrate and differentiate in the slices. Instead of using homozygous hCSF1 expression to provide human microglia with a competitive advantage over mouse microglia, mouse microglia were continuously depleted in CSC. In the absence of mouse microglia, the lower binding affinity of mCSF1 to hCSF1R would not play a major role and would still suffice to induce CSF1R downstream signaling for iMic differentiation and survival. This hypothesis would also explain why a stop of the depletion in CSC led to a repopulation of the murine microglia that replaced the already integrated human iMics (Figure 4.10 C). Although only a few murine microglia remain after depletion, they then have a competitive advantage over human iMics once the depletion is stopped.

This hypothesis is also supported by the recent publication that attempted to develop CSC. Similar to us, the authors also used WT mice and depleted the endogenous mouse microglia. However, instead of depleting throughout the entire experiment with a mouse specific anti-CSF1R antibody, they depleted the endogenous microglia with PLX3397 or Clodronate. Of the two methods, Clodronate provided the more efficient depletion and resulted in a grafting efficiency of about 80 %, while PLX3397

prevented integration of human microglia, likely due to remaining substance in the tissue. Additionally, after grafting, the slices were supplemented with hCSF1, hence providing human microglia with enough trophic support to not be replaced by remaining murine microglia (Ogaki et al. 2022). This approach resembles the heterozygous hCSF1 mice of the Hasselmann et al. study in which neither human nor mouse microglia had a competitive advantage, resulting in lower grafting efficiency for human microglia compared to the homozygous knock-in mice (Hasselmann et al. 2019).

Interestingly, models for chimeric mice with xenotransplanted microglia only rely on hCSF1 knock-in but do not require the expression of hIL34. An important difference between the two ligands is their expression pattern. CSF1 is mostly expressed by astrocytes, oligodendrocytes and microglia while IL34 is mainly expressed by neurons leading to regional differences in the expression (Badimon et al. 2020; Easley-Neal et al. 2019). CSF1 is mainly expressed in the white matter, while IL34 is mainly expressed in the gray matter. Despite low levels of hCSF1 and only mIL34 present in the gray matter, transplantation of microglia in the gray matter is as efficient as in the white matter in chimeric mice (Hasselmann et al. 2019; Svoboda et al. 2019). This indicates that mIL34 is indeed able to bind hCSF1R at a normal level and that cross-species binding to CSF1R is only impaired for CSF1 but not for IL34. For CSC, this would mean that trophic support for iMics is at a normal level in the gray matter areas of the hippocampus and potential low affinity binding would only occur in the white matter areas. Nevertheless, iMic integration and survival in CSC is very homogenous and no obvious impaired integration is observable for certain areas.

In order to further investigate cross-species binding of CSF1R and its ligands, more detailed biochemical assays are necessary. First, receptor-ligand binding assays could reveal differences in the affinity of the receptor-ligand binding. Second, activation of downstream-signaling of CSF1R could be assessed by Western Blot analysis of phosphorylated CSF1R and other downstream targets such as phosphorylated ERK which only occurs upon activation of the receptor (Liu et al. 2012; Stanley and Chitu 2014).

2.3 Chimeric slice cultures to model neurodegenerative diseases

A major advantage of CSC is that they are independent of the mouse model. No matter which model needs to be used for an assay, mouse microglia can be replaced by human iMics as described. Hence, CSC can be combined with existing mouse OBSC models for various neurological conditions. Current models involving the use of OBSC include neurotoxicity assays and small-scale screening as well as models for neurodegenerative diseases such as tauopathies, prion disease, AD and synucleinopathies (Croft et al. 2019; Falsig and Aguzzi 2008; Humpel 2015). An important caveat for the combination of CSC with neurodegenerative disease models is that microglial replacement should be performed before pathology induction if possible. The reason for this is that plaque-associated microglia in a

mouse model of AD were reported to be less dependent on CSF1R signaling and hence could not be depleted by PLX5622 (Spangenberg et al. 2019). Induction of pathology including a disease-associated microglial phenotype before microglial replacement could thus impair the efficiency of the replacement.

In my laboratory, we established OBSC-based models for AD-like amyloid plaque formation and αsyn-seeding induced synucleinopathy (Barth et al. 2021; Novotny et al. 2016). As a proof-of-principle experiment, a combination of CSC with our previously established, seeded model for synucleinopathy was performed to demonstrate the variability of CSC. To this end, HSC are seeded with synthetic αsyn-pff. For our model of synucleinopathy, we demonstrated that HSC prepared from both WT and A53T-αsyn transgenic mice can be used. A53T mice are characterized by the overexpression of human αsyn with the A53T mutation that makes αsyn more aggregation-prone. The mice suffer from prominent motor symptoms and have neuronal αsyn inclusions reminiscent of the inclusions occurring in PD (van der Putten et al. 2000). Consequently, seeding of A53T-transgenic HSC accelerates and enhances the development of αsyn inclusions. Seeded A53T cultures develop prominent αsyn inclusions within a week. In contrast to that seeded WT cultures need five weeks to develop a similar amount of αsyn inclusions (Barth et al. 2021). Seeding of WT cultures hence serves as a more physiological, slower way of inducing synucleinopathies in HSC while A53T cultures are suitable for experiments for which fast and/or strong αsyn pathology is necessary. Despite the midbrain being the most affected brain region in PD, the use of the hippocampus as brain region of interest for the generation of a model for seeded synucleinopathies has two major advantages. First, the organization of the hippocampus with axonal connections that are outside the hippocampus only to and from the entorhinal cortex. This limits axonal damage during the preparation procedure and thus reduces synaptic rearrangement (Gähwiler et al. 1997). Second, the well-known axonal connections within the hippocampus facilitates the investigation of mechanisms of spreading alongside axonal connections as demonstrated in Barth et al. Nevertheless, neuronal pathology and specific susceptibility of dopaminergic neurons cannot be modeled in HSC and are thus a disadvantage.

2.3.1 Microglial inclusions in chimeric slice cultures with synucleinopathy

In another recent publication of the laboratory, we discovered prominent microglial inclusions in transgenic mouse models of PD (Tanriöver et al. 2020). We were also able to model these inclusions in our seeded synucleinopathy HSC model. However, five weeks after seeding, microglial inclusions were only prominent in seeded A53T HSC and almost completely absent in seeded WT HSC (Barth et al. 2021). Most likely, due to the delayed time course of WT cultures, they would nevertheless occur at some point in WT slices as well. Nevertheless, to test if human microglia would also develop αsyn inclusions in seeded CSC, I used CSC based on the A53T background to obtain a stronger induction of

αsyn pathology. I seeded A53T-CSC at 14 DIV with αsyn-pff and quantified microglial inclusions three and five weeks after seeding. In order to visualize microglial inclusions, αsyn inclusions were stained with the amyloid-binding dye hFTAA. Then, co-localizing signal of hFTAA with microglial Iba1 was quantified. First, I found several microglia that had typical αsyn inclusions (Figure 4.18 B). These inclusions are typically non-compact structures that are positive for hFTAA. Their size can range from almost non-detectable to soma-sized and with higher resolution microscopes these inclusions appear wool-like, indicating a filamentous structure of the inclusions (Tanriöver et al. 2020). In Tanriöver et al., my laboratory could show that microglial inclusions are C-terminally truncated and therefore not detected by pS129-staining. Thus, it is possible that the inclusions are derived from phagocytosed material that can only partially be digested by microglia and then accumulates within microglia. The αsyn inclusions within microglia are thus comprised of the N-terminus and the NAC-domain of αsyn (Tanriöver et al. 2020). The C-terminus of αsyn is thought to protect the NAC-domain from fibrillization, suggesting that C-terminal truncation of αsyn by microglia could have effects on the aggregation propensities of αsyn (Gallardo, Escalona-Noguero, and Sot 2020). The C-terminal truncation of αsyn in microglia and the resulting lack of the epitope for the binding of pS129-antibodies that are widely used to detect αsyn pathology could also be a reason why microglial inclusions have been overlooked so far.

Second, I found that the percentage of iMics that were positive for αsyn inclusions doubled from three to five weeks post seeding. Moreover, the relative volume of LCO-signal within iMics increased four-fold, demonstrating that microglial inclusions are not only derived from the seeded material but also from ongoing pathology within the tissue, similar to what we showed in regular HSC (Barth et al. 2021) (Figure 4.18 C, D). Additionally, this showed that αsyn within microglial inclusions is not only redistributed between microglia to share the burden, as suggested by Scheiblich et al. (Scheiblich et al. 2021), but that more αsyn is incorporated into microglial inclusions. The most likely assumption for the origin of microglial αsyn inclusions is that it is phagocytosed material from neurons that is then processed and C-terminally truncated within microglia, but not fully degraded and thus accumulates. This is supported by the time-delay between the occurrence of pS129-lesions and microglial inclusions (Barth et al. 2021). A second possibility is that αsyn inclusions are additionally amplified in microglia. Microglia were shown to express low levels of αsyn which could also be incorporated into microglial inclusions (Austin et al. 2006; Zhang et al. 2016). This could be tested by using αsyn knock-out iMics in the same experiment as described above.

Besides the origin of microglial inclusions, another open question is what happens in the event of microglial cell death. A permanent increase in the amount of LCO-positive signal within microglia would eventually lead to an ‘overloading’ of microglia with αsyn inclusions. Although Scheiblich et al.

showed that microglia are able to share their αsyn-burden via nanotubes which reduces the inflammatory signature and cytotoxicity, it is unclear how microglial inclusions are processed within microglia (Scheiblich et al. 2021). How much αsyn can be degraded by microglia? Are microglial inclusions eventually released via exosomes? Once coping mechanisms such as degradation, exocytosis of αsyn or direct transfer to αsyn-inclusion naïve cells via nanotubes are exhausted, the increasing amount of cytotoxicity would most likely lead to microglial death and the microglial inclusions would be released into the extracellular space. However, αsyn has so far only been described as intracellular inclusions in the form of Lewy bodies and Lewy neurites, but not in the extracellular space (Spillantini et al. 1997). There are two major questions that influence the relevance of this hypothesis. First, are microglial inclusions occurring in PD patients and if so to an extent that this hypothetical situation of microglial 'overload' would occur or is the amount of αsyn pathology in the used slice culture system too artificial and too high? Second, what is happening in case αsyn inclusions are released into the extracellular space? Is the released material capable to induce further seeding and spreading of the disease or is it just phagocytosed by another microglia that is able to degrade it, at least partially? To answer these questions, human PD tissue needs to be studied further in order to determine the extent of microglial inclusions in the human disease. Furthermore, isolation and amplification of the microglial seeds with subsequent seeding of HSC with these microglial seeds will help to determine the role of microglia in the spreading of αsyn pathology. Lastly, the role of microglia in the spreading of αsyn pathology can also be studied by live cell imaging of microglial inclusions in combination with organelle tracking.

2.3.2 Response of iMics in chimeric slice cultures with synucleinopathy

Besides the presence of microglial inclusions, the response of iMics to the seeded synucleinopathy was also characterized. To achieve a less artificial pathology, WT CSC that have slower disease progression compared to A53T CSC were used. The cytokine profile of iMics in CSC showed peaks after 48 hours for all four tested cytokines but then came back to baseline levels, except for IL8, for which concentrations stayed slightly elevated over the following weeks (Figure 4.19). In PD, CSF levels for TNFα, IL1β and IL6 are increased (Joers et al. 2017). Serum IL8 is positively correlated with disease severity in PD patients, while in CSF, IL-8 levels show a higher variability over the day compared to healthy controls (Eidson et al. 2017). Due to the comparably high volume of the slice culture medium (1.2 ml / well), it is reasonable to assume that the dilution of TNFα, IL1β and IL6 was so high that potential elevated levels were not detectable anymore when compared to the control. A possible solution for this problem would be to culture slice cultures on smaller inserts that are designed for 24-well plates. In other experiments in my laboratory, we used the smaller inserts with a culture medium volume of 300 µl for one slice per insert, but smaller volumes of down to 200 µl might be possible to

use. In our regular 6-well plates we use 400 µl per slice, so that using 24-plates with small inserts would significantly increase all cytokine concentrations.

A strong initial cytokine reaction compared to a weaker chronic reaction for all cytokines is similar to previous observations for acute and chronic LPS stimulation of CSC. However, the reasons for this might be different. Additionally, the cytokine reaction to αsyn-pathology was much weaker compared to LPS (Figure 4.14). For the LPS stimulation, a high concentration was used that was hypothesized to elicit a strong response as proof-of-principle experiment. For the induction of synucleinopathy, however, a WT background was selected for the CSC generation that led to a slow, less artificial disease progression compared to more severe models such as A53T slices. Hence, the stimulation of microglia by αsyn is expected to be smaller. The initial peak of the αsyn experiment is most likely derived from the reaction to the initial seed. After the initial seed is processed, the subsequent progression of the pathology is much slower and thus does not reflect an immune tolerance mechanism as suspected for LPS.

Furthermore, five weeks after seeding, profound microgliosis demonstrated by higher iMic densities compared to untreated CSC was observed, a finding which is similar to the findings in PD (Joers et al. 2017; Smajić et al. 2022) (Figure 4.18 A). At this timepoint, scRNAseq analysis was performed and the transcriptomic profile was compared to the baseline situation before seeding and unseeded control CSC at the endpoint. iMics in seeded CSC showed a downregulation of homeostatic markers and a general upregulation of genes associated with antigen presentation, inflammasome, complement, lipid metabolism, phagocytosis and other DAM genes, similar to the ageing-associated iMics at the same timepoint (Figure 4.20). Compared to the age-matched control CSC, seeded CSC showed reduced upregulation of the IRM phenotype of microglial, demonstrating a differential regulation to the age-associated processes in the untreated CSC. Moreover, classical DAM markers APOE, TREM2 and TYROBP were stronger upregulated in CSC with synucleinopathy (Keren-Shaul et al. 2017). Besides classical DAM markers, that were originally described for AD, a strong upregulation of genes was found that were also reported to be upregulated in microglia of PD patients, namely IL1B and SPP1, genes involved in the inflammatory response and phagocytosis (Smajić et al. 2022). This demonstrates that CSC with seeded synucleinopathy are a valid model to study synucleinopathy *in vitro* and that CSC can most likely also be adapted for the study of other models of neurological diseases. Similar to the characterization experiments of CSC, more detailed scRNAseq analysis to detect distinct clusters of microglia has not yet been performed. These could reveal how well iMics in CSC are mimicking microglia in PD patients. Furthermore, this will show if further studies should focus more on CSC generated from midbrain OBSC and if the brain-region dependency of the microglial phenotype also has implications on the response to neurodegenerative pathology.

2.4 Chimeric slice cultures (Summary)

As an *in vitro* model, CSC have several drawbacks that are common to this type of model system. First, survival of CSC was so far only shown until 12 weeks *in vitro*, a short time period compared to the slow progression of many neurodegenerative diseases. Second, while precisely modeling cell-cell interactions within the brain, CSC lack interactions with the periphery of the brain. The existing vasculature within the brain becomes dysfunctional upon culturing and a functional blood brain barrier is missing (Humpel 2015). In light of recent trends in the field of neurodegeneration, a lack of these interactions might be an important, limiting factor of CSC. Recent high impact publications highlight an important role of the interactions of the brain with immune cells derived from the bone marrow of the skull and the glymphatic system, processes that can only be studied *in vivo* (Jorfi, Maaser-Hecker, and Tanzi 2023; Da Mesquita et al. 2018). Similarly, many neurological diseases involve the vasculature of the brain and the functionality of the blood brain barrier. Examples of this are stroke and cerebral amyloid angiopathy caused by deposition of Aβ in vessel walls. The simplicity of CSC and their limited time of survival hence limits their range of applications.

On the other hand, CSC combine several advantages of both *in vitro* models and microglia xenotransplantation models. CSC are scalable and can be used for low throughput screens. At the same time, CSC save animal numbers compared to *in* vivo experiments since several conditions can be tested in slices prepared from one pup. Like chimeric mice, CSC provide microglia with a complex tissue environment that induces a close to *in vivo* transcriptional profile (see section V.2.1.2) but on the other hand do not rely on immunodeficient mouse models. In contrast to brain organoids, however, CSC do not only provide a complex 3D-environment but are also well-defined in terms of their cellular composition. Moreover, CSC do not require a specialized mouse line and thus can mostly be prepared from WT mice or even be used with already existing models of various neurological diseases. This limits the complicated and time- and labor-consuming generation of novel mouse models.

The use of iPSC opens up the opportunity to investigate the effect of microglia-specific mutations of target genes. Mutations can be induced at the iPSC stage and thus do not spill into undesired cell types of the slice culture. Furthermore, iPSC can be derived from patients and subsequently be used to generate CSC to investigate patient-specific phenotypes. For experimental read-outs, CSC are easily accessible for a broad range of methods, including low throughput screens. They generate cell numbers that are high enough for single-cell RNA-sequencing when pooling several slices and can be used for 2-Photon live cell imaging without complicated surgical procedures.

Overall, CSC will be a useful addition to the methodological spectrum in microglia research as the trend in the field goes towards more complex models that investigate human microglia in an environment that is as close as possible to *in vivo*.

3 Conclusion and Outlook

In this PhD thesis, I present two main projects, firstly *in vivo* experiments to observe the homeostasis of the microglial network by targeted cell death of individual microglia and secondly the development of chimeric slice cultures with human iMics.

Unfortunately, during the *in vivo* project, I faced problems in establishing the mouse model, which I was able to explain with further experiments to analyze the recombination efficiency of the two transgenes by CreERT. I found that recombination of tdTomato and iDTR rarely, if ever, occurred in the same cell. In addition, the transgenes were most likely not recombined to the same extent due to differences in the length between the two loxP-sites flanking the STOP-cassette. I also ruled out other approaches for targeted microglial cell death, such as 2Phatal and photosensitizing proteins. So the only possible solution for this project would have been to create a new mouse model with a fusion protein of a red fluorescent protein and iDTR. With this model, the fluorescent marker protein would always be expressed in the iDTR expressing cells to allow the identification of the targeted cell.

Due to these challenges, which are not uncommon for *in vivo* experiments, a novel chimeric *in vitro* model was developed to facilitate further microglial research on this and other topics. To this end, established HSC models were combined with human iPSC-derived microglia to generate CSC. The endogenous mouse microglial cells were specifically depleted and replaced with iPSC-derived microglial progenitor cells. Subsequently, these cells differentiated into iMics that morphologically, functionally and transcriptionally resembled microglia *in vivo*. This work also showed how microglia-specific mutations of CSF1R through mutant iPSC lines can affect the microglial network and that iMics are dependent on CSF1R signaling via cross-species ligand-receptor interactions for their differentiation and survival. In a seeded synucleinopathy model, iMics adapt a phenotype associated with neurodegeneration, demonstrating that CSC can be used to model neurodegenerative diseases. CSC have thus proven to be a valid model for studying the homeostasis of human microglial networks *in vitro* under different conditions.

In future applications, CSC could be used as an alternative approach for a follow-up study to the *in vivo* project of this thesis. Despite being an *in vitro* system, iMics in CSC adapt a homeostatic phenotype, making them suitable for studying the homeostasis of the microglial network. Due to their easy accessibility, they allow cell-type-specific manipulations of microglia and the use of 2Phatal, photosensitizing proteins or fusion proteins of iDTR and a fluorescent reporter for targeted ablation of microglia would be facilitated.

In addition, the field of microglia will benefit enormously from CSC. CSC are a scalable, easily accessible *in vitro* model for studying human microglia with an *in vivo*-like phenotype that can be adapted to various existing OBSC models of neurological diseases.

Finally, research into neurodegenerative diseases would benefit from even more complex chimeric *in vitro* systems. There are already xenotransplantation models for astrocytes and neurons in mice that have shown a human-specific neuronal susceptibility to Alzheimer's disease (Balusu et al. 2023). A similar approach is theoretically possible for CSC to generate double- or triple-chimeric slice cultures.

Overall, CSCs with human iMics are a novel *in vitro* system that bridge the gap between current *in vitro* models and xenotransplanted chimeric mice in the spectrum of model systems for the study of microglia. They are one of the most complex *in vitro* models and induce a microglia phenotype reminiscent of microglia *in vivo*.

VI References

Abdel-Haq, Reem, Johannes C. M. Schlachetzki, Christopher K. Glass, and Sarkis K. Mazmanian. 2019. "Microbiome–Microglia Connections via the Gut–Brain Axis." *Journal of Experimental Medicine* 216(1):41–59.

Abiega, Oihane, Sol Beccari, Irune Diaz-Aparicio, Agnes Nadjar, Sophie Layé, Quentin Leyrolle, Diego Gómez-Nicola, María Domercq, Alberto Pérez-Samartín, Víctor Sánchez-Zafra, Iñaki Paris, Jorge Valero, Julie C. Savage, Chin-Wai Hui, Marie-Ève Tremblay, Juan J. P. Deudero, Amy L. Brewster, Anne E. Anderson, Laura Zaldumbide, Lara Galbarriatu, Ainhoa Marinas, Maria dM. Vivanco, Carlos Matute, Mirjana Maletic-Savatic, Juan M. Encinas, and Amanda Sierra. 2016. "Neuronal Hyperactivity Disturbs ATP Microgradients, Impairs Microglial Motility, and Reduces Phagocytic Receptor Expression Triggering Apoptosis/Microglial Phagocytosis Uncoupling." *PLOS Biology* 14(5):e1002466.

Absinta, Martina, Dragan Maric, Marjan Gharagozloo, Thomas Garton, Matthew D. Smith, Jing Jin, Kathryn C. Fitzgerald, Anya Song, Poching Liu, Jing Ping Lin, Tianxia Wu, Kory R. Johnson, Dorian B. McGavern, Dorothy P. Schafer, Peter A. Calabresi, and Daniel S. Reich. 2021. "A Lymphocyte–Microglia–Astrocyte Axis in Chronic Active Multiple Sclerosis." *Nature* 597(7878):709–14.

Abud, Edsel M., Ricardo N. Ramirez, Eric S. Martinez, Luke M. Healy, Cecilia H. H. Nguyen, Sean A. Newman, Andriy V Yeromin, Vanessa M. Scarfone, Samuel E. Marsh, Cristhian Fimbres, Chad A. Caraway, Gianna M. Fote, Abdullah M. Madany, Anshu Agrawal, Rakez Kayed, Karen H. Gylys, Michael D. Cahalan, Brian J. Cummings, Jack P. Antel, Ali Mortazavi, Monica J. Carson, Wayne W. Poon, and Mathew Blurton-Jones. 2017. "IPSC-Derived Human Microglia-like Cells to Study Neurological Diseases." *Neuron* 94(2):278-293.e9.

Ahn, Sung-Min, Kyunghee Byun, Kun Cho, Jin Young Kim, Jong Shin Yoo, Deokhoon Kim, Sun Ha Paek, Seung U. Kim, Richard J. Simpson, and Bonghee Lee. 2008. "Human Microglial Cells Synthesize Albumin in Brain." *PloS One* 3(7):e2829.

Ajami, Bahareh, Jami L. Bennett, Charles Krieger, Wolfram Tetzlaff, and Fabio M. V. Rossi. 2007. "Local Self-Renewal Can Sustain CNS Microglia Maintenance and Function throughout Adult Life." *Nature Neuroscience* 10(12):1538–43.

Åkerblom, Malin, Rohit Sachdeva, Luis Quintino, Erika Elgstrand Wettergren, Katie Z. Chapman, Giuseppe Manfre, Olle Lindvall, Cecilia Lundberg, and Johan Jakobsson. 2013. "Visualization and Genetic Modification of Resident Brain Microglia Using Lentiviral Vectors Regulated by MicroRNA-9." *Nature Communications* 4(1):1770.

Alzheimer, A., R. A. Stelzmann, H. N. Schnitzlein, and F. R. Murtagh. 1995. "An English Translation of Alzheimer's 1907 Paper, 'Uber Eine Eigenartige Erkankung Der Hirnrinde'." *Clinical Anatomy (New York, N.Y.)* 8(6):429–31.

Andjelkovic, A. V, B. Nikolic, J. S. Pachter, and N. Zecevic. 1998. "Macrophages/Microglial Cells in Human Central Nervous System during Development: An Immunohistochemical Study." *Brain Research* 814(1):13–25.

Andrews, Shea J., Brian Fulton-Howard, and Alison Goate. 2020. "Interpretation of Risk Loci from Genome-Wide Association Studies of Alzheimer's Disease." *The Lancet. Neurology* 19(4):326–35.

Anon. 2023. "2023 Alzheimer's Disease Facts and Figures." *Alzheimer's & Dementia* 19(4):1598–1695.

Askew, Katharine, Kaizhen Li, Adrian Olmos-alonso, Olga Garaschuk, V. Hugh Perry, Diego Gomez-nicola, Katharine Askew, Kaizhen Li, Adrian Olmos-alonso, Fernando Garcia-moreno, Yajie Liang, Philippa Richardson, Mark S. Cragg, Olga Garaschuk, V. Hugh Perry, and Diego Gomez-nicola. 2017. "Coupled Proliferation and Apoptosis Maintain the Rapid Turnover of Microglia in the Adult Brain Article Coupled Proliferation and Apoptosis Maintain the Rapid Turnover of Microglia in the Adult Brain." 391–405.

Auer, Franziska, Stavros Vagionitis, and Tim Czopka. 2018. "Evidence for Myelin Sheath Remodeling in the CNS Revealed by In Vivo Imaging." *Current Biology : CB* 28(4):549-559.e3.

Austin, Susan A., Angela M. Floden, Eric J. Murphy, and Colin K. Combs. 2006. "Alpha-Synuclein Expression Modulates Microglial Activation Phenotype." *The Journal of Neuroscience : The Official Journal of the Society for Neuroscience* 26(41):10558–63.

Badimon, Ana, Hayley J. Strasburger, Pinar Ayata, Xinhong Chen, Aditya Nair, Ako Ikegami, Philip Hwang, Andrew

T. Chan, Steven M. Graves, Joseph O. Uweru, Carola Ledderose, Munir Gunes Kutlu, Michael A. Wheeler, Anat Kahan, Masago Ishikawa, Ying Chih Wang, Yong Hwee E. Loh, Jean X. Jiang, D. James Surmeier, Simon C. Robson, Wolfgang G. Junger, Robert Sebra, Erin S. Calipari, Paul J. Kenny, Ukpong B. Eyo, Marco Colonna, Francisco J. Quintana, Hiroaki Wake, Viviana Gradinaru, and Anne Schaefer. 2020. "Negative Feedback Control of Neuronal Activity by Microglia." *Nature* 586(7829):417–23.

Balusu, Sriram, Katrien Horré, Nicola Thrupp, Katleen Craessaerts, An Snellinx, Lutgarde Serneels, Dries T'Syen, Iordana Chrysidou, Amaia M. Arranz, Annerieke Sierksma, Joel Simrén, Thomas K. Karikari, Henrik Zetterberg, Wei-Ting Chen, Dietmar Rudolf Thal, Evgenia Salta, Mark Fiers, and Bart De Strooper. 2023. "MEG3 Activates Necroptosis in Human Neuron Xenografts Modeling Alzheimer's Disease." *Science (New York, N.Y.)* 381(6663):1176–82.

Barry-Carroll, Liam, Philip Greulich, Abigail R. Marshall, Kristoffer Riecken, Boris Fehse, Katharine E. Askew, Kaizhen Li, Olga Garaschuk, David A. Menassa, and Diego Gomez-Nicola. 2023. "Microglia Colonize the Developing Brain by Clonal Expansion of Highly Proliferative Progenitors, Following Allometric Scaling." *Cell Reports* 42(5):112425.

Barth, Melanie, Mehtap Bacioglu, Niklas Schwarz, Renata Novotny, Janine Brandes, Marc Welzer, Sonia Mazzitelli, Lisa M. Häsler, Manuel Schweighauser, Thomas V. Wuttke, Deborah Kronenberg-Versteeg, Karina Fog, Malene Ambjørn, Ania Alik, Ronald Melki, Philipp J. Kahle, Derya R. Shimshek, Henner Koch, Mathias Jucker, and Gaye Tanriöver. 2021. "Microglial Inclusions and Neurofilament Light Chain Release Follow Neuronal α-Synuclein Lesions in Long-Term Brain Slice Cultures." *Molecular Neurodegeneration* 16(1):1–17.

Baxter, Paul S., Owen Dando, Katie Emelianova, Xin He, Sean McKay, Giles E. Hardingham, and Jing Qiu. 2021. "Microglial Identity and Inflammatory Responses Are Controlled by the Combined Effects of Neurons and Astrocytes." *Cell Reports* 34(12):108882.

Beckmann, Nicolau, Elisa Giorgetti, Anna Neuhaus, Stefan Zurbruegg, Nathalie Accart, Paul Smith, Julien Perdoux, Ludovic Perrot, Mark Nash, Sandrine Desrayaud, Peter Wipfli, Wilfried Frieauff, and Derya R. Shimshek. 2018. "Brain Region-Specific Enhancement of Remyelination and Prevention of Demyelination by the CSF1R Kinase Inhibitor BLZ945." *Acta Neuropathologica Communications* 6(1):9.

Benner, Brooke, Logan Good, Dionisia Quiroga, Thomas E. Schultz, Mahmoud Kassem, William E. Carson, Mathew A. Cherian, Sagar Sardesai, and Robert Wesolowski. 2020. "Pexidartinib, a Novel Small Molecule CSF-1R Inhibitor in Use for Tenosynovial Giant Cell Tumor: A Systematic Review of Pre-Clinical and Clinical Development." *Drug Design, Development and Therapy* 14:1693–1704.

Bennett, F. Chris, Mariko L. Bennett, Fazeela Yaqoob, Sara B. Mulinyawe, Gerald A. Grant, Melanie Hayden Gephart, Edward D. Plowey, and Ben A. Barres. 2018. "A Combination of Ontogeny and CNS Environment Establishes Microglial Identity." *Neuron* 98(6):1170-1183.e8.

Bennett, Mariko L., F. Chris Bennett, Shane A. Liddelow, Bahareh Ajami, Jennifer L. Zamanian, Nathaniel B. Fernhoff, Sara B. Mulinyawe, Christopher J. Bohlen, Aykezar Adil, Andrew Tucker, Irving L. Weissman, Edward F. Chang, Gordon Li, Gerald A. Grant, Melanie G. Hayden Gephart, and Ben A. Barres. 2016. "New Tools for Studying Microglia in the Mouse and Human CNS." *Proceedings of the National Academy of Sciences* 113(12):E1738–46.

Billingsley, K. J., S. Bandres-Ciga, S. Saez-Atienzar, and A. B. Singleton. 2018. "Genetic Risk Factors in Parkinson's Disease." *Cell and Tissue Research* 373(1):9–20.

Blasi, E., R. Barluzzi, V. Bocchini, R. Mazzolla, and F. Bistoni. 1990. "Immortalization of Murine Microglial Cells by a V-raf</Em> / v-myc</Em> Carrying Retrovirus." *Journal of Neuroimmunology* 27(2):229–37.

Bodnar, Brittany, Yongang Zhang, Jinbiao Liu, Yuan Lin, Peng Wang, Zhengyu Wei, Sami Saribas, Yuanjun Zhu, Fang Li, Xu Wang, Wenli Yang, Qingsheng Li, Wen-Zhe Ho, and Wenhui Hu. 2021. "Novel Scalable and Simplified System to Generate Microglia-Containing Cerebral Organoids From Human Induced Pluripotent Stem Cells." *Frontiers in Cellular Neuroscience* 15:682272.

Bohlen, Christopher J., F. Chris Bennett, Andrew F. Tucker, Hannah Y. Collins, Sara B. Mulinyawe, and Ben A. Barres. 2017. "Diverse Requirements for Microglial Survival, Specification, and Function Revealed by Defined-Medium Cultures." *Neuron* 94(4):759-773.e8.

Borst, Katharina, Anaelle Aurelie Dumas, and Marco Prinz. 2021. "Microglia: Immune and Non-Immune Functions." *Immunity* 54(10):2194–2208.

Boza-Serrano, Antonio, Juan F. Reyes, Nolwen L. Rey, Hakon Leffler, Luc Bousset, Ulf Nilsson, Patrik Brundin, Jose Luis Venero, Miguel Angel Burguillos, and Tomas Deierborg. 2014. "The Role of Galectin-3 in α-Synuclein-Induced Microglial Activation." *Acta Neuropathologica Communications* 2:156.

Braak, Heiko, Kelly Del Tredici, Udo Rub, Rob A. I. de Vos, Ernst N. H. Jansen Steur, and Eva Braak. 2003. "Staging of Brain Pathology Related to Sporadic Parkinson's Disease." *Neurobiology of Aging* 24(2):197–211.

Brawek, Bianca, Yajie Liang, Daria Savitska, Kaizhen Li, Natalie Fomin-Thunemann, Yury Kovalchuk, Elizabeta Zirdum, Johan Jakobsson, and Olga Garaschuk. 2017. "A New Approach for Ratiometric in Vivo Calcium Imaging of Microglia." *Scientific Reports* 7(1):1–13.

Brettschneider, Johannes, Kelly Del Tredici, Virginia M. Y. Lee, and John Q. Trojanowski. 2015. "Spreading of Pathology in Neurodegenerative Diseases: A Focus on Human Studies." *Nature Reviews Neuroscience* 16(2):109–20.

Brown, Guy C. and Jonas J. Neher. 2014. "Microglial Phagocytosis of Live Neurons." *Nature Reviews. Neuroscience* 15(4):209–16.

Bruttger, Julia, Khalad Karram, Simone Wortge, Tommy Regen, Federico Marini, Nicola Hoppmann, Matthias Klein, Thomas Blank, Simon Yona, Yochai Wolf, Matthias Mack, Emmanuel Pinteaux, Werner Muller, Frauke Zipp, Harald Binder, Tobias Bopp, Marco Prinz, Steffen Jung, and Ari Waisman. 2015. "Genetic Cell Ablation Reveals Clusters of Local Self-Renewing Microglia in the Mammalian Central Nervous System." *Immunity* 43(1):92–106.

Buch, Thorsten, Frank L. Heppner, Christine Tertilt, Tobias J. A. J. Heinen, Marcel Kremer, F. Thomas Wunderlich, Steffen Jung, and Ari Waisman. 2005. "A Cre-Inducible Diphtheria Toxin Receptor Mediates Cell Lineage Ablation after Toxin Administration." *Nature Methods* 2(6):419–26.

Buckley, C., M. T. Carvalho, L. K. Young, S. A. Rider, C. McFadden, C. Berlage, R. F. Verdon, J. M. Taylor, J. M. Girkin, and J. J. Mullins. 2017. "Precise Spatio-Temporal Control of Rapid Optogenetic Cell Ablation with Mem-KillerRed in Zebrafish." *Scientific Reports* 7(1):5096.

Bulina, Maria E., Dmitriy M. Chudakov, Olga V Britanova, Yurii G. Yanushevich, Dmitry B. Staroverov, Tatyana V Chepurnykh, Ekaterina M. Merzlyak, Maria A. Shkrob, Sergey Lukyanov, and Konstantin A. Lukyanov. 2006. "A Genetically Encoded Photosensitizer." *Nature Biotechnology* 24(1):95–99.

Busch, Robert, Richard A. Neese, Mohamad Awada, Gregory M. Hayes, and Marc K. Hellerstein. 2007. "Measurement of Cell Proliferation by Heavy Water Labeling." *Nature Protocols* 2(12):3045–57.

Cadiz, Mika P., Tanner D. Jensen, Jonathon P. Sens, Kuixi Zhu, Won-Min Song, Bin Zhang, Mark Ebbert, Rui Chang, and John D. Fryer. 2022. "Culture Shock: Microglial Heterogeneity, Activation, and Disrupted Single-Cell Microglial Networks in Vitro." *Molecular Neurodegeneration* 17(1):26.

Cha, Jeong-Heon, Mee Young Chang, James A. Richardson, and Leon Eidels. 2003. "Transgenic Mice Expressing the Diphtheria Toxin Receptor Are Sensitive to the Toxin." *Molecular Microbiology* 49(1):235–40.

Chadarevian, Jean Paul, Sonia I. Lombroso, Graham C. Peet, Jonathan Hasselmann, Christina Tu, Dave E. Marzan, Joia Capocchi, Freddy S. Purnell, Kelsey M. Nemec, Alina Lahian, Adrian Escobar, Whitney England, Sai Chaluvadi, Carleigh A. O'Brien, Fazeela Yaqoob, William H. Aisenberg, Matias Porras-Paniagua, Mariko L. Bennett, Hayk Davtyan, Robert C. Spitale, Mathew Blurton-Jones, and F. Chris Bennett. 2022. "Engineering an Inhibitor-Resistant Human CSF1R Variant for Microglia Replacement." *Journal of Experimental Medicine* 220(3):e20220857.

Chapman, Timothy W., Genaro E. Olveda, Xhoela Bame, Elizabeth Pereira, and Robert A. Hill. 2023. "Oligodendrocyte Death Initiates Synchronous Remyelination to Restore Cortical Myelin Patterns in Mice." *Nature Neuroscience* 26(4):555–69.

Chappell-Maor, Louise, Masha Kolesnikov, Jung Seok Kim, Anat Shemer, Zhana Haimon, Jonathan Grozovski, Sigalit Boura-Halfon, Takahiro Masuda, Marco Prinz, and Steffen Jung. 2020. "Comparative Analysis of CreER Transgenic Mice for the Study of Brain Macrophages: A Case Study." *European Journal of Immunology* 50(3):353–62.

Chen, Xiaoying, Maria Firulyova, Melissa Manis, Jasmin Herz, Igor Smirnov, Ekaterina Aladyeva, Chanung Wang, Xin Bao, Mary Beth Finn, Hao Hu, Irina Shchukina, Min Woo Kim, Carla M. Yuede, Jonathan Kipnis, Maxim N. Artyomov, Jason D. Ulrich, and David M. Holtzman. 2023. "Microglia-Mediated T Cell Infiltration Drives Neurodegeneration in Tauopathy." *Nature* 615(7953):668–77.

Chiu, Isaac M., Emiko T. A. Morimoto, Hani Goodarzi, Jennifer T. Liao, Sean O'Keeffe, Hemali P. Phatnani, Michael Muratet, Michael C. Carroll, Shawn Levy, Saeed Tavazoie, Richard M. Myers, and Tom Maniatis. 2013. "A Neurodegeneration-Specific Gene-Expression Signature of Acutely Isolated Microglia from an Amyotrophic Lateral Sclerosis Mouse Model." *Cell Reports* 4(2):385–401.

Choi, Insup, Yuanxi Zhang, Steven P. Seegobin, Mathilde Pruvost, Qian Wang, Kerry Purtell, Bin Zhang, and Zhenyu Yue. 2020. "Microglia Clear Neuron-Released α-Synuclein via Selective Autophagy and Prevent Neurodegeneration." *Nature Communications* 11(1).

Choi, Myunghwan, Taeyun Ku, Kyuha Chong, Jonghee Yoon, and Chulhee Choi. 2011. "Minimally Invasive Molecular Delivery into the Brain Using Optical Modulation of Vascular Permeability." *Proceedings of the National Academy of Sciences of the United States of America* 108(22):9256–61.

Choi, Woong, Shahin Zibaee, Ross Jakes, Louise C. Serpell, Bazbek Davletov, R. Anthony Crowther, and Michel Goedert. 2004. "Mutation E46K Increases Phospholipid Binding and Assembly into Filaments of Human Alpha-Synuclein." *FEBS Letters* 576(3):363–68.

Colombo, Gloria, Ryan John A. Cubero, Lida Kanari, Alessandro Venturino, Rouven Schulz, Martina Scolamiero, Jens Agerberg, Hansruedi Mathys, Li-Huei Tsai, Wojciech Chachólski, Kathryn Hess, and Sandra Siegert. 2022. "A Tool for Mapping Microglial Morphology, MorphOMICs, Reveals Brain-Region and Sex-Dependent Phenotypes." *Nature Neuroscience* 25(10):1379–93.

Colonna, Marco and Oleg Butovsky. 2017. "Microglia Function in the Central Nervous System during Health and Neurodegeneration." *Annual Review of Immunology* 35:441–68.

Colton, C. A. and D. L. Gilbert. 1987. "Production of Superoxide Anions by a CNS Macrophage, the Microglia." *FEBS Letters* 223(2):284–88.

Coniglio, Salvatore J., Eliseo Eugenin, Kostantin Dobrenis, E. Richard Stanley, Brian L. West, Marc H. Symons, and Jeffrey E. Segall. 2012. "Microglial Stimulation of Glioblastoma Invasion Involves Epidermal Growth Factor Receptor (EGFR) and Colony Stimulating Factor 1 Receptor (CSF-1R) Signaling." *Molecular Medicine* 18(3):519–27.

Conway, James G., Brad McDonald, Janet Parham, Barry Keith, David W. Rusnak, Eva Shaw, Marilyn Jansen, Peiyuan Lin, Alan Payne, Renae M. Crosby, Jennifer H. Johnson, Lloyd Frick, Min-Hwa Jasmine Lin, Scott Depee, Sarva Tadepalli, Bart Votta, Ian James, Karen Fuller, Timothy J. Chambers, Frederick C. Kull, Stanley D. Chamberlain, and Jeff T. Hutchins. 2005. "Inhibition of Colony-Stimulating-Factor-1 Signaling in Vivo with the Orally Bioavailable CFMS Kinase Inhibitor GW2580." *Proceedings of the National Academy of Sciences* 102(44):16078–83.

Croft, C. L., H. S. Futch, B. D. Moore, and T. E. Golde. 2019. "Organotypic Brain Slice Cultures to Model Neurodegenerative Proteinopathies." *Molecular Neurodegeneration* 14(1):45.

Cronk, James C., Anthony J. Filiano, Antoine Louveau, Ioana Marin, Rachel Marsh, Emily Ji, Dylan H. Goldman, Igor Smirnov, Nicholas Geraci, Scott Acton, Christopher C. Overall, and Jonathan Kipnis. 2018. "Peripherally Derived Macrophages Can Engraft the Brain Independent of Irradiation and Maintain an Identity Distinct from Microglia." *Journal of Experimental Medicine* 215(6):1627–47.

Cserép, Csaba, Balázs Pósfai, Nikolett Lénárt, Rebeka Fekete, Zsófia I. László, Zsolt Lele, Barbara Orsolits, Gábor Molnár, Steffanie Heindl, Anett D. Schwarcz, Katinka Ujvári, Zsuzsanna Környei, Krisztina Tóth, Eszter Szabadits, Beáta Sperlágh, Mária Baranyi, László Csiba, Tibor Hortobágyi, Zsófia Maglóczky, Bernadett Martinecz, Gábor Szabó, Ferenc Erdélyi, Róbert Szipocs, Michael M. Tamkun, Benno Gesierich, Marco Duering, István Katona, Arthur Liesz, Gábor Tamás, and Ádám Dénes. 2020. "Microglia Monitor and Protect Neuronal Function through Specialized Somatic Purinergic Junctions." *Science* 367(6477):528–37.

Czapiga, M. and C. A. Colton. 1999. "Function of Microglia in Organotypic Slice Cultures." *Journal of Neuroscience Research* 56(6):644–51.

Dai, Xu-Ming, Gregory R. Ryan, Andrew J. Hapel, Melissa G. Dominguez, Robert G. Russell, Sara Kapp, Vonetta Sylvestre, and E. Richard Stanley. 2002. "Targeted Disruption of the Mouse Colony-Stimulating Factor 1 Receptor Gene Results in Osteopetrosis, Mononuclear Phagocyte Deficiency, Increased Primitive Progenitor Cell Frequencies, and Reproductive Defects." *Blood* 99(1):111–20.

Damani, Mausam R., Lian Zhao, Aurora M. Fontainhas, Juan Amaral, Robert N. Fariss, and Wai T. Wong. 2011. "Age-Related Alterations in the Dynamic Behavior of Microglia." *Aging Cell* 10(2):263–76.

Damisah, Eyiyemisi C., Robert A. Hill, Anupama Rai, Fuyi Chen, Carla V Rothlin, Sourav Ghosh, and Jaime Grutzendler. 2020. “Astrocytes and Microglia Play Orchestrated Roles and Respect Phagocytic Territories during Neuronal Corpse Removal in Vivo.” 1–13.

Daniel, Mayer, Fischer Heike, Schneider Urs, Heimrich Bernd, and Schwemmle Martin. 2005. “Borna Disease Virus Replication in Organotypic Hippocampal Slice Cultures from Rats Results in Selective Damage of Dentate Granule Cells.” *Journal of Virology* 79(18):11716–23.

Danzer, Karin M., Lisa R. Kranich, Wolfgang P. Ruf, Ozge Cagsal-Getkin, Ashley R. Winslow, Liya Zhu, Charles R. Vanderburg, and Pamela J. McLean. 2012. “Exosomal Cell-to-Cell Transmission of Alpha Synuclein Oligomers.” *Molecular Neurodegeneration* 7(1):42.

Davalos, Dimitrios, Jaime Grutzendler, Guang Yang, Jiyun V. Kim, Yi Zuo, Steffen Jung, Dan R. Littman, Michael L. Dustin, and Wen Biao Gan. 2005. “ATP Mediates Rapid Microglial Response to Local Brain Injury in Vivo.” *Nature Neuroscience* 8(6):752–58.

Dawson, Ted M., Todd E. Golde, and Clotilde Lagier-Tourenne. 2018. “Animal Models of Neurodegenerative Diseases.” *Nature Neuroscience* 21(10):1370–79.

Delbridge, Alex R. D., Dann Huh, Margot Brickelmaier, Jeremy C. Burns, Chris Roberts, Ravi Challa, Naideline Raymond, Patrick Cullen, Thomas M. Carlile, Katelin A. Ennis, Mei Liu, Chao Sun, Normand E. Allaire, Marianna Foos, Hui Hsin Tsai, Nathalie Franchimont, Richard M. Ransohoff, Cherie Butts, and Michael Mingueneau. 2020. “Organotypic Brain Slice Culture Microglia Exhibit Molecular Similarity to Acutely-Isolated Adult Microglia and Provide a Platform to Study Neuroinflammation.” *Frontiers in Cellular Neuroscience* 14(December).

Distéfano-Gagné, Félix, Sara Bitarafan, Steve Lacroix, and David Gosselin. 2023. “Roles and Regulation of Microglia Activity in Multiple Sclerosis: Insights from Animal Models.” *Nature Reviews Neuroscience* 24(7):397–415.

Dolan, Michael-John, Martine Therrien, Saša Jereb, Tushar Kamath, Vahid Gazestani, Trevor Atkeson, Samuel E. Marsh, Aleksandrina Goeva, Neal M. Lojek, Sarah Murphy, Cassandra M. White, Julia Joung, Bingxu Liu, Francesco Limone, Kevin Eggan, Nir Hacohen, Bradley E. Bernstein, Christopher K. Glass, Ville Leinonen, Mathew Blurton-Jones, Feng Zhang, Charles B. Epstein, Evan Z. Macosko, and Beth Stevens. 2023. “Exposure of IPSC-Derived Human Microglia to Brain Substrates Enables the Generation and Manipulation of Diverse Transcriptional States in Vitro.” *Nature Immunology* 24(8):1382–90.

Dolmetsch, Ricardo and Daniel H. Geschwind. 2011. “The Human Brain in a Dish: The Promise of IPSC-Derived Neurons.” *Cell* 145(6):831–34.

Douvaras, Panagiotis, Bruce Sun, Minghui Wang, Ilya Kruglikov, Gregory Lallos, Matthew Zimmer, Cecile Terrenoire, Bin Zhang, Sam Gandy, Eric Schadt, Donald O. Freytes, Scott Noggle, and Valentina Fossati. 2017. “Directed Differentiation of Human Pluripotent Stem Cells to Microglia.” *Stem Cell Reports* 8(6):1516–24.

Dräger, Nina M., Sydney M. Sattler, Cindy Tzu-Ling Huang, Olivia M. Teter, Kun Leng, Sayed Hadi Hashemi, Jason Hong, Giovanni Aviles, Claire D. Clelland, Lihong Zhan, Joe C. Udeochu, Lay Kodama, Andrew B. Singleton, Mike A. Nalls, Justin Ichida, Michael E. Ward, Faraz Faghri, Li Gan, and Martin Kampmann. 2022. “A CRISPRi/a Platform in Human IPSC-Derived Microglia Uncovers Regulators of Disease States.” *Nature Neuroscience* 25(9):1149–62.

Drazin, R., J. Kandel, and R. J. Collier. 1971. “Structure and Activity of Diphtheria Toxin. II. Attack by Trypsin at a Specific Site within the Intact Toxin Molecule.” *The Journal of Biological Chemistry* 246(5):1504–10.

Dubbelaar, Marissa L., Laura Kracht, Bart J. L. Eggen, and Erik W. G. M. Boddeke. 2018. “The Kaleidoscope of Microglial Phenotypes.” *Frontiers in Immunology* 9:1753.

Easley-Neal, Courtney, Oded Foreman, Neeraj Sharma, Ali A. Zarrin, and Robby M. Weimer. 2019. “CSF1R Ligands IL-34 and CSF1 Are Differentially Required for Microglia Development and Maintenance in White and Gray Matter Brain Regions.” *Frontiers in Immunology* 10(September).

Efthymiou, Anastasia G. and Alison M. Goate. 2017. “Late Onset Alzheimer’s Disease Genetics Implicates Microglial Pathways in Disease Risk.” *Molecular Neurodegeneration* 12(1):43.

Eidson, Lori N., George T. Kannarkat, Christopher J. Barnum, Jianjun Chang, Jaegwon Chung, Chelsea Caspell-Garcia, Peggy Taylor, Brit Mollenhauer, Michael G. Schlossmacher, Larry Ereshefsky, Mark Yen, Catherine

Kopil, Mark Frasier, Kenneth Marek, Vicki S. Hertzberg, and Malú G. Tansey. 2017. "Candidate Inflammatory Biomarkers Display Unique Relationships with Alpha-Synuclein and Correlate with Measures of Disease Severity in Subjects with Parkinson's Disease." *Journal of Neuroinflammation* 14(1):1–16.

Elmore, Monica R. P., Lindsay A. Hohsfield, Enikö A. Kramár, Lilach Soreq, Rafael J. Lee, Stephanie T. Pham, Allison R. Najafi, Elizabeth E. Spangenberg, Marcelo A. Wood, Brian L. West, and Kim N. Green. 2018. "Replacement of Microglia in the Aged Brain Reverses Cognitive, Synaptic, and Neuronal Deficits in Mice." *Aging Cell* 17(6).

Elmore, Monica R. P., Allison R. Najafi, Maya A. Koike, Nabil N. Dagher, Elizabeth E. Spangenberg, Rachel A. Rice, Masashi Kitazawa, Bernice Matusow, Hoa Nguyen, Brian L. West, and Kim N. Green. 2014. "Colony-Stimulating Factor 1 Receptor Signaling Is Necessary for Microglia Viability, Unmasking a Microglia Progenitor Cell in the Adult Brain." *Neuron* 82(2):380–97.

Eme-Scolan, Elisa and Samantha J. Dando. 2020. "Tools and Approaches for Studying Microglia In Vivo." *Frontiers in Immunology* 11:583647.

Erblich, Bryna, Liyin Zhu, Anne M. Etgen, Kostantin Dobrenis, and Jeffrey W. Pollard. 2011. "Absence of Colony Stimulation Factor-1 Receptor Results in Loss of Microglia, Disrupted Brain Development and Olfactory Deficits." *PLOS ONE* 6(10):e26317.

Ertürk, Ali, Yuanyuan Wang, and Morgan Sheng. 2014. "Local Pruning of Dendrites and Spines by Caspase-3-Dependent and Proteasome-Limited Mechanisms." *The Journal of Neuroscience : The Official Journal of the Society for Neuroscience* 34(5):1672–88.

Eugène, Emmanuel, Françoise Cluzeaud, Carmen Cifuentes-Diaz, Desdemona Fricker, Caroline Le Duigou, Stephane Clemenceau, Michel Baulac, Jean-Christophe Poncer, and Richard Miles. 2014. "An Organotypic Brain Slice Preparation from Adult Patients with Temporal Lobe Epilepsy." *Journal of Neuroscience Methods* 235:234–44.

Eyo, Ukpong B., Ashley Bispo, Junting Liu, Sruchika Sabu, Rong Wu, Victoria L. DiBona, Jiaying Zheng, Madhuvika Murugan, Huaye Zhang, Yamei Tang, and Long-Jun Wu. 2018. "The GluN2A Subunit Regulates Neuronal NMDA Receptor-Induced Microglia-Neuron Physical Interactions." *Scientific Reports* 8(1):828.

Eyo, Ukpong B., Mingshu Mo, Min-Hee Yi, Madhuvika Murugan, Junting Liu, Rohan Yarlagadda, David J. Margolis, Pingyi Xu, and Long-Jun Wu. 2018. "P2Y12R-Dependent Translocation Mechanisms Gate the Changing Microglial Landscape." *Cell Reports* 23(4):959–66.

Falsig, Jeppe and Adriano Aguzzi. 2008. "The Prion Organotypic Slice Culture Assay--POSCA." *Nature Protocols* 3(4):555–62.

Fantin, Alessandro, Joaquim M. Vieira, Gaia Gestri, Laura Denti, Quenten Schwarz, Sergey Prykhozhij, Francesca Peri, Stephen W. Wilson, and Christiana Ruhrberg. 2010. "Tissue Macrophages Act as Cellular Chaperones for Vascular Anastomosis Downstream of VEGF-Mediated Endothelial Tip Cell Induction." *Blood* 116(5):829–40.

Fattorelli, Nicola, Anna Martinez-Muriana, Leen Wolfs, Ivana Geric, Bart De Strooper, and Renzo Mancuso. 2021. "Stem-Cell-Derived Human Microglia Transplanted into Mouse Brain to Study Human Disease." *Nature Protocols* 16(2):1013–33.

Faust, Travis E., Philip A. Feinberg, Ciara O'Connor, Riki Kawaguchi, Andrew Chan, Hayley Strasburger, Maximilian Frosch, Margaret A. Boyle, Takahiro Masuda, Lukas Amann, Klaus-Peter Knobeloch, Marco Prinz, Anne Schaefer, and Dorothy P. Schafer. 2023. "A Comparative Analysis of Microglial Inducible Cre Lines." *Cell Reports* 42(9):113031.

Feil, R., J. Brocard, B. Mascrez, M. LeMeur, D. Metzger, and P. Chambon. 1996. "Ligand-Activated Site-Specific Recombination in Mice." *Proceedings of the National Academy of Sciences of the United States of America* 93(20):10887–90.

Fellner, Lisa, Regina Irschick, Kathrin Schanda, Markus Reindl, Lars Klimaschewski, Werner Poewe, Gregor K. Wenning, and Nadia Stefanova. 2013. "Toll-like Receptor 4 Is Required for α-Synuclein Dependent Activation of Microglia and Astroglia." *Glia* 61(3):349–60.

Feng, Linjuan, Hsuan Lo, Zhaoxiang Hong, Jiahao Zheng, Yuhong Yan, Zucheng Ye, Xiaochun Chen, and Xiaodong Pan. 2023. "Microglial LRRK2-Mediated NFATc1 Attenuates α-Synuclein Immunotoxicity in Association with CX3CR1-Induced Migration and the Lysosome-Initiated Degradation." *Glia* (January):1–19.

Feng, Yang, Chuyun Zheng, Yajun Zhang, Changyang Xing, Wenbin Cai, Ruru Li, Jianzong Chen, and Yunyou Duan. 2019. "Triptolide Inhibits Preformed Fibril-Induced Microglial Activation by Targeting the MicroRNA155-5p/SHIP1 Pathway" edited by R. Morishita. *Oxidative Medicine and Cellular Longevity* 2019:6527638.

Ferrucci, Luigi, Marta Gonzalez-Freire, Elisa Fabbri, Eleanor Simonsick, Toshiko Tanaka, Zenobia Moore, Shabnam Salimi, Felipe Sierra, and Rafael de Cabo. 2020. "Measuring Biological Aging in Humans: A Quest." *Aging Cell* 19(2):e13080.

Filipello, Fabia, Raffaella Morini, Irene Corradini, Valerio Zerbi, Alice Canzi, Bernadeta Michalski, Marco Erreni, Marija Markicevic, Chiara Starvaggi-Cucuzza, Karel Otero, Laura Piccio, Francesca Cignarella, Fabio Perrucci, Matteo Tamborini, Marco Genua, Lawrence Rajendran, Elisabetta Menna, Stefania Vetrano, Margaret Fahnestock, Rosa Chiara Paolicelli, and Michela Matteoli. 2018. "The Microglial Innate Immune Receptor TREM2 Is Required for Synapse Elimination and Normal Brain Connectivity." *Immunity* 48(5):979-991.e8.

Formella, Isabel, Adam J. Svahn, Rowan A. W. Radford, Emily K. Don, Nicholas J. Cole, Alison Hogan, Albert Lee, Roger S. Chung, and Marco Morsch. 2018. "Real-Time Visualization of Oxidative Stress-Mediated Neurodegeneration of Individual Spinal Motor Neurons in Vivo." *Redox Biology* 19:226–34.

Frade, José María and Yves-Alain Barde. 1998. "Microglia-Derived Nerve Growth Factor Causes Cell Death in the Developing Retina." *Neuron* 20(1):35–41.

Franco, Rafael and Diana Fernández-Suárez. 2015. "Alternatively Activated Microglia and Macrophages in the Central Nervous System." *Progress in Neurobiology* 131:65–86.

Fu, Hongjun, John Hardy, and Karen E. Duff. 2018. "Selective Vulnerability in Neurodegenerative Diseases." *Nature Neuroscience* 21(10):1350–58.

Füger, Petra, Jasmin K. Hefendehl, Karthik Veeraraghavalu, Ann-christin Wendeln, Christine Schlosser, Ulrike Obermüller, Bettina M. Wegenast-braun, Jonas J. Neher, Peter Martus, Shinichi Kohsaka, Martin Thunemann, Robert Feil, Sangram S. Sisodia, Angelos Skodras, and Mathias Jucker. 2017. "Microglia Turnover with Aging and in an Alzheimer ' s Model via Long-Term in Vivo Single-Cell Imaging." 20(10).

Fujiwara, Hideo, Masato Hasegawa, Naoshi Dohmae, Akiko Kawashima, Eliezer Masliah, Matthew S. Goldberg, Jie Shen, Koji Takio, and Takeshi Iwatsubo. 2002. "A-Synuclein Is Phosphorylated in Synucleinopathy Lesions." *Nature Cell Biology* 4(2):160–64.

Gähwiler, B. H., M. Capogna, D. Debanne, R. A. McKinney, and S. M. Thompson. 1997. "Organotypic Slice Cultures: A Technique Has Come of Age." *Trends in Neurosciences* 20(10):471–77.

Galatro, Thais F., Inge R. Holtman, Antonio M. Lerario, Ilia D. Vainchtein, Nieske Brouwer, Paula R. Sola, Mariana M. Veras, Tulio F. Pereira, Renata E. P. Leite, Thomas Möller, Paul D. Wes, Mari C. Sogayar, Jon D. Laman, Wilfred Den Dunnen, Carlos A. Pasqualucci, Sueli M. Oba-Shinjo, Erik W. G. M. Boddeke, Suely K. N. Marie, and Bart J. L. Eggen. 2017. "Transcriptomic Analysis of Purified Human Cortical Microglia Reveals Age-Associated Changes." *Nature Neuroscience* 20(8):1162–71.

Gallardo, José, Carmen Escalona-Noguero, and Begoña Sot. 2020. "Role of α-Synuclein Regions in Nucleation and Elongation of Amyloid Fiber Assembly." *ACS Chemical Neuroscience* 11(6):872–79.

Gate, David, Emma Tapp, Olivia Leventhal, Marian Shahid, Tim J. Nonninger, Andrew C. Yang, Katharina Strempfl, Michael S. Unger, Tobias Fehlmann, Hamilton Oh, Divya Channappa, Victor W. Henderson, Andreas Keller, Ludwig Aigner, Douglas R. Galasko, Mark M. Davis, Kathleen L. Poston, and Tony Wyss-Coray. 2021. "CD4(+) T Cells Contribute to Neurodegeneration in Lewy Body Dementia." *Science (New York, N.Y.)* 374(6569):868–74.

Geirsdottir, Laufey, Eyal David, Hadas Keren-Shaul, Assaf Weiner, Stefan Cornelius Bohlen, Jana Neuber, Adam Balic, Amir Giladi, Fadi Sheban, Charles-Antoine Dutertre, Christine Pfeifle, Francesca Peri, Antonella Raffo-Romero, Jacopo Vizioli, Kaspar Matiasek, Christian Scheiwe, Stephan Meckel, Kerstin Mätz-Rensing, Franziska van der Meer, Finnbogi Rutur Thormodsson, Christine Stadelmann, Noga Zilkha, Tali Kimchi, Florent Ginhoux, Igor Ulitsky, Daniel Erny, Ido Amit, and Marco Prinz. 2019. "Cross-Species Single-Cell Analysis Reveals Divergence of the Primate Microglia Program." *Cell* 179(7):1609-1622.e16.

Ginhoux, Florent, Melanie Greter, Marylene Leboeuf, Sayan Nandi, Peter See, Solen Gokhan, Mark F. Mehler, Simon J. Conway, Lai Guan Ng, E. Richard Stanley, Igor M. Samokhvalov, and Miriam Merad. 2010. "Fate Mapping Analysis Reveals That Adult Microglia Derive from Primitive Macrophages." *Science (New York, N.Y.)* 330(6005):841–45.

Glaser, Stefan, Konstantinos Anastassiadis, and A. Francis Stewart. 2005. “Current Issues in Mouse Genome Engineering.” *Nature Genetics* 37(11):1187–93.

Glenner, G. G. and C. W. Wong. 1984. “Alzheimer’s Disease: Initial Report of the Purification and Characterization of a Novel Cerebrovascular Amyloid Protein.” *Biochemical and Biophysical Research Communications* 120(3):885–90.

Goddery, Emma N., Cori E. Fain, Chloe G. Lipovsky, Katayoun Ayasoufi, Lila T. Yokanovich, Courtney S. Malo, Roman H. Khadka, Zachariah P. Tritz, Fang Jin, Michael J. Hansen, and Aaron J. Johnson. 2021. “Microglia and Perivascular Macrophages Act as Antigen Presenting Cells to Promote CD8 T Cell Infiltration of the Brain .” *Frontiers in Immunology* 12.

Goedert, Michel. 2015. “Alzheimer’s and Parkinson’s Diseases: The Prion Concept in Relation to Assembled Aβ, Tau, and α-Synuclein.” *Science* 349(6248):1255555.

Goedert, Michel, Ross Jakes, and Maria Grazia Spillantini. 2017. “The Synucleinopathies: Twenty Years On.” *Journal of Parkinson’s Disease* 7(s1):S51–69.

Gordon, Aaron, Se-Jin Yoon, Stephen S. Tran, Christopher D. Makinson, Jin Young Park, Jimena Andersen, Alfredo M. Valencia, Steve Horvath, Xinshu Xiao, John R. Huguenard, Sergiu P. Pașca, and Daniel H. Geschwind. 2021. “Long-Term Maturation of Human Cortical Organoids Matches Key Early Postnatal Transitions.” *Nature Neuroscience* 24(3):331–42.

Gordon, Richard, Eduardo A. Albornoz, Daniel C. Christie, Monica R. Langley, Vinod Kumar, Susanna Mantovani, Avril A. B. Robertson, Mark S. Butler, Dominic B. Rowe, Luke A. O’Neill, Anumantha G. Kanthasamy, Kate Schroder, Matthew A. Cooper, and Trent M. Woodruff. 2018. “Inflammasome Inhibition Prevents α-Synuclein Pathology and Dopaminergic Neurodegeneration in Mice.” *Science Translational Medicine* 10(465):eaah4066.

Gosselin, David, Dylan Skola, Nicole G. Coufal, Inge R. Holtman, Johannes C. M. Schlachetzki, Eniko Sajti, Baptiste N. Jaeger, Carolyn O’Connor, Conor Fitzpatrick, Martina P. Pasillas, Monique Pena, Amy Adair, David D. Gonda, Michael L. Levy, Richard M. Ransohoff, Fred H. Gage, and Christopher K. Glass. 2017. “An Environment-Dependent Transcriptional Network Specifies Human Microglia Identity.” *Science* 356(6344):1248–59.

Grabiec, Urszula, Tim Hohmann, Niels Hammer, and Faramarz Dehghani. 2017. “Organotypic Hippocampal Slice Cultures As a Model to Study Neuroprotection and Invasiveness of Tumor Cells.” *Journal of Visualized Experiments : JoVE* (126).

Green, Kim N., Joshua D. Crapser, and Lindsay A. Hohsfield. 2020. “To Kill a Microglia: A Case for CSF1R Inhibitors.” *Trends in Immunology* 41(9):771–84.

Grozdanov, Veselin and Karin M. Danzer. 2018. “Release and Uptake of Pathologic Alpha-Synuclein.” *Cell and Tissue Research* 373(1):175–82.

Grundke-Iqbal, I., K. Iqbal, Y. C. Tung, M. Quinlan, H. M. Wisniewski, and L. I. Binder. 1986. “Abnormal Phosphorylation of the Microtubule-Associated Protein Tau (Tau) in Alzheimer Cytoskeletal Pathology.” *Proceedings of the National Academy of Sciences of the United States of America* 83(13):4913–17.

Guneykaya, Dilansu, Andranik Ivanov, Daniel Perez Hernandez, Verena Haage, Bartosz Wojtas, Niklas Meyer, Meron Maricos, Philipp Jordan, Alice Buonfiglioli, Bartlomiej Gielniewski, Natalia Ochocka, Cagla Cömert, Corinna Friedrich, Lorena Suarez Artiles, Bozena Kaminska, Philipp Mertins, Dieter Beule, Helmut Kettenmann, and Susanne A. Wolf. 2018. “Transcriptional and Translational Differences of Microglia from Male and Female Brains.” *Cell Reports* 24(10):2773-2783.e6.

Guo, Min, Jian Wang, Yanxin Zhao, Yiwei Feng, Sida Han, Qiang Dong, Mei Cui, and Kim Tieu. 2020. “Microglial Exosomes Facilitate α-Synuclein Transmission in Parkinson’s Disease.” *Brain : A Journal of Neurology* 143(5):1476–97.

Haenseler, Walther, Stephen N. Sansom, Julian Buchrieser, Sarah E. Newey, Craig S. Moore, Francesca J. Nicholls, Satyan Chintawar, Christian Schnell, Jack P. Antel, Nicholas D. Allen, M. Zameel Cader, Richard Wade-Martins, William S. James, and Sally A. Cowley. 2017. “A Highly Efficient Human Pluripotent Stem Cell Microglia Model Displays a Neuronal-Co-Culture-Specific Expression Profile and Inflammatory Response.” *Stem Cell Reports* 8(6):1727–42.

Hagemeyer, Nora, Klara Maria Hanft, Maria Anna Akriditou, Nicole Unger, Eun S. Park, E. Richard Stanley, Ori

Staszewski, Leda Dimou, and Marco Prinz. 2017. “Microglia Contribute to Normal Myelinogenesis and to Oligodendrocyte Progenitor Maintenance during Adulthood.” *Acta Neuropathologica* 134(3):441–58.

Hailer, N. P., J. D. Jarhult, and R. Nitsch. 1996. “Resting Microglial Cells in Vitro: Analysis of Morphology and Adhesion Molecule Expression in Organotypic Hippocampal Slice Cultures.” *Glia* 18(4):319–31.

Hammond, Timothy R., Connor Dufort, Lasse Dissing-Olesen, Stefanie Giera, Adam Young, Alec Wysoker, Alec J. Walker, Frederick Gergits, Michael Segel, James Nemesh, Samuel E. Marsh, Arpiar Saunders, Evan Macosko, Florent Ginhoux, Jinmiao Chen, Robin J. M. Franklin, Xianhua Piao, Steven A. McCarroll, and Beth Stevens. 2019. “Single-Cell RNA Sequencing of Microglia throughout the Mouse Lifespan and in the Injured Brain Reveals Complex Cell-State Changes.” *Immunity* 50(1):253-271.e6.

Han, Jinming, Violeta Chitu, E. Richard Stanley, Zbigniew K. Wszolek, Virginija Danylaité Karrenbauer, and Robert A. Harris. 2022. “Inhibition of Colony Stimulating Factor-1 Receptor (CSF-1R) as a Potential Therapeutic Strategy for Neurodegenerative Diseases: Opportunities and Challenges.” *Cellular and Molecular Life Sciences* 79(4):219.

Han, Xiaoning, Qian Li, Xi Lan, Leena El-Mufti, Honglei Ren, and Jian Wang. 2019. “Microglial Depletion with Clodronate Liposomes Increases Proinflammatory Cytokine Levels, Induces Astrocyte Activation, and Damages Blood Vessel Integrity.” *Molecular Neurobiology* 56(9):6184–96.

Hardy, John. 2010. “Genetic Analysis of Pathways to Parkinson Disease.” *Neuron* 68(2):201–6.

Hasselmann, Jonathan and Mathew Blurton-Jones. 2020. “Human IPSC-Derived Microglia: A Growing Toolset to Study the Brain’s Innate Immune Cells.” *Glia* 68(4):721–39.

Hasselmann, Jonathan, Morgan A. Coburn, Whitney England, Dario X. Figueroa Velez, Sepideh Kiani Shabestari, Christina H. Tu, Amanda McQuade, Mahshad Kolahdouzan, Karla Echeverria, Christel Claes, Taylor Nakayama, Ricardo Azevedo, Nicole G. Coufal, Claudia Z. Han, Brian J. Cummings, Hayk Davtyan, Christopher K. Glass, Luke M. Healy, Sunil P. Gandhi, Robert C. Spitale, and Mathew Blurton-Jones. 2019. “Development of a Chimeric Model to Study and Manipulate Human Microglia In Vivo.” *Neuron* 103(6):1016-1033.e10.

Healy, Luke M., Jo Anne Stratton, Tanja Kuhlmann, and Jack Antel. 2022. “The Role of Glial Cells in Multiple Sclerosis Disease Progression.” *Nature Reviews Neurology* 18(4):237–48.

Hedegaard, Anne, Szymon Stodolak, William S. James, and Sally A. Cowley. 2020. “Honing the Double-Edged Sword: Improving Human IPSC-Microglia Models.” *Frontiers in Immunology* 11:614972.

Hefendehl, Jasmin K., David Milford, Daniel Eicke, Bettina M. Wegenast-Braun, Michael E. Calhoun, Stefan A. Grathwohl, Mathias Jucker, and Christian Liebig. 2012. “Repeatable Target Localization for Long-Term in Vivo Imaging of Mice with 2-Photon Microscopy.” *Journal of Neuroscience Methods* 205(2):357–63.

Hefendehl, Jasmin K., Jonas J. Neher, Rafael B. Suhs, Shinichi Kohsaka, Angelos Skodras, Mathias Jucker, Rafael B. Sühs, Shinichi Kohsaka, Angelos Skodras, and Mathias Jucker. 2014. “Homeostatic and Injury-Induced Microglia Behavior in the Aging Brain.” *Aging Cell* 13(1):60–69.

Heng, Yang, Marissa L. Dubbelaar, Suely K. N. Marie, Erik W. G. M. Boddeke, and Bart J. L. Eggen. 2021. “The Effects of Postmortem Delay on Mouse and Human Microglia Gene Expression.” *Glia* 69(4):1053–60.

Henn, Anja, Søren Lund, Maj Hedtjärn, Andreé Schrattenholz, Peter Pörzgen, and Marcel Leist. 2009. “The Suitability of BV2 Cells as Alternative Model System for Primary Microglia Cultures or for Animal Experiments Examining Brain Inflammation.” *ALTEX* 26(2):83–94.

Heppner, F. L., T. Skutella, N. P. Hailer, D. Haas, and R. Nitsch. 1998. “Activated Microglial Cells Migrate towards Sites of Excitotoxic Neuronal Injury inside Organotypic Hippocampal Slice Cultures.” *The European Journal of Neuroscience* 10(10):3284–90.

Heppner, Frank L., Melanie Greter, Denis Marino, Jeppe Falsig, Gennadij Raivich, Nadine Hövelmeyer, Ari Waisman, Thomas Rülicke, Marco Prinz, Josef Priller, Burkhard Becher, and Adriano Aguzzi. 2005. “Experimental Autoimmune Encephalomyelitis Repressed by Microglial Paralysis.” *Nature Medicine* 11(2):146–52.

Hickman, Suzanne E., Elizabeth K. Allison, and Joseph El Khoury. 2008. “Microglial Dysfunction and Defective β-Amyloid Clearance Pathways in Aging Alzheimer's Disease Mice.” *The Journal of Neuroscience* 28(33):8354 LP – 8360.

Hickman, Suzanne, Saef Izzy, Pritha Sen, Liza Morsett, and Joseph El Khoury. 2018. “Microglia in Neurodegeneration.” *Nature Neuroscience* 21(10):1359–69.

Hierro-Bujalance, Carmen, Brian J. Bacskai, and Monica Garcia-Alloza. 2018. “In Vivo Imaging of Microglia With Multiphoton Microscopy.” *Frontiers in Aging Neuroscience* 10:218.

Hill, Robert A., Eyiyemisi C. Damisah, Fuyi Chen, Alex C. Kwan, and Jaime Grutzendler. 2017. “Targeted Two-Photon Chemical Apoptotic Ablation of Defined Cell Types in Vivo.” *Nature Communications* 8:15837.

Hirasawa, T., K. Ohsawa, Y. Imai, Y. Ondo, C. Akazawa, S. Uchino, and S. Kohsaka. 2005. “Visualization of Microglia in Living Tissues Using Iba1-EGFP Transgenic Mice.” *Journal of Neuroscience Research* 81(3):357–62.

Hollingworth, Paul, Denise Harold, Rebecca Sims, Amy Gerrish, Jean-Charles Lambert, Minerva M. Carrasquillo, Richard Abraham, Marian L. Hamshere, Jaspreet Singh Pahwa, Valentina Moskvina, Kimberley Dowzell, Nicola Jones, Alexandra Stretton, Charlene Thomas, Alex Richards, Dobril Ivanov, Caroline Widdowson, Jade Chapman, Simon Lovestone, John Powell, Petroula Proitsi, Michelle K. Lupton, Carol Brayne, David C. Rubinsztein, Michael Gill, Brian Lawlor, Aoibhinn Lynch, Kristelle S. Brown, Peter A. Passmore, David Craig, Bernadette McGuinness, Stephen Todd, Clive Holmes, David Mann, A. David Smith, Helen Beaumont, Donald Warden, Gordon Wilcock, Seth Love, Patrick G. Kehoe, Nigel M. Hooper, Emma R. L. C. Vardy, John Hardy, Simon Mead, Nick C. Fox, Martin Rossor, John Collinge, Wolfgang Maier, Frank Jessen, Eckart Rüther, Britta Schürmann, Reiner Heun, Heike Kölsch, Hendrik van den Bussche, Isabella Heuser, Johannes Kornhuber, Jens Wiltfang, Martin Dichgans, Lutz Frölich, Harald Hampel, John Gallacher, Michael Hüll, Dan Rujescu, Ina Giegling, Alison M. Goate, John S. K. Kauwe, Carlos Cruchaga, Petra Nowotny, John C. Morris, Kevin Mayo, Kristel Sleegers, Karolien Bettens, Sebastiaan Engelborghs, Peter P. De Deyn, Christine Van Broeckhoven, Gill Livingston, Nicholas J. Bass, Hugh Gurling, Andrew McQuillin, Rhian Gwilliam, Panagiotis Deloukas, Ammar Al-Chalabi, Christopher E. Shaw, Magda Tsolaki, Andrew B. Singleton, Rita Guerreiro, Thomas W. Mühleisen, Markus M. Nöthen, Susanne Moebus, Karl-Heinz Jöckel, Norman Klopp, H. Erich Wichmann, V. Shane Pankratz, Sigrid B. Sando, Jan O. Aasly, Maria Barcikowska, Zbigniew K. Wszolek, Dennis W. Dickson, Neill R. Graff-Radford, Ronald C. Petersen, Cornelia M. van Duijn, Monique M. B. Breteler, M. Arfan Ikram, Anita L. DeStefano, Annette L. Fitzpatrick, Oscar Lopez, Lenore J. Launer, Sudha Seshadri, Claudine Berr, Dominique Campion, Jacques Epelbaum, Jean-François Dartigues, Christophe Tzourio, Annick Alpérovitch, Mark Lathrop, Thomas M. Feulner, Patricia Friedrich, Caterina Riehle, Michael Krawczak, Stefan Schreiber, Manuel Mayhaus, S. Nicolhaus, Stefan Wagenpfeil, Stacy Steinberg, Hreinn Stefansson, Kari Stefansson, Jon Snaedal, Sigurbjörn Björnsson, Palmi V Jonsson, Vincent Chouraki, Benjamin Genier-Boley, Mikko Hiltunen, Hilkka Soininen, Onofre Combarros, Diana Zelenika, Marc Delepine, Maria J. Bullido, Florence Pasquier, Ignacio Mateo, Ana Frank-Garcia, Elisa Porcellini, Olivier Hanon, Eliecer Coto, Victoria Alvarez, Paolo Bosco, Gabriele Siciliano, Michelangelo Mancuso, Francesco Panza, Vincenzo Solfrizzi, Benedetta Nacmias, Sandro Sorbi, Paola Bossù, Paola Piccardi, Beatrice Arosio, Giorgio Annoni, Davide Seripa, Alberto Pilotto, Elio Scarpini, Daniela Galimberti, Alexis Brice, Didier Hannequin, Federico Licastro, Lesley Jones, Peter A. Holmans, Thorlakur Jonsson, Matthias Riemenschneider, Kevin Morgan, Steven G. Younkin, Michael J. Owen, Michael O’Donovan, Philippe Amouyel, and Julie Williams. 2011. “Common Variants at ABCA7, MS4A6A/MS4A4E, EPHA1, CD33 and CD2AP Are Associated with Alzheimer’s Disease.” *Nature Genetics* 43(5):429–35.

Honjo, T., Y. Nishizuka, I. Kato, and O. Hayaishi. 1971. “Adenosine Diphosphate Ribosylation of Aminoacyl Transferase II and Inhibition of Protein Synthesis by Diphtheria Toxin.” *The Journal of Biological Chemistry* 246(13):4251–60.

Horvath, Ryan J., Nancy Nutile-McMenemy, Matthew S. Alkaitis, and Joyce A. Deleo. 2008. “Differential Migration, LPS-Induced Cytokine, Chemokine, and NO Expression in Immortalized BV-2 and HAPI Cell Lines and Primary Microglial Cultures.” *Journal of Neurochemistry* 107(2):557–69.

Hou, Jinchao, Yun Chen, Gary Grajales-Reyes, and Marco Colonna. 2022. “TREM2 Dependent and Independent Functions of Microglia in Alzheimer’s Disease.” *Molecular Neurodegeneration* 17(1):84.

Huang, Yubin, Zhen Xu, Shanshan Xiong, Fangfang Sun, Guangrong Qin, Guanglei Hu, Jingjing Wang, Lei Zhao, Yu-Xiang Liang, Tianzhun Wu, Zhonghua Lu, Mark S. Humayun, Kwok-Fai So, Yihang Pan, Ningning Li, Ti-Fei Yuan, Yanxia Rao, and Bo Peng. 2018. “Repopulated Microglia Are Solely Derived from the Proliferation of Residual Microglia after Acute Depletion.” *Nature Neuroscience* 21(4):530–40.

Hughes, Craig D., Minee L. Choi, Mina Ryten, Lee Hopkins, Anna Drews, Juan A. Botía, Maria Iljina, Margarida Rodrigues, Sarah A. Gagliano, Sonia Gandhi, Clare Bryant, and David Klenerman. 2019. “Picomolar Concentrations of Oligomeric Alpha-Synuclein Sensitizes TLR4 to Play an Initiating Role in Parkinson’s

Disease Pathogenesis." *Acta Neuropathologica* 137(1):103–20.

Humpel, C. 2015. "Organotypic Brain Slice Cultures: A Review." *Neuroscience* 305:86–98.

Ising, Christina, Carmen Venegas, Shuangshuang Zhang, Hannah Scheiblich, Susanne V Schmidt, Ana Vieira-Saecker, Stephanie Schwartz, Shadi Albasset, Roisin M. McManus, Dario Tejera, Angelika Griep, Francesco Santarelli, Frederic Brosseron, Sabine Opitz, James Stunden, Maximilian Merten, Rakez Kayed, Douglas T. Golenbock, David Blum, Eicke Latz, Luc Buee, and Michael T. Heneka. 2019. "NLRP3 Inflammasome Activation Drives Tau Pathology." *Nature* 575(7784):669–73.

Jin, Mengmeng, Ranjie Xu, Le Wang, Mahabub Maraj Alam, Ziyuan Ma, Sining Zhu, Alessandra C. Martini, Azadeh Jadali, Matteo Bernabucci, Ping Xie, Kelvin Y. Kwan, Zhiping P. Pang, Elizabeth Head, Ying Liu, Ronald P. Hart, and Peng Jiang. 2022. "Type-I-Interferon Signaling Drives Microglial Dysfunction and Senescence in Human IPSC Models of Down Syndrome and Alzheimer's Disease." *Cell Stem Cell* 29(7):1135-1153.e8.

Jo, Junghyun, Yixin Xiao, Alfred Xuyang Sun, Engin Cukuroglu, Hoang-Dai Tran, Jonathan Göke, Zi Ying Tan, Tzuen Yih Saw, Cheng-Peow Tan, Hidayat Lokman, Younghwan Lee, Donghoon Kim, Han Seok Ko, Seong-Oh Kim, Jae Hyeon Park, Nam-Joon Cho, Thomas M. Hyde, Joel E. Kleinman, Joo Heon Shin, Daniel R. Weinberger, Eng King Tan, Hyunsoo Shawn Je, and Huck-Hui Ng. 2016. "Midbrain-like Organoids from Human Pluripotent Stem Cells Contain Functional Dopaminergic and Neuromelanin-Producing Neurons." *Cell Stem Cell* 19(2):248–57.

Joers, Valerie, Malú G. Tansey, Giovanna Mulas, and Anna R. Carta. 2017. "Microglial Phenotypes in Parkinson's Disease and Animal Models of the Disease." *Progress in Neurobiology* 155:57–75.

Jorfi, Mehdi, Anna Maaser-Hecker, and Rudolph E. Tanzi. 2023. "The Neuroimmune Axis of Alzheimer's Disease." *Genome Medicine* 15(1):6.

Joshi, P., E. Turola, A. Ruiz, A. Bergami, D. D. Libera, L. Benussi, P. Giussani, G. Magnani, G. Comi, G. Legname, R. Ghidoni, R. Furlan, M. Matteoli, and C. Verderio. 2014. "Microglia Convert Aggregated Amyloid-β into Neurotoxic Forms through the Shedding of Microvesicles." *Cell Death and Differentiation* 21(4):582–93.

Jucker, Mathias and Lary C. Walker. 2018. "Propagation and Spread of Pathogenic Protein Assemblies in Neurodegenerative Diseases." *Nature Neuroscience* 21(10):1341–49.

Jucker, Mathias and Lary C. Walker. 2023. "Alzheimer's Disease: From Immunotherapy to Immunoprevention." *Cell* 186(20):4260–70.

Jung, S., J. Aliberti, P. Graemmel, M. J. Sunshine, G. W. Kreutzberg, A. Sher, and D. R. Littman. 2000. "Analysis of Fractalkine Receptor CX(3)CR1 Function by Targeted Deletion and Green Fluorescent Protein Reporter Gene Insertion." *Molecular and Cellular Biology* 20(11):4106–14.

Jung, Steffen, Derya Unutmaz, Phillip Wong, Gen-Ichiro Sano, Kenia De los Santos, Tim Sparwasser, Shengji Wu, Sri Vuthoori, Kyung Ko, Fidel Zavala, Eric G. Pamer, Dan R. Littman, and Richard A. Lang. 2002. "In Vivo Depletion of CD11c+ Dendritic Cells Abrogates Priming of CD8+ T Cells by Exogenous Cell-Associated Antigens." *Immunity* 17(2):211–20.

Kaiser, Tobias and Guoping Feng. 2019. "Tmem119-EGFP and Tmem119-CreERT2 Transgenic Mice for Labeling and Manipulating Microglia." *Eneuro* 6(4):ENEURO.0448-18.2019.

Keller, Daniel, Csaba Erö, and Henry Markram. 2018. "Cell Densities in the Mouse Brain: A Systematic Review." *Frontiers in Neuroanatomy* 12(October).

Keren-Shaul, Hadas, Amit Spinrad, Assaf Weiner, Orit Matcovitch-Natan, Raz Dvir-Szternfeld, Tyler K. Ulland, Eyal David, Kuti Baruch, David Lara-Astaiso, Beata Toth, Shalev Itzkovitz, Marco Colonna, Michal Schwartz, and Ido Amit. 2017. "A Unique Microglia Type Associated with Restricting Development of Alzheimer's Disease." *Cell* 169(7):1276-1290.e17.

Kim, Jung-Seok, Masha Kolesnikov, Shany Peled-Hajaj, Isabelle Scheyltjens, Yuan Xia, Sebastien Trzebanski, Zhana Haimon, Anat Shemer, Alisa Lubart, Hannah Van Hove, Louise Chappell-Maor, Sigalit Boura-Halfon, Kiavash Movahedi, Pablo Blinder, and Steffen Jung. 2021. "A Binary Cre Transgenic Approach Dissects Microglia and CNS Border-Associated Macrophages." *Immunity* 54(1):176-190.e7.

Klichinsky, Michael, Marco Ruella, Olga Shestova, Xueqing Maggie Lu, Andrew Best, Martha Zeeman, Maggie Schmierer, Konrad Gabrusiewicz, Nicholas R. Anderson, Nicholas E. Petty, Katherine D. Cummins, Feng Shen, Xinhe Shan, Kimberly Veliz, Kristin Blouch, Yumi Yashiro-Ohtani, Saad S. Kenderian, Miriam Y. Kim,

Roddy S. O'Connor, Stephen R. Wallace, Miroslaw S. Kozlowski, Dylan M. Marchione, Maksim Shestov, Benjamin A. Garcia, Carl H. June, and Saar Gill. 2020. "Human Chimeric Antigen Receptor Macrophages for Cancer Immunotherapy." *Nature Biotechnology* 38(8):947–53.

Kopec, K. K. and R. T. Carroll. 1998. "Alzheimer's Beta-Amyloid Peptide 1-42 Induces a Phagocytic Response in Murine Microglia." *Journal of Neurochemistry* 71(5):2123–31.

Kordower, Jeffrey H., Yaping Chu, Robert A. Hauser, Thomas B. Freeman, and C. Warren Olanow. 2008. "Lewy Body–like Pathology in Long-Term Embryonic Nigral Transplants in Parkinson's Disease." *Nature Medicine* 14(5):504–6.

Kosik, K. S., C. L. Joachim, and D. J. Selkoe. 1986. "Microtubule-Associated Protein Tau (Tau) Is a Major Antigenic Component of Paired Helical Filaments in Alzheimer Disease." *Proceedings of the National Academy of Sciences of the United States of America* 83(11):4044–48.

Krabbe, Grietje, Annett Halle, Vitali Matyash, Jan L. Rinnenthal, Gina D. Eom, Ulrike Bernhardt, Kelly R. Miller, Stefan Prokop, Helmut Kettenmann, and Frank L. Heppner. 2013. "Functional Impairment of Microglia Coincides with Beta-Amyloid Deposition in Mice with Alzheimer-Like Pathology." *PLOS ONE* 8(4):e60921.

Krasemann, Susanne, Charlotte Madore, Ron Cialic, Caroline Baufeld, Narghes Calcagno, Rachid El Fatimy, Lien Beckers, Elaine O'Loughlin, Yang Xu, Zain Fanek, David J. Greco, Scott T. Smith, George Tweet, Zachary Humulock, Tobias Zrzavy, Patricia Conde-Sanroman, Mar Gacias, Zhiping Weng, Hao Chen, Emily Tjon, Fargol Mazaheri, Kristin Hartmann, Asaf Madi, Jason D. Ulrich, Markus Glatzel, Anna Worthmann, Joerg Heeren, Bogdan Budnik, Cynthia Lemere, Tsuneya Ikezu, Frank L. Heppner, Vladimir Litvak, David M. Holtzman, Hans Lassmann, Howard L. Weiner, Jordi Ochando, Christian Haass, and Oleg Butovsky. 2017. "The TREM2-APOE Pathway Drives the Transcriptional Phenotype of Dysfunctional Microglia in Neurodegenerative Diseases." *Immunity* 47(3):566-581.e9.

Krauser, Joel A., Yi Jin, Markus Walles, Ulrike Pfaar, James Sutton, Marion Wiesmann, Daniel Graf, Veronique Pflimlin-Fritschy, Thierry Wolf, Gian Camenisch, and Piet Swart. 2015. "Phenotypic and Metabolic Investigation of a CSF-1R Kinase Receptor Inhibitor (BLZ945) and Its Pharmacologically Active Metabolite." *Xenobiotica* 45(2):107–23.

Kuhlmann, Tanja, Samuel Ludwin, Alexandre Prat, Jack Antel, Wolfgang Brück, and Hans Lassmann. 2017. "An Updated Histological Classification System for Multiple Sclerosis Lesions." *Acta Neuropathologica* 133(1):13–24.

Lancaster, Madeline A. and Juergen A. Knoblich. 2014. "Generation of Cerebral Organoids from Human Pluripotent Stem Cells." *Nature Protocols* 9(10):2329–40.

Lancaster, Madeline A., Magdalena Renner, Carol-Anne Martin, Daniel Wenzel, Louise S. Bicknell, Matthew E. Hurles, Tessa Homfray, Josef M. Penninger, Andrew P. Jackson, and Juergen A. Knoblich. 2013. "Cerebral Organoids Model Human Brain Development and Microcephaly." *Nature* 501(7467):373–79.

Lang, Anthony E. and Andres M. Lozano. 1998. "Parkinson's Disease." *New England Journal of Medicine* 339(15):1044–53.

Lawson, L. J., V. H. Perry, P. Dri, and S. Gordon. 1990. "Heterogeneity in the Distribution and Morphology of Microglia in the Normal Adult Mouse Brain." *Neuroscience* 39(1):151–70.

Lee, Christopher Z. W., Tatsuya Kozaki, and Florent Ginhoux. 2018. "Studying Tissue Macrophages in Vitro: Are IPSC-Derived Cells the Answer?" *Nature Reviews Immunology* 18(11):716–25.

Lei, Fengyang, Naiwen Cui, Chengxin Zhou, James Chodosh, Demetrios G. Vavvas, and Eleftherios I. Paschalis. 2020. "CSF1R Inhibition by a Small-Molecule Inhibitor Is Not Microglia Specific; Affecting Hematopoiesis and the Function of Macrophages." *Proceedings of the National Academy of Sciences* 117(38):23336–38.

Li, Jia-Yi, Elisabet Englund, Janice L. Holton, Denis Soulet, Peter Hagell, Andrew J. Lees, Tammaryn Lashley, Niall P. Quinn, Stig Rehncrona, Anders Björklund, Håkan Widner, Tamas Revesz, Olle Lindvall, and Patrik Brundin. 2008. "Lewy Bodies in Grafted Neurons in Subjects with Parkinson's Disease Suggest Host-to-Graft Disease Propagation." *Nature Medicine* 14(5):501–3.

Li, Jia, Ken Chen, Liyin Zhu, and Jeffrey W. Pollard. 2006. "Conditional Deletion of the Colony Stimulating Factor-1 Receptor (c-Fms Proto-Oncogene) in Mice." *Genesis (New York, N.Y. : 2000)* 44(7):328–35.

Li, Jie-Qiong, Lan Tan, and Jin-Tai Yu. 2014. "The Role of the LRRK2 Gene in Parkinsonism." *Molecular*

Neurodegeneration 9(1):47.

Li, Na, Tessandra Stewart, Lifu Sheng, Min Shi, Eugene M. Cilento, Yufeng Wu, Jau-Syong Hong, and Jing Zhang. 2020. "Immunoregulation of Microglial Polarization: An Unrecognized Physiological Function of α-Synuclein." *Journal of Neuroinflammation* 17(1):272.

Liddelow, Shane A., Kevin A. Guttenplan, Laura E. Clarke, Frederick C. Bennett, Christopher J. Bohlen, Lucas Schirmer, Mariko L. Bennett, Alexandra E. Münch, Won Suk Chung, Todd C. Peterson, Daniel K. Wilton, Arnaud Frouin, Brooke A. Napier, Nikhil Panicker, Manoj Kumar, Marion S. Buckwalter, David H. Rowitch, Valina L. Dawson, Ted M. Dawson, Beth Stevens, and Ben A. Barres. 2017. "Neurotoxic Reactive Astrocytes Are Induced by Activated Microglia." *Nature* 541(7638):481–87.

Lin, Rui, Youtong Zhou, Ting Yan, Ruiyu Wang, Heng Li, Zhaofa Wu, Xinshuang Zhang, Xiangyu Zhou, Fei Zhao, Li Zhang, Yulong Li, and Minmin Luo. 2022. "Directed Evolution of Adeno-Associated Virus for Efficient Gene Delivery to Microglia." *Nature Methods* 19(8):976–85.

Liu, Guiyou, Yongquan Liu, Qinghua Jiang, Yongshuai Jiang, Rennan Feng, Liangcai Zhang, Zugen Chen, Keshen Li, and Jiafeng Liu. 2016. "Convergent Genetic and Expression Datasets Highlight TREM2 in Parkinson's Disease Susceptibility." *Molecular Neurobiology* 53(7):4931–38.

Liu, Heli, Cindy Leo, Xiaoyan Chen, Brian R. Wong, Lewis T. Williams, Haishan Lin, and Xiaolin He. 2012. "The Mechanism of Shared but Distinct CSF-1R Signaling by the Non-Homologous Cytokines IL-34 and CSF-1." *Biochimica et Biophysica Acta* 1824(7):938–45.

Liu, Jiexi, Fei Wang, Yang Qin, and Xiaolan Feng. 2021. "Advances in the Genetically Engineered KillerRed for Photodynamic Therapy Applications." *International Journal of Molecular Sciences* 22(18).

Liu, Yingjun, Assunta Senatore, Silvia Sorce, Mario Nuvolone, Jingjing Guo, Zeynep H. Gümüş, and Adriano Aguzzi. 2022. "Brain Aging Is Faithfully Modelled in Organotypic Brain Slices and Accelerated by Prions." *Communications Biology* 5(1):1–11.

Liu, Yiting, Katherine S. Given, Erin L. Dickson, Gregory P. Owens, Wendy B. Macklin, and Jeffrey L. Bennett. 2019. "Concentration-Dependent Effects of CSF1R Inhibitors on Oligodendrocyte Progenitor Cells Ex Vivo and in Vivo." *Experimental Neurology* 318:32–41.

Liu, Yong U., Yanlu Ying, Yujiao Li, Ukpong B. Eyo, Tingjun Chen, Jiaying Zheng, Anthony D. Umpierre, Jia Zhu, Dale B. Bosco, Hailong Dong, and Long Jun Wu. 2019. "Neuronal Network Activity Controls Microglial Process Surveillance in Awake Mice via Norepinephrine Signaling." *Nature Neuroscience* 22(11):1771–81.

van Lochem, E. G., V. H. J. van der Velden, H. K. Wind, J. G. te Marvelde, N. A. C. Westerdaal, and J. J. M. van Dongen. 2004. "Immunophenotypic Differentiation Patterns of Normal Hematopoiesis in Human Bone Marrow: Reference Patterns for Age-Related Changes and Disease-Induced Shifts." *Cytometry. Part B, Clinical Cytometry* 60(1):1–13.

Lund, Harald, Melanie Pieber, Roham Parsa, Jinming Han, David Grommisch, Ewoud Ewing, Lara Kular, Maria Needhamsen, Alexander Espinosa, Emma Nilsson, Anna K. Överby, Oleg Butovsky, Maja Jagodic, Xing-Mei Zhang, and Robert A. Harris. 2018. "Competitive Repopulation of an Empty Microglial Niche Yields Functionally Distinct Subsets of Microglia-like Cells." *Nature Communications* 9(1):4845.

Luo, Chongyuan, Madeline A. Lancaster, Rosa Castanon, Joseph R. Nery, Juergen A. Knoblich, and Joseph R. Ecker. 2016. "Cerebral Organoids Recapitulate Epigenomic Signatures of the Human Fetal Brain." *Cell Reports* 17(12):3369–84.

Lynch, Marina A. 2022. "Exploring Sex-Related Differences in Microglia May Be a Game-Changer in Precision Medicine." *Frontiers in Aging Neuroscience* 14:868448.

MacDonald, Kelli P. A., James S. Palmer, Stephen Cronau, Elke Seppanen, Stuart Olver, Neil C. Raffelt, Rachel Kuns, Allison R. Pettit, Andrew Clouston, Brandon Wainwright, Dan Branstetter, Jeffrey Smith, Raymond J. Paxton, Douglas Pat Cerretti, Lynn Bonham, Geoffrey R. Hill, and David A. Hume. 2010. "An Antibody against the Colony-Stimulating Factor 1 Receptor Depletes the Resident Subset of Monocytes and Tissue- and Tumor-Associated Macrophages but Does Not Inhibit Inflammation." *Blood* 116(19):3955–63.

Madisen, Linda, Theresa A. Zwingman, Susan M. Sunkin, Seung Wook Oh, Hatim A. Zariwala, Hong Gu, Lydia L. Ng, Richard D. Palmiter, Michael J. Hawrylycz, Allan R. Jones, Ed S. Lein, and Hongkui Zeng. 2010. "A Robust and High-Throughput Cre Reporting and Characterization System for the Whole Mouse Brain." *Nature Neuroscience* 13(1):133–40.

Madry, Christian, Vasiliki Kyrargyri, I. Lorena Arancibia-Cárcamo, Renaud Jolivet, Shinichi Kohsaka, Robert M. Bryan, and David Attwell. 2018. “Microglial Ramification, Surveillance, and Interleukin-1β Release Are Regulated by the Two-Pore Domain K^+ Channel THIK-1.” *Neuron* 97(2):299-312.e6.

Maezawa, Izumi, Pavel I. Zimin, Heike Wulff, and Lee-Way Jin. 2011. “Amyloid-Beta Protein Oligomer at Low Nanomolar Concentrations Activates Microglia and Induces Microglial Neurotoxicity.” *The Journal of Biological Chemistry* 286(5):3693–3706.

Maguire, Emily, Natalie Connor-Robson, Bethany Shaw, Rachel O’Donoghue, Nina Stöberl, and Hazel Hall-Roberts. 2022. “Assaying Microglia Functions In Vitro.” *Cells* 11(21).

Mancuso, Renzo, Johanna Van Den Daele, Nicola Fattorelli, Leen Wolfs, Sriram Balusu, Oliver Burton, Adrian Liston, Annerieke Sierksma, Yannick Fourne, Suresh Poovathingal, Amaia Arranz-mendiguren, Carlo Sala Frigerio, Christel Claes, Lutgarde Serneels, Tom Theys, V. Hugh Perry, Catherine Verfaillie, Mark Fiers, and Bart De Strooper. 2019. “Stem-Cell-Derived Human Microglia Transplanted in Mouse Brain to Study Human Disease.” *Nature Neuroscience* 22(December).

Mari, Carina, Murat Karabiyikoglu, Michael L. Goris, Jonathan F. Tait, Midori Anne Yenari, and Francis G. Blankenberg. 2004. “Detection of Focal Hypoxic-Ischemic Injury and Neuronal Stress in a Rodent Model of Unilateral MCA Occlusion/Reperfusion Using Radiolabeled Annexin V.” *European Journal of Nuclear Medicine and Molecular Imaging* 31(5):733–39.

Marschallinger, Julia, Tal Iram, Macy Zardeneta, Song E. Lee, Benoit Lehallier, Michael S. Haney, John V. Pluvinage, Vidhu Mathur, Oliver Hahn, David W. Morgens, Justin Kim, Julia Tevini, Thomas K. Felder, Heimo Wolinski, Carolyn R. Bertozzi, Michael C. Bassik, Ludwig Aigner, and Tony Wyss-Coray. 2020. “Lipid-Droplet-Accumulating Microglia Represent a Dysfunctional and Proinflammatory State in the Aging Brain.” *Nature Neuroscience* 23(2):194–208.

Marzan, Dave E., Valérie Brügger-Verdon, Brian L. West, Shane Liddelow, Jayshree Samanta, and James L. Salzer. 2021. “Activated Microglia Drive Demyelination via CSF1R Signaling.” *Glia* 69(6):1583–1604.

Mastorakos, Panagiotis, Nicole Mihelson, Marie Luby, Scott R. Burks, Kory Johnson, Amie W. Hsia, Jaclyn Witko, Joseph A. Frank, Lawrence Latour, and Dorian B. McGavern. 2021. “Temporally Distinct Myeloid Cell Responses Mediate Damage and Repair after Cerebrovascular Injury.” *Nature Neuroscience* 24(2):245–58.

Masuch, Annette, Rianne van der Pijl, Lisa Füner, Yochai Wolf, Bart Eggen, Erik Boddeke, and Knut Biber. 2016. “Microglia Replenished OHSC: A Culture System to Study in Vivo like Adult Microglia.” *Glia* 64(8):1285–97.

Masuda, Takahiro, Lukas Amann, Roman Sankowski, Ori Staszewski, Maximilian Lenz, Paolo d´Errico, Nicolas Snaidero, Marta Joana Costa Jordão, Chotima Böttcher, Katrin Kierdorf, Steffen Jung, Josef Priller, Thomas Misgeld, Andreas Vlachos, Melanie Meyer-Luehmann, Klaus-Peter Knobeloch, and Marco Prinz. 2020. “Author Correction: Novel Hexb-Based Tools for Studying Microglia in the CNS.” *Nature Immunology* 21(10):1302.

Masuda, Takahiro, Roman Sankowski, Ori Staszewski, Chotima Böttcher, Lukas Amann, Sagar, Christian Scheiwe, Stefan Nessler, Patrik Kunz, Geert van Loo, Volker Arnd Coenen, Peter Christoph Reinacher, Anna Michel, Ulrich Sure, Ralf Gold, Dominic Grün, Josef Priller, Christine Stadelmann, and Marco Prinz. 2019. “Spatial and Temporal Heterogeneity of Mouse and Human Microglia at Single-Cell Resolution.” *Nature* 566(7744):388–92.

McKinsey, Gabriel L., Carlos O. Lizama, Amber E. Keown-Lang, Abraham Niu, Nicolas Santander, Amara Larpthaveesarp, Elin Chee, Fernando F. Gonzalez, and Thomas D. Arnold. 2020. “A New Genetic Strategy for Targeting Microglia in Development and Disease” edited by I. M. Chiu, S. Rath, I. M. Chiu, B. Stevens, and A. Sierra. *ELife* 9:e54590.

McLellan, Micheal A., Nadia A. Rosenthal, and Alexander R. Pinto. 2017. “Cre-LoxP-Mediated Recombination: General Principles and Experimental Considerations.” *Current Protocols in Mouse Biology* 7(1):1–12.

McNamara, Niamh B., David A. D. Munro, Nadine Bestard-Cuche, Akiko Uyeda, Jeroen F. J. Bogie, Alana Hoffmann, Rebecca K. Holloway, Irene Molina-Gonzalez, Katharine E. Askew, Stephen Mitchell, William Mungall, Michael Dodds, Carsten Dittmayer, Jonathan Moss, Jamie Rose, Stefan Szymkowiak, Lukas Amann, Barry W. McColl, Marco Prinz, Tara L. Spires-Jones, Werner Stenzel, Karen Horsburgh, Jerome J. A. Hendriks, Clare Pridans, Rieko Muramatsu, Anna Williams, Josef Priller, and Veronique E. Miron. 2023. “Microglia Regulate Central Nervous System Myelin Growth and Integrity.” *Nature* 613(7942):120–29.

McQuade, Amanda, Morgan Coburn, Christina H. Tu, Jonathan Hasselmann, Hayk Davtyan, and Mathew Blurton-Jones. 2018. “Development and Validation of a Simplified Method to Generate Human Microglia from Pluripotent Stem Cells.” *Molecular Neurodegeneration* 13(1):67.

Da Mesquita, Sandro, Antoine Louveau, Andrea Vaccari, Igor Smirnov, R. Chase Cornelison, Kathryn M. Kingsmore, Christian Contarino, Suna Onengut-Gumuscu, Emily Farber, Daniel Raper, Kenneth E. Viar, Romie D. Powell, Wendy Baker, Nisha Dabhi, Robin Bai, Rui Cao, Song Hu, Stephen S. Rich, Jennifer M. Munson, M. Beatriz Lopes, Christopher C. Overall, Scott T. Acton, and Jonathan Kipnis. 2018. “Functional Aspects of Meningeal Lymphatics in Ageing and Alzheimer’s Disease.” *Nature* 560(7717):185–91.

Mhyre, Timothy R., James T. Boyd, Robert W. Hamill, and Kathleen A. Maguire-Zeiss. 2012. “Parkinson’s Disease.” *Sub-Cellular Biochemistry* 65:389–455.

Middlebrook, John L. and Rebecca B. Dorland. 1977. “Response of Cultured Mammalian Cells to the Exotoxins of Pseudomonas Aeruginosa and Corynebacterium Diphtheriae: Differential Cytotoxicity.” *Canadian Journal of Microbiology* 23(2):183–89.

Mildner, Alexander, Hauke Schmidt, Mirko Nitsche, Doron Merkler, Uwe-Karsten Hanisch, Matthias Mack, Mathias Heikenwalder, Wolfgang Brück, Josef Priller, and Marco Prinz. 2007. “Microglia in the Adult Brain Arise from Ly-6ChiCCR2+ Monocytes Only under Defined Host Conditions.” *Nature Neuroscience* 10(12):1544–53.

Mills, William A., AnnaLin M. Woo, Shan Jiang, Joelle Martin, Dayana Surendran, Matthew Bergstresser, Ian F. Kimbrough, Ukpong B. Eyo, Michael V Sofroniew, and Harald Sontheimer. 2022. “Astrocyte Plasticity in Mice Ensures Continued Endfoot Coverage of Cerebral Blood Vessels Following Injury and Declines with Age.” *Nature Communications* 13(1):1794.

Mittelbronn, M., K. Dietz, H. J. Schluesener, and R. Meyermann. 2001. “Local Distribution of Microglia in the Normal Adult Human Central Nervous System Differs by up to One Order of Magnitude.” *Acta Neuropathologica* 101(3):249–55.

Moseman, E. Ashley, Alexa C. Blanchard, Debasis Nayak, and Dorian B. McGavern. 2020. “T Cell Engagement of Cross-Presenting Microglia Protects the Brain from a Nasal Virus Infection.” *Science Immunology* 5(48):1–14.

Muffat, Julien, Yun Li, Attya Omer, Ann Durbin, Irene Bosch, Grisilda Bakiasi, Edward Richards, Aaron Meyer, Lee Gehrke, and Rudolf Jaenisch. 2018. “Human Induced Pluripotent Stem Cell-Derived Glial Cells and Neural Progenitors Display Divergent Responses to Zika and Dengue Infections.” *Proceedings of the National Academy of Sciences of the United States of America* 115(27):7117–22.

Muffat, Julien, Yun Li, Bingbing Yuan, Maisam Mitalipova, Attya Omer, Sean Corcoran, Grisilda Bakiasi, Li-Huei Tsai, Patrick Aubourg, Richard M. Ransohoff, and Rudolf Jaenisch. 2016. “Efficient Derivation of Microglia-like Cells from Human Pluripotent Stem Cells.” *Nature Medicine* 22(11):1358–67.

Nagai, A., E. Nakagawa, K. Hatori, H. B. Choi, J. G. McLarnon, M. A. Lee, and S. U. Kim. 2001. “Generation and Characterization of Immortalized Human Microglial Cell Lines: Expression of Cytokines and Chemokines.” *Neurobiology of Disease* 8(6):1057–68.

Nemes-Baran, Ashley D., Donovan R. White, and Tara M. DeSilva. 2020. “Fractalkine-Dependent Microglial Pruning of Viable Oligodendrocyte Progenitor Cells Regulates Myelination.” *Cell Reports* 32(7):108047.

Nimmerjahn, Axel, Frank Kirchhoff, and Fritjof Helmchen. 2005. “Resting Microglial Cells Are Highly Dynamic Surveillants of Brain Parenchyma in Vivo.” *Science (New York, N.Y.)* 308(5726):1314–18.

Nissen, Jillian C., Kaitlyn K. Thompson, Brian L. West, and Stella E. Tsirka. 2018. “Csf1R Inhibition Attenuates Experimental Autoimmune Encephalomyelitis and Promotes Recovery.” *Experimental Neurology* 307:24–36.

Norden, Diana M., Megan M. Muccigrosso, and Jonathan P. Godbout. 2015. “Microglial Priming and Enhanced Reactivity to Secondary Insult in Aging, and Traumatic CNS Injury, and Neurodegenerative Disease.” *Neuropharmacology* 96:29–41.

Novotny, Renata, Franziska Langer, Jasmin Mahler, Angelos Skodras, Andreas Vlachos, Bettina M. Wegenast-Braun, Stephan A. Kaeser, Jonas J. Neher, Yvonne S. Eisele, Marie J. Pietrowski, K. Peter R. Nilsson, Thomas Deller, Matthias Staufenbiel, Bernd Heimrich, and Mathias Jucker. 2016. “Conversion of Synthetic Abeta to In Vivo Active Seeds and Amyloid Plaque Formation in a Hippocampal Slice Culture Model.” *The Journal of*

Neuroscience : The Official Journal of the Society for Neuroscience 36(18):5084–93.

Ogaki, Ari, Yuji Ikegaya, and Ryuta Koyama. 2022. "Replacement of Mouse Microglia With Human Induced Pluripotent Stem Cell (HiPSC)-Derived Microglia in Mouse Organotypic Slice Cultures." *Frontiers in Cellular Neuroscience* 16:918442.

Olah, Marta, Vilas Menon, Naomi Habib, Mariko F. Taga, Yiyi Ma, Christina J. Yung, Maria Cimpean, Anthony Khairallah, Guillermo Coronas-Samano, Roman Sankowski, Dominic Grün, Alexandra A. Kroshilina, Danielle Dionne, Rani R. Sarkis, Garth R. Cosgrove, Jeffrey Helgager, Jeffrey A. Golden, Page B. Pennell, Marco Prinz, Jean Paul G. Vonsattel, Andrew F. Teich, Julie A. Schneider, David A. Bennett, Aviv Regev, Wassim Elyaman, Elizabeth M. Bradshaw, and Philip L. De Jager. 2020. "Single Cell RNA Sequencing of Human Microglia Uncovers a Subset That Is Associated with Alzheimer's Disease." *Nature Communications*.

Olah, Marta, Ellis Patrick, Alexandra Chloe Villani, Jishu Xu, Charles C. White, Katie J. Ryan, Paul Piehowski, Alifiya Kapasi, Parham Nejad, Maria Cimpean, Sarah Connor, Christina J. Yung, Michael Frangieh, Allison McHenry, Wassim Elyaman, Vlad Petyuk, Julie A. Schneider, David A. Bennett, Philip L. De Jager, and Elizabeth M. Bradshaw. 2018. "A Transcriptomic Atlas of Aged Human Microglia." *Nature Communications* 9(1):1–8.

Olesen, Mads N., Josefine R. Christiansen, Steen Vang Petersen, Poul Henning Jensen, Wojciech Paslawski, Marina Romero-Ramos, and Vanesa Sanchez-Guajardo. 2018. "CD4 T Cells React to Local Increase of α-Synuclein in a Pathology-Associated Variant-Dependent Manner and Modify Brain Microglia in Absence of Brain Pathology." *Heliyon* 4(1):e00513.

Olmedillas, Maria, Bianca Brawek, Kaizhen Li, Cris Richter, and Olga Garaschuk. 2023. "Plaque Vicinity as a Hotspot of Microglial Turnover in a Mouse Model of Alzheimer ' s Disease." (July):1–18.

Ormel, Paul R., Renata Vieira de Sá, Emma J. van Bodegraven, Henk Karst, Oliver Harschnitz, Marjolein A. M. Sneeboer, Lill Eva Johansen, Roland E. van Dijk, Nicky Scheefhals, Amber Berdenis van Berlekom, Eduardo Ribes Martínez, Sandra Kling, Harold D. MacGillavry, Leonard H. van den Berg, René S. Kahn, Elly M. Hol, Lot D. de Witte, and R. Jeroen Pasterkamp. 2018. "Microglia Innately Develop within Cerebral Organoids." *Nature Communications* 9(1):1–14.

Outeiro, Tiago Fleming, David J. Koss, Daniel Erskine, Lauren Walker, Marzena Kurzawa-Akanbi, David Burn, Paul Donaghy, Christopher Morris, John-Paul Taylor, Alan Thomas, Johannes Attems, and Ian McKeith. 2019. "Dementia with Lewy Bodies: An Update and Outlook." *Molecular Neurodegeneration* 14(1):5.

Paloneva, Juha, Tuula Manninen, Grant Christman, Karine Hovanes, Jami Mandelin, Rolf Adolfsson, Marino Bianchin, Thomas Bird, Roxana Miranda, Andrea Salmaggi, Lisbeth Tranebjærg, Yrjö Konttinen, and Leena Peltonen. 2002. "Mutations in Two Genes Encoding Different Subunits of a Receptor Signaling Complex Result in an Identical Disease Phenotype." *The American Journal of Human Genetics* 71(3):656–62.

Pandya, Hetal, Michael J. Shen, David M. Ichikawa, Andrea B. Sedlock, Yong Choi, Kory R. Johnson, Gloria Kim, Mason A. Brown, Abdel G. Elkahloun, Dragan Maric, Colin L. Sweeney, Selamawit Gossa, Harry L. Malech, Dorian B. McGavern, and John K. Park. 2017. "Differentiation of Human and Murine Induced Pluripotent Stem Cells to Microglia-like Cells." *Nature Neuroscience* 20(5):753–59.

Pantazis, Caroline B., Andrian Yang, Erika Lara, Justin A. McDonough, Cornelis Blauwendraat, Lirong Peng, Hideyuki Oguro, Jitendra Kanaujiya, Jizhong Zou, David Sebesta, Gretchen Pratt, Erin Cross, Jeffrey Blockwick, Philip Buxton, Lauren Kinner-Bibeau, Constance Medura, Christopher Tompkins, Stephen Hughes, Marianita Santiana, Faraz Faghri, Mike A. Nalls, Daniel Vitale, Shannon Ballard, Yue A. Qi, Daniel M. Ramos, Kailyn M. Anderson, Julia Stadler, Priyanka Narayan, Jason Papademetriou, Luke Reilly, Matthew P. Nelson, Sanya Aggarwal, Leah U. Rosen, Peter Kirwan, Venkat Pisupati, Steven L. Coon, Sonja W. Scholz, Theresa Priebe, Miriam Öttl, Jian Dong, Marieke Meijer, Lara J. M. Janssen, Vanessa S. Lourenco, Rik van der Kant, Dennis Crusius, Dominik Paquet, Ana Caroline Raulin, Guojun Bu, Aaron Held, Brian J. Wainger, Rebecca M. C. Gabriele, Jackie M. Casey, Selina Wray, Dad Abu-Bonsrah, Clare L. Parish, Melinda S. Beccari, Don W. Cleveland, Emmy Li, Indigo V. L. Rose, Martin Kampmann, Carles Calatayud Aristoy, Patrik Verstreken, Laurin Heinrich, Max Y. Chen, Birgitt Schüle, Dan Dou, Erika L. F. Holzbaur, Maria Clara Zanellati, Richa Basundra, Mohanish Deshmukh, Sarah Cohen, Richa Khanna, Malavika Raman, Zachary S. Nevin, Madeline Matia, Jonas Van Lent, Vincent Timmerman, Bruce R. Conklin, Katherine Johnson Chase, Ke Zhang, Salome Funes, Daryl A. Bosco, Lena Erlebach, Marc Welzer, Deborah Kronenberg-Versteeg, Guochang Lyu, Ernest Arenas, Elena Coccia, Lily Sarrafha, Tim Ahfeldt, John C. Marioni, William C. Skarnes, Mark R. Cookson, Michael E. Ward, and Florian T. Merkle. 2022. "A Reference Human Induced Pluripotent Stem Cell Line for Large-Scale Collaborative Studies." *Cell Stem Cell* 29(12):1685-1702.e22.

Paolicelli, Rosa C., Giulia Bolasco, Francesca Pagani, Laura Maggi, Maria Scianni, Patrizia Panzanelli, Maurizio Giustetto, Tiago Alves Ferreira, Eva Guiducci, Laura Dumas, Davide Ragozzino, and Cornelius T. Gross. 2011. "Synaptic Pruning by Microglia Is Necessary for Normal Brain Development." *Science* 333(6048):1456–58.

Paolicelli, Rosa C., Amanda Sierra, Beth Stevens, Marie Eve Tremblay, Adriano Aguzzi, Bahareh Ajami, Ido Amit, Etienne Audinat, Ingo Bechmann, Mariko Bennett, Frederick Bennett, Alain Bessis, Knut Biber, Staci Bilbo, Mathew Blurton-Jones, Erik Boddeke, Dora Brites, Bert Brône, Guy C. Brown, Oleg Butovsky, Monica J. Carson, Bernardo Castellano, Marco Colonna, Sally A. Cowley, Colm Cunningham, Dimitrios Davalos, Philip L. De Jager, Bart de Strooper, Adam Denes, Bart J. L. Eggen, Ukpong Eyo, Elena Galea, Sonia Garel, Florent Ginhoux, Christopher K. Glass, Ozgun Gokce, Diego Gomez-Nicola, Berta González, Siamon Gordon, Manuel B. Graeber, Andrew D. Greenhalgh, Pierre Gressens, Melanie Greter, David H. Gutmann, Christian Haass, Michael T. Heneka, Frank L. Heppner, Soyon Hong, David A. Hume, Steffen Jung, Helmut Kettenmann, Jonathan Kipnis, Ryuta Koyama, Greg Lemke, Marina Lynch, Ania Majewska, Marzia Malcangio, Tarja Malm, Renzo Mancuso, Takahiro Masuda, Michela Matteoli, Barry W. McColl, Veronique E. Miron, Anna Victoria Molofsky, Michelle Monje, Eva Mracsko, Agnes Nadjar, Jonas J. Neher, Urte Neniskyte, Harald Neumann, Mami Noda, Bo Peng, Francesca Peri, V. Hugh Perry, Phillip G. Popovich, Clare Pridans, Josef Priller, Marco Prinz, Davide Ragozzino, Richard M. Ransohoff, Michael W. Salter, Anne Schaefer, Dorothy P. Schafer, Michal Schwartz, Mikael Simons, Cody J. Smith, Wolfgang J. Streit, Tuan Leng Tay, Li Huei Tsai, Alexei Verkhratsky, Rommy von Bernhardi, Hiroaki Wake, Valérie Wittamer, Susanne A. Wolf, Long Jun Wu, and Tony Wyss-Coray. 2022. "Microglia States and Nomenclature: A Field at Its Crossroads." *Neuron* 110(21):3458–83.

Pappenheimer Jr., A. M., Annabel A. Harper, Michael Moynihan, and Jeremy P. Brockes. 1982. "Diphtheria Toxin and Related Proteins: Effect of Route of Injection on Toxicity and the Determination of Cytotoxicity for Various Cultured Cells." *The Journal of Infectious Diseases* 145(1):94–102.

Parhizkar, Samira, Thomas Arzberger, Matthias Brendel, Gernot Kleinberger, Maximilian Deussing, Carola Focke, Brigitte Nuscher, Monica Xiong, Alireza Ghasemigharagoz, Natalie Katzmarski, Susanne Krasemann, Stefan F. Lichtenthaler, Stephan A. Müller, Alessio Colombo, Laura Sebastian Monasor, Sabina Tahirovic, Jochen Herms, Michael Willem, Nadine Pettkus, Oleg Butovsky, Peter Bartenstein, Dieter Edbauer, Axel Rominger, Ali Ertürk, Stefan A. Grathwohl, Jonas J. Neher, David M. Holtzman, Melanie Meyer-Luehmann, and Christian Haass. 2019. "Loss of TREM2 Function Increases Amyloid Seeding but Reduces Plaque-Associated ApoE." *Nature Neuroscience* 22(2):191–204.

Park, Dong Shin, Tatsuya Kozaki, Satish Kumar Tiwari, Marco Moreira, Ahad Khalilnezhad, Federico Torta, Nicolas Olivié, Chung Hwee Thiam, Oniko Liani, Aymeric Silvin, Wint Wint Phoo, Liang Gao, Alexander Triebl, Wai Kin Tham, Leticia Gonçalves, Wan Ting Kong, Sethi Raman, Xiao Meng Zhang, Garett Dunsmore, Charles Antoine Dutertre, Salanne Lee, Jia Min Ong, Akhila Balachander, Shabnam Khalilnezhad, Josephine Lum, Kaibo Duan, Ze Ming Lim, Leonard Tan, Ivy Low, Kagistia Hana Utami, Xin Yi Yeo, Sylvaine Di Tommaso, Jean-William Dupuy, Balazs Varga, Ragnhildur Thora Karadottir, Mufeeda Changaramvally Madathummal, Isabelle Bonne, Benoit Malleret, Zainab Yasin Binte, Ngan Wei Da, Yingrou Tan, Wei Jie Wong, Jinqiu Zhang, Jinmiao Chen, Radoslaw M. Sobota, Shanshan W. Howland, Lai Guan Ng, Frédéric Saltel, David Castel, Jacques Grill, Veronique Minard, Salvatore Albani, Jerry K. Y. Chan, Morgane Sonia Thion, Sang Yong Jung, Markus R. Wenk, Mahmoud A. Pouladi, Claudia Pasqualini, Veronique Angeli, Olivier N. F. Cexus, and Florent Ginhoux. 2023. "IPS-Cell-Derived Microglia Promote Brain Organoid Maturation via Cholesterol Transfer." *Nature* 623(7986):397–405.

Parkhurst, Christopher N., Guang Yang, Ipe Ninan, Jeffrey N. Savas, John R. 3rd Yates, Juan J. Lafaille, Barbara L. Hempstead, Dan R. Littman, and Wen-Biao Gan. 2013. "Microglia Promote Learning-Dependent Synapse Formation through Brain-Derived Neurotrophic Factor." *Cell* 155(7):1596–1609.

Paşca, Anca M., Steven A. Sloan, Laura E. Clarke, Yuan Tian, Christopher D. Makinson, Nina Huber, Chul Hoon Kim, Jin-Young Park, Nancy A. O'Rourke, Khoa D. Nguyen, Stephen J. Smith, John R. Huguenard, Daniel H. Geschwind, Ben A. Barres, and Sergiu P. Paşca. 2015. "Functional Cortical Neurons and Astrocytes from Human Pluripotent Stem Cells in 3D Culture." *Nature Methods* 12(7):671–78.

Patani, R., M. Balaratnam, A. Vora, and R. Reynolds. 2007. "Remyelination Can Be Extensive in Multiple Sclerosis despite a Long Disease Course." *Neuropathology and Applied Neurobiology* 33(3):277–87.

Pérez, María José, Dina Ivanyuk, Vasiliki Panagiotakopoulou, Gabriele Di Napoli, Stefanie Kalb, Dario Brunetti, Rawaa Al-Shaana, Stephan A. Kaeser, Sabine Anne-Kristin Fraschka, Mathias Jucker, Massimo Zeviani, Carlo Viscomi, and Michela Deleidi. 2021. "Loss of Function of the Mitochondrial Peptidase PITRM1 Induces

Proteotoxic Stress and Alzheimer's Disease-like Pathology in Human Cerebral Organoids." *Molecular Psychiatry* 26(10):5733–50.

Perry, V. Hugh, James A. R. Nicoll, and Clive Holmes. 2010. "Microglia in Neurodegenerative Disease." *Nature Reviews Neurology* 6(4):193–201.

Petrelli, Francesco, Luca Pucci, and Paola Bezzi. 2016. "Astrocytes and Microglia and Their Potential Link with Autism Spectrum Disorders." *Frontiers in Cellular Neuroscience* 10:21.

Pletnev, Sergei, Nadya G. Gurskaya, Nadya V Pletneva, Konstantin A. Lukyanov, Dmitri M. Chudakov, Vladimir I. Martynov, Vladimir O. Popov, Mikhail V Kovalchuk, Alexander Wlodawer, Zbigniew Dauter, and Vladimir Pletnev. 2009. "Structural Basis for Phototoxicity of the Genetically Encoded Photosensitizer KillerRed." *The Journal of Biological Chemistry* 284(46):32028–39.

Polymeropoulos, M. H., C. Lavedan, E. Leroy, S. E. Ide, A. Dehejia, A. Dutra, B. Pike, H. Root, J. Rubenstein, R. Boyer, E. S. Stenroos, S. Chandrasekharappa, A. Athanassiadou, T. Papapetropoulos, W. G. Johnson, A. M. Lazzarini, R. C. Duvoisin, G. Di Iorio, L. I. Golbe, and R. L. Nussbaum. 1997. "Mutation in the Alpha-Synuclein Gene Identified in Families with Parkinson's Disease." *Science (New York, N.Y.)* 276(5321):2045–47.

Popova, Galina, Sarah S. Soliman, Chang N. Kim, Matthew G. Keefe, Kelsey M. Hennick, Samhita Jain, Tao Li, Dario Tejera, David Shin, Bryant B. Chhun, Christopher S. McGinnis, Matthew Speir, Zev J. Gartner, Shalin B. Mehta, Maximilian Haeussler, Keith B. Hengen, Richard R. Ransohoff, Xianhua Piao, and Tomasz J. Nowakowski. 2021. "Human Microglia States Are Conserved across Experimental Models and Regulate Neural Stem Cell Responses in Chimeric Organoids." *Cell Stem Cell* 28(12):2153-2166.e6.

Prinz, Marco, Steffen Jung, and Josef Priller. 2019. "Microglia Biology: One Century of Evolving Concepts." *Cell* 179(2):292–311.

Prusiner, Stanley B. 1982. "Novel Proteinaceous Infectious Particles Cause Scrapie." *Science* 216(4542):136–44.

Prusiner, Stanley B. 2012. "Cell Biology. A Unifying Role for Prions in Neurodegenerative Diseases." *Science (New York, N.Y.)* 336(6088):1511–13.

Prusiner, Stanley B. 2013. "Biology and Genetics of Prions Causing Neurodegeneration." *Annual Review of Genetics* 47:601–23.

van der Putten, H., K. H. Wiederhold, A. Probst, S. Barbieri, C. Mistl, S. Danner, S. Kauffmann, K. Hofele, W. P. Spooren, M. A. Ruegg, S. Lin, P. Caroni, B. Sommer, M. Tolnay, and G. Bilbe. 2000. "Neuropathology in Mice Expressing Human Alpha-Synuclein." *The Journal of Neuroscience : The Official Journal of the Society for Neuroscience* 20(16):6021–29.

Qian, Xuyu, Hongjun Song, and Guo-Li Ming. 2019. "Brain Organoids: Advances, Applications and Challenges." *Development (Cambridge, England)* 146(8).

Qin, Liya, Jun He, Richard N. Hanes, Olivera Pluzarev, Jau Shyong Hong, and Fulton T. Crews. 2008. "Increased Systemic and Brain Cytokine Production and Neuroinflammation by Endotoxin Following Ethanol Treatment." *Journal of Neuroinflammation* 5:1–17.

Quadrato, Giorgia, Tuan Nguyen, Evan Z. Macosko, John L. Sherwood, Sung Min Yang, Daniel R. Berger, Natalie Maria, Jorg Scholvin, Melissa Goldman, Justin P. Kinney, Edward S. Boyden, Jeff W. Lichtman, Ziv M. Williams, Steven A. McCarroll, and Paola Arlotta. 2017. "Cell Diversity and Network Dynamics in Photosensitive Human Brain Organoids." *Nature* 545(7652):48–53.

Rademakers, Rosa, Matt Baker, Alexandra M. Nicholson, Nicola J. Rutherford, Nicole Finch, Alexandra Soto-Ortolaza, Jennifer Lash, Christian Wider, Aleksandra Wojtas, Mariely Dejesus-Hernandez, Jennifer Adamson, Naomi Kouri, Christina Sundal, Elizabeth A. Shuster, Jan Aasly, James MacKenzie, Sigrun Roeber, Hans A. Kretzschmar, Bradley F. Boeve, David S. Knopman, Ronald C. Petersen, Nigel J. Cairns, Bernardino Ghetti, Salvatore Spina, James Garbern, Alexandros C. Tselis, Ryan Uitti, Pritam Das, Jay A. Van Gerpen, James F. Meschia, Shawn Levy, Daniel F. Broderick, Neill Graff-Radford, Owen A. Ross, Bradley B. Miller, Russell H. Swerdlow, Dennis W. Dickson, and Zbigniew K. Wszolek. 2012. "Mutations in the Colony Stimulating Factor 1 Receptor (CSF1R) Gene Cause Hereditary Diffuse Leukoencephalopathy with Spheroids." *Nature Genetics* 44(2):200–205.

Ransohoff, Richard M. 2016. "A Polarizing Question: Do M1 and M2 Microglia Exist?" *Nature Neuroscience* 19:987.

Rathinam, Chozhavendan, William T. Poueymirou, Jose Rojas, Andrew J. Murphy, David M. Valenzuela, George D. Yancopoulos, Anthony Rongvaux, Elizabeth E. Eynon, Markus G. Manz, and Richard A. Flavell. 2011. "Efficient Differentiation and Function of Human Macrophages in Humanized CSF-1 Mice." *Blood* 118(11):3119–28.

Réu, Pedro, Azadeh Khosravi, Samuel Bernard, Jeff E. Mold, Mehran Salehpour, Kanar Alkass, Shira Perl, John Tisdale, Göran Possnert, Henrik Druid, and Jonas Frisén. 2017. "The Lifespan and Turnover of Microglia in the Human Brain." *Cell Reports* 20(4):779–84.

Riazi, Kiarash, Michael A. Galic, J. Brent Kuzmiski, Winnie Ho, Keith A. Sharkey, and Quentin J. Pittman. 2008. "Microglial Activation and TNFα Production Mediate Altered CNS Excitability Following Peripheral Inflammation." *Proceedings of the National Academy of Sciences of the United States of America* 105(44):17151–56.

Righi, M., L. Mori, G. De Libero, M. Sironi, A. Biondi, A. Mantovani, S. D. Donini, and P. Ricciardi-Castagnoli. 1989. "Monokine Production by Microglial Cell Clones." *European Journal of Immunology* 19(8):1443–48.

Rogers, Justin T., Josh M. Morganti, Adam D. Bachstetter, Charles E. Hudson, Melinda M. Peters, Bethany A. Grimmig, Edwin J. Weeber, Paula C. Bickford, and Carmelina Gemma. 2011. "CX3CR1 Deficiency Leads to Impairment of Hippocampal Cognitive Function and Synaptic Plasticity." *The Journal of Neuroscience : The Official Journal of the Society for Neuroscience* 31(45):16241–50.

de Rojas, Itziar, Sonia Moreno-Grau, Niccolo Tesi, Benjamin Grenier-Boley, Victor Andrade, Iris E. Jansen, Nancy L. Pedersen, Najada Stringa, Anna Zettergren, Isabel Hernández, Laura Montrreal, Carmen Antúnez, Anna Antonell, Rick M. Tankard, Joshua C. Bis, Rebecca Sims, Céline Bellenguez, Inés Quintela, Antonio González-Perez, Miguel Calero, Emilio Franco-Macías, Juan Macías, Rafael Blesa, Laura Cervera-Carles, Manuel Menéndez-González, Ana Frank-García, Jose Luís Royo, Fermin Moreno, Raquel Huerto Vilas, Miquel Baquero, Mónica Diez-Fairen, Carmen Lage, Sebastián García-Madrona, Pablo García-González, Emilio Alarcón-Martín, Sergi Valero, Oscar Sotolongo-Grau, Abbe Ullgren, Adam C. Naj, Afina W. Lemstra, Alba Benaque, Alba Pérez-Cordón, Alberto Benussi, Alberto Rábano, Alessandro Padovani, Alessio Squassina, Alexandre de Mendonça, Alfonso Arias Pastor, Almar A. L. Kok, Alun Meggy, Ana Belén Pastor, Ana Espinosa, Anaïs Corma-Gómez, Angel Martín Montes, Ángela Sanabria, Anita L. DeStefano, Anja Schneider, Annakaisa Haapasalo, Anne Kinhult Ståhlbom, Anne Tybjærg-Hansen, Annette M. Hartmann, Annika Spottke, Arturo Corbatón-Anchuelo, Arvid Rongve, Barbara Borroni, Beatrice Arosio, Benedetta Nacmias, Børge G. Nordestgaard, Brian W. Kunkle, Camille Charbonnier, Carla Abdelnour, Carlo Masullo, Carmen Martínez Rodríguez, Carmen Muñoz-Fernandez, Carole Dufouil, Caroline Graff, Catarina B. Ferreira, Caterina Chillotti, Chandra A. Reynolds, Chiara Fenoglio, Christine Van Broeckhoven, Christopher Clark, Claudia Pisanu, Claudia L. Satizabal, Clive Holmes, Dolores Buiza-Rueda, Dag Aarsland, Dan Rujescu, Daniel Alcolea, Daniela Galimberti, David Wallon, Davide Seripa, Edna Grünblatt, Efthimios Dardiotis, Emrah Düzel, Elio Scarpini, Elisa Conti, Elisa Rubino, Ellen Gelpi, Eloy Rodriguez-Rodriguez, Emmanuelle Duron, Eric Boerwinkle, Evelyn Ferri, Fabrizio Tagliavini, Fahri Küçükali, Florence Pasquier, Florentino Sanchez-Garcia, Francesca Mangialasche, Frank Jessen, Gaël Nicolas, Geir Selbæk, Gemma Ortega, Geneviève Chêne, Georgios Hadjigeorgiou, Giacomina Rossi, Gianfranco Spalletta, Giorgio Giaccone, Giulia Grande, Giuliano Binetti, Goran Papenberg, Harald Hampel, Henri Bailly, Henrik Zetterberg, Hilkka Soininen, Ida K. Karlsson, Ignacio Alvarez, Ildebrando Appollonio, Ina Giegling, Ingmar Skoog, Ingvild Saltvedt, Innocenzo Rainero, Irene Rosas Allende, Jakub Hort, Janine Diehl-Schmid, Jasper Van Dongen, Jean-Sebastien Vidal, Jenni Lehtisalo, Jens Wiltfang, Jesper Qvist Thomassen, Johannes Kornhuber, Jonathan L. Haines, Jonathan Vogelgsang, Juan A. Pineda, Juan Fortea, Julius Popp, Jürgen Deckert, Katharina Buerger, Kevin Morgan, Klaus Fließbach, Kristel Sleegers, Laura Molina-Porcel, Lena Kilander, Leonie Weinhold, Lindsay A. Farrer, Li-San Wang, Luca Kleineidam, Lucia Farotti, Lucilla Parnetti, Lucio Tremolizzo, Lucrezia Hausner, Luisa Benussi, Lutz Froelich, M. Arfan Ikram, M. Candida Deniz-Naranjo, Magda Tsolaki, Maitée Rosende-Roca, Malin Löwenmark, Marc Hulsman, Marco Spallazzi, Margaret A. Pericak-Vance, Margaret Esiri, María Bernal Sánchez-Arjona, Maria Carolina Dalmasso, María Teresa Martínez-Larrad, Marina Arcaro, Markus M. Nöthen, Marta Fernández-Fuertes, Martin Dichgans, Martin Ingelsson, Martin J. Herrmann, Martin Scherer, Martin Vyhnalek, Mary H. Kosmidis, Mary Yannakoulia, Matthias Schmid, Michael Ewers, Michael T. Heneka, Michael Wagner, Michela Scamosci, Miia Kivipelto, Mikko Hiltunen, Miren Zulaica, Montserrat Alegret, Myriam Fornage, Natalia Roberto, Natasja M. van Schoor, Nazib M. Seidu, Nerisa Banaj, Nicola J. Armstrong, Nikolaos Scarmeas, Norbert Scherbaum, Oliver Goldhardt, Oliver Hanon, Oliver Peters, Olivia Anna Skrobot, Olivier Quenez, Ondrej Lerch, Paola Bossù, Paolo Caffarra, Paolo Dionigi Rossi, Paraskevi Sakka, Patrizia Mecocci, Per Hoffmann, Peter A. Holmans, Peter Fischer, Peter Riederer, Qiong Yang, Rachel Marshall, Rajesh N. Kalaria, Richard Mayeux, Rik Vandenberghe, Roberta Cecchetti, Roberta Ghidoni, Ruth

Frikke-Schmidt, Sandro Sorbi, Sara Hägg, Sebastiaan Engelborghs, Seppo Helisalmi, Sigrid Botne Sando, Silke Kern, Silvana Archetti, Silvia Boschi, Silvia Fostinelli, Silvia Gil, Silvia Mendoza, Simon Mead, Simona Ciccone, Srdjan Djurovic, Stefanie Heilmann-Heimbach, Steffi Riedel-Heller, Teemu Kuulasmaa, Teodoro Del Ser, Thibaud Lebouvier, Thomas Polak, Tiia Ngandu, Timo Grimmer, Valentina Bessi, Valentina Escott-Price, Vilmantas Giedraitis, Vincent Deramecourt, Wolfgang Maier, Xueqiu Jian, Yolande A. L. Pijnenburg, Patrick Gavin Kehoe, Guillermo Garcia-Ribas, Pascual Sánchez-Juan, Pau Pastor, Jordi Pérez-Tur, Gerard Piñol-Ripoll, Adolfo Lopez de Munain, Jose María García-Alberca, María J. Bullido, Victoria Álvarez, Alberto Lleó, Luis M. Real, Pablo Mir, Miguel Medina, Philip Scheltens, Henne Holstege, Marta Marquié, María Eugenia Sáez, Ángel Carracedo, Philippe Amouyel, Gerard D. Schellenberg, Julie Williams, Sudha Seshadri, Cornelia M. van Duijn, Karen A. Mather, Raquel Sánchez-Valle, Manuel Serrano-Ríos, Adelina Orellana, Lluís Tárraga, Kaj Blennow, Martijn Huisman, Ole A. Andreassen, Danielle Posthuma, Jordi Clarimón, Mercè Boada, Wiesje M. van der Flier, Alfredo Ramirez, Jean-Charles Lambert, Sven J. van der Lee, and Agustín Ruiz. 2021. “Common Variants in Alzheimer’s Disease and Risk Stratification by Polygenic Risk Scores.” *Nature Communications* 12(1):3417.

Rojo, Rocío, Anna Raper, Derya D. Ozdemir, Lucas Lefevre, Kathleen Grabert, Evi Wollscheid-Lengeling, Barry Bradford, Melanie Caruso, Iveta Gazova, Alejandra Sánchez, Zofia M. Lisowski, Joana Alves, Irene Molina-Gonzalez, Hayk Davtyan, Rebecca J. Lodge, James D. Glover, Robert Wallace, David A. D. Munro, Eyal David, Ido Amit, Véronique E. Miron, Josef Priller, Stephen J. Jenkins, Giles E. Hardingham, Mathew Blurton-Jones, Neil A. Mabbott, Kim M. Summers, Peter Hohenstein, David A. Hume, and Clare Pridans. 2019. “Deletion of a Csf1r Enhancer Selectively Impacts CSF1R Expression and Development of Tissue Macrophage Populations.” *Nature Communications* 10(1):3215.

Ronaldson, Patrick T. and Thomas P. Davis. 2020. “Regulation of Blood–Brain Barrier Integrity by Microglia in Health and Disease: A Therapeutic Opportunity.” *Journal of Cerebral Blood Flow and Metabolism* 40(1_suppl):S6–24.

Rooijen, Nico Van and Annemarie Sanders. 1994. “Liposome Mediated Depletion of Macrophages: Mechanism of Action, Preparation of Liposomes and Applications.” *Journal of Immunological Methods* 174(1):83–93.

Rosario, Awilda M., Pedro E. Cruz, Carolina Ceballos-Diaz, Michael R. Strickland, Zoe Siemienski, Meghan Pardo, Keri-Lyn Schob, Andrew Li, George V Aslanidi, Arun Srivastava, Todd E. Golde, and Paramita Chakrabarty. 2016. “Microglia-Specific Targeting by Novel Capsid-Modified AAV6 Vectors.” *Molecular Therapy. Methods & Clinical Development* 3:16026.

Rosin, Jessica M., Siddharth R. Vora, and Deborah M. Kurrasch. 2018. “Depletion of Embryonic Microglia Using the CSF1R Inhibitor PLX5622 Has Adverse Sex-Specific Effects on Mice, Including Accelerated Weight Gain, Hyperactivity and Anxiolytic-like Behaviour.” *Brain, Behavior, and Immunity* 73:682–97.

Rubino, Stephen J., Lior Mayo, Isabella Wimmer, Victoria Siedler, Florian Brunner, Simon Hametner, Asaf Madi, Amanda Lanser, Thais Moreira, Dustin Donnelly, Laura Cox, Rafael Machado Rezende, Oleg Butovsky, Hans Lassmann, and Howard L. Weiner. 2018. “Acute Microglia Ablation Induces Neurodegeneration in the Somatosensory System.” *Nature Communications* 9(1):4578.

Ruedl, Christiane and Steffen Jung. 2018. “DTR-Mediated Conditional Cell Ablation—Progress and Challenges.” *European Journal of Immunology* 48(7):1114–19.

Ruiz-González, Rubén, Aitziber L. Cortajarena, Sara H. Mejias, Montserrat Agut, Santi Nonell, and Cristina Flors. 2013. “Singlet Oxygen Generation by the Genetically Encoded Tag MiniSOG.” *Journal of the American Chemical Society* 135(26):9564–67.

Sabate-Soler, Sonia, Sarah Louise Nickels, Cláudia Saraiva, Emanuel Berger, Ugne Dubonyte, Kyriaki Barmpa, Yan Jun Lan, Tsukasa Kouno, Javier Jarazo, Graham Robertson, Jafar Sharif, Haruhiko Koseki, Christian Thome, Jay W. Shin, Sally A. Cowley, and Jens C. Schwamborn. 2022. “Microglia Integration into Human Midbrain Organoids Leads to Increased Neuronal Maturation and Functionality.” *Glia* 70(7):1267–88.

Saito, Michiko, Takao Iwawaki, Choji Taya, Hiromichi Yonekawa, Munehiro Noda, Yoshiaki Inui, Eisuke Mekada, Yukio Kimata, Akio Tsuru, and Kenji Kohno. 2001. “Diphtheria Toxin Receptor–Mediated Conditional and Targeted Cell Ablation in Transgenic Mice.” *Nature Biotechnology* 19(8):746–50.

Sakaguchi, Hideya, Taisuke Kadoshima, Mika Soen, Nobuhiro Narii, Yoshihito Ishida, Masatoshi Ohgushi, Jun Takahashi, Mototsugu Eiraku, and Yoshiki Sasai. 2015. “Generation of Functional Hippocampal Neurons from Self-Organizing Human Embryonic Stem Cell-Derived Dorsomedial Telencephalic Tissue.” *Nature Communications* 6.

Sala Frigerio, Carlo, Leen Wolfs, Nicola Fattorelli, Nicola Thrupp, Iryna Voytyuk, Inga Schmidt, Renzo Mancuso, Wei Ting Chen, Maya E. Woodbury, Gyan Srivastava, Thomas Möller, Eloise Hudry, Sudeshna Das, Takaomi Saido, Eric Karran, Bradley Hyman, V. Hugh Perry, Mark Fiers, and Bart De Strooper. 2019. "The Major Risk Factors for Alzheimer's Disease: Age, Sex, and Genes Modulate the Microglia Response to Aβ Plaques." *Cell Reports* 27(4):1293-1306.e6.

Salamanca, Luis, Naguib Mechawar, Keith K. Murai, Rudi Balling, David S. Bouvier, and Alexander Skupin. 2019. "MIC-MAC: An Automated Pipeline for High-Throughput Characterization and Classification of Three-Dimensional Microglia Morphologies in Mouse and Human Postmortem Brain Samples." *Glia* 67(8):1496–1509.

Dos Santos, Sandra E., Marcelle Medeiros, Jairo Porfirio, William Tavares, Leila Pessôa, Lea Grinberg, Renata E. P. Leite, Renata E. L. Ferretti-Rebustini, Claudia K. Suemoto, Wilson Jacob Filho, Stephen C. Noctor, Chet C. Sherwood, Jon H. Kaas, Paul R. Manger, and Suzana Herculano-Houzel. 2020. "Similar Microglial Cell Densities across Brain Structures and Mammalian Species: Implications for Brain Tissue Function." *The Journal of Neuroscience : The Official Journal of the Society for Neuroscience* 40(24):4622–43.

Santuy, Andrea, Laura Tomás-Roca, José-Rodrigo Rodríguez, Juncal González-Soriano, Fei Zhu, Zhen Qiu, Seth G. N. Grant, Javier DeFelipe, and Angel Merchan-Perez. 2020. "Estimation of the Number of Synapses in the Hippocampus and Brain-Wide by Volume Electron Microscopy and Genetic Labeling." *Scientific Reports* 10(1):14014.

Sarkisyan, Karen S., Olga A. Zlobovskaya, Dmitry A. Gorbachev, Nina G. Bozhanova, George V Sharonov, Dmitriy B. Staroverov, Evgeny S. Egorov, Anastasia V Ryabova, Kyril M. Solntsev, Alexander S. Mishin, and Konstantin A. Lukyanov. 2015. "KillerOrange, a Genetically Encoded Photosensitizer Activated by Blue and Green Light." *PLOS ONE* 10(12):e0145287.

Sauer, B. 1998. "Inducible Gene Targeting in Mice Using the Cre/Lox System." *Methods (San Diego, Calif.)* 14(4):381–92.

Sauer, Brian and Nancy Henderson. 1989. "Cre-Stimulated Recombination at LoxP-Containing DNA Sequences Placed into the Mammalian Genome." *Nucleic Acids Research* 17(1):147–61.

Schafer, Dorothy P., Emily K. Lehrman, Amanda G. Kautzman, Ryuta Koyama, Alan R. Mardinly, Ryo Yamasaki, Richard M. Ransohoff, Michael E. Greenberg, Ben A. Barres, and Beth Stevens. 2012. "Microglia Sculpt Postnatal Neural Circuits in an Activity and Complement-Dependent Manner." *Neuron* 74(4):691–705.

Schafer, Simon T., Abed AlFatah Mansour, Johannes C. M. Schlachetzki, Monique Pena, Saeed Ghassemzadeh, Lisa Mitchell, Amanda Mar, Daphne Quang, Sarah Stumpf, Irene Santisteban Ortiz, Addison J. Lana, Clara Baek, Raghad Zaghal, Christopher K. Glass, Axel Nimmerjahn, and Fred H. Gage. 2023. "An in Vivo Neuroimmune Organoid Model to Study Human Microglia Phenotypes." *Cell* 186(10):2111-2126.e20.

Scheiblich, Hannah, Cira Dansokho, Dilek Mercan, Susanne V Schmidt, Luc Bousset, Lena Wischhof, Frederik Eikens, Alexandru Odainic, Jasper Spitzer, Angelika Griep, Stephanie Schwartz, Daniele Bano, Eicke Latz, Ronald Melki, and Michael T. Heneka. 2021. "Microglia Jointly Degrade Fibrillar Alpha-Synuclein Cargo by Distribution through Tunneling Nanotubes." *Cell* 184(20):5089-5106.e21.

Schindelin, Johannes, Ignacio Arganda-Carreras, Erwin Frise, Verena Kaynig, Mark Longair, Tobias Pietzsch, Stephan Preibisch, Curtis Rueden, Stephan Saalfeld, Benjamin Schmid, Jean-Yves Tinevez, Daniel James White, Volker Hartenstein, Kevin Eliceiri, Pavel Tomancak, and Albert Cardona. 2012. "Fiji: An Open-Source Platform for Biological-Image Analysis." *Nature Methods* 9(7):676–82.

Schreiber, Heidi A., Jakob Loschko, Roos A. Karssemeijer, Amelia Escolano, Matthew M. Meredith, Daniel Mucida, Pierre Guermonprez, and Michel C. Nussenzweig. 2013. "Intestinal Monocytes and Macrophages Are Required for T Cell Polarization in Response to Citrobacter Rodentium." *The Journal of Experimental Medicine* 210(10):2025–39.

Schulz, Christian, Elisa Gomez Perdiguero, Laurent Chorro, Heather Szabo-Rogers, Nicolas Cagnard, Katrin Kierdorf, Marco Prinz, Bishan Wu, Sten Eirik W. Jacobsen, Jeffrey W. Pollard, Jon Frampton, Karen J. Liu, and Frederic Geissmann. 2012. "A Lineage of Myeloid Cells Independent of Myb and Hematopoietic Stem Cells." *Science* 336(6077):86–90.

Schwarz, N., B. Uysal, M. Welzer, J. C. Bahr, N. Layer, H. Löffler, K. Stanaitis, P. A. Harshad, Y. G. Weber, U. B. S. Hedrich, J. B. Honegger, A. Skodras, A. J. Becker, T. V. Wuttke, and H. Koch. 2019. "Long-Term Adult Human Brain Slice Cultures as a Model System to Study Human CNS Circuitry and Disease." *ELife* 8.

Schwarz, Niklas, Ulrike B. S. Hedrich, Hannah Schwarz, Harshad P A, Nele Dammeier, Eva Auffenberg, Francesco Bedogni, Jurgen B. Honegger, Holger Lerche, Thomas V Wuttke, and Henner Koch. 2017. "Human Cerebrospinal Fluid Promotes Long-Term Neuronal Viability and Network Function in Human Neocortical Organotypic Brain Slice Cultures." *Scientific Reports* 7(1):12249.

Serpell, L. C., J. Berriman, R. Jakes, M. Goedert, and R. A. Crowther. 2000. "Fiber Diffraction of Synthetic Alpha-Synuclein Filaments Shows Amyloid-like Cross-Beta Conformation." *Proceedings of the National Academy of Sciences of the United States of America* 97(9):4897–4902.

Sharma, Kaushik, Kanchan Bisht, and Ukpong B. Eyo. 2021. "A Comparative Biology of Microglia Across Species." *Frontiers in Cell and Developmental Biology* 9:652748.

Shi, Jiayuan, Li Hua, Danielle Harmer, Peishan Li, and Guangwen Ren. 2018. "Cre Driver Mice Targeting Macrophages BT - Macrophages: Methods and Protocols." Pp. 263–75 in, edited by G. Rousselet. New York, NY: Springer New York.

Shi, Yanhong, Haruhisa Inoue, Joseph C. Wu, and Shinya Yamanaka. 2017. "Induced Pluripotent Stem Cell Technology: A Decade of Progress." *Nature Reviews Drug Discovery* 16(2):115–30.

Sieff, C. A. 1987. "Hematopoietic Growth Factors." *The Journal of Clinical Investigation* 79(6):1549–57.

Sierra, Amanda, Juan M. Encinas, Juan J. P. Deudero, Jessica H. Chancey, Grigori Enikolopov, Linda S. Overstreet-Wadiche, Stella E. Tsirka, and Mirjana Maletic-Savatic. 2010. "Microglia Shape Adult Hippocampal Neurogenesis through Apoptosis-Coupled Phagocytosis." *Cell Stem Cell* 7(4):483–95.

Sierra, Amanda, Rosa C. Paolicelli, and Helmut Kettenmann. 2019. "Cien Años de Microglía: Milestones in a Century of Microglial Research." *Trends in Neurosciences* 42(11):778–92.

Sims, Rebecca, Sven J. van der Lee, Adam C. Naj, Céline Bellenguez, Nandini Badarinarayan, Johanna Jakobsdottir, Brian W. Kunkle, Anne Boland, Rachel Raybould, Joshua C. Bis, Eden R. Martin, Benjamin Grenier-Boley, Stefanie Heilmann-Heimbach, Vincent Chouraki, Amanda B. Kuzma, Kristel Sleegers, Maria Vronskaya, Agustin Ruiz, Robert R. Graham, Robert Olaso, Per Hoffmann, Megan L. Grove, Badri N. Vardarajan, Mikko Hiltunen, Markus M. Nöthen, Charles C. White, Kara L. Hamilton-Nelson, Jacques Epelbaum, Wolfgang Maier, Seung-Hoan Choi, Gary W. Beecham, Cécile Dulary, Stefan Herms, Albert V Smith, Cory C. Funk, Céline Derbois, Andreas J. Forstner, Shahzad Ahmad, Hongdong Li, Delphine Bacq, Denise Harold, Claudia L. Satizabal, Otto Valladares, Alessio Squassina, Rhodri Thomas, Jennifer A. Brody, Liming Qu, Pascual Sánchez-Juan, Taniesha Morgan, Frank J. Wolters, Yi Zhao, Florentino Sanchez Garcia, Nicola Denning, Myriam Fornage, John Malamon, Maria Candida Deniz Naranjo, Elisa Majounie, Thomas H. Mosley, Beth Dombroski, David Wallon, Michelle K. Lupton, Josée Dupuis, Patrice Whitehead, Laura Fratiglioni, Christopher Medway, Xueqiu Jian, Shubhabrata Mukherjee, Lina Keller, Kristelle Brown, Honghuang Lin, Laura B. Cantwell, Francesco Panza, Bernadette McGuinness, Sonia Moreno-Grau, Jeremy D. Burgess, Vincenzo Solfrizzi, Petra Proitsi, Hieab H. Adams, Mariet Allen, Davide Seripa, Pau Pastor, L. Adrienne Cupples, Nathan D. Price, Didier Hannequin, Ana Frank-García, Daniel Levy, Paramita Chakrabarty, Paolo Caffarra, Ina Giegling, Alexa S. Beiser, Vilmantas Giedraitis, Harald Hampel, Melissa E. Garcia, Xue Wang, Lars Lannfelt, Patrizia Mecocci, Gudny Eiriksdottir, Paul K. Crane, Florence Pasquier, Virginia Boccardi, Isabel Henández, Robert C. Barber, Martin Scherer, Lluis Tarraga, Perrie M. Adams, Markus Leber, Yuning Chen, Marilyn S. Albert, Steffi Riedel-Heller, Valur Emilsson, Duane Beekly, Anne Braae, Reinhold Schmidt, Deborah Blacker, Carlo Masullo, Helena Schmidt, Rachelle S. Doody, Gianfranco Spalletta, W. T. Jr Longstreth, Thomas J. Fairchild, Paola Bossù, Oscar L. Lopez, Matthew P. Frosch, Eleonora Sacchinelli, Bernardino Ghetti, Qiong Yang, Ryan M. Huebinger, Frank Jessen, Shuo Li, M. Ilyas Kamboh, John Morris, Oscar Sotolongo-Grau, Mindy J. Katz, Chris Corcoran, Melanie Dunstan, Amy Braddel, Charlene Thomas, Alun Meggy, Rachel Marshall, Amy Gerrish, Jade Chapman, Miquel Aguilar, Sarah Taylor, Matt Hill, Mònica Díez Fairén, Angela Hodges, Bruno Vellas, Hilkka Soininen, Iwona Kloszewska, Makrina Daniilidou, James Uphill, Yogen Patel, Joseph T. Hughes, Jenny Lord, James Turton, Annette M. Hartmann, Roberta Cecchetti, Chiara Fenoglio, Maria Serpente, Marina Arcaro, Carlo Caltagirone, Maria Donata Orfei, Antonio Ciaramella, Sabrina Pichler, Manuel Mayhaus, Wei Gu, Alberto Lleó, Juan Fortea, Rafael Blesa, Imelda S. Barber, Keeley Brookes, Chiara Cupidi, Raffaele Giovanni Maletta, David Carrell, Sandro Sorbi, Susanne Moebus, Maria Urbano, Alberto Pilotto, Johannes Kornhuber, Paolo Bosco, Stephen Todd, David Craig, Janet Johnston, Michael Gill, Brian Lawlor, Aoibhinn Lynch, Nick C. Fox, John Hardy, Roger L. Albin, Liana G. Apostolova, Steven E. Arnold, Sanjay Asthana, Craig S. Atwood, Clinton T. Baldwin, Lisa L. Barnes, Sandra Barral, Thomas G. Beach, James T. Becker, Eileen H. Bigio, Thomas D. Bird, Bradley F. Boeve, James D. Bowen, Adam Boxer, James R. Burke, Jeffrey M. Burns, Joseph D. Buxbaum, Nigel J. Cairns, Chuanhai Cao,

Chris S. Carlson, Cynthia M. Carlsson, Regina M. Carney, Minerva M. Carrasquillo, Steven L. Carroll, Carolina Ceballos Diaz, Helena C. Chui, David G. Clark, David H. Cribbs, Elizabeth A. Crocco, Charles DeCarli, Malcolm Dick, Ranjan Duara, Denis A. Evans, Kelley M. Faber, Kenneth B. Fallon, David W. Fardo, Martin R. Farlow, Steven Ferris, Tatiana M. Foroud, Douglas R. Galasko, Marla Gearing, Daniel H. Geschwind, John R. Gilbert, Neill R. Graff-Radford, Robert C. Green, John H. Growdon, Ronald L. Hamilton, Lindy E. Harrell, Lawrence S. Honig, Matthew J. Huentelman, Christine M. Hulette, Bradley T. Hyman, Gail P. Jarvik, Erin Abner, Lee-Way Jin, Gyungah Jun, Anna Karydas, Jeffrey A. Kaye, Ronald Kim, Neil W. Kowall, Joel H. Kramer, Frank M. LaFerla, James J. Lah, James B. Leverenz, Allan I. Levey, Ge Li, Andrew P. Lieberman, Kathryn L. Lunetta, Constantine G. Lyketsos, Daniel C. Marson, Frank Martiniuk, Deborah C. Mash, Eliezer Masliah, Wayne C. McCormick, Susan M. McCurry, Andrew N. McDavid, Ann C. McKee, Marsel Mesulam, Bruce L. Miller, Carol A. Miller, Joshua W. Miller, John C. Morris, Jill R. Murrell, Amanda J. Myers, Sid O'Bryant, John M. Olichney, Vernon S. Pankratz, Joseph E. Parisi, Henry L. Paulson, William Perry, Elaine Peskind, Aimee Pierce, Wayne W. Poon, Huntington Potter, Joseph F. Quinn, Ashok Raj, Murray Raskind, Barry Reisberg, Christiane Reitz, John M. Ringman, Erik D. Roberson, Ekaterina Rogaeva, Howard J. Rosen, Roger N. Rosenberg, Mark A. Sager, Andrew J. Saykin, Julie A. Schneider, Lon S. Schneider, William W. Seeley, Amanda G. Smith, Joshua A. Sonnen, Salvatore Spina, Robert A. Stern, Russell H. Swerdlow, Rudolph E. Tanzi, Tricia A. Thornton-Wells, John Q. Trojanowski, Juan C. Troncoso, Vivianna M. Van Deerlin, Linda J. Van Eldik, Harry V Vinters, Jean Paul Vonsattel, Sandra Weintraub, Kathleen A. Welsh-Bohmer, Kirk C. Wilhelmsen, Jennifer Williamson, Thomas S. Wingo, Randall L. Woltjer, Clinton B. Wright, Chang-En Yu, Lei Yu, Fabienne Garzia, Feroze Golamaully, Gislain Septier, Sebastien Engelborghs, Rik Vandenberghe, Peter P. De Deyn, Carmen Muñoz Fernadez, Yoland Aladro Benito, Hakan Thonberg, Charlotte Forsell, Lena Lilius, Anne Kinhult-Stählbom, Lena Kilander, RoseMarie Brundin, Letizia Concari, Seppo Helisalmi, Anne Maria Koivisto, Annakaisa Haapasalo, Vincent Dermecourt, Nathalie Fievet, Olivier Hanon, Carole Dufouil, Alexis Brice, Karen Ritchie, Bruno Dubois, Jayanadra J. Himali, C. Dirk Keene, JoAnn Tschanz, Annette L. Fitzpatrick, Walter A. Kukull, Maria Norton, Thor Aspelund, Eric B. Larson, Ron Munger, Jerome I. Rotter, Richard B. Lipton, María J. Bullido, Albert Hofman, Thomas J. Montine, Eliecer Coto, Eric Boerwinkle, Ronald C. Petersen, Victoria Alvarez, Fernando Rivadeneira, Eric M. Reiman, Maura Gallo, Christopher J. O'Donnell, Joan S. Reisch, Amalia Cecilia Bruni, Donald R. Royall, Martin Dichgans, Mary Sano, Daniela Galimberti, Peter St George-Hyslop, Elio Scarpini, Debby W. Tsuang, Michelangelo Mancuso, Ubaldo Bonuccelli, Ashley R. Winslow, Antonio Daniele, Chuang-Kuo Wu, Oliver Peters, Benedetta Nacmias, Matthias Riemenschneider, Reinhard Heun, Carol Brayne, David C. Rubinsztein, Jose Bras, Rita Guerreiro, Ammar Al-Chalabi, Christopher E. Shaw, John Collinge, David Mann, Magda Tsolaki, Jordi Clarimón, Rebecca Sussams, Simon Lovestone, Michael C. O'Donovan, Michael J. Owen, Timothy W. Behrens, Simon Mead, Alison M. Goate, Andre G. Uitterlinden, Clive Holmes, Carlos Cruchaga, Martin Ingelsson, David A. Bennett, John Powell, Todd E. Golde, Caroline Graff, Philip L. De Jager, Kevin Morgan, Nilufer Ertekin-Taner, Onofre Combarros, Bruce M. Psaty, Peter Passmore, Steven G. Younkin, Claudine Berr, Vilmundur Gudnason, Dan Rujescu, Dennis W. Dickson, Jean-François Dartigues, Anita L. DeStefano, Sara Ortega-Cubero, Hakon Hakonarson, Dominique Campion, Merce Boada, John Keoni Kauwe, Lindsay A. Farrer, Christine Van Broeckhoven, M. Arfan Ikram, Lesley Jones, Jonathan L. Haines, Christophe Tzourio, Lenore J. Launer, Valentina Escott-Price, Richard Mayeux, Jean-François Deleuze, Najaf Amin, Peter A. Holmans, Margaret A. Pericak-Vance, Philippe Amouyel, Cornelia M. van Duijn, Alfredo Ramirez, Li-San Wang, Jean-Charles Lambert, Sudha Seshadri, Julie Williams, and Gerard D. Schellenberg. 2017. "Rare Coding Variants in PLCG2, ABI3, and TREM2 Implicate Microglial-Mediated Innate Immunity in Alzheimer's Disease." *Nature Genetics* 49(9):1373–84.

Smajić, Semra, Cesar A. Prada-Medina, Zied Landoulsi, Jenny Ghelfi, Sylvie Delcambre, Carola Dietrich, Javier Jarazo, Jana Henck, Saranya Balachandran, Sinthuja Pachchek, Christopher M. Morris, Paul Antony, Bernd Timmermann, Sascha Sauer, Sandro L. Pereira, Jens C. Schwamborn, Patrick May, Anne Grünewald, and Malte Spielmann. 2022. "Single-Cell Sequencing of Human Midbrain Reveals Glial Activation and a Parkinson-Specific Neuronal State." *Brain : A Journal of Neurology* 145(3):964–78.

Song, Liqing, Xuegang Yuan, Zachary Jones, Cynthia Vied, Yu Miao, Mark Marzano, Thien Hua, Qing-Xiang Amy Sang, Jingjiao Guan, Teng Ma, Yi Zhou, and Yan Li. 2019. "Functionalization of Brain Region-Specific Spheroids with Isogenic Microglia-like Cells." *Scientific Reports* 9(1):11055.

Spangenberg, Elizabeth E., Rafael J. Lee, Allison R. Najafi, Rachel A. Rice, Monica R. P. Elmore, Mathew Blurton-Jones, Brian L. West, and Kim N. Green. 2016. "Eliminating Microglia in Alzheimer's Mice Prevents Neuronal Loss without Modulating Amyloid-β Pathology." *Brain* 139(4):1265–81.

Spangenberg, Elizabeth, Paul L. Severson, Lindsay A. Hohsfield, Joshua Crapser, Jiazhong Zhang, Elizabeth A.

Burton, Ying Zhang, Wayne Spevak, Jack Lin, Nicole Y. Phan, Gaston Habets, Andrey Rymar, Garson Tsang, Jason Walters, Marika Nespi, Parmveer Singh, Stephanie Broome, Prabha Ibrahim, Chao Zhang, Gideon Bollag, Brian L. West, and Kim N. Green. 2019. "Sustained Microglial Depletion with CSF1R Inhibitor Impairs Parenchymal Plaque Development in an Alzheimer's Disease Model." *Nature Communications* 10(1):1–21.

Speicher, Anna M., Heinz Wiendl, Sven G. Meuth, and Matthias Pawlowski. 2019. "Generating Microglia from Human Pluripotent Stem Cells: Novel in Vitro Models for the Study of Neurodegeneration." *Molecular Neurodegeneration* 14(1):46.

Spillantini, M. G., R. A. Crowther, R. Jakes, N. J. Cairns, P. L. Lantos, and M. Goedert. 1998. "Filamentous Alpha-Synuclein Inclusions Link Multiple System Atrophy with Parkinson's Disease and Dementia with Lewy Bodies." *Neuroscience Letters* 251(3):205–8.

Spillantini, M. G., M. L. Schmidt, V. M. Lee, J. Q. Trojanowski, R. Jakes, and M. Goedert. 1997. "Alpha-Synuclein in Lewy Bodies." *Nature* 388(6645):839–40.

Spillantini, Maria Grazia and Michel Goedert. 2018. "Neurodegeneration and the Ordered Assembly of α-Synuclein." *Cell and Tissue Research* 373(1):137–48.

Stanley, E. Richard and Violeta Chitu. 2014. "CSF-1 Receptor Signaling in Myeloid Cells." *Cold Spring Harbor Perspectives in Biology* 6(6).

Stansley, Branden, Jan Post, and Kenneth Hensley. 2012. "A Comparative Review of Cell Culture Systems for the Study of Microglial Biology in Alzheimer's Disease." *Journal of Neuroinflammation* 9:115.

Stifter, Sebastian A. and Melanie Greter. 2020. "STOP Floxing around: Specificity and Leakiness of Inducible Cre/LoxP Systems." *European Journal of Immunology* 50(3):338–41.

Stöberl, Nina, Emily Maguire, Elisa Salis, Bethany Shaw, and Hazel Hall-Roberts. 2023. "Human IPSC-Derived Glia Models for the Study of Neuroinflammation." *Journal of Neuroinflammation* 20(1):231.

Stoppini, L., P. A. Buchs, and D. Muller. 1991. "A Simple Method for Organotypic Cultures of Nervous Tissue." *Journal of Neuroscience Methods* 37(2):173–82.

Streit, Wolfgang J., Nicole W. Sammons, Amanda J. Kuhns, and D. Larry Sparks. 2004. "Dystrophic Microglia in the Aging Human Brain." *Glia* 45(2):208–12.

Stremmel, C., R. Schuchert, F. Wagner, R. Thaler, T. Weinberger, R. Pick, E. Mass, H. C. Ishikawa-Ankerhold, A. Margraf, S. Hutter, R. Vagnozzi, S. Klapproth, J. Frampton, S. Yona, C. Scheiermann, J. D. Molkentin, U. Jeschke, M. Moser, M. Sperandio, S. Massberg, F. Geissmann, and C. Schulz. 2018. "Yolk Sac Macrophage Progenitors Traffic to the Embryo during Defined Stages of Development." *Nature Communications* 9(1).

Sun, Na, Matheus B. Victor, Yongjin P. Park, Xushen Xiong, Aine Ni Scannail, Noelle Leary, Shaniah Prosper, Soujanya Viswanathan, Xochitl Luna, Carles A. Boix, Benjamin T. James, Yosuke Tanigawa, Kyriaki Galani, Hansruedi Mathys, Xueqiao Jiang, Ayesha P. Ng, David A. Bennett, Li-Huei Tsai, and Manolis Kellis. 2023. "Human Microglial State Dynamics in Alzheimer’s Disease Progression." *Cell* 186(20):4386-4403.e29.

Sveinbjornsdottir, Sigurlaug. 2016. "The Clinical Symptoms of Parkinson's Disease." *Journal of Neurochemistry* 139(S1):318–24.

Svoboda, Devon S., M. Inmaculada Barrasa, Jian Shu, Rosalie Rietjens, Shupei Zhang, Maya Mitalipova, Peter Berube, Dongdong Fu, Leonard D. Shultz, George W. Bell, and Rudolf Jaenisch. 2019. "Human IPSC-Derived Microglia Assume a Primary Microglia-like State after Transplantation into the Neonatal Mouse Brain." *Proceedings of the National Academy of Sciences of the United States of America* 116(50):25293–303.

Tada, Mari, Takuya Konno, Masayoshi Tada, Toshiyuki Tezuka, Takeshi Miura, Naomi Mezaki, Ken ichi Okazaki, Musashi Arakawa, Kyoko Itoh, Toru Yamamoto, Hideaki Yokoo, Nobuaki Yoshikura, Kenji Ishihara, Masao Horie, Hirohide Takebayashi, Yasuko Toyoshima, Makoto Naito, Osamu Onodera, Masatoyo Nishizawa, Hitoshi Takahashi, Takeshi Ikeuchi, and Akiyoshi Kakita. 2016. "Characteristic Microglial Features in Patients with Hereditary Diffuse Leukoencephalopathy with Spheroids." *Annals of Neurology* 80(4):554–65.

Takahashi, Kazutoshi and Shinya Yamanaka. 2006. "Induction of Pluripotent Stem Cells from Mouse Embryonic and Adult Fibroblast Cultures by Defined Factors." *Cell* 126(4):663–76.

Takasato, Minoru, Kenji Osafune, Yuko Matsumoto, Yuki Kataoka, Nobuaki Yoshida, Hiroko Meguro, Hiroyuki

Aburatani, Makoto Asashima, and Ryuichi Nishinakamura. 2004. “Identification of Kidney Mesenchymal Genes by a Combination of Microarray Analysis and Sall1-GFP Knockin Mice.” *Mechanisms of Development* 121(6):547–57.

Takata, Kazuyuki, Yoshihisa Kitamura, Mana Saeki, Maki Terada, Sachiko Kagitani, Risa Kitamura, Yasuhiro Fujikawa, Alfred Maelicke, Hidekazu Tomimoto, Takashi Taniguchi, and Shun Shimohama. 2010. “Galantamine-Induced Amyloid-{beta} Clearance Mediated via Stimulation of Microglial Nicotinic Acetylcholine Receptors.” *The Journal of Biological Chemistry* 285(51):40180–91.

Takata, Kazuyuki, Tatsuya Kozaki, Christopher Zhe Wei Lee, Morgane Sonia Thion, Masayuki Otsuka, Shawn Lim, Kagistia Hana Utami, Kerem Fidan, Dong Shin Park, Benoit Malleret, Svetoslav Chakarov, Peter See, Donovan Low, Gillian Low, Marta Garcia-Miralles, Ruizhu Zeng, Jinqiu Zhang, Chi Ching Goh, Ahmet Gul, Sandra Hubert, Bernett Lee, Jinmiao Chen, Ivy Low, Nurhidaya Binte Shadan, Josephine Lum, Tay Seok Wei, Esther Mok, Shohei Kawanishi, Yoshihisa Kitamura, Anis Larbi, Michael Poidinger, Laurent Renia, Lai Guan Ng, Yochai Wolf, Steffen Jung, Tamer Önder, Evan Newell, Tara Huber, Eishi Ashihara, Sonia Garel, Mahmoud A. Pouladi, and Florent Ginhoux. 2017. “Induced-Pluripotent-Stem-Cell-Derived Primitive Macrophages Provide a Platform for Modeling Tissue-Resident Macrophage Differentiation and Function.” *Immunity* 47(1):183-198.e6.

Takemoto, Kiwamu, Tomoki Matsuda, Naoki Sakai, Donald Fu, Masanori Noda, Susumu Uchiyama, Ippei Kotera, Yoshiyuki Arai, Masataka Horiuchi, Kiichi Fukui, Tokiyoshi Ayabe, Fuyuhiko Inagaki, Hiroshi Suzuki, and Takeharu Nagai. 2013. “SuperNova, a Monomeric Photosensitizing Fluorescent Protein for Chromophore-Assisted Light Inactivation.” *Scientific Reports* 3:2629.

Tanaka, Yoshiaki, Bilal Cakir, Yangfei Xiang, Gareth J. Sullivan, and In-Hyun Park. 2020. “Synthetic Analyses of Single-Cell Transcriptomes from Multiple Brain Organoids and Fetal Brain.” *Cell Reports* 30(6):1682-1689.e3.

Tanriöver, Gaye, Mehtap Bacioglu, Manuel Schweighauser, Jasmin Mahler, Bettina M. Wegenast-Braun, Angelos Skodras, Ulrike Obermüller, Melanie Barth, Deborah Kronenberg-Versteeg, K. Peter R. Nilsson, Derya R. Shimshek, Philipp J. Kahle, Yvonne S. Eisele, and Mathias Jucker. 2020. “Prominent Microglial Inclusions in Transgenic Mouse Models of α-Synucleinopathy That Are Distinct from Neuronal Lesions.” *Acta Neuropathologica Communications* 8(1):1–11.

Tay, Tuan Leng, Dominic Mai, Jana Dautzenberg, Francisco Fernández-Klett, Gen Lin, Sagar, Moumita Datta, Anne Drougard, Thomas Stempfl, Alberto Ardura-Fabregat, Ori Staszewski, Anca Margineanu, Anje Sporbert, Lars M. Steinmetz, J. Andrew Pospisilik, Steffen Jung, Josef Priller, Dominic Grün, Olaf Ronneberger, and Marco Prinz. 2017. “A New Fate Mapping System Reveals Context-Dependent Random or Clonal Expansion of Microglia.” *Nature Neuroscience* 20:793.

Taylor, Deanna L., Fleur Jones, Eva S. F. Chen Seho Kubota, and Jennifer M. Pocock. 2005. “Stimulation of Microglial Metabotropic Glutamate Receptor MGlu2 Triggers Tumor Necrosis Factor α-Induced Neurotoxicity in Concert with Microglial-Derived Fas Ligand.” *Journal of Neuroscience* 25(11):2952–64.

Thomsen, Majken B., Sara A. Ferreira, Anna C. Schacht, Jan Jacobsen, Mette Simonsen, Cristine Betzer, Poul H. Jensen, David J. Brooks, Anne M. Landau, and Marina Romero-Ramos. 2021. “PET Imaging Reveals Early and Progressive Dopaminergic Deficits after Intra-Striatal Injection of Preformed Alpha-Synuclein Fibrils in Rats.” *Neurobiology of Disease* 149:105229.

Timmerman, Raissa, Saskia M. Burm, and Jeffrey J. Bajramovic. 2018. “An Overview of in Vitro Methods to Study Microglia.” *Frontiers in Cellular Neuroscience* 12(August):1–12.

Ubhi, Kiren, Phillip Low, and Eliezer Masliah. 2011. “Multiple System Atrophy: A Clinical and Neuropathological Perspective.” *Trends in Neurosciences* 34(11):581–90.

Ueno, Masaki, Yuki Fujita, Tatsuhide Tanaka, Yuka Nakamura, Junichi Kikuta, Masaru Ishii, and Toshihide Yamashita. 2013. “Layer v Cortical Neurons Require Microglial Support for Survival during Postnatal Development.” *Nature Neuroscience* 16(5):543–51.

Vahsen, Björn F., Elizabeth Gray, Ana Candalija, Kaitlyn M. L. Cramb, Jakub Scaber, Ruxandra Dafinca, Antigoni Katsikoudi, Yinyan Xu, Lucy Farrimond, Richard Wade-Martins, William S. James, Martin R. Turner, Sally A. Cowley, and Kevin Talbot. 2022. “Human IPSC Co-Culture Model to Investigate the Interaction between Microglia and Motor Neurons.” *Scientific Reports* 12(1):12606.

Vainchtein, Ilia D., Gregory Chin, Frances S. Cho, Kevin W. Kelley, John G. Miller, Elliott C. Chien, Shane A.

Liddelow, Phi T. Nguyen, Hiromi Nakao-Inoue, Leah C. Dorman, Omar Akil, Satoru Joshita, Ben A. Barres, Jeanne T. Paz, Ari B. Molofsky, and Anna V Molofsky. 2018. “Astrocyte-Derived Interleukin-33 Promotes Microglial Synapse Engulfment and Neural Circuit Development.” *Science* 359(6381):1269–73.

Varvel, Nicholas H., Stefan A. Grathwohl, Frank Baumann, Christian Liebig, Andrea Bosch, Richard M. Ransohoff, and Mathias Jucker. 2012. “Microglial Repopulation Model Reveals a Robust Homeostatic Process for Replacing CNS Myeloid Cells.” 2–7.

Velasco, Silvia, Amanda J. Kedaigle, Sean K. Simmons, Allison Nash, Marina Rocha, Giorgia Quadrato, Bruna Paulsen, Lan Nguyen, Xian Adiconis, Aviv Regev, Joshua Z. Levin, and Paola Arlotta. 2019. “Individual Brain Organoids Reproducibly Form Cell Diversity of the Human Cerebral Cortex.” *Nature* 570(7762):523–27.

Venegas, Carmen, Sathish Kumar, Bernardo S. Franklin, Tobias Dierkes, Rebecca Brinkschulte, Dario Tejera, Ana Vieira-Saecker, Stephanie Schwartz, Francesco Santarelli, Markus P. Kummer, Angelika Griep, Ellen Gelpi, Michael Beilharz, Dietmar Riedel, Douglas T. Golenbock, Matthias Geyer, Jochen Walter, Eicke Latz, and Michael T. Heneka. 2017. “Microglia-Derived ASC Specks Crossseed Amyloid-β in Alzheimer’s Disease.” *Nature* 552(7685):355–61.

Vidal-Itriago, Andrés, Rowan A. W. Radford, Jason A. Aramideh, Cindy Maurel, Natalie M. Scherer, Emily K. Don, Albert Lee, Roger S. Chung, Manuel B. Graeber, and Marco Morsch. 2022. “Microglia Morphophysiological Diversity and Its Implications for the CNS.” *Frontiers in Immunology* 13:997786.

Villa, Alessandro, Paolo Gelosa, Laura Castiglioni, Mauro Cimino, Nicoletta Rizzi, Giovanna Pepe, Federica Lolli, Elena Marcello, Luigi Sironi, Elisabetta Vegeto, and Adriana Maggi. 2018. “Sex-Specific Features of Microglia from Adult Mice.” *Cell Reports* 23(12):3501–11.

Waisman, Ari, Florent Ginhoux, Melanie Greter, and Julia Bruttger. 2015. “Homeostasis of Microglia in the Adult Brain: Review of Novel Microglia Depletion Systems.” *Trends in Immunology* 36(10):625–36.

Wang, Shoutang and Marco Colonna. 2019. “Microglia in Alzheimer’s Disease: A Target for Immunotherapy.” *Journal of Leukocyte Biology* 106(1):219–27.

Wang, Xu, Lian Zhao, Jun Zhang, Robert N. Fariss, Wenxin Ma, Friedrich Kretschmer, Minhua Wang, Hao Hua Qian, Tudor C. Badea, Jeffrey S. Diamond, Wen-Biao Gan, Jerome E. Roger, and Wai T. Wong. 2016. “Requirement for Microglia for the Maintenance of Synaptic Function and Integrity in the Mature Retina.” *The Journal of Neuroscience : The Official Journal of the Society for Neuroscience* 36(9):2827–42.

Warden, Anna S., Claudia Han, Emily Hansen, Samantha Trescott, Celina Nguyen, Roy Kim, Danielle Schafer, Avalon Johnson, Madison Wright, Gabriela Ramirez, Mark Lopez-Sanchez, and Nicole G. Coufal. 2023. “Tools for Studying Human Microglia: In Vitro and in Vivo Strategies.” *Brain, Behavior, and Immunity* 107:369–82.

Wendeln, Ann-Christin, Karoline Degenhardt, Lalit Kaurani, Michael Gertig, Thomas Ulas, Gaurav Jain, Jessica Wagner, Lisa M. Hasler, Katleen Wild, Angelos Skodras, Thomas Blank, Ori Staszewski, Moumita Datta, Tonatiuh Pena Centeno, Vincenzo Capece, Md Rezaul Islam, Cemil Kerimoglu, Matthias Staufenbiel, Joachim L. Schultze, Marc Beyer, Marco Prinz, Mathias Jucker, Andre Fischer, and Jonas J. Neher. 2018. “Innate Immune Memory in the Brain Shapes Neurological Disease Hallmarks.” *Nature* 556(7701):332–38.

Wes, Paul D., Inge R. Holtman, Erik W. G. M. Boddeke, Thomas Möller, and Bart J. L. Eggen. 2016. “Next Generation Transcriptomics and Genomics Elucidate Biological Complexity of Microglia in Health and Disease.” *Glia* 64(2):197–213.

Wickham, Jenny, Andrea Corna, Niklas Schwarz, Betül Uysal, Nikolas Layer, Jürgen B. Honegger, Thomas V Wuttke, Henner Koch, and Günther Zeck. 2020. “Human Cerebrospinal Fluid Induces Neuronal Excitability Changes in Resected Human Neocortical and Hippocampal Brain Slices.” *Frontiers in Neuroscience* 14:283.

Williams, Daniel C., Rachid El Bejjani, Paula Mugno Ramirez, Sean Coakley, Shin Ae Kim, Hyewon Lee, Quan Wen, Aravi Samuel, Hang Lu, Massimo A. Hilliard, and Marc Hammarlund. 2013. “Rapid and Permanent Neuronal Inactivation in Vivo via Subcellular Generation of Reactive Oxygen with the Use of KillerRed.” *Cell Reports* 5(2):553–63.

Wlodarczyk, Agnieszka, Inge R. Holtman, Martin Krueger, Nir Yogev, Julia Bruttger, Reza Khorooshi, Anouk Benmamar-Badel, Jelkje J. de Boer-Bergsma, Nellie A. Martin, Khalad Karram, Isabella Kramer, Erik WGM Boddeke, Ari Waisman, Bart JL Eggen, and Trevor Owens. 2017. “A Novel Microglial Subset Plays a Key Role in Myelinogenesis in Developing Brain.” *The EMBO Journal* 36(22):3292–3308.

Wood, J. G., S. S. Mirra, N. J. Pollock, and L. I. Binder. 1986. “Neurofibrillary Tangles of Alzheimer Disease Share Antigenic Determinants with the Axonal Microtubule-Associated Protein Tau (Tau).” *Proceedings of the National Academy of Sciences of the United States of America* 83(11):4040–43.

Xia, Yun, Guoxin Zhang, Chao Han, Kai Ma, Xingfang Guo, Fang Wan, Liang Kou, Sijia Yin, Ling Liu, Jinsha Huang, Nian Xiong, and Tao Wang. 2019. “Microglia as Modulators of Exosomal Alpha-Synuclein Transmission.” *Cell Death & Disease* 10(3):174.

Xu, Ranjie, Andrew J. Boreland, Xiaoxi Li, Caroline Erickson, Mengmeng Jin, Colm Atkins, Zhiping P. Pang, Brian P. Daniels, and Peng Jiang. 2021. “Developing Human Pluripotent Stem Cell-Based Cerebral Organoids with a Controllable Microglia Ratio for Modeling Brain Development and Pathology.” *Stem Cell Reports* 16(8):1923–37.

Xu, Zhen, Yubin Huang, Lin Cai, Shuai Gao, Taohui Liu, Fanzhuo Zeng, Yafei Wang, Wenxu Wang, Ti-fei Yuan, Hengli Tian, Yousheng Shu, Feifan Guo, Wei Lu, Ying Mao, Xifan Mei, Yanxia Rao, and Bo Peng. 2023. “Transcriptional and Epigenetic Decoding of the Microglial Aging Process.”

Xu, Zhen, Yanxia Rao, Yubin Huang, Tian Zhou, Rui Feng, Shanshan Xiong, Ti-Fei Yuan, Shan Qin, Yijie Lu, Xin Zhou, Xiaoyu Li, Bo Qin, Ying Mao, and Bo Peng. 2020. “Efficient Strategies for Microglia Replacement in the Central Nervous System.” *Cell Reports* 32(6):108041.

Yuan, Peng, Carlo Condello, C. Dirk Keene, Yaming Wang, Thomas D. Bird, Steven M. Paul, Wenjie Luo, Marco Colonna, David Baddeley, and Jaime Grutzendler. 2016. “TREM2 Haplodeficiency in Mice and Humans Impairs the Microglia Barrier Function Leading to Decreased Amyloid Compaction and Severe Axonal Dystrophy.” *Neuron* 90(4):724–39.

Zhan, Lihong, Li Fan, Lay Kodama, Peter Dongmin Sohn, Man Ying Wong, Gergey Alzaem Mousa, Yungui Zhou, Yaqiao Li, and Li Gan. 2020. “A Mac2-Positive Progenitor-like Microglial Population Is Resistant to Csf1r Inhibition in Adult Mouse Brain.” *ELife* 9:1–22.

Zhan, Lihong, Grietje Krabbe, Fei Du, Ian Jones, Meredith C. Reichert, Maria Telpoukhovskaia, Lay Kodama, Chao Wang, Seo-hyun Cho, Faten Sayed, Yaqiao Li, David Le, Yungui Zhou, Yin Shen, Brian West, and Li Gan. 2019. “Proximal Recolonization by Self-Renewing Microglia Re-Establishes Microglial Homeostasis in the Adult Mouse Brain.” *PLOS Biology* 17(2):e3000134.

Zhan, Yang, Rosa C. Paolicelli, Francesco Sforazzini, Laetitia Weinhard, Giulia Bolasco, Francesca Pagani, Alexei L. Vyssotski, Angelo Bifone, Alessandro Gozzi, Davide Ragozzino, and Cornelius T. Gross. 2014. “Deficient Neuron-Microglia Signaling Results in Impaired Functional Brain Connectivity and Social Behavior.” *Nature Neuroscience* 17(3):400–406.

Zhang, Wendiao, Jiamei Jiang, Zhenhong Xu, Hongye Yan, Beisha Tang, Chunyu Liu, Chao Chen, and Qingtuan Meng. 2023. “Microglia-Containing Human Brain Organoids for the Study of Brain Development and Pathology.” *Molecular Psychiatry* 28(1):96–107.

Zhang, Ye, Steven A. Sloan, Laura E. Clarke, Christine Caneda, Colton A. Plaza, Paul D. Blumenthal, Hannes Vogel, Gary K. Steinberg, Michael S. B. Edwards, Gordon Li, John A. Duncan III, Samuel H. Cheshier, Lawrence M. Shuer, Edward F. Chang, Gerald A. Grant, Melanie G. Hayden Gephart, and Ben A. Barres. 2016. “Purification and Characterization of Progenitor and Mature Human Astrocytes Reveals Transcriptional and Functional Differences with Mouse.” *Neuron* 89(1):37–53.

Zhao, Xueze, Jiangping Liu, Jiangli Fan, Hui Chao, and Xiaojun Peng. 2021. “Recent Progress in Photosensitizers for Overcoming the Challenges of Photodynamic Therapy: From Molecular Design to Application.” *Chemical Society Reviews* 50(6):4185–4219.

Zhou, Tian, Yuxin Li, Xiaoyu Li, Fanzhuo Zeng, Yanxia Rao, Yang He, Yafei Wang, Meizhen Liu, Dali Li, Zhen Xu, Xin Zhou, Siling Du, Fugui Niu, Jiyun Peng, Xifan Mei, Sheng-Jian Ji, Yousheng Shu, Wei Lu, Feifan Guo, Tianzhun Wu, Ti-Fei Yuan, Ying Mao, and Bo Peng. 2022. “Microglial Debris Is Cleared by Astrocytes via C4b-Facilitated Phagocytosis and Degraded via RUBICON-Dependent Noncanonical Autophagy in Mice.” *Nature Communications* 13(1):6233.

Zimprich, Alexander, Saskia Biskup, Petra Leitner, Peter Lichtner, Matthew Farrer, Sarah Lincoln, Jennifer Kachergus, Mary Hulihan, Ryan J. Uitti, Donald B. Calne, A. Jon Stoessl, Ronald F. Pfeiffer, Nadja Patenge, Iria Carballo Carbajal, Peter Vieregge, Friedrich Asmus, Bertram Müller-Myhsok, Dennis W. Dickson, Thomas Meitinger, Tim M. Strom, Zbigniew K. Wszolek, and Thomas Gasser. 2004. “Mutations in LRRK2 Cause Autosomal-Dominant Parkinsonism with Pleomorphic Pathology.” *Neuron* 44(4):601–7.

VII Statement of contributions

1 New mouse model does not allow to induce targeted microglia cell death to investigate microglial network homeostasis *in vivo*

Marc Welzer, Deborah Kronenberg-Versteeg, Jasmin Hefendehl, Bettina Wegenast-Braun, Angelos Skodras, Susanne Feil, Robert Feil, Mathias Jucker

Personal contribution: Experimental design and planning of the study (Figures 4.1, 4.2; together with BWB, AS, RF, MJ); Mouse injections; Cranial window surgery (training by JH); Mouse preparation and fixation; (2-Photon *in* vivo) microscopy (together with AS; assisted by DKV); Brain sectioning; Immunofluorescent staining; Image analysis (Figures 4.3, 4.4); Dosing experiment for Tam and DT (Figure 4.3); Microglia isolation (together with DKV); FACS (Figure 4.5; Together with DKV); DNA isolation; Design of PCR strategy and primers (Figure 4.6; together with DKV, SF, RF); PCR incl. analysis (Figure 4.7); DNA purification; Sanger sequencing analysis (Figure 4.8); statistical analysis; figure design and preparation

Others: Vera Pichler and Carina Leibssle performed earmarking and genotyping of mice; Sanger sequencing was performed by LGC genomics, Berlin

2 Development of a novel chimeric *in vitro* model to investigate human microglial network homeostasis and neurodegeneration

Marc Welzer*, Lena Erlebach*, Anika Bühler, Gamze Özata, Marta Vilademunt-Alcaide, Vasiliki Pangiotakopoulou, Ulrike Obermüller, Marius Lambert, Derya R. Shimshek, Ronald Melki, Peter R. Nilsson, Angelos Skodras, Jonas Neher, Mathias Jucker, Deborah Kronenberg-Versteeg

*contributed equally

Personal contribution: Experimental design and planning of the study (together with LE, JN, MJ, DKV); iPSC culture and microglia differentiation (mostly by LE, assisted by MW, AB, GÖ, VP); iMic precursor harvesting and grafting (mostly by LE, assisted by MW, GÖ); preparation of hippocampal slice cultures (together with LE); maintenance of hippocampal slice cultures incl. microglia depletion (together with LE, AB, VP); slice culture fixation (together with LE, AB, VP); Microglia isolation for scRNAseq (together with LE); scRNAseq data visualization (Figures 4.15, 4.22, together with DKV); immunofluorescent staining (together with LE, UO); LCO staining; Confocal imaging (Figures 4.9-4.12, 4.18-4.20, together with LE); 2-Photon live cell imaging; Calcium imaging; Quantification of microglia (Figures 4.9-4.12, 4.18, 4.20, together with LE); Morphological and network analysis of microglia (Figure 4.12); Analysis of microglia dynamics (Figure 4.13); Analysis of MSD measurements (Figure 4.14, 4.21, together with LE, DKV); Calcium imaging analysis (Figure 4.16); Analysis of microglial inclusions (Figure 4.20); statistical analysis (together with LE, DKV); figure design and preparation (together with LE, MJ, DKV)

Others: Vera Pichler and Carina Leibssle performed earmarking; AB and Carina Leibssle performed mouse genotyping; AB performed media collection for cytokine measurements; DRS provided the transgenic mouse model; RM provided the αsyn pff; PRN provided the LCO-dyes pFTAA and hFTAA; HK provided human *ex vivo* tissue; LE performed the LPS treatment, iMic monoculture experiments (Figure 4.17) and 10x scRNAseq library generation; Single-cell RNA sequencing was performed by the NGS competence center Tübingen; DKV and Dr. Jun-Hoe Lee performed scRNAseq analysis; ML performed MSD measurements; MVA established LPS treatments in CSC

VIII Abbreviations

°C	Degrees Celsius
4-AP	4-Aminopyridine
AAV	adeno-associated virus
Aβ	Amyloid beta
AD	Alzheimer's disease
ALS	Amyotrophic lateral sclerosis
ARM	Activated response microglia
αsyn	Alpha synuclein
B6	Black 6 or C57BL/6 mouse strain
BDNF	brain derived neurotrophic factor
CD11b	Cluster of differentiation molecule 11B, also known as ITGAM
CD45	Cluster of differentiation molecule 45, also known as PTPRC
CO_2	Carbon dioxide
CreERT2	Cre recombinase fused to a mutant estrogen ligand-binding domain
CSC	Chimeric slice culture
CSF1(R)	Colony stimulating factor 1 (receptor)
CX3CR1	CX3C motif chemokine receptor 1
DAM	Disease-associated microglia
DEGs	Differentially-expressed genes
DIV	Days in vitro
DLB	Dementia with Lewy Bodies
DNA	Deoxyribonucleic acid
DT	Diphtheria toxin
(E)GFP	(Enhanced) green fluorescent protein
EB	Embryoid body

FACS	Fluorescence-activated cell sorting
FTLD	Frontotemporal lobar degeneration
GWAS	Genome-wide association studies
h	Hours
(h)TMEM119	(human) transmembrane protein 119
Het	Heterozygous
hFTAA	heptamer-formyl thiophene acetic acid
Hom	Homozygous
HSC	Hippocampal slice culture
HSVTK	herpes simplex virus thymidine kinase
Iba1	ionized calcium-binding adapter molecule 1, also known as AIF1
iDTR	Cre-inducible diphtheria toxin receptor
IGF1	Insulin-like growth factor 1
IL	Interleukin
iMic	iPSC-derived microglia
iMicros	iPSC-derived microglia-like cells
iPSC	Induced pluripotent stem cells
IRM	Interferon response microglia
(k)bp	(kilo)base pair
KO	Knock-out
LCO	Luminescent conjugated oligothiophenes
loxP	Locus of X-over P1
LPS	Lipopolysaccharide
M	Molar
MHC	Major Histocompatibility Complex
min	Minute(s)

ml	Milliliters
mM	Millimolar
mm^3	cubic millimeter
MS	Multiple sclerosis
MSA	Multiple System Atrophy
n	Number of technical/biological replicates
NaCl	Sodium chloride
NND	Nearest neighbor distance
OBSC	Organotypic brain slice culture(s)
ON	Over night
PCR	Polymerase chain reaction
PD	Parkinson's disease
pFTAA	pentamer-formyl thiophene acetic acid
Pre-iMics	iMic precursors
pS129	Phosphorylation at serine 129
PU.1	Transcription factor also known as SP1
R26	Rosa26-locus
RNA	Ribonucleic acid
ROI	Region of interest
ROS	Reactive oxygen species
RT	Room temperature
scRNAseq	Single-cell RNA sequencing
STEM101	Antibody specific to human Ku80
Tam	Tamoxifen
tdTom	tdTomato
TGFβ	Transforming Growth Factor beta

TNFα	Tumor necrosis factor alpha
TREM2	Triggering receptor expressed on myeloid cells 2
TYROBP	TYRO protein tyrosine kinase-binding protein
VEGF	Vascular Endothelial Growth Factor
WT	Wildtype
µm	Micrometer
µM	Micromolar
μm^3	cubic micrometer

IX Acknowledgment

First of all, I would like to express my deepest gratitude to Prof. Dr. Mathias Jucker for his great guidance throughout my two PhD projects and his permanent support. He was always a great mentor and always helped me to stay focused on the important parts of the projects.

I would also like to thank Prof. Dr. Olga Garaschuk and Prof. Dr. Cornelius Schwarz for their support as members of my scientific advisory board. I always appreciated the thoughtful input and constructive criticism during our meetings. Additionally, I would like to thank Prof. Dr. Katja Schenke-Layland for serving on my thesis board.

Next, my deep gratitude goes to Dr. Deborah Kronenberg-Versteeg for her outstanding support with lab-related and private matters and for her great input, also for this thesis. Deborah was always there for me, no matter at which time of the day I pitched ideas to her. I would also like to thank Lena Erlebach, not only for all the fun time we had outside of the lab but also for being a fantastic lab partner.

I would also like to express my deepest gratitude to everyone in the department of 'Cellular Neurology' at the Hertie Institute for the support and great time. Special thanks go to all fellow PhD students, I spent so much time with, in the PhD office and in private: Thank you to Dr. Melanie Barth (also for mentoring me in my first years in the lab), Carina Bergmann (also for being a great office buddy), Lena Erlebach, Dr. Christine Rother, Ying Xu, Teresa Bartling, Sinja Buchner and Antonia Keller. Special thanks go to Dr. Gaye Tanriöver for mentoring me, to Vasiliki Panagiotakopoulou for her fantastic support and great conversations, to Marius Lambert, Anika Bühler and Katleen Wild for keeping the lab running, to Jörg Odenthal and Vera Pichler for their help with animal work, and to Stephan Käser for statistical help, great input and his help with animal protocols.

This work would not have been possible without great collaborations within the Tübingen NeuroCampus and outside with special thanks to Prof. Dr. Jasmin Hefendehl for teaching me the cranial window surgery.

My deepest gratitude also goes to Dr. Jessica Wagner for a great time in and outside of the lab, and especially for proof-reading my thesis.

Most importantly, I would like to thank my family and friends for their permanent support not only during my PhD but also before. Thank you to my parents who always supported me during every step of my career. Last but not least, thank you to Katrin and Theresa who always brought me joy, supported me, helped me through difficult days during the PhD and always make me smile with their love. I am lucky to have you around me.

X Supplementary Material

1 Genotyping PCRs

1.1 R26-tdTomato

1.1.1 Primer

```
tdTom-F:    5’CTC TGC TGC CTC CTG GCT TCT 3’
tdTom-tg_R: 5’TCA ATG GGC GGG GGT CGT T 3’
tdTom-wt_R: 5’CGA GGC GGA TCA CAA GCA ATA 3’
```

1.1.2 Protocol

Table 10.1 PCR mix tdTomato

H2O:	5.25 µl
tdTom-F	0.25 µl
tdTom -tg_R	0.25 µl
tdTom -wt_R	0.25 µl
Mastermix (Sigma-Aldrich)	10 µl
	16 µl
Tissue Extract	4 µl
	20 µl

1.	Incubate at	95 °C	for	5´
2.	Incubate at	95 °C	for	10 s
3.	Incubate at	61 °C	for	30 s
4.	Incubate at	72 °C	for	30 s

Repeat steps 2 – 4 35 more times

5.	Incubate at	72 °C	for	5´
6.	Incubate at	4 °C	forever	

Products: Transgenic: 270 bp

WT: 350 bp

1.2 CD11b-CreERT2

1.2.1 Primer

```
CD11b-Cre Fw:  5’GCT GCC ACG ACC AAG TGA CAG CAA TG 3’
CD11b-Cre Rev: 5’GTA GTT ATT CGG ATC ATC AGC TAC AC 3’
KO2F:          5’CCA CGC AGG ATC ACG ATG 3’
KO1R:          5’TCT GCG TTC AAG GCT CGT CC 3’
```

1.2.2 Protocol

Table 10.2 PCR mix CD11b-Cre

H2O:	5.1 µl
CD11b-Cre Fw	0.25 µl
CD11b-Cre Rev	0.25 µl
K02F	0.2 µl
K01R	0.2 µl
Mastermix (Sigma-Aldrich)	10 µl
	16 µl
Tissue Extract	4 µl
	20 µl

1.	Incubate at	95 °C	for	5´
2.	Incubate at	95 °C	for	10 s
3.	Incubate at	58 °C	for	30 s
4.	Incubate at	72 °C	for	30 s

Repeat steps 2 – 4 35 more times

5.	Incubate at	72 °C	for	5´
6.	Incubate at	4 °C	forever	

Products: Transgenic: 450 bp

WT control: 400 bp

1.3 R26-iDTR

1.3.1 Primer

ROSA26-F: 5'AAA GTC GCT CTG AGT TGT TAT 3'
ROSA26-tg_R: 5'CAT CAA GGA AAC CCT GGA CTA CTG 3'
ROSA26-wt_R: 5'GGA GCG GGA GAA ATG GAT ATG 3'

1.3.2 Protocol

Table 10.3 PCR mix iDTR

H2O:	5.6 µl
ROSA26-F	0.1 µl
ROSA26-tg_R	0.1 µl
ROSA26-wt_R	0.2 µl
Mastermix (Sigma-Aldrich)	10 µl
	16 µl
Tissue Extract	4 µl
	20 µl

1. Incubate at 94 °C for 2´
2. Incubate at 94 °C for 45 s
3. Incubate at 60 °C for 45 s
4. Incubate at 72 °C for 1´

Repeat steps 2 – 4 35 more times

5. Incubate at 72 °C for 2´
6. Incubate at 4 °C forever

Products: Transgenic: 241 bp

WT: 600 bp

1.4 Iba1-EGFP

1.4.1 Primer

EGFP Fw: 5'AAG TTC ATC TGC ACC ACC G 3'
EGFP Rev: 5'CGG CCA TGA TAT AGA CGT TG 3'
KO2F: 5'CCA CGC AGG ATC ACG ATG 3'
KO1R: 5'TCT GCG TTC AAG GCT CGT CC 3'

1.4.2 Protocol

Table 10.4 PCR mix Iba1-EGFP

H2O:	5.3 µl
EGFP Fw	0.25 µl
EGFP Rev	0.25 µl
K02F	0.1 µl
K01R	0.1 µl
Mastermix (Sigma-Aldrich)	10 µl
	16 µl
Tissue Extract	4 µl
	20 µl

1. Incubate at 95 °C for 5´
2. Incubate at 95 °C for 45 s
3. Incubate at 60 °C for 45 s
4. Incubate at 72 °C for 45 s

Repeat steps 2 – 4 35 more times

5. Incubate at 72 °C for 10´
6. Incubate at 4 °C forever

Products: Transgenic: 375 bp

WT control: 400 bp

1.5 Thy1-hA53T-αSyn

1.5.1 Primer

```
aSYN-s1 Fw:  5’TGT AGG CTC CAA AAC CAA GG 3’
aSYN-s1 Rev: 5’TGT CAG GAT CCA CAG GCA TA 3’
KO2F:        5’CCA CGC AGG ATC ACG ATG 3’
KO1R:        5’TCT GCG TTC AAG GCT CGT CC 3’
```

1.5.2 Protocol

Table 10.5 PCR mix A53T

H_2O:	5 µl
aSYN-s1 Fw	0.3 µl
aSYN -s1 rev	0.3 µl
K02F	0.2 µl
K01R	0.2 µl
Mastermix (Sigma-Aldrich)	10 µl
	16 µl
Tissue Extract	4 µl
	20 µl

1.	Incubate at	95 °C	for	5´
2.	Incubate at	95 °C	for	45 s
3.	Incubate at	64 °C	for	45 s
4.	Incubate at	72 °C	for	45 s

Repeat steps 2 – 4 35 more times

5.	Incubate at	72 °C	for	10´
6.	Incubate at	4 °C	forever	

Products: Transgenic: 284 bp

WT control: 400 bp

2 Sanger sequencing - Alignments

2.1 GFP only – NaCl Forward

Alignment of Sequence_1: [iDTRlinear_Cre-recombination.xdna] with Sequence_2: [Untreated_GFPonly_F.txt.xdna]

```
Seq_1  1201  CCTTCCCCCTCTTCCCTCGTGATCTGCAACTCCAGTCTTTCTAGCATCTGTAGGGCGCAG  1260

Seq_2  1     ------------------------------------------------------------  0


Seq_1  1261  TAGTCCAGGGTTTCCTTGATGATGTCATACTTATCCTGTCCCTTTTTTTTCCACAGCTCG  1320
                                     | |   |       |||||| ||||   ||||||
Seq_2  1     -------------------------GAGA--CA-ATCTGTCCTTTTATTTCA--AGCTCG  30


Seq_1  1321  CGGTTGAGGACAAACTCTTCGCGGTCTTTCCAGTGGTTATTAATTAAATAACTTCGTATA  1380
             |||||||||||| |||||||||||||||||||||||||   ||||||||||||||||||
Seq_2  31    CGGTTGAGGACAA-CTCTTCGCGGTCTTTCCAGTGGTTA---ATTAAATAACTTCGTATA  86


Seq_1  1381  GCATACATTATACGAAGTTATCGGCGCGCCGATATCGAATTCGCCACCATGAAGCTGCTG  1440
             ||||||||||||||||||||||||||||||||||||||||||||||||||||||||||||
Seq_2  87    GCATACATTATACGAAGTTATCGGCGCGCCGATATCGAATTCGCCACCATGAAGCTGCTG  146


Seq_1  1441  CCGTCGGTGGTGCTGAAGCTCCTTCTGGCTGCAGTTCTTTCGGCACTGGTGACTGGCGAG  1500
             ||||||||||||||||||||||||||||||||||||||||||||||||||||||||||||
Seq_2  147   CCGTCGGTGGTGCTGAAGCTCCTTCTGGCTGCAGTTCTTTCGGCACTGGTGACTGGCGAG  206


Seq_1  1501  AGCCTGGAGCAGCTTCGGAGAGGGCTAGCTGCTGGAACCAGCAACCCGGACCCTTCCACT  1560
             ||||||||||||||||||||||||||||||||||||||||||||||||||||||||||||
Seq_2  207   AGCCTGGAGCAGCTTCGGAGAGGGCTAGCTGCTGGAACCAGCAACCCGGACCCTTCCACT  266


Seq_1  1561  GGATCTACGGACCAGCTGCTACGCCTAGGAGGCGGCCGGGACCGGAAAGTCCGTGACTTG  1620
             ||||||||||||||||||||||||||||||||||||||||||||||||||||||||||||
Seq_2  267   GGATCTACGGACCAGCTGCTACGCCTAGGAGGCGGCCGGGACCGGAAAGTCCGTGACTTG  326
Seq_1  1621  CAAGAGGCAGATCTGGACCTTTTGAGAGTCACTTTATCCTCCAAGCCACAAGCACTGGCC  1680
             ||||||||||||||||||||||||||||||||||||||||||||||||||||||||||||
```

```
Seq_2  327   CAAGAGGCAGATCTGGACCTTTTGAGAGTCACTTTATCCTCCAAGCCACAAGCACTGGCC  386


Seq_1  1681  ACACCAAGCAAGGAGGAGCACGGGAAAAGAAAGAAGAAAGGCAAGGGACTAGGGAAGAAG  1740
              ||||||||||||||||||||||||||||||||||||||||||||||||||||||||||||
Seq_2  387   ACACCAAGCAAGGAGGAGCACGGGAAAAGAAAGAAGAAAGGCAAGGGACTAGGGAAGAAG  446


Seq_1  1741  AGGGACCCATGTCTTCGGAAATACAAGGACTTCTGCATCCACGGAGAATGCAAATATGTG  1800
              ||||||||||||||||||||||||||||||||||||||||||||||||||||||||||||
Seq_2  447   AGGGACCCATGTCTTCGGAAATACAAGGACTTCTGCATCCACGGAGAATGCAAATATGTG  506


Seq_1  1801  AAGGAGCTCCGGGCTCCCTCCTGCATCTGCCACCCAGGTTACCATGGAGAGAGGTGTCAT  1860
              ||||||||||||||||||||||||||||||||||||||||||||||||||||||||||||
Seq_2  507   AAGGAGCTCCGGGCTCCCTCCTGCATCTGCCACCCAGGTTACCATGGAGAGAGGTGTCAT  566


Seq_1  1861  GGGCTGAGCCTCCCAGTGGAAAATCGCTTATATACCTATGACCATACAACTATCCTGGCT  1920
              ||||||||||||||||||||||||||||||||||||||||||||||||||||||||||||
Seq_2  567   GGGCTGAGCCTCCCAGTGGAAAATCGCTTATATACCTATGACCATACAACTATCCTGGCT  626


Seq_1  1921  GTGGTGGCCGTGGTGCTGTCCTCTGTCTGTCTGCTGGTCATCGTGGGGCTTCTCATGTTT  1980
              ||||||||||||||||||||||||||||||||||||||||||||||||||||||||||||
Seq_2  627   GTGGTGGCCGTGGTGCTGTCCTCTGTCTGTCTGCTGGTCATCGTGGGGCTTCTCATGTTT  686


Seq_1  1981  AGGTACCATAGGAGAGGTGGTTATGATGTGGAAAACGAAGAGAAAGTGAAGTTGGGCATG  2040
              ||||||||||||||||||||||||||||||||||||||||||||||||||||||||||||
Seq_2  687   AGGTACCATAGGAGAGGTGGTTATGATGTGGAAAACGAAGAGAAAGTGAAGTTGGGCATG  746


Seq_1  2041  ACTAATTCCCACCCGGATCTCAGACATGATAAGATACATTGATGAGTTTGGACAAACCAC  2100
              ||||||||||||||||||||||||
Seq_2  747   ACTAATTCCCACCCGGATCTCAGA----------------------------------  770
```

Features [Seq_1]:

LoxP : [1368 : 1401]

DTR : [1429 : 2079]

ROSA26_tg_R : [1258 : 1281]

2.2 GFP only – NaCl Reverse

Alignment of Sequence_1: [iDTRlinear_Cre-recombination.xdna] with Sequence_2: [Untreated_GFPonly_R.txt.xdna]

```
Seq_1  1254  GGCGCAGTAGTCCAGGGTTTCCTTGATGATGTCATACTTATCCTGTCCCTTTTTTTTCCA  1313
                    ||||||||||||||||||||||||||||||||||||||||||||||||||||||
Seq_2  771   ---------GTCCAGGGTTTCCTTGATGATGTCATACTTATCCTGTCCCTTTTTTTTCCA  721


Seq_1  1314  CAGCTCGCGGTTGAGGACAAACTCTTCGCGGTCTTTCCAGTGGTTATTAATTAAATAACT  1373
             |||||||||||||||||||||||||||||||||||||||||||||   ||||||||||||
Seq_2  720   CAGCTCGCGGTTGAGGACAAACTCTTCGCGGTCTTTCCAGTGGTTA---ATTAAATAACT  664


Seq_1  1374  TCGTATAGCATACATTATACGAAGTTATCGGCGCGCCGATATCGAATTCGCCACCATGAA  1433
             ||||||||||||||||||||||||||||||||||||||||||||||||||||||||||||
Seq_2  663   TCGTATAGCATACATTATACGAAGTTATCGGCGCGCCGATATCGAATTCGCCACCATGAA  604


Seq_1  1434  GCTGCTGCCGTCGGTGGTGCTGAAGCTCCTTCTGGCTGCAGTTCTTTCGGCACTGGTGAC  1493
             ||||||||||||||||||||||||||||||||||||||||||||||||||||||||||||
Seq_2  603   GCTGCTGCCGTCGGTGGTGCTGAAGCTCCTTCTGGCTGCAGTTCTTTCGGCACTGGTGAC  544


Seq_1  1494  TGGCGAGAGCCTGGAGCAGCTTCGGAGAGGGCTAGCTGCTGGAACCAGCAACCCGGACCC  1553
             ||||||||||||||||||||||||||||||||||||||||||||||||||||||||||||
Seq_2  543   TGGCGAGAGCCTGGAGCAGCTTCGGAGAGGGCTAGCTGCTGGAACCAGCAACCCGGACCC  484


Seq_1  1554  TTCCACTGGATCTACGGACCAGCTGCTACGCCTAGGAGGCGGCCGGGACCGGAAAGTCCG  1613
             ||||||||||||||||||||||||||||||||||||||||||||||||||||||||||||
Seq_2  483   TTCCACTGGATCTACGGACCAGCTGCTACGCCTAGGAGGCGGCCGGGACCGGAAAGTCCG  424


Seq_1  1614  TGACTTGCAAGAGGCAGATCTGGACCTTTTGAGAGTCACTTTATCCTCCAAGCCACAAGC  1673
             ||||||||||||||||||||||||||||||||||||||||||||||||||||||||||||
Seq_2  423   TGACTTGCAAGAGGCAGATCTGGACCTTTTGAGAGTCACTTTATCCTCCAAGCCACAAGC  364


Seq_1  1674  ACTGGCCACACCAAGCAAGGAGGAGCACGGGAAAAGAAAGAAGAAAGGCAAGGGACTAGG  1733
             ||||||||||||||||||||||||||||||||||||||||||||||||||||||||||||
Seq_2  363   ACTGGCCACACCAAGCAAGGAGGAGCACGGGAAAAGAAAGAAGAAAGGCAAGGGACTAGG  304
```

```
Seq_1  1734  GAAGAAGAGGGACCCATGTCTTCGGAAATACAAGGACTTCTGCATCCACGGAGAATGCAA  1793
             ||||||||||||||||||||||||||||||||||||||||||||||||||||||||||||
Seq_2  303   GAAGAAGAGGGACCCATGTCTTCGGAAATACAAGGACTTCTGCATCCACGGAGAATGCAA  244


Seq_1  1794  ATATGTGAAGGAGCTCCGGGCTCCCTCCTGCATCTGCCACCCAGGTTACCATGGAGAGAG  1853
             ||||||||||||||||||||||||||||||||||||||||||||||||||||||||||||
Seq_2  243   ATATGTGAAGGAGCTCCGGGCTCCCTCCTGCATCTGCCACCCAGGTTACCATGGAGAGAG  184


Seq_1  1854  GTGTCATGGGCTGAGCCTCCCAGTGGAAAATCGCTTATATACCTATGACCATACAACTAT  1913
             ||||||||||||||||||||||||||||||||||||||||||||||||||||||||||||
Seq_2  183   GTGTCATGGGCTGAGCCTCCCAGTGGAAAATCGCTTATATACCTATGACCATACAACTAT  124


Seq_1  1914  CCTGGCTGTGGTGGCCGTGGTGCTGTCCTCTGTCTGTCTGCTGGTCATCGTGGGGCTTCT  1973
             ||||||||||||||||||||||||||||||||||||||||||||||||||||||||||||
Seq_2  123   CCTGGCTGTGGTGGCCGTGGTGCTGTCCTCTGTCTGTCTGCTGGTCATCGTGGGGCTTCT  64


Seq_1  1974  CATGTTTAGGTACCATAGGAGAGGTGGTTATGATGTGGAAA-ACGAAGAGAAAGTGAAGT  2032
             ||||||||||||||||||||||||||||||||||||||||  || |    ||  |||||
Seq_2  63    CATGTTTAGGTACCATAGGAGAGGTGGTTATGATGTGGAAATTCG-AAGAGAAAGGAAGT  5


Seq_1  2033  TGGGCATGACTAATTCCCACCCGGATCTCAGACATGATAAGATACATTGATGAGTTTGGA  2092
              |
Seq_2  4     AGCC----------------------------------------------------  1
```

Features [Seq_1]:

LoxP : [1368 : 1401]

DTR : [1429 : 2079]

ROSA26_tg_R : [1258 : 1281]

2.3 GFP only – DT Forward

Alignment of Sequence_1: [iDTRlinear_Cre-recombination.xdna] with Sequence_2: [DT_GFPonly_F.txt.xdna]

```
Seq_1  1201  CCTTCCCCCTCTTCCCTCGTGATCTGCAACTCCAGTCTTTCTAGCATCTGTAGGGCGCAG  1260

Seq_2  1     ------------------------------------------------------------  0


Seq_1  1261  TAGTCCAGGGTTTCCTTGATGATGTCATACTTATCCTGTCCCTTTTTTTTCCACAGCTCG  1320

Seq_2  1     ------------------------------------------------------------  0


Seq_1  1321  CGGTTGAGGACAAACTCTTCGCGGTCTTTCCAGTGGTTATTAATTAAATAACTTCGTATA  1380

Seq_2  1     ------------------------------------------------------------  0


Seq_1  1381  GCATACATTATACGAAGTTATCGGCGCGCCGATATCGAATTCGCCACCATGAAGCTGCTG  1440

Seq_2  1     ------------------------------------------------------------  0


Seq_1  1441  CCGTCGGTGGTGCTGAAGCTCCTTCTGGCTGCAGTTCTTTCGGCACTGGTGACTGGCGAG  1500

Seq_2  1     ------------------------------------------------------------  0


Seq_1  1501  AGCCTGGAGCAGCTTCGGAGAGGGCTAGCTGCTGGAACCAGCAACCCGGACCCTTCCACT  1560

Seq_2  1     ------------------------------------------------------------  0


Seq_1  1561  GGATCTACGGACCAGCTGCTACGCCTAGGAGGCGGCCGGGACCGGAAAGTCCGTGACTTG  1620

Seq_2  1     ------------------------------------------------------------  0


Seq_1  1621  CAAGAGGCAGATCTGGACCTTTTGAGAGTCACTTTATCCTCCAAGCCACAAGCACTGGCC  1680

Seq_2  1     ------------------------------------------------------------  0
```

```
Seq_1  1681  ACACCAAGCAAGGAGGAGCACGGGAAAAGAAAGAAGAAAGGCAAGGGACTAGGGAAGAAG  1740

Seq_2  1     ------------------------------------------------------------  0


Seq_1  1741  AGGGACCCATGTCTTCGGAAATACAAGGACTTCTGCATCCACGGAGAATGCAAATATGTG  1800

Seq_2  1     ------------------------------------------------------------  0


Seq_1  1801  AAGGAGCTCCGGGCTCCCTCCTGCATCTGCCACCCAGGTTACCATGGAGAGAGGTGTCAT  1860

Seq_2  1     ------------------------------------------------------------  0


Seq_1  1861  GGGCTGAGCCTCCCAGTGGAAAATCGCTTATATACCTATGACCATACAACTATCCTGGCT  1920

Seq_2  1     ------------------------------------------------------------  0


Seq_1  1921  GTGGTGGCCGTGGTGCTGTCCTCTGTCTGTCTGCTGGTCATCGTGGGGCTTCTCATGTTT  1980

Seq_2  1     ------------------------------------------------------------  0


Seq_1  1981  AGGTACCATAGGAGAGGTGGTTATGATGTGGAAAACGAAGAGAAAGTGAAGTTGGGCATG  2040

Seq_2  1     ------------------------------------------------------------  0


Seq_1  2041  ACTAATTCCCACCCGGATCTCAGACATGATAAGATACATTGATGAGTTTGGACAAACCAC  2100

Seq_2  1     ------------------------------------------------------------  0


Features [Seq_1]:
LoxP           : [1368 : 1401]
DTR            : [1429 : 2079]
ROSA26_tg_R    : [1258 : 1281]
```

2.4 GFP only – DT Reverse

Alignment of Sequence_1: [iDTRlinear_Cre-recombination.xdna] with Sequence_2: [DT_GFPonly_R.txt.xdna]

```
Seq_1  1201  CCTTCCCCCTCTTCCCTCGTGATCTGCAACTCCAGTCTTTCTAGCATCTGTAGGGCGCAG  1260

Seq_2  2780  ------------------------------------------------------------  2781


Seq_1  1261  TAGTCCAGGGTTTCCTTGATGATGTCATACTTATCCTGTCCCTTTTTTTTCCACAGCTCG  1320

Seq_2  2780  ------------------------------------------------------------  2781


Seq_1  1321  CGGTTGAGGACAAACTCTTCGCGGTCTTTCCAGTGGTTATTAATTAAATAACTTCGTATA  1380

Seq_2  2780  ------------------------------------------------------------  2781


Seq_1  1381  GCATACATTATACGAAGTTATCGGCGCGCCGATATCGAATTCGCCACCATGAAGCTGCTG  1440

Seq_2  2780  ------------------------------------------------------------  2781


Seq_1  1441  CCGTCGGTGGTGCTGAAGCTCCTTCTGGCTGCAGTTCTTTCGGCACTGGTGACTGGCGAG  1500

Seq_2  2780  ------------------------------------------------------------  2781


Seq_1  1501  AGCCTGGAGCAGCTTCGGAGAGGGCTAGCTGCTGGAACCAGCAACCCGGACCCTTCCACT  1560

Seq_2  2780  ------------------------------------------------------------  2781


Seq_1  1561  GGATCTACGGACCAGCTGCTACGCCTAGGAGGCGGCCGGGACCGGAAAGTCCGTGACTTG  1620

Seq_2  2780  ------------------------------------------------------------  2781


Seq_1  1621  CAAGAGGCAGATCTGGACCTTTTGAGAGTCACTTTATCCTCCAAGCCACAAGCACTGGCC  1680

Seq_2  2780  ------------------------------------------------------------  2781
```

```
Seq_1   1681  ACACCAAGCAAGGAGGAGCACGGGAAAAGAAAGAAGAAAGGCAAGGGACTAGGGAAGAAG  1740

Seq_2   2780  ------------------------------------------------------------  2781


Seq_1   1741  AGGGACCCATGTCTTCGGAAATACAAGGACTTCTGCATCCACGGAGAATGCAAATATGTG  1800

Seq_2   2780  ------------------------------------------------------------  2781


Seq_1   1801  AAGGAGCTCCGGGCTCCCTCCTGCATCTGCCACCCAGGTTACCATGGAGAGAGGTGTCAT  1860

Seq_2   2780  ------------------------------------------------------------  2781


Seq_1   1861  GGGCTGAGCCTCCCAGTGGAAAATCGCTTATATACCTATGACCATACAACTATCCTGGCT  1920

Seq_2   2780  ------------------------------------------------------------  2781


Seq_1   1921  GTGGTGGCCGTGGTGCTGTCCTCTGTCTGTCTGCTGGTCATCGTGGGGCTTCTCATGTTT  1980

Seq_2   2780  ------------------------------------------------------------  2781


Seq_1   1981  AGGTACCATAGGAGAGGTGGTTATGATGTGGAAAACGAAGAGAAAGTGAAGTTGGGCATG  2040

Seq_2   2780  ------------------------------------------------------------  2781


Seq_1   2041  ACTAATTCCCACCCGGATCTCAGACATGATAAGATACATTGATGAGTTTGGACAAACCAC  2100

Seq_2   2780  ------------------------------------------------------------  2781
```

Features [Seq_1]:

LoxP : [1368 : 1401]

DTR : [1429 : 2079]

ROSA26_tg_R : [1258 : 1281]

XI Scripts and Macros

1.1.1 Laser injury

Normalization

```
%%select folder with xls-files containing scatter plot coordinates
filename= input ('Name of output-file? ','s');
folder=uigetdir;
cd(folder);

%%Find all excel files in folder
matfiles = dir(fullfile(folder, '*.xls*'));
nfiles = length(matfiles);

%%summarize all excel files of one image in one variable
for i = 1 : nfiles
   data=readtable(matfiles(i).name);
   x=[];
   y=[];
   for j = 2: height(data)
       xvalue=str2double(cell2mat(data{j,1}));
       yvalue=str2double(cell2mat(data{j,3}));
       x=[x xvalue];
       y=[y yvalue];
   end
   alldata.x(i)={x};
   alldata.y(i)={y};
end

%Search min & max for each timepoint
for i= 1 : nfiles
    alldata.max(i)=max(alldata.y{i});
    alldata.min(i)=min(alldata.y{i});
end

%Normalize all timepoints to global max and min
globalmax=max(alldata.max);
globalmin=min(alldata.min);
for i= 1: nfiles
        alldata.y{i}=(alldata.y{i}-globalmin)/(globalmax-globalmin)*100;
end
```

```
save(strcat(filename,'.mat'),'alldata');
```

Summary

```
%%select folder with mat-files containing normalized scatter plot
coordinates
filename= input ('Name of output-file? ','s');
folder=uigetdir;
cd(folder);
timepoints=16;

%%Find all mat files in folder
matfiles = dir(fullfile(folder, '*.mat*'));
nfiles = length(matfiles);
for timepoint= 0:timepoints
%%summarize all mat files of one analysis in one variable
    for i = 1 : nfiles
        data=open(matfiles(i).name);
        if i==1
            summary.x=data.alldata.x{i}';
            leng=length(data.alldata.x{i});
        else
            if length(data.alldata.x{i})<leng
                leng=length(data.alldata.x{i});
                summary.x=data.alldata.x{i}';
            end
        end
        summary.y{i}=data.alldata.y{timepoint+1}';
    end

    output=zeros(leng,nfiles+1);
    output(:,1)=summary.x;
    for i = 1: nfiles
        y=summary.y{i};
        output(:,i+1)=y(1:leng);
    end

    output=array2table(output);
    output.Properties.VariableNames{1}='x';
    for i = 1 : nfiles
        output.Properties.VariableNames{i+1}=char(matfiles(i).name);
    end
    fulloutput.timepoint{timepoint+1}=output;
end

save(strcat(filename,'.mat'),'fulloutput');
```

1.1.2 Calcium imaging

Part 1 – FIJI

Parts of the code were copied from user 'Biovoxxel (Jan Brocher) from https://forum.image.sc/t/using-macro-to-open-lif-tif-files/33853/5, accessed on April 20, 2023

```
//@ File (label = "Input directory", style = "directory") chosenDir

inputDir = chosenDir + File.separator;

var acceptedNonBioFormatsFiles = "jpg, jpeg, tif, png, bmp, gif, avi, ijm, txt";

run("Bio-Formats Macro Extensions");

processBioFormatFiles(inputDir);

function processBioFormatFiles(currentDirectory) {

	fileList = getFileList(currentDirectory);

	for (file = 0; file < fileList.length; file++) {

		Ext.isThisType(currentDirectory + fileList[file], supportedFileFormat);

		if (supportedFileFormat=="true" && !matches(acceptedNonBioFormatsFiles, ".*" + substring(fileList[file], lengthOf(fileList[file])-3) + ".*")) {
			Ext.setId(currentDirectory + fileList[file]);
			Ext.getSeriesCount(seriesCount);

			for (series = 1; series <= seriesCount; series++) {
				//record the Bio-Formats importer with the setup you need if different from below and change accordingly
				run("Bio-Formats Importer", "open=[" + currentDirectory + fileList[file] + "] autoscale color_mode=Composite rois_import=[ROI manager] view=Hyperstack stack_order=XYCZT series_"+series);
				runMyMacro();
			}

		} else if (matches(acceptedNonBioFormatsFiles, ".*" + substring(fileList[file], lengthOf(fileList[file])-3) + ".*")) {

			open(currentDirectory + fileList[file]);
			runMyMacro();

		} else if (endsWith(fileList[file], "/")) {
```

```
                    processBioFormatFiles(currentDirectory + fileList[file]);

            }
      }
}

function runMyMacro() {
getDimensions(width, height, channels, slices, frames);
if (frames > 3) {
      oldfileName=getTitle();
      //print(oldfileName);
      unwanted_part="/";
      slash=indexOf(oldfileName,unwanted_part);
      fileName=substring(oldfileName, slash+1, oldfileName.length);
      //print(fileName)
      rename(fileName);
      run("Duplicate...", "use");
      setAutoThreshold("Default dark");
      setOption("BlackBackground", true);
      run("Convert to Mask");
      run("Analyze Particles...", "size=100000-Infinity clear add");
      selectWindow(fileName);
      close("Log");
      k=1;
      for (i = 1; i < 17; i++) {
            for (j = 1; j < 17; j++) {
                  makeRectangle(64*(i-1), 64*(j-1), 64, 64);
                  roiManager("Add");
                  k=k+1;
            }
      }
      a1 = newArray(147);
      for (i=0; i<a1.length; i++) {
       a1[i] = i+1;
      }

      roiManager("Select", a1);
      run("Time Series Analyzer V3");
      wait(1000);
      run("IJ   Robot",   "order=Left_Click   x_point=116   y_point=105   delay=300
keypress=[]");
      wait(10000);
      close("Time Trace Average");
```

```
	selectWindow("Time Trace(s)");
	saveAs("Results", "C:/Users/Marc/Desktop/Calcium_traces/" + fileName + "_part1.csv");
	close(fileName + "_part1.csv");

	a2 = newArray(k-148);
	for (i=0; i<a2.length; i++) {
	 a2[i] = i+148;
	}

	selectWindow("DUP_" + fileName);
	roiManager("Select", a2);
	run("Time Series Analyzer V3");
	wait(1000);
	run("IJ Robot", "order=Left_Click x_point=116 y_point=105 delay=300 keypress=[]");
	wait(10000);
	close("Time Trace Average");
	selectWindow("Time Trace(s)");
	saveAs("Results", "C:/Users/Marc/Desktop/Calcium_traces/" + fileName + "_part2.csv");
	close(fileName + "_part2.csv");

	roiManager("Deselect");
	roiManager("Delete");
}
close("*");
}
```

Part 2 – MATLAB

```
%% Get directory and find all xls files in that directory
dname = uigetdir('C:\');
cd (dname);
matfiles = dir(fullfile(dname, '*.csv'));
nfiles = length(matfiles);
set(groot,'defaultLineLineWidth',1.5)

%% Remove unwanted part1 and part2 from filename as preparation to merge
xls-files
for k = 1 : nfiles
    name=matfiles(k).name;
    if contains(name,'part1') == 1
        newname = erase(name,"_part1");
    elseif contains(name,'part2') == 1
        newname = erase(name,"_part2");
    end
    matfiles(k).name2 = newname;
end
```

```
%% Find unique filenames and merge xls-files to one file per condition
for k = 1: nfiles
    allfiles{k,1} = matfiles(k).name2;
end
allfiles = string(allfiles);
filenames = unique(allfiles);
nfilenames = length(filenames);

for k = 1 : nfilenames
    index = find(allfiles == filenames(k));
    data{k,1} = filenames(k);
    for i = 1 : length(index)
        data{k,i+1} = readmatrix(matfiles(index(i)).name);
        [rows,columns] = size(data{k,i+1});
        data{k,i+1} = data{k,i+1}(1:rows,1:columns-2);
    end
    for i = 2 : length(index)
        data{k,2} = [data{k,2} data{k,i+1}];
    end
    for i = 2 : length(index)
        data{k,i+1} = [];
    end
end

%% Processing of each file separately and summarizing in results table

for k = 1 : nfilenames
    a = data{k,2};

    %% Find files for which FIJI had a bug
    zero = find(a == 0);
    if zero >= 1
        disp ('Error in file ' + filenames(k))
    else
        %% Detect spikes and measure amplitude with rolling average of 10
timepoints
        [rows,columns] = size(a);
        spikes = zeros(rows, columns);
        amplitudes = zeros(rows, columns);
        for i = 1 : columns
            b = a(:,i);
            for j = 11 : rows
                rollingaverage = mean(b(j-10:j-1));
                if b(j) > rollingaverage * 1.005
                    spikes(j,i) = 1;
                    amplitudes(j,i) = (b(j)/rollingaverage-1)*100;
                end
            end
            %% Find peak of Spike and count only this as spike
            for j = 2 : rows
                if spikes(j,i) == 1 && spikes(j-1,i) == 1
                    incr= 1;
                    if j < rows
                        while j+incr <= rows && spikes(j+incr,i) == 1
                        incr = incr + 1;
                        end
                    end
                    amps = [amplitudes(j-1 : j-1+incr,i)];
                    sptime = find(amps == max(amps));
                    spikesreset = zeros (incr+1,1);
                    spikesreset(sptime,1) = 1;
                    spikes(j-1 : j-1+incr,i) = spikesreset;
```

```
        end
    end

    for j = 1 : rows
        amplitudes(j,i) = amplitudes(j,i) * spikes(j,i);
    end
end

%% Plot spikes for all regions
for i = 1 : columns
    sptimes{i} = find(spikes(:,i) ==1)/10;
end

figure('Units','normalized','Position',[0 0 0.3 1])
ax = subplot(2,1,1); hold on

for i = 1 : length(sptimes)
    spks = sptimes{i}';
    xspikes = repmat(spks,3,1);
    yspikes = nan(size(xspikes));

    if ~isempty(yspikes)
        yspikes(1,:) = i-1;
        yspikes(2,:) = i;
    end
    plot(xspikes, yspikes, 'Color', 'k')
end
ax.XLim = [0 180];
ax.YLim = [0 length(sptimes)];
ax.XLabel.String = 'Time [s]';
ax.YLabel.String = 'Regions';
set(gca,'linewidth',1.5)
set(gca,'FontSize',20)

%% Spike histogram

all = [];
for i = 1: length(sptimes)
    all = [all; sptimes{i}];
end

ax = subplot(2,1,2);
nbins = 900;
h = histogram(all,nbins);
h.FaceColor = 'k';

ax.XLim = [0 180];
ax.XLabel.String = 'Time [s]';
ax.YLabel.String = 'Spikes/Bin';
set(gca,'linewidth',1.5)
saveas(gcf, data{k,1} + '.jpg');

%% Calculation of analysis parameters
%% Average amplitude and spike firing rate per region
amplitudes (amplitudes == 0) = [];
averageamplitude = mean(amplitudes,'all');

spikesum = sum(spikes,'all');
time = 180;
spikerate = spikesum/(time*columns);
```

```
        %% Synchronized activity as defined as synchronous activity in 10+
region in bins of 200 ms with filter to avoid double count of adjacent bins
        histo=h.Values;
        [rows2, columns2] = size(histo);
        for i = 2 : columns2
            if histo(1,i) > 0 && histo(1,i-1) > 0
                incr= 1;
                if i < columns2
                    while i+incr <= columns2 && histo(1,i+incr) > 0
                    incr = incr + 1;
                    end
                end
                maxHisto = [histo(1,i-1 : i-1+incr)];
                peaktime = find(maxHisto == max(maxHisto));
                peaksreset = zeros (incr+1,1);
                peaksreset(peaktime,1) = max(maxHisto);
                histo(1,i-1 : i-1+incr) = peaksreset;
            end
        end
        idx = histo >= 10;
        synchspikes = sum(idx(:));
        synchspikerate = synchspikes/time;

        %% Put parameters in data array
        data{k,3} = averageamplitude;
        data{k,4} = spikerate;
        data{k,5} = synchspikerate;
    end
end

%% Save cell array with data as Excel-file
T = cell2table(data);
T = removevars(T,{'data2'});
T.Properties.VariableNames("data1") = "Filename";
T.Properties.VariableNames("data3") = "Average Amplitude";
T.Properties.VariableNames("data4") = "Spike Rate";
T.Properties.VariableNames("data5") = "Synchronous Spike Rate";
writetable(T,'Results.xlsx');
clear
```

XII List of Figures

XIII List of Tables